

4/2184/250

NUMERICAL ELECTROMAGNETIC MODELING

OF A SMALL APERTURE HELICAL-FED

REFLECTOR ANTENNA

A Thesis Presented to

The Faculty of the

Fritz J. and Dolores H. Russ
College of Engineering and Technology

Ohio University

In Partial Fulfillment

of the Requirement for the Degree

Master of Science

by

Chin-Yuan Cheng

August, 1998

Thesis
M
1998
CHENG

OHIO UNIVERSITY
LIBRARY

Acknowledgments

I would like to extend my appreciation to all my friends and family who made this thesis possible. With their consistent support and enthusiastic help, I was able to conduct and present my research.

A special thank you goes to Dr. Michael Braasch, my academic director, who has broadened my view. By giving me extensive support and continually sharing knowledge about this project, he assured that I was able to overcome the challenges one by one. Dr. Roger Radcliff has earned my respect for his extensive knowledge about antennas. He offered me many precious ideas; when I had hard time in finding appropriate software, he shed light to guide me in the right direction. My appreciation goes to Dr. Frank van Graas for helping me measure the dimensions of the helibowl.

Thanks also go to Dr. Simbo Odunaiya for being my mentor and friend. Even under extreme personal circumstances, he still helped me. I would like to thank Michael

DiBenedetto and dB Systems Inc. for offering information about the helibowl antenna and providing details about the measurement of the helibowl's radiation pattern.

My friend, Rick Cooper, generously gave me support by letting me use his valuable MatNec software and assisting me in working out software difficulties. I, too, want to thank Dianne Bouvier for reviewing this paper and helping me with my English writing.

I am deeply indebted to Yuling, my wife, and Shania and Megan, my two children. It was only through Yuling's unselfish support and encouragement that I was able to finish my research and complete my thesis. A heartfelt thank you goes to all three for making everything possible.

Table of Contents

	<u>Page</u>
Acknowledgments	iii
Table of Contents	v
List of Figures	vii
Chapter 1 Introduction	1
Chapter 2 Background - GPS Antennas and Signal Reception Issues	3
2.1 General Overview - What is Multipath?	4
2.2 Historical Actions - Adopted Solutions	7
2.2.1 Multipath Limiting Receiver Architectures	7
2.2.2 Post-Processing Techniques	7
2.2.3 Antenna Siting	8
2.2.4 Antennas Design	8
2.3 Specific Approach of the Research	8
2.3.1 NEC-BSC (Numerical Electromagnetic Code - Basic Scattering Code)	13
2.3.2 Numerical Electromagnetic Code (NEC)	14
2.3.3 MININEC	14
2.3.4 Electromagnetic Surface Patch Code (ESP)	15
2.3.5 Triangular Surface Patch Code	15
2.3.6 General Electromagnetic Model for the Analysis of Complex Systems (GEMACS)	16

Chapter 3	Derivation of Equations	17
3.1	Integral Equation (IE)	18
3.1.1	Introduction to integral equation (IE)	18
3.1.2	Derivation of Integral Equations (IE)	19
3.2	Theorem of the Method of Moments (MOM)	23
3.2.1	Introduction to Method of Moments (MOM)	23
3.2.2	Derivation of Method of Moments (MOM)	24
Chapter 4	Validation on the $\lambda/4$ Monopole Above a Conducting Plane	28
4.1	Measured Data	30
4.2	Simulation Result	33
Chapter 5	Simulation on the Helibowl Antenna	39
5.1	Measured Data	40
5.2	Simulation Results	51
5.2.1	Model One: First One with Less Detail	52
5.2.2	Model Two: Modified Helical Part	80
5.2.3	Model Three: With the Circular Plate Added	88
5.3	Extensive Simulations on Two Models with Their Shapes Changed	97
Chapter 6	Conclusion and Recommendations	113
6.1	Conclusion	113
6.2	Recommendations for Future Work	115
References		117
Appendix A	About NEC-2	120
Appendix B	Programs of Some Visualization and Converting Tools	122
Appendix C	NEC-2 Input Files for the $\lambda/4$ monopoles in Chapter 4	129
Appendix D	Measured Data for the Helibowl Antenna (Measured by dB Systems Inc.)	147
Appendix E	The Simulation Results of those Helibowl Models as Mentioned in Sections 5.2.3 & 5.3	154

List of Figures

<u>Figure</u>	<u>Page</u>
1. Figure 2.1 - Illustration shows the cause of multipath	5
2. Figure 2.2 - GPS signal distorted by multipath	6
3. Figure 2.3.1 - Pictures of the helibowl antenna	10
4. Figure 2.3.2 - Measured patterns of the helibowl at azimuth angle $\phi = 0^\circ$ and 90°	12
5. Figure 3.1.1 - Geometry of a line source above a two-dimensional finite width strip	21
6. Figure 4.1.1 - Total radiation pattern of $\lambda/4$ monopole above a square plane. (Reference: Balanis, C.A., Antenna Theory: Analysis and Design, John Wiley & Sons, Inc., 1982, p. 519)	31
7. Figure 4.1.2 - Total radiation pattern of $\lambda/4$ monopole above a circular plane. (Reference: Balanis, C.A., Antenna Theory: Analysis and Design, John Wiley & Sons, Inc., 1982, p. 515)	32
8. Figure 4.2.1 - Geometry of wire-grid model of the $\lambda/4$ monopole above a square plane, frequency at 1 GHz	35
9. Figure 4.2.2 - Geometry of wire-grid model of the $\lambda/4$ monopole above a circular plane, frequency at 1 GHz	36

10.	Figure 4.2.3 - Simulation result (total radiation pattern) for Figure 4.2.1	37
11.	Figure 4.2.4 - Simulation result (total radiation pattern) for Figure 4.2.2	38
12.	Figure 5.1.1 - Helibowl antenna's geometric configuration. (Figure provided courtesy of dB Systems, Inc.)	41
13.	Figure 5.1.3a - Measured horizontal pattern of the helibowl at azimuth angle $\phi = 0^\circ$	43
14.	Figure 5.1.3b - Measured horizontal pattern of the helibowl at azimuth angle $\phi = 0^\circ$	44
15.	Figure 5.1.4a - Measured horizontal pattern of the helibowl at azimuth angle $\phi = 90^\circ$	45
16.	Figure 5.1.4b - Measured horizontal pattern of the helibowl at azimuth angle $\phi = 90^\circ$	46
17.	Figure 5.1.5a - Measured vertical pattern of the helibowl at azimuth angle $\phi = 0^\circ$	47
18.	Figure 5.1.5b - Measured vertical pattern of the helibowl at azimuth angle $\phi = 0^\circ$	48
19.	Figure 5.1.6a - Measured vertical pattern of the helibowl at azimuth angle $\phi = 90^\circ$	49
20.	Figure 5.1.6b - Measured vertical pattern of the helibowl at azimuth angle $\phi = 90^\circ$	50
21.	Figure 5.2.1a - Geometry of the wire-grid model for helibowl in Section 5.2.1	53
22.	Figure 5.2.1b - 2-D geometry of the wire-grid model for helibowl in Section 5.2.1	54
23.	Figure 5.2.2 - Vertical radiation patterns for helibowl model in Section 5.2.1, Simple helix, No circular plate, $\phi = 0^\circ$ and 90° , 1575 MHz	56
24.	Figure 5.2.3 - Vertical radiation pattern for helibowl model in Section 5.2.1, Simple helix, No circular plate, $\phi = 0^\circ$, 1575 MHz	57

25.	Figure 5.2.4 - Vertical radiation pattern for helibowl model in Section 5.2.1, Simple helix, No circular plate, $\phi = 90^\circ$, 1575 MHz	58
26.	Figure 5.2.5 - Horizontal radiation patterns for helibowl model in Section 5.2.1, Simple helix, No circular plate, $\phi = 0^\circ$ and 90° , 1575 MHz	59
27.	Figure 5.2.6 - Horizontal radiation pattern for helibowl model in Section 5.2.1, Simple helix, No circular plate, $\phi = 0^\circ$, 1575 MHz	60
28.	Figure 5.2.7 - Horizontal radiation pattern for helibowl model in Section 5.2.1, Simple helix, No circular plate, $\phi = 90^\circ$, 1575 MHz	61
29.	Figure 5.2.8 - Vertical radiation patterns for helibowl model in Section 5.2.1, Simple helix, No circular plate, $\phi = 22.5^\circ$ and 112.5° , 1575 MHz	62
30.	Figure 5.2.9 - Vertical radiation pattern for helibowl model in Section 5.2.1, Simple helix, No circular plate, $\phi = 22.5^\circ$, 1575 MHz	63
31.	Figure 5.2.10 - Vertical radiation pattern for helibowl model in Section 5.2.1, Simple helix, No circular plate, $\phi = 112.5^\circ$, 1575 MHz	64
32.	Figure 5.2.11 - Horizontal radiation patterns for helibowl model in Section 5.2.1, Simple helix, No circular plate, $\phi = 22.5^\circ$ and 112.5° , 1575 MHz	65
33.	Figure 5.2.12 - Horizontal radiation pattern for helibowl model in Section 5.2.1, Simple helix, No circular plate, $\phi = 22.5^\circ$, 1575 MHz	66
34.	Figure 5.2.13 - Horizontal radiation pattern for helibowl model in Section 5.2.1, Simple helix, No circular plate, $\phi = 112.5^\circ$, 1575 MHz	67
35.	Figure 5.2.14 - Vertical radiation patterns for helibowl model in Section 5.2.1, Simple helix, No circular plate, $\phi = 45^\circ$ and 135° , 1575 MHz	68

36.	Figure 5.2.15 - Vertical radiation pattern for helibowl model in Section 5.2.1, Simple helix, No circular plate, $\phi = 45^\circ$, 1575 MHz	69
37.	Figure 5.2.16 - Vertical radiation pattern for helibowl model in Section 5.2.1, Simple helix, No circular plate, $\phi = 135^\circ$, 1575 MHz	70
38.	Figure 5.2.17 - Horizontal radiation patterns for helibowl model in Section 5.2.1, Simple helix, No circular plate, $\phi = 45^\circ$ and 135° , 1575 MHz	71
39.	Figure 5.2.18 - Horizontal radiation pattern for helibowl model in Section 5.2.1, Simple helix, No circular plate, $\phi = 45^\circ$, 1575 MHz	72
40.	Figure 5.2.19 - Horizontal radiation pattern for helibowl model in Section 5.2.1, Simple helix, No circular plate, $\phi = 135^\circ$, 1575 MHz	73
41.	Figure 5.2.20 - Vertical radiation patterns for helibowl model in Section 5.2.1, Simple helix, No circular plate, $\phi = 67.5^\circ$ and 157.5° , 1575 MHz	74
42.	Figure 5.2.21 - Vertical radiation pattern for helibowl model in Section 5.2.1, Simple helix, No circular plate, $\phi = 67.5^\circ$, 1575 MHz	75
43.	Figure 5.2.22 - Vertical radiation pattern for helibowl model in Section 5.2.1, Simple helix, No circular plate, $\phi = 157.5^\circ$, 1575 MHz	76
44.	Horizontal radiation patterns for helibowl model in Section 5.2.1, Simple helix, No circular plate, $\phi = 67.5^\circ$ and 157.5° , 1575 MHz	77
45.	Horizontal radiation pattern for helibowl model in Section 5.2.1, Simple helix, No circular plate, $\phi = 67.5^\circ$, 1575 MHz	78
46.	Horizontal radiation pattern for helibowl model in Section 5.2.1, Simple helix, No circular plate, $\phi = 157.5^\circ$, 1575 MHz	79

47.	Figure 5.2.26 - Geometry of the wire-grid model for helibowl in Section 5.2.2, Ribbon Helix	81
48.	Figure 5.2.27 - Vertical radiation patterns for helibowl model in Section 5.2.2, Ribbon helix, No circular plate, $\phi = 0^\circ$ and 90° , 1575 MHz	82
49.	Figure 5.2.28 - Vertical radiation pattern for helibowl model in Section 5.2.2, Ribbon helix, No circular plate, $\phi = 0^\circ$, 1575 MHz	83
50.	Figure 5.2.29 - Vertical radiation pattern for helibowl model in Section 5.2.2, Ribbon helix, No circular plate, $\phi = 90^\circ$, 1575 MHz	84
51.	Figure 5.2.30 - Horizontal radiation patterns for helibowl model in Section 5.2.2, Ribbon helix, No circular plate, $\phi = 0^\circ$ And 90° , 1575 MHz	85
52.	Figure 5.2.31 - Horizontal radiation pattern for helibowl model in Section 5.2.2, Ribbon helix, No circular plate, $\phi = 0^\circ$, 1575 MHz	86
53.	Figure 5.2.32 - Horizontal radiation pattern for helibowl model in Section 5.2.2, Ribbon helix, No circular plate, $\phi = 90^\circ$, 1575 MHz	87
54.	Figure 5.2.33 - Geometry of the wire-grid model for helibowl in Section 5.2.3, Simple helix, with circular plate	89
55.	Figure 5.2.34 - Vertical radiation patterns for helibowl model in Section 5.2.3, Simple helix, With circular plate, $\phi = 0^\circ$ and 90° , 1575 MHz	91
56.	Figure 5.2.35 - Vertical radiation pattern for helibowl model in Section 5.2.3, Simple helix, With circular plate, $\phi = 0^\circ$, 1575 MHz	92
57.	Figure 5.2.36 - Vertical radiation pattern for helibowl model in Section 5.2.3, Simple helix, With circular plate, $\phi = 90^\circ$, 1575 MHz	93

58.	Figure 5.2.37 - Horizontal radiation patterns for helibowl model in Section 5.2.3, Simple helix, With circular plate, $\phi = 0^\circ$ and 90° , 1575 MHz	94
59.	Figure 5.2.38 - Horizontal radiation pattern for helibowl model in Section 5.2.3, Simple helix, With circular plate, $\phi = 0^\circ$, 1575 MHz	95
60.	Figure 5.2.39 - Horizontal radiation pattern for helibowl model in Section 5.2.3, Simple helix, With circular plate, $\phi = 90^\circ$, 1575 MHz	96
61.	Figure 5.3.1 - Geometry of the wire-grid model for helibowl in Section 5.3, Bowl's diameter doubled	98
62.	Figure 5.3.2 - Vertical radiation patterns for helibowl model in Section 5.3, Bowl's diameter doubled, $\phi = 0^\circ$ and 90° , 1575 MHz	99
63.	Figure 5.3.3 - Vertical radiation pattern for helibowl model in Section 5.3, Bowl's diameter doubled, $\phi = 0^\circ$, 1575 MHz	100
64.	Figure 5.3.4 - Vertical radiation pattern for helibowl model in Section 5.3, Bowl's diameter doubled, $\phi = 90^\circ$, 1575 MHz	101
65.	Figure 5.3.5 - Horizontal radiation patterns for helibowl model in Section 5.3, bowl's diameter doubled, $\phi = 0^\circ$ and 90° , 1575 MHz	102
66.	Figure 5.3.6 - Horizontal radiation pattern for helibowl model in Section 5.3, bowl's diameter doubled, $\phi = 0^\circ$, 1575 MHz	103
67.	Figure 5.3.7 - Horizontal radiation pattern for helibowl model in Section 5.3, bowl's diameter doubled, $\phi = 90^\circ$, 1575 MHz	104
68.	Figure 5.3.8 - Geometry of the wire-grid model for helibowl in Section 5.3, Length of the helix doubled	105
69.	Figure 5.3.9 - Vertical radiation patterns for helibowl model in Section 5.3, Length of the helix doubled, $\phi = 0^\circ$ and 90° , 1575 MHz	106
70.	Figure 5.3.10 - Vertical radiation pattern for helibowl model in Section 5.3, Length of the helix doubled, $\phi = 0^\circ$, 1575 MHz	107

71.	Figure 5.3.11 - Vertical radiation pattern for helibowl model in Section 5.3, Length of the helix doubled, $\phi = 90^\circ$, 1575 MHz	108
72.	Figure 5.3.12 - Horizontal radiation patterns for helibowl model in Section 5.3, Length of the helix doubled, $\phi = 0^\circ$ and 90° , 1575 MHz	109
73.	Figure 5.3.13 - Horizontal radiation pattern for helibowl model in Section 5.3, Length of the helix doubled, $\phi = 0^\circ$, 1575 MHz	110
74.	Figure 5.3.14 - Horizontal radiation pattern for helibowl model in Section 5.3, Length of the helix doubled, $\phi = 90^\circ$, 1575 MHz	111
75.	Figure E-1 Total radiation pattern for original helibowl at $\phi = 0^\circ$	155
76.	Figure E-2 Total radiation pattern for original helibowl at $\phi = 90^\circ$	156
77.	Figure E-3 Total radiation pattern for helibowl with double sized bowl at $\phi = 0^\circ$	157
78.	Figure E-4 Total radiation pattern for helibowl with double sized bowl at $\phi = 90^\circ$	158
79.	Figure E-5 Total radiation pattern for helibowl with length of helix doubled at $\phi = 0^\circ$	159
80.	Figure E-6 Total radiation pattern for helibowl with length of helix doubled at $\phi = 90^\circ$	160

Chapter 1

Introduction

Any antenna system may introduce interference into its associated receiver. The multipath effect is one of the major interference sources that prevent communication, navigation and surveillance systems from functioning correctly. Multipath is the phenomenon where a signal is received through multiple paths due to reflection and diffraction. However, because the reflected and diffracted signals travel longer paths, the multipath is also delayed when compared to the direct signal. In addition, the multipath is usually weaker than the direct. This reduces the impact of multipath on the receiver but it does not eliminate it.

Multipath is the dominant error source in differential GPS (DGPS) applications [1]. Ground reference stations experience the most serious problem, which results from the multipath [2]. For fixed sites, the most effective multipath control technique is antenna

pattern shaping [2, 3]. Antennas such as choke-rings, reflectors and stacked arrays have been designed to limit multipath [3]. For the current DGPS landing system design [2], a stacked array antenna is used to track low elevation satellites and either a choke-ring antenna or a reflector antenna is used to track high elevation satellites. The stacked array has proven to be effective in reducing multipath [2]. However, the reflector antenna, known as a helibowl, has never been rigorously analyzed.

This thesis will describe the results of this research which investigated the performance of the helibowl antenna. Through use of NEC-2 (Numerical Electromagnetics Code), the derived results from the simulation will be able to compare with the measured data from the experiment. This approach will be proved to be correct. The validated model can then be used as a tool for future efforts to optimize helibowl performance.

Chapter 2

Background - GPS Antennas and Signal Reception Issues

In GPS (Global Positioning System) applications, the clarity of the antenna reception plays a very important role in the whole operation of GPS control. Antennas have been designed specifically to reduce sensitivity to multipath. Research [4] has shown that multipath distorts the PRN (Pseudorandom Noise) code such that ranging error can be on the order of tens of meters. It also changes the phase of the carrier itself. In some cases, the GPS monitor station receivers have lost lock of satellite signals because of this [6]. In order to achieve better operation, we need to know how to limit the effect of multipath.

In this chapter, multipath is discussed along with the adopted action to reduce multipath. In section 3 of this chapter, the approach will be described along with why it is a viable way to solve the multipath problem.

2.1 General Overview - What is Multipath?

There are two major unwanted effects which will downgrade the DGPS accuracy. One is called multipath and the other, shadowing effect, as shown in Figure 2.1. These effects will contribute to the errors incurred in the receiver measurement process. In the latter, there are not many things we can do but pull ourselves out of the shadow area. In the multipath effect, we have some ideas about how to reduce interference. Multipath mitigation techniques for GPS have been the subject of extensive research and the research still continues [5].

Multipath is presented by the indirect or reflected version of the original signal. Because the multipath signal is a reflected or diffracted signal, it will be attenuated and delayed (in comparison with the genuine or direct signal) at reception. When the GPS antenna receives such an erroneous signal as well as the original (or direct) signal, the original signal will be distorted (Figure 2.2) and thus results in the shift of zero crossing of the correlation peak. In this case, if the error goes beyond the tolerance range, the result will be an erroneous pseudorange determination or, under even worse conditions, GPS satellite signal receiver tracking loops may lose lock of the GPS signal.

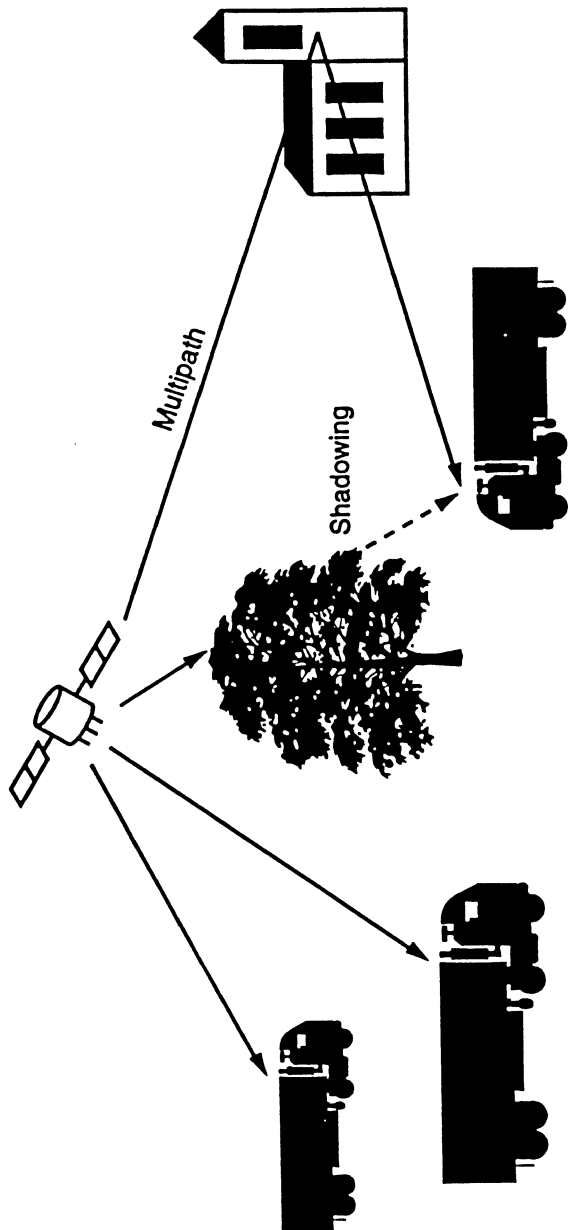


Figure 2.1 - Illustration shows the cause of multipath
(Illustration drawn from: Kaplan, E.D., Understanding GPS: Principles and Applications, Artech House Publishers, Boston, 1996, p.256.)

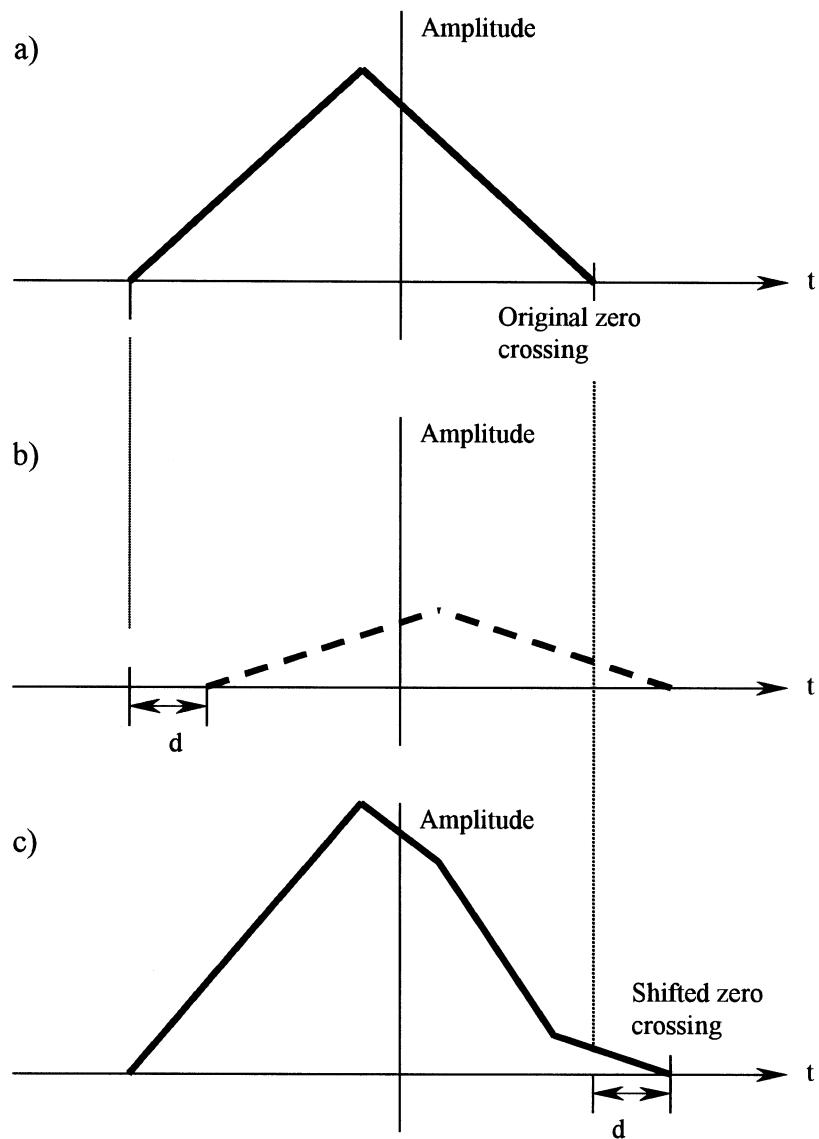


Figure 2.2 - GPS Signal distorted by multipath:

- (a) Solid line represents the direct GPS correlation peak
- (b) Dashed line represents the scaled and delayed indirect correlation peak.
- (c) Distortion causes the zero crossing of the curve to be shifted time d .

2.2 Historical Actions - Adopted Solutions

In this section, current techniques to reduce the effects of multipath will be discussed.

2.2.1 Multipath Limiting Receiver Architectures

A variety of receiver designs have been developed to reduce sensitivity to multipath [5]. These designs include the narrow correlator, strobe correlator and multipath estimating delay lock loop (MEDLL). None of these designs, however, reduce errors due to short delay multipath. "Short" in this case, refers to delays less than 0.1 PRN chip. To GPS ground station receiver, the C/A-code has a chipping rate of 1.023×10^6 chips/sec and the P(Y)-code has a chipping rate of 10.23×10^6 chips/sec. The duration per PRN chip is 977.52ns long for C/A-code or 97.72ns long for P(Y)-code. Therefore, 0.1 PRN chip is roughly equal to 97.75ns for C/A-code and 9.78ns for P(Y)-code.

2.2.2 Post-Processing Techniques

Filtering schemes such as Kalman filtering and complementary filtering have been developed to reduce multipath error after the pseudorange and carrier-phase measurements have been formed [17-19]. These techniques, however, only reduce high frequency multipath errors while leaving the low frequency and bias errors untouched.

2.2.3 Antenna Siting

Some success has been achieved by choosing a location for the antenna where multipath is negligible. In many instances, however, it is either impractical to do this or a good location simply does not exist.

2.2.4 Antennas Design

This technique involves the design of antennas or the combination of antennas. Because multipath generally arrives along with signals from satellites at low elevation angles, an antenna (or a combination of antennas) is designed to receive signals from elevation angles greater than 5 degrees with normal gain and attenuate the rest. Factors like the shape of the antenna, the height of antenna housing and the arrangement of antenna elements will be considered in order to improve receiver performance.

2.3 Specific Approach of the Research

The work described here focused on analysis of a GPS antenna known as a 'heli-bowl.' The antenna has good coverage of the upper hemisphere and has significant attenuation below the horizon.

The final goal of the research presented here focused on analyzing the helibowl antenna by changing its shape. Basically, this idea is similar to the approach mentioned in section 2.2.4. The antennas with different shapes were analyzed to help people understand what is the relationship between the antenna's dimensions and its radiation pattern. Before the analysis is accomplished, a series of analyzing procedure must be built first. This procedure has to be proved correct before any further research can be continued. The development of a simulation to analyze helibowl-type antennas is the main goal of this research.

First, a simple wire-grid model was developed based on the NEC-2 input format. The results of this simulation were compared with published data from a textbook. Once a favorable comparison was obtained, work proceeded to build another model, that is, the helibowl antenna. Simulation results were compared with the experimental (measured) data obtained from dB Systems Incorporated, Salt Lake City, Utah and Mike DiBenedetto of the Avionics Engineering Center of Ohio University. The thesis work was completed once the modeled and measured data compared favorably. The ultimate goal is to develop an optimum DGPS reference antenna and a key first step is a validated model. Our research and observations are just the beginning in this field and hopefully will lead to future development until the ideal GPS antennas are designed.

The helibowl is a bowl-shape reflector antenna with a helical excitation element attached within the bowl (see Figure 2.3.1). The helibowl was originally developed by Don

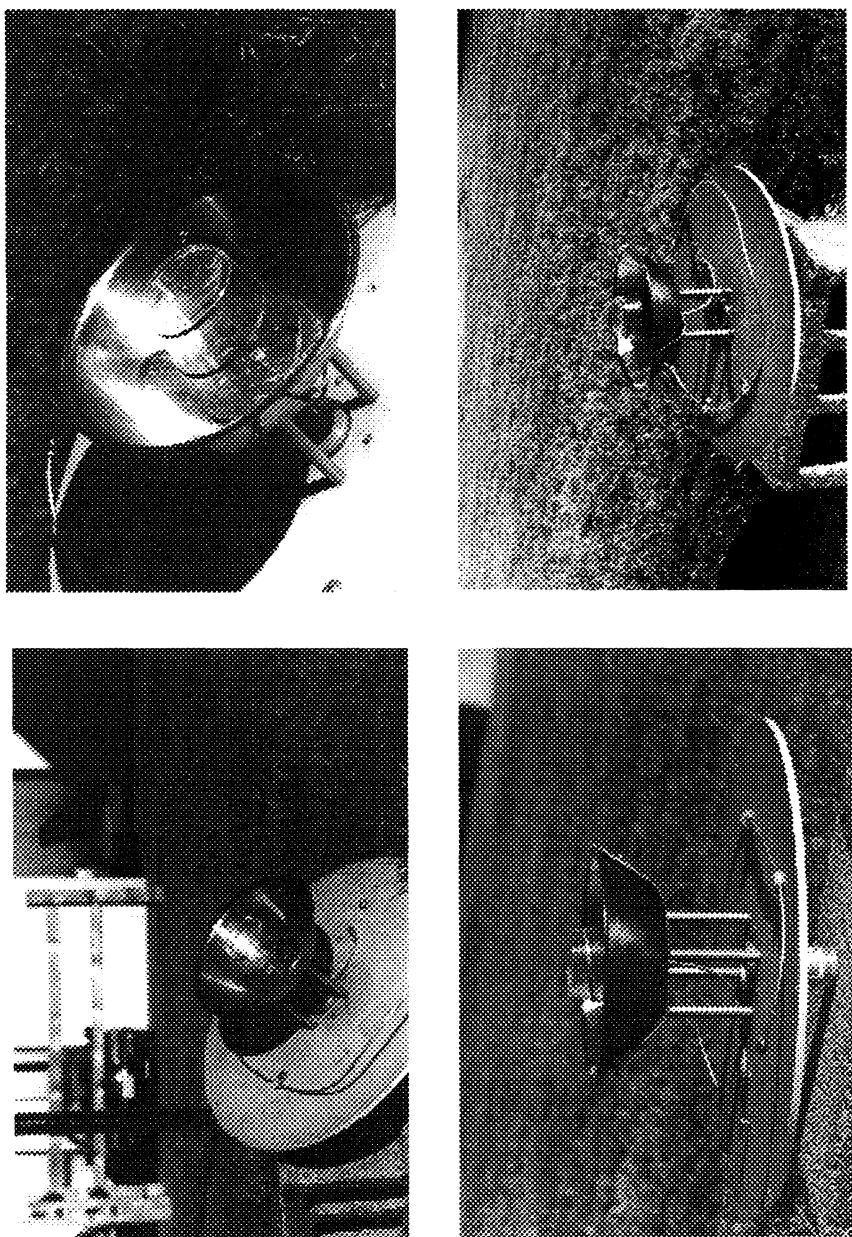


Figure 2.3.1 - Pictures of the helibowl antenna

Spitzmesser at the Jet Propulsion Laboratory (JPL) in Pasadena [20]. The concept was an extension of the helicone antenna developed and reported by Carver in 1967 [21]. The "helibowl" was well-used by many of the GPS ground stations and experimental facilities around the world.

The helibowl has a radiation pattern as shown in Figure 2.3.2. This pattern is measured when the bowl's opening is upright, like a cereal bowl on your table. As shown in its radiation patterns, the antenna has better reception between 0 degrees (topmost) and about 100 degrees (10 degrees under the ground). The reception below 100 degrees will go down to -30 dB and less. If the relationship between its pattern and its shape can be analyzed successfully, a better helibowl antenna that rejects the multipath efficiently will be found.

How will this helibowl antenna be modeled? First of all, a wire-grid model, which was constructed by hundreds of segments of conducting wires, was built. The contour of this mesh model was made to follow the shape of the helibowl as closely as possible. After developing an NEC-2 model, a simulation was performed to calculate the radiation pattern. For more information about how to use NEC-2 code, please see [Appendix A] or "Numerical Electromagnetics code (NEC) - Method of Moments", part III: User's Guide" [9]. Once the NEC-2 program finished the calculation, a program written in Matlab language in Appendix B was used to help us read the results.

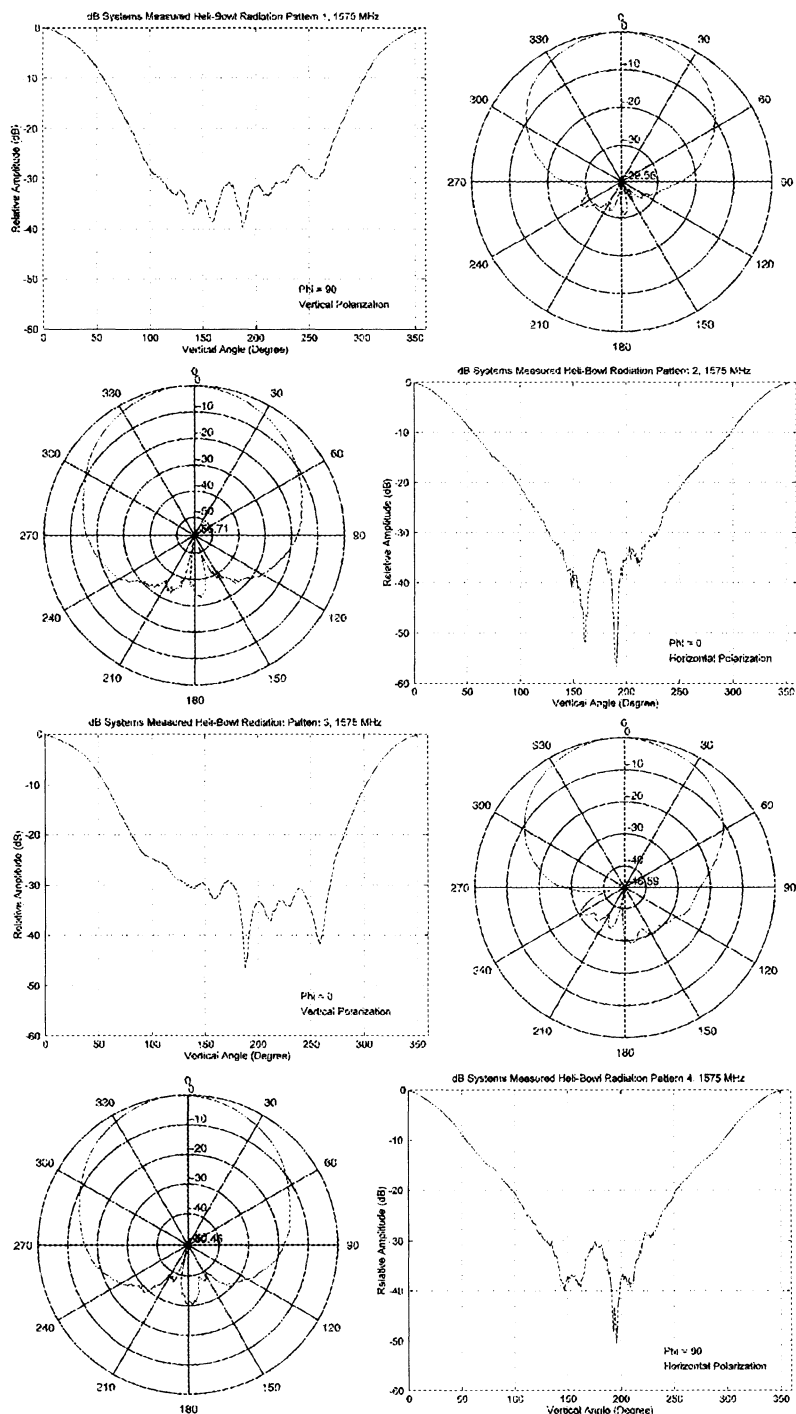


Figure 2.3.2 - Measured patterns of the helibowl at azimuth angle $\phi = 0^\circ$ and 90°

The wire-grid modeling approach has been applied in many situations, especially those that need to deal with the far-field quantities such as radiation patterns and radar cross sections [10]. Other modeling methods like surface patch modeling for this research have been considered, too. The surface patch modeling approach has the advantage in calculating both far-field and near-field patterns [11]. However, it's not easy to use in simulating curved surfaces such as the helibowl. In the end, the wire-grid modeling method was adopted for this research at the final decision. Below is the brief comparison of some available numerical electromagnetic modeling codes.

2.3.1 NEC-BSC (Numerical Electromagnetic Code - Basic Scattering Code)

NEC-BSC is the code for the electromagnetic analysis of the radiation from antennas, in the presence of complex scattering structures at high frequency. Simulation of the scattering structures is accomplished by using combinations of perfectly conducting multiple flat plates, finite elliptic cylinders, composite cone frustums, and finite composite ellipsoids.

The code also has a limited finite thin dielectric slab capability. This dielectric capability can be used as an isolated thin slab which can simulate composite material, an absorber-coated ground plane or a radome, etc. Software is developed by The ElectroScience Lab of Ohio State University, and is based on UTD (uniform geometrical theory of diffraction, also referred to as the modern geometrical theory of diffraction.)

2.3.2 Numerical Electromagnetic Code (NEC)

NEC is one of the most popular numerical electromagnetic codes in the world. It was first introduced to the world by Lawrence Livermore Laboratory in 1970's. This code is written based on the theory of MFIE (magnetic field integral equation) and its numerical solutions are implemented with the MOM (method of moments). It simulates the antenna and scattering objects via wire-grid modeling or surface-patch modeling, however, surface-modeling is not recommended by the author when using in the far-zone case. The newer version of NEC may have a better and more sophisticated implementation to solve this issue.

2.3.3 MININEC

MININEC was written, compiled and brought to the world by John Rockway. The code was originally written in BASIC language and now has been transited to Fortran language. MININEC is believed to be the striped-down version of NEC, designed especially for slow personal computers in the 1980's. Just like NEC, MININEC is based on the theory of MFIE. The most current version of MININEC adopted the triangular basis function for its numerical solution and results in greater accuracy. Many ham radio users and amateur antenna designers still use it today.

2.3.4 Electromagnetic Surface Patch Code (ESP)

ESP is developed by The ElectroScience Lab of Ohio State University. ESP is based upon the piecewise sinusoidal reaction formulation (basically equivalent to the EFIE, electric field integral equation) for wires and surfaces. It allows users to model the scattering surface by using piecewise sinusoidal (PWS) rectangular patches.

This surface-patch modeling code has the following advantages over the wire-grid modeling code:

- (1) Fewer modes per square wavelength of surface area are required. Larger surface can be modeled by using fewer surface patches if the target surface is simple enough.
- (2) The results are not so dependent upon the specific grid geometry used.
- (3) Surface patch model gives a more accurate approximation of the currents on a surface. Currents are correctly presented through the use of vector expression.

Since the ESP code is implemented according to the theory of EFIE, unlike NEC, the surface object it models does not need to be a closed surface.

2.3.5 Triangular Surface Patch Code

Triangular surface patch code is very similar to ESP. The major difference between triangular surface patch code and ESP is that, the former allows users to use triangular patches to model the surface object instead of piecewise rectangular patches. The original idea was brought out mainly by Rao [24].

2.3.6 General Electromagnetic Model for the Analysis of Complex Systems (GEMACS)

GEMACS can be used to model complex scattering geometry. It employs GTD and MOM as its theoretic base. The capabilities of this code include performing simulations in the presence of some specific weather situations such as cloud water, rainwater, cloud ice, and snow. However, GEMACS's installation involves many complicated procedures and readings. This disadvantage may intimidate many potential users.

Chapter 3

Derivation of Equations

One of the well-known numerical solutions for analyzing electromagnetic problems is NEC, which is short for Numerical Electromagnetics Code. This computer code combines an integral equation for smooth surfaces with one for wire modeling to provide a convenient and accurate modeling of any structure. It's built by using the numerical solution of the integral equation (IE) for the currents induced on the structure by sources or incident fields. In Electromagnetic theory, NEC employs an integral equation (IE) to accomplish the analysis. In order to apply the code to the computer simulation, NEC also employs the method of moments (MOM). Before starting to prove the validity of applying NEC to our helibowl case, it is necessary to take a brief look at the theorem of IE and MOM.

This computer code, NEC-2, has successfully applied the numerical solution of the integral equation for induced currents (i.e., MFIE or EFIE) to solve many of the antenna problems. In this chapter, the theory of the Integral Equation will be described briefly. In addition, the theorem of Method of Moments (MOM) will be described and will explain how NEC-2 analysis can be accomplished by using these numerical solutions.

3.1 Integral Equation (IE)

3.1.1 Introduction to integral equation (IE)

The integral equation technique (IE) casts the solution for the induced current in the form of an integral equation where the unknown induced current density is part of the integrand. By applying computer techniques such as the method of moments (MOM), the integral equation can be solved for the induced current density. To proceed, the total induced current density found here will be used to find out what the scattering electric field and magnetic field of the conducting object are.

It is worth noting that there are many other methods other than the IE (for example, Geometrical Optics, Physical Optics, Modal Solutions and Geometrical Theory of Diffraction (GTD)) to help antenna designers calculate the fields scattered by arbitrary objects. However, those methods mentioned above are not as accurate as IE. They may provide excellent calculation for the problem of a simple conducting plane or edge

problem, but they are not suitable to analyze the helibowl, which combines a helical antenna and a bowl-shaped reflector. In order to derive more accurate representations of the fields, the IE is the best choice.

3.1.2 Derivation of Integral Equations (IE)

Two of the most popular forms of the integral equation (IE) for time-harmonic electromagnetics are the electric field integral equation (EFIE) and the magnetic field integral equation (MFIE). Both approaches (MFIE and EFIE) take advantage of one special situation, that is, the boundary conditions. In order to employ the boundary conditions, we start our observation point on the target conducting surface, then move on to deal with the boundary conditions problem. In addition, it is important to note that the EFIE enforces the boundary conditions on the tangential electric field and MFIE enforces the boundary conditions on the tangential components of the magnetic field.

In the EFIE case:

The total tangential electric field on the conducting surface ($r = r_s$) is equal to zero. So, we have:

$$E_t^{total} = E_t^s(r = r_s) + E_t^i(r = r_s) = 0 \quad (3.1.1)$$

Where,

E_t^{total} : Total tangential electric field on the conducting surface.

E_t^s : Scattered electric field radiated by the induced current density J_s .

E_t^i : Tangential component of the incident electric field due to a source located anywhere on or outside the conducting body.

Similarly, in the MFIE case:

The free surface currents, $J_s(r = r_s)$, do not exist on a normal conducting surface where the conductivity is finite. Therefore, we have:

$$J_s(r = r_s) = \hat{n} \times H^{total}(r = r_s) = \hat{n} \times [H^i(r = r_s) + H^s(r = r_s)] = 0 \quad (3.1.2)$$

where,

H^{total} : Total magnetic field on the conducting surface.

\hat{n} : Unit normal vector which is perpendicular to the conducting surface

H^s : Scattered magnetic field radiated by the induced current density J_s .

H^i : Incident magnetic field due to a source located anywhere on or outside the conducting body.

Now, let us use a simple example to help us understand integral equation (IE). Please refer to Fig 3.1.1. The figure shows the geometry of a line source above a two-dimensional finite width strip.

Example 3.1 (illustrated in Figure 3.1.1):

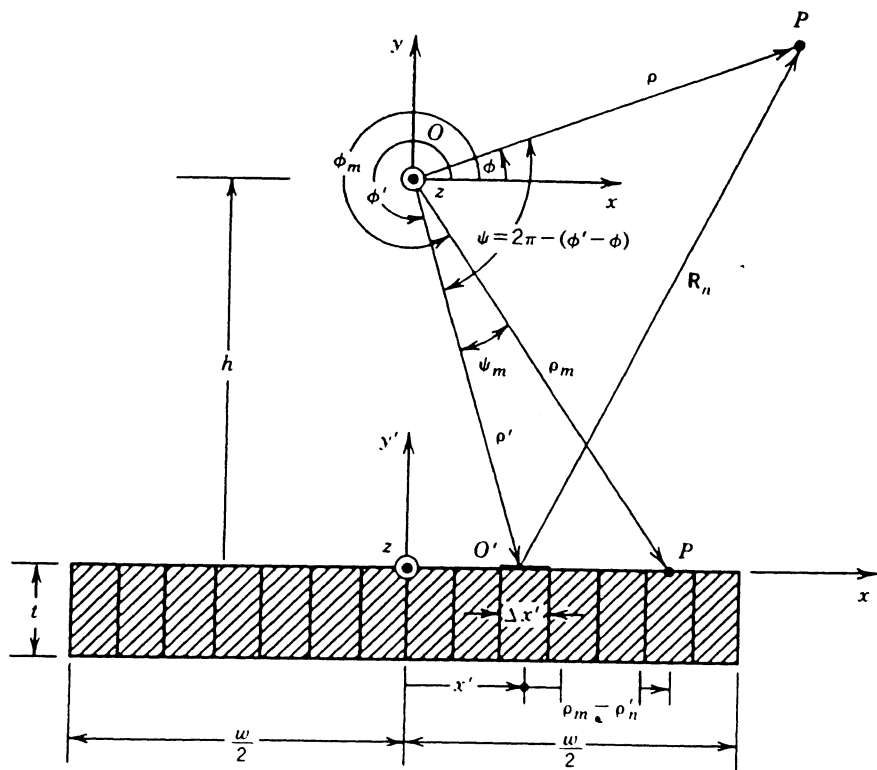


Figure 3.1.1 - Geometry of a line source above a two-dimensional finite width strip
 (Illustration drawn from: Balanis, C.A., Advanced Engineering
 Electromagnetics, Wiley, New York, 1989, p. 678)

Referring to Figure 3.1.1, the electric field, $E_t^i(\rho)$, generated by a line source with a constant current, I_z , is:

$$E_t^i(\rho) = -\frac{\beta^2}{4\omega\epsilon} I_z H_0^{(2)}(\beta\rho) \quad (3.1.3)$$

where,

$H_0^{(2)}$: The Hankel function of the second kind of order zero.

ω : Angular frequency.

β : Phase constant (rad/m).

ϵ : Permittivity of the finite width strip.

Part of the field, $E_t^i(\rho)$, is directed to the strip and induces on it a linear current density,

J_z , that:

$$J_z(x')\Delta x' = \Delta I_z(x') \quad (3.1.4)$$

If we let $\Delta x' \rightarrow 0$, Equation (3.1.4) can be written as:

$$J_z(x')dx' = dI_z(x') \quad (3.1.5)$$

The scattering field, $E_t^s(\rho)$, generated by the induced current density, J_z , now can be written as:

$$\begin{aligned} E_t^s(\rho) &= -\frac{\beta^2}{4\omega\epsilon} \left(\sum_{n=1}^N \Delta I_z(x'_n) \right) H_0^{(2)}(\beta|\rho - \rho'|) \\ &= -\frac{\beta^2}{4\omega\epsilon} \sum_{n=1}^N H_0^{(2)}(\beta|\rho - \rho'|) J_z(x'_n) \Delta x'_n \\ &= -\frac{\beta^2}{4\omega\epsilon} \int_{-w/2}^{w/2} H_0^{(2)}(\beta|\rho - \rho'|) J_z(x') dx' \end{aligned} \quad (3.1.6)$$

Now we choose an observation point on the conducting surface (i.e., $\rho = \rho_m$). We have tangential total electric field equal to zero.

$$E_t^{total}(\rho_m) = 0 \Rightarrow E_t^i(\rho_m) + E_t^s(\rho_m) = 0 \quad (3.1.7)$$

So,

$$-\frac{\beta^2 I_z}{4\omega\epsilon} H_0^{(2)}(\beta\rho_m) = \frac{\beta^2}{4\omega\epsilon} \int_{-\omega/2}^{\omega/2} J_z(x') H_0^{(2)}(\beta|\rho_m - \rho|) dx' \quad (3.1.8)$$

Therefore, the EFIE expression for this example is:

$$H_0^{(2)}(\beta\rho_m) = - \int_{-\omega/2}^{\omega/2} J_z(x') H_0^{(2)}(\beta|\rho_m - \rho|) dx' \quad (3.1.9)$$

We can now calculate the induced current density $J_z(x')$ by applying the moment method and then have those electric fields. For more details about the integral equation (IE), please refer to [12].

3.2 Theorem of the Method of Moments (MOM)

3.2.1 Introduction to Method of Moments (MOM)

Now the electric field integral equation (EFIE) presentation from Example 3.1 is given by equation (3.1.9). The next target is to find out what the induced current density, $J_z(x')$, is. However, the above equation (3.1.9) is rather difficult to solve by hand. A closed-form solution of equation (3.1.9) will not be obtained without considerable effort. This is

why analytical techniques such as the method of moments (MOM) have to be employed to determine approximate solutions.

The method of moments (Harrington, 1968) [13], which was extended to include electromagnetic problems, is analytically simple but requires large amounts of computation. Essentially it reduces the associated integral equation to a system of linear algebraic equations in N unknowns where the N unknowns are usually coefficients of some appropriate expansion of the value to be determined. In radiation problems, the value mentioned above usually refers to the induced current on the surface of the conducting object [14]. However, with the rapid development of computing machines, the problem of requiring large amounts of computation stated above can be solved. Therefore, it becomes more and more applicable.

To interpret the application of the Method of Moments, the theory of MOM will be explained in pure math in Section 3.2.2.

3.2.2 Derivation of Method of Moments (MOM)

Here, the method of moments is presented. First let,

f : Unknown function to be determined

L : Linear operator

g : Known (given) forcing function

$$\text{and } L(f) = g \quad (3.2.1)$$

Further, let,

$$f = \sum_{j=1}^N \alpha_j f_j \quad (3.2.2)$$

Where

f_j : The j^{th} known expansion functions or basis function

α_j : Expansion Coefficient of f_j functions

[Note]: When the number N increases, the approximation of function, f , will increase also.

Now we substitute function, f , in Equation (3.2.1) with Equation (3.2.2):

$$L(f) = L\left(\sum_{j=1}^N \alpha_j f_j\right) = g \quad (3.2.3)$$

Since L is a linear operator, we have:

$$L\left(\sum_{j=1}^N \alpha_j f_j\right) = \sum_{j=1}^N \alpha_j L(f_j) \quad (3.2.4)$$

So,

$$\sum_{j=1}^N \alpha_j L(f_j) = g \quad (3.2.5)$$

Take the inner product of both sides of Equation (3.2.5) with w_m , the so-called testing or weighting function. Substitute Equation (3.2.5) to Equation (3.2.6):

$$\langle w_m, \sum_{j=1}^N \alpha_j L(f_j) \rangle = \langle w_m, g \rangle \quad (3.2.6)$$

Then,

$$\sum_{j=1}^N \alpha_j \langle w_m, L(f_j) \rangle = \langle w_m, g \rangle \quad (3.2.7)$$

Now, simplify the calculation in Equation (3.2.7) by letting w_m equal to a Dirac delta function. Equation (3.2.7) is reduced to a system of linear algebraic equations in N unknowns and can be written as:

$$[\langle w_m, L(f_j) \rangle][\alpha_j] = [g_m] \quad (3.2.8)$$

Further, we let:

$$[l_{mj}] = [\langle w_m, L(f_j) \rangle] \quad (3.2.9)$$

Equation (3.2.8) can be reduced to:

$$[l_{mj}][\alpha_j] = [g_m] \quad (3.2.10)$$

Hence, α_j can be determined by:

$$[\alpha_j] = [l_{mj}]^{-1}[g_m] \quad (3.2.11)$$

Therefore, we have our answer:

$$[f] = [f_j][\alpha_j] \quad (3.2.12)$$

That is,

$$f = \alpha_1 f_1 + \alpha_2 f_2 + \alpha_3 f_3 + \dots + \alpha_N f_N \quad (3.2.13)$$

Now, the unknown function, f , is determined. However, there is still a problem in calculating the value at a specific point. This calculation could turn out to be tedious and computationally expensive if the basis functions are chosen randomly. Sometimes, in

order to reduce the complexity of calculation, the pulse functions or the triangle pulse functions are used as the basis function of the unknown function. Therefore:

$$f = \alpha_1 \delta(S - S_1) + \alpha_2 \delta(S - S_2) + \alpha_3 \delta(S - S_3) + \dots + \alpha_N \delta(S - S_N) \quad (3.2.14)$$

This is called the point-matching method. The value of f at a certain point S_m ($m=1,2,\dots,N$) is α_m , the coefficient of the m^{th} expansion function.

Chapter 4

Validation on the 1/4 - Wavelength Monopole above a Conducting Plane

Before modeling the helibowl, it is prudent to use the electromagnetic code to model an antenna with known properties. Two sets of antennas of different types with known experimental data were modeled. In this chapter, the testing models were two 1/4-wavelength monopole antennas placed above a square or circular conducting plane. The data for validation will be based on the published data found in [15]. The simulation result will be compared with the experimental (measured) data to make sure that the simulation is correct. Then it will be possible to move on to analyze the helibowl antenna in chapter 5.

One thing worth noting is that, in the real world, short monopoles are used which are buried inside the horn antennas as the detectors to probe the strength of the fields. By putting the detector horizontally or vertically, they can measure the horizontal or vertical

electric field. They don't measure the total electric field directly. The NEC-2 program also shows only two split electric fields. However, in this chapter, the reference data is shown in the form of the total field. For the work here, a program was written to help convert two split fields obtained from our simulation into one total field. These conversion programs can be found in Appendix B, as well as some visualization tools used to display the rectangular and polar patterns of fields. The programs were written in Matlab. The conversion program to convert two fields into one is based on the following calculations.

First, let:

\vec{E}_h : Horizontal electric field

\vec{E}_v : Vertical electric field

θ_h : The phase of E_h

θ_v : The phase of E_v

Consider the vector operation, we have the total field (E_t):

$$\vec{E}_t = \vec{E}_h + \vec{E}_v \quad (4.1)$$

So, we have the magnitude of \vec{E}_t :

$$|\vec{E}_t| = |\vec{E}_h + \vec{E}_v| \quad (4.2)$$

$$\therefore |\vec{E}_t| = [(\vec{E}_h \cos(\theta_h) + \vec{E}_v \cos(\theta_v))^2 + (\vec{E}_h \sin(\theta_h) + \vec{E}_v \sin(\theta_v))^2]^{1/2} \quad (4.3)$$

It is now possible to convert NEC-2 output data to total field data. In the next chapter, results using the separated electric fields only will be given.

4.1 Measured Data

The measured data to be used here for the 1/4-wavelength monopoles above the conducting planes was done by C. A. Balanis in his book, Antenna Theory [15]. As shown in Figures 4.1.1 and 4.1.2, the two 1/4-wavelength monopoles are sitting above two conducting planes, one square and one circular. A voltage source is attached to the bottom end of each monopole. The length of each side of the square plane is two wavelengths long and the diameter of the circular plane is 4 feet long. The principal elevation plane amplitude patterns were measured when the antennas were operating at the frequency of 1 GHz.

Now consider the radiation patterns. Figures 4.1.1 and 4.1.2 also show the polar-form patterns for the two antennas. The simulation result obtained in Section 4.2 will be compared with these two patterns.

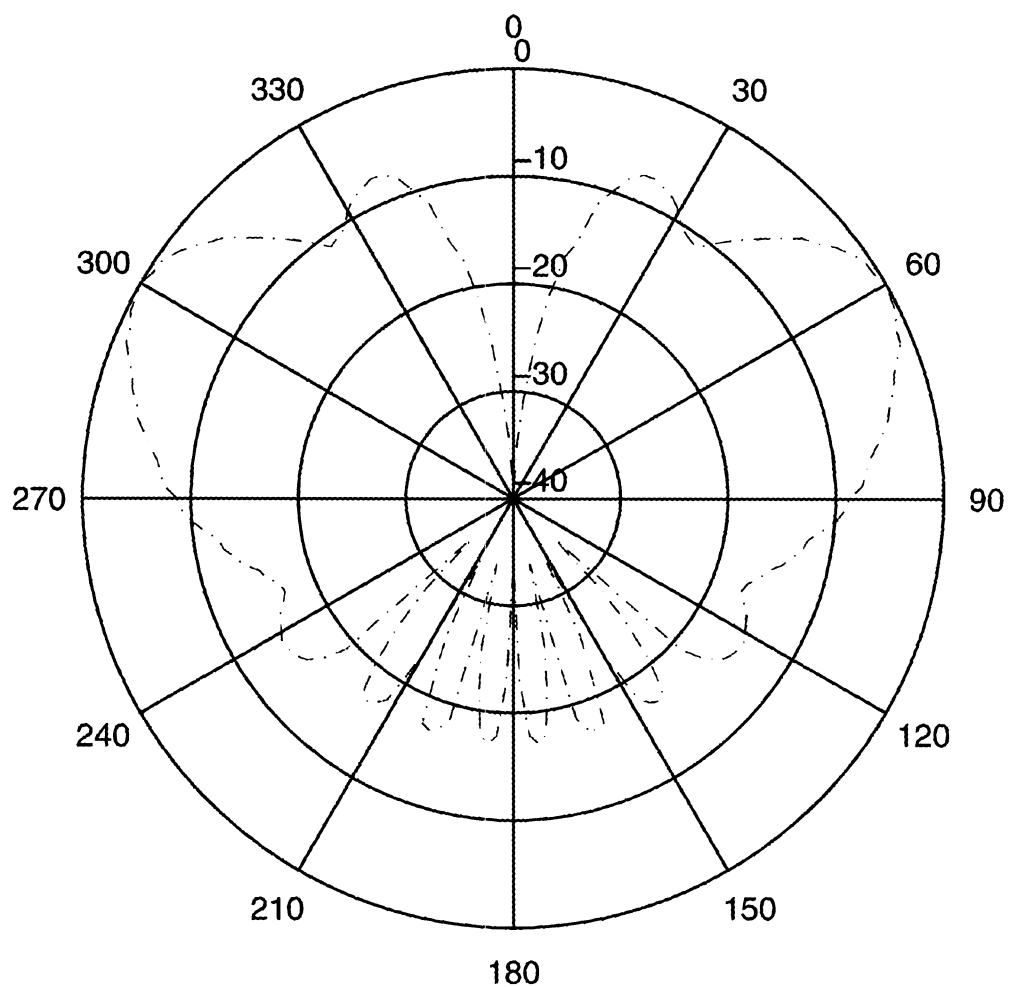


Figure 4.1.1 - Total radiation pattern of $\lambda/4$ monopole above a square ground plane.
(reference: Balanis, C.A., Antenna Theory: Analysis and Design, John Wiley & Sons, Inc., 1982, p. 519)

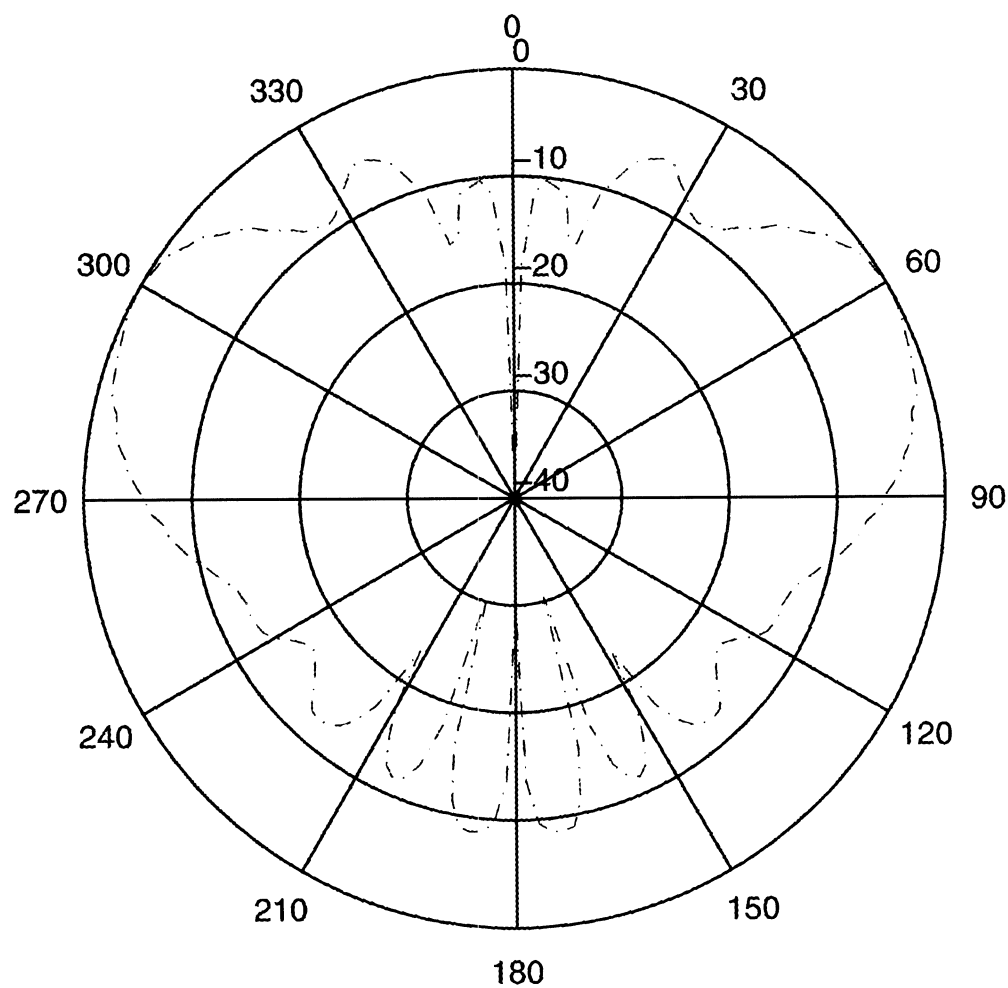


Figure 4.1.2 - Total radiation pattern of $\lambda/4$ monopole above a circular ground plane.
(reference: Balanis, C.A., Antenna Theory: Analysis and Design, John Wiley & Sons, Inc., 1982, p. 515)

4.2 Simulation Result

Through many options, wire-grid models were chosen to build the two 1/4-wavelength monopoles above conducting planes. Figure 4.2.1 and 4.2.2 show the frameworks of these wire-grid models.

Two NEC-2 input files were developed for NEC-2 to run. Arbitrary voltage sources were chosen since the power consumption or the quantity of the fields is not of interest. Instead, the relative amplitude of the fields is of greatest importance. Hence the arbitrary applied voltage sources with different quantity will not affect the observations. The Appendices B-1 and B-3 have the NEC-2 input files for each case. Figures 4.2.3 and 4.2.4 show the polar-form of our simulation result. The Appendices B-2 and B-4 show the computation details in numbers.

Another thing worth noting here is that, at $\theta = 0^\circ$ and 180° , the intensity of field of a monopole is actually equal to minus infinity ($-\infty$). Even though NEC-2 won't show the correct number due to the computing limitation, the number could still be very small. If a clamp to limit the minimum is not used, the pattern will be meaningless. For example, the pattern of the simulation result in this section will look like a circle with two cracks at $\theta = 0^\circ$ and 180° when no clamp is functioning. The rest of the nulls will be indistinguishable because those nulls have been flattened down. In order to compare the

simulation data with published data, a clamp is set at -40 dB. This helps compare the patterns.

Compared to Figures 4.1.1 and 4.1.2, the simulation data in Figures 4.2.3 and 4.2.4 does not exactly overlap the measured data, but the butterfly configuration is nearly identical. After the computation error was taken into account, this approach can be considered to be on the right track. Now, the helibowl antenna can be modeled.

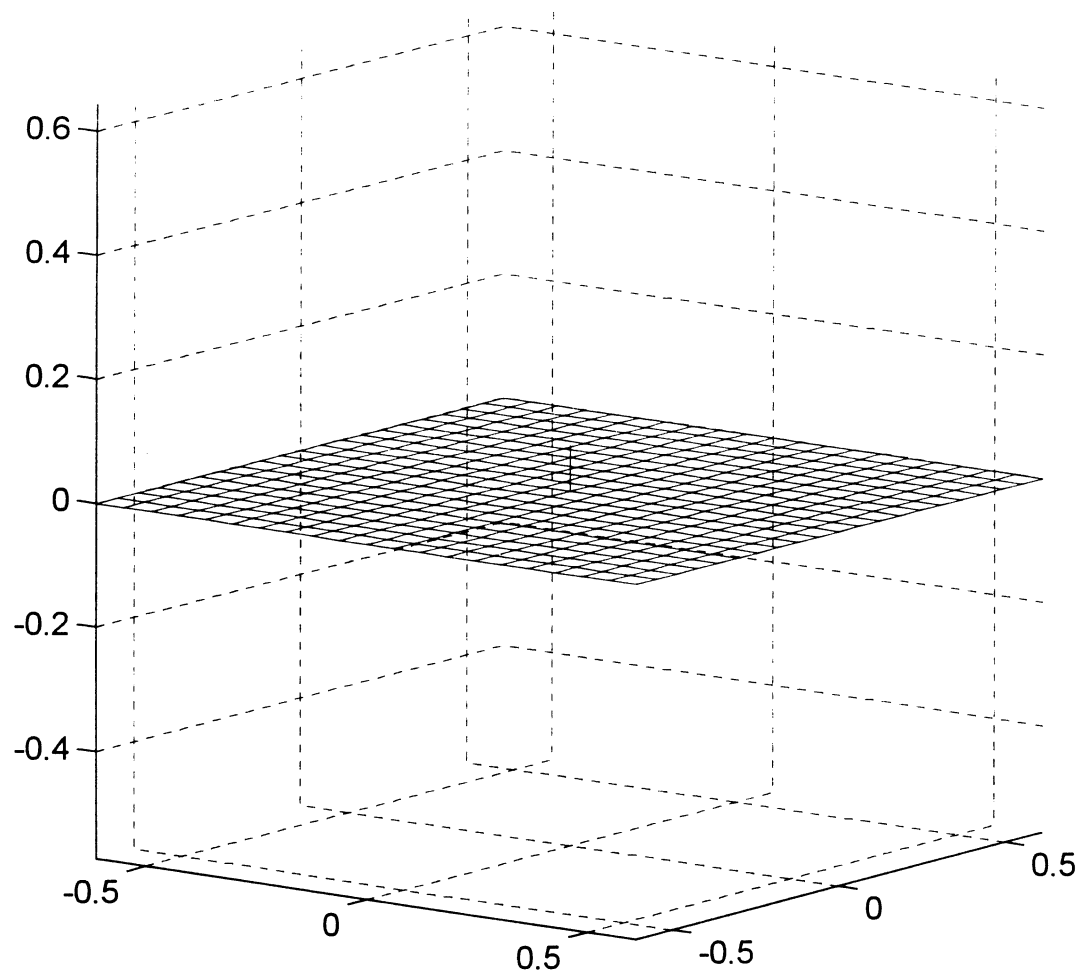


Figure 4.2.1 - Geometry of wire-grid model of the $\lambda/4$ monopole
above a square plane, frequency at 1 GHz

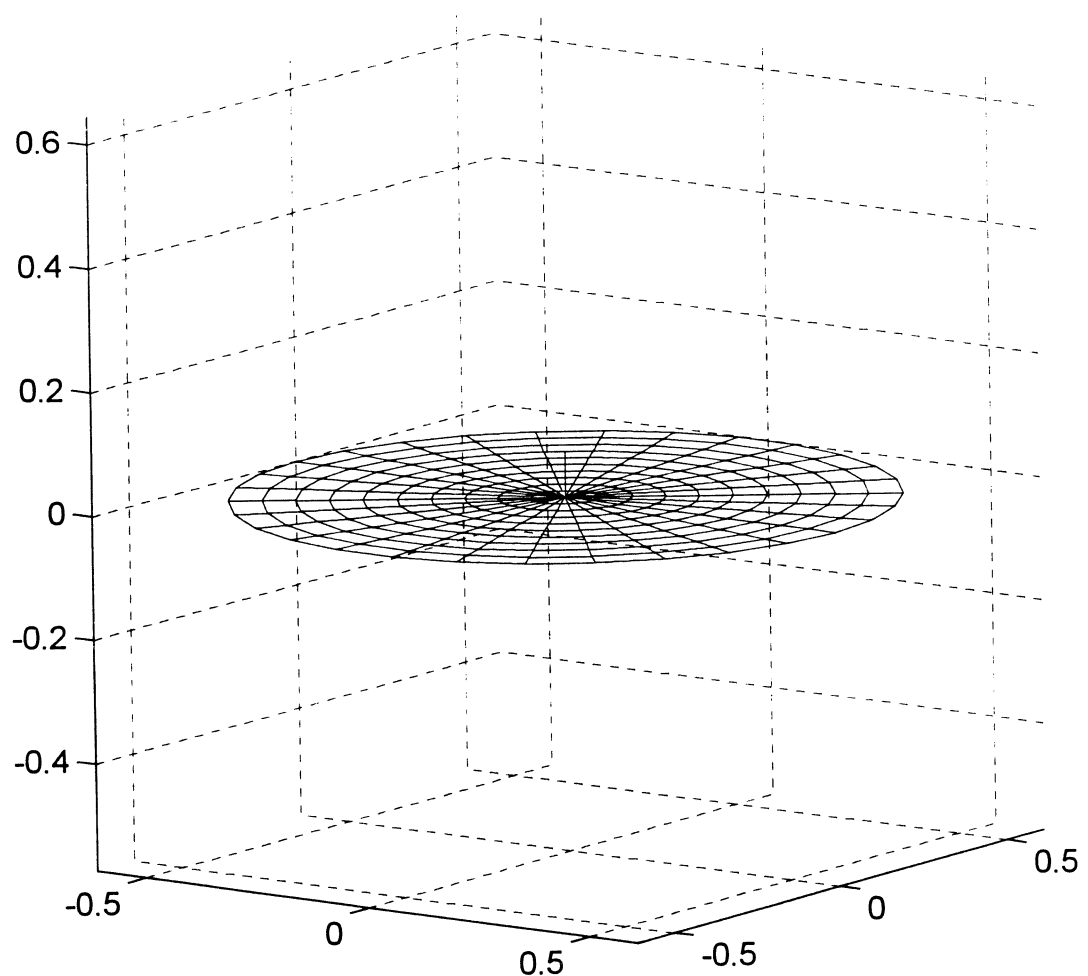


Figure 4.2.2 - Geometry of wire-grid model of the $\lambda/4$ monopole
above a circular plane, frequency at 1 GHz

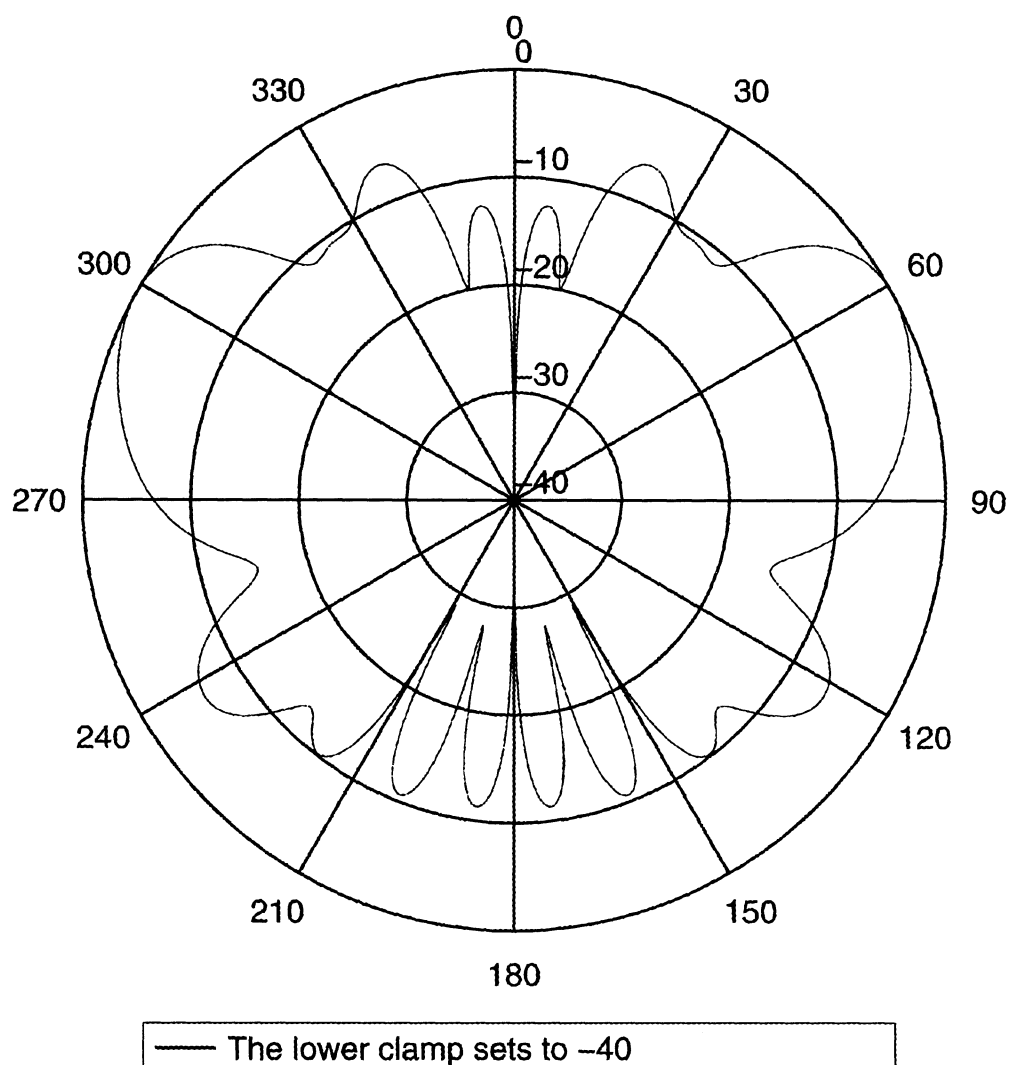


Figure 4.2.3 - Simulation result (total radiation pattern) for Figure 4.2.1

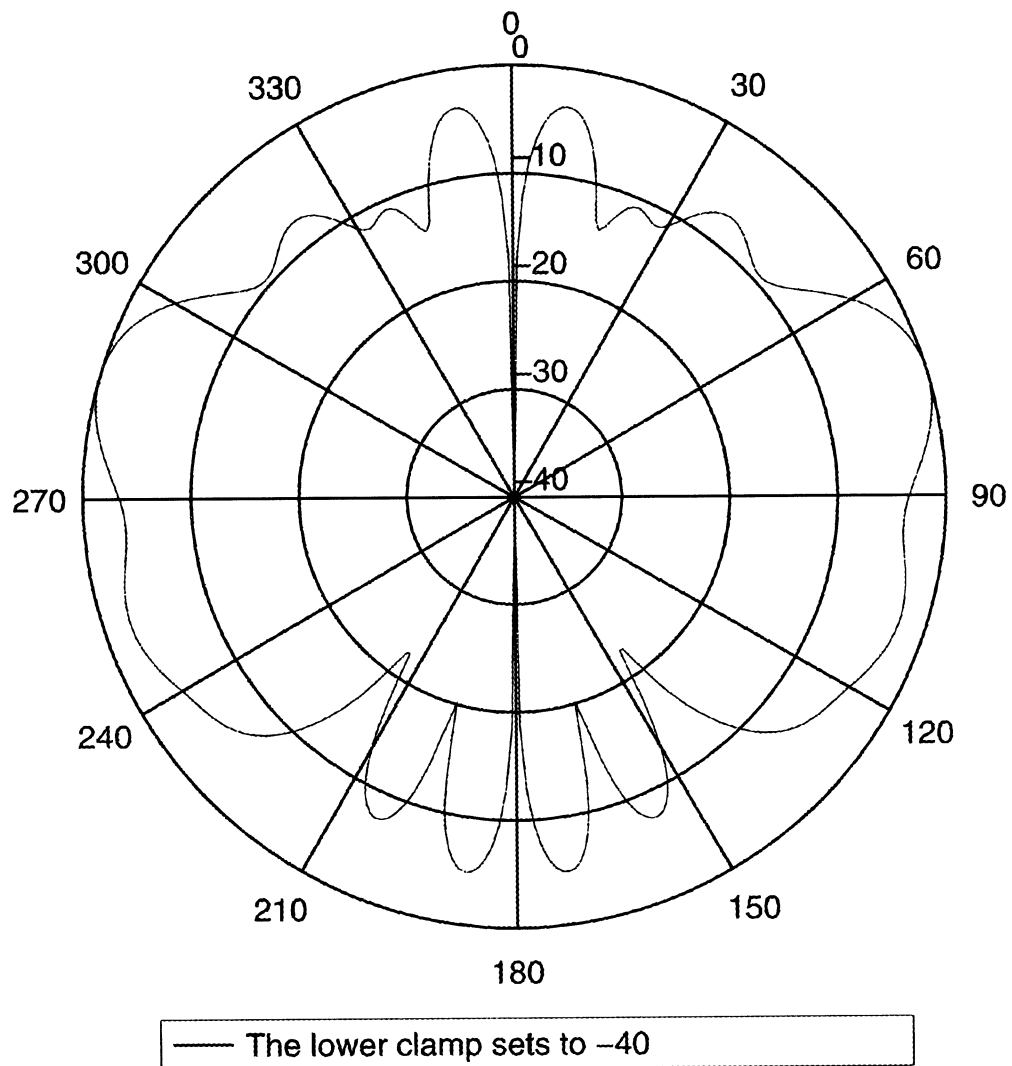


Figure 4.2.4 - Simulation result (total radiation pattern) for Figure 4.2.2

Chapter 5

Simulation on the Helibowl Antenna

In this chapter, the simulation procedure on the helibowl antenna will be described and discussed as well as the results obtained from the simulation. The primary goal is to develop a series of processes, which can be used to simulate any helibowl of any shape. Of course, the correctness of the approach is also an important factor. It will be discussed as well.

At the end of this chapter, two extensive simulations on two helibowls with different shapes will be performed. Brief discussion about the relationship between the helibowl's radiation patterns and right shapes will be made. A prediction on how to improve the performance of helibowls in order to meet the DGPS's requirements will be made, too.

5.1 Measured Data

The helibowl antenna was designed and built by Don Spitzmesser at JPL. The dB Systems Inc. has performed many experiments to collect information about the helibowl's radiation pattern. The data collected by dB Systems Inc. will be used as the basis from which to compare the simulation results.

The helibowl's geometric configuration and actual photos are shown in Figures 5.1.1 and 2.3.1 respectively. The helibowl consists of two major parts -- the aluminum bowl and the tapered-end helical antenna wound on an inverted cup. The helical antenna and the cup are placed in the middle of the bowl, but they do not touch the bowl. In the middle of the bowl, a hole was cut out to let one end of the helix go through the bowl to the other side. A voltage source will attach to that end of the helical antenna. The whole antenna setup included the helibowl; a 16½-inch wide, 1/4-inch thick circular plate; an overhead radome; four supporting rods; cables; bolts and nuts. It was placed on a stand about 20 feet high while the measurement was proceeding. The antenna was considered to be in free space. The probe (or detector) was a small dipole within a rectangular horn. Because the simulation interest falls in GPS bands, the frequency was set at 1,575 MHz (GPS L1 band).

According to the experimental result obtained at dB Systems Inc. in June 1997 [22], the helibowl's radiation patterns were measured at two different azimuth angles (ϕ), namely,

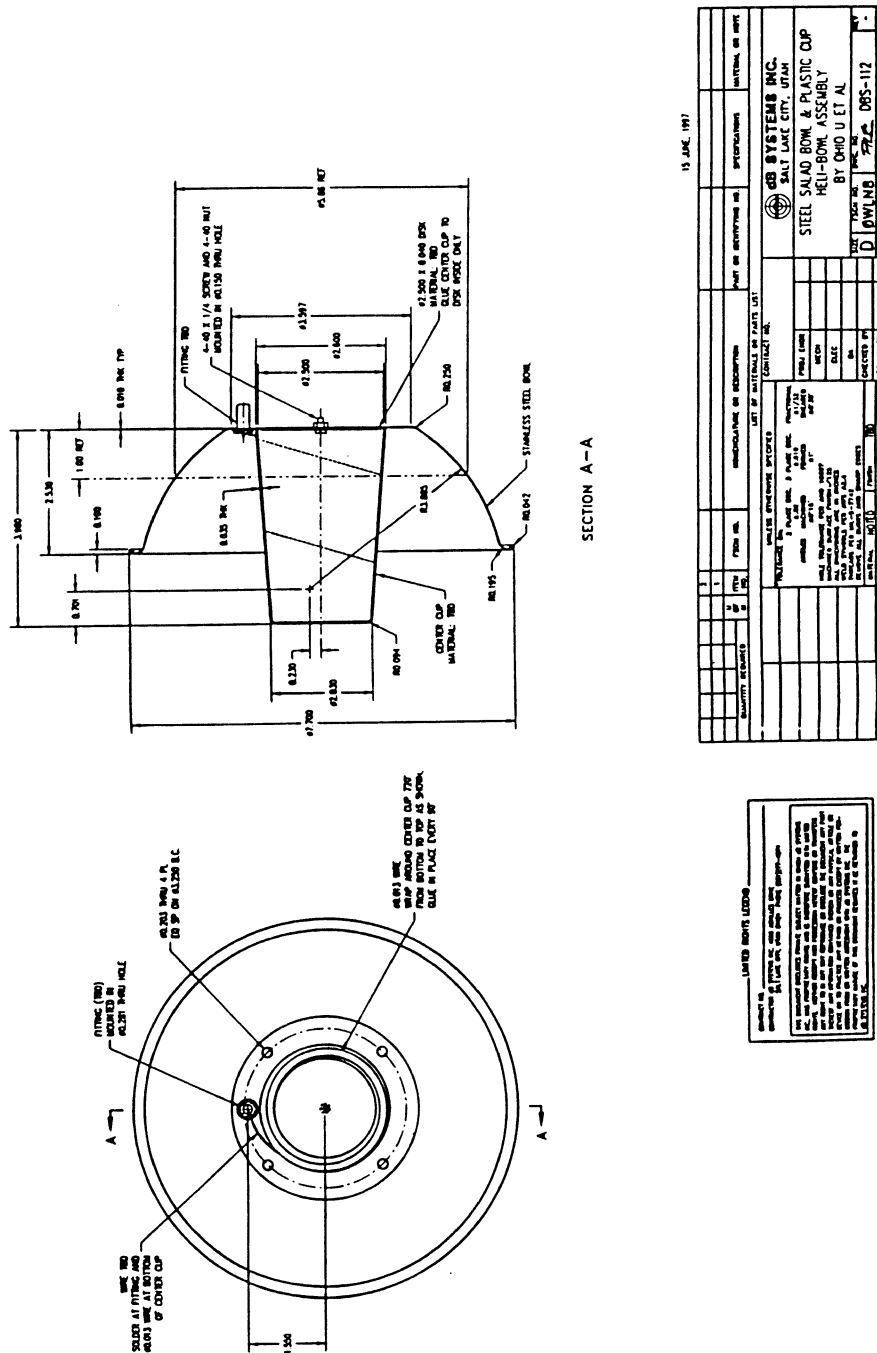


**Figure 5.1.1 - Helibowl antenna's geometric configuration
(Figure provided courtesy of dB Systems, Inc.)**

0 degree and 90 degrees. The reason why the experiment was done twice is simply because the helibowl antenna is not symmetrical. After the first measurement, the antenna had to be turned 90 degrees horizontally for the next measurement. At each angle, both the vertical polarization field and the horizontal polarization field were recorded. Now, consider Figures 5.1.3, 5.1.4, 5.1.5 and 5.1.6. They are the helibowl's radiation patterns, as measured by dB Systems.

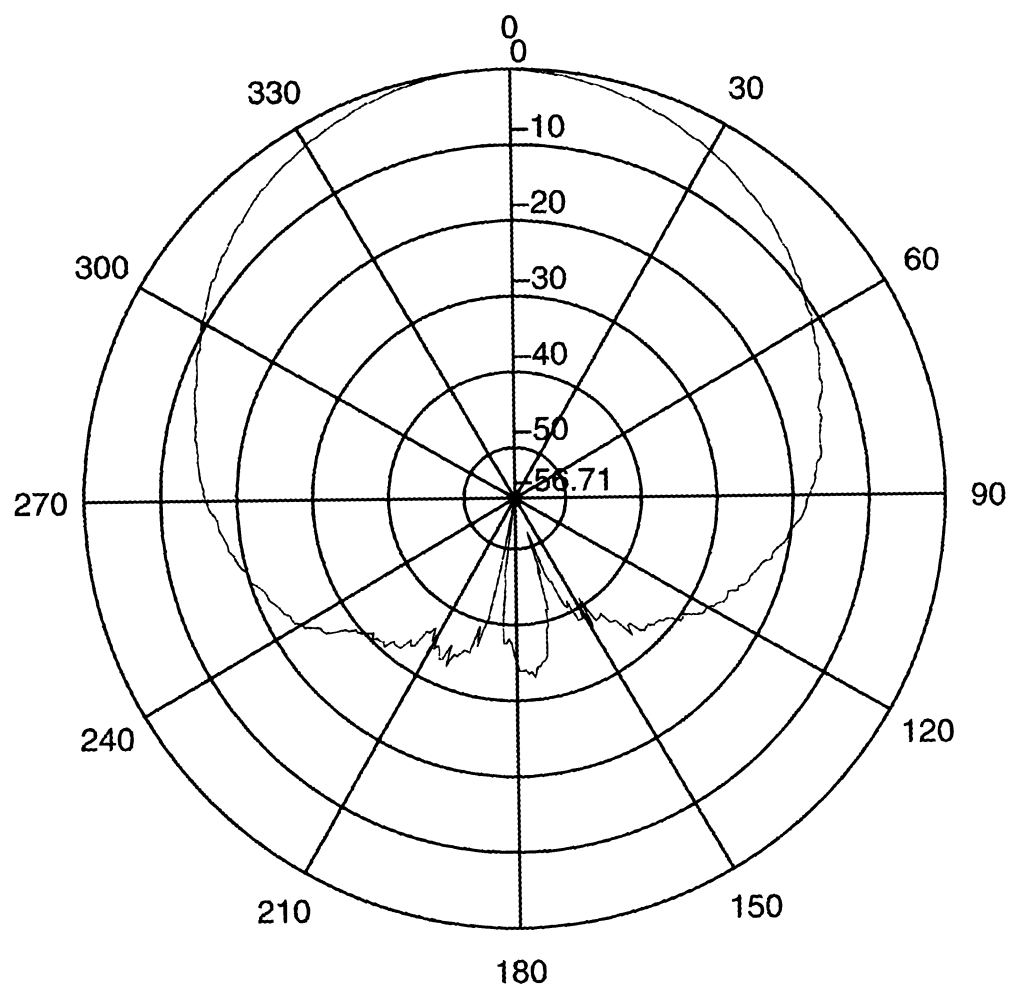


Figure 5.1.3a - Measured horizontal polarization pattern of the helibowl at azimuth angle $\phi = 0^\circ$

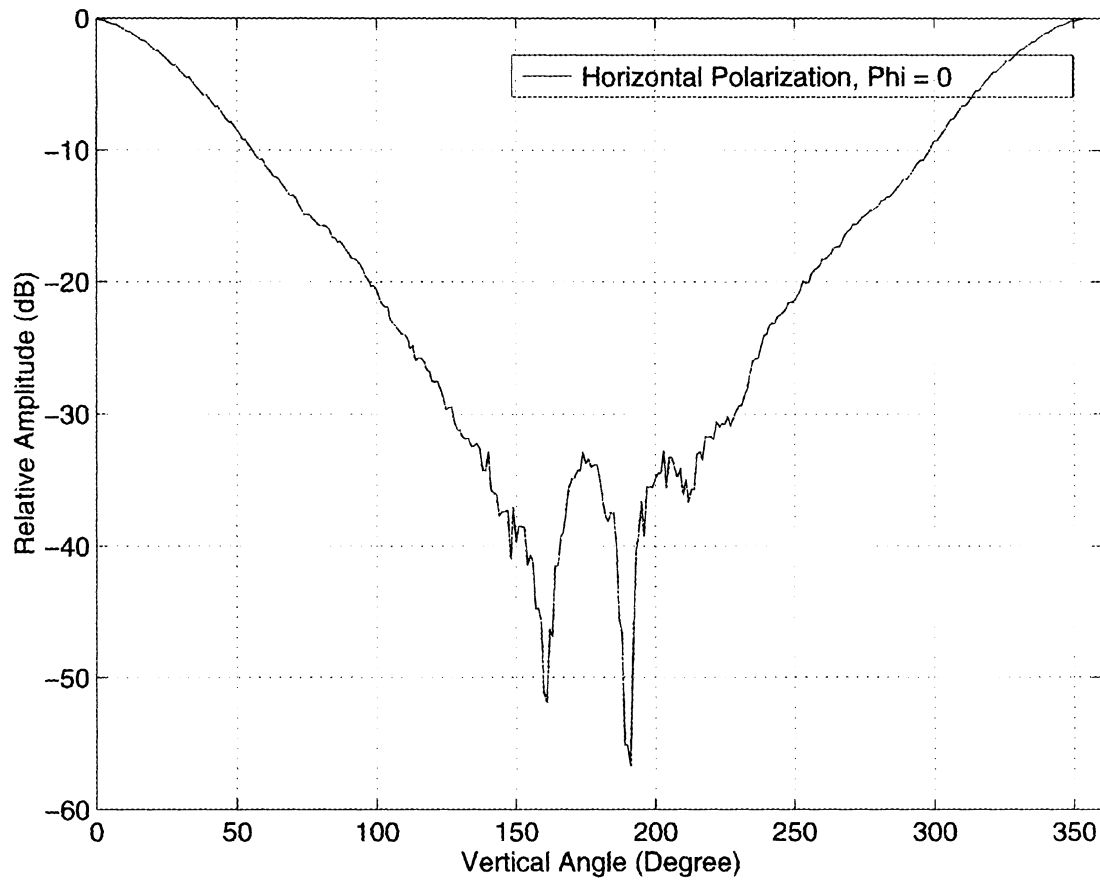


Figure 5.1.3b - Measured horizontal polarization pattern of the helibowl at azimuth angle $\phi = 0^\circ$

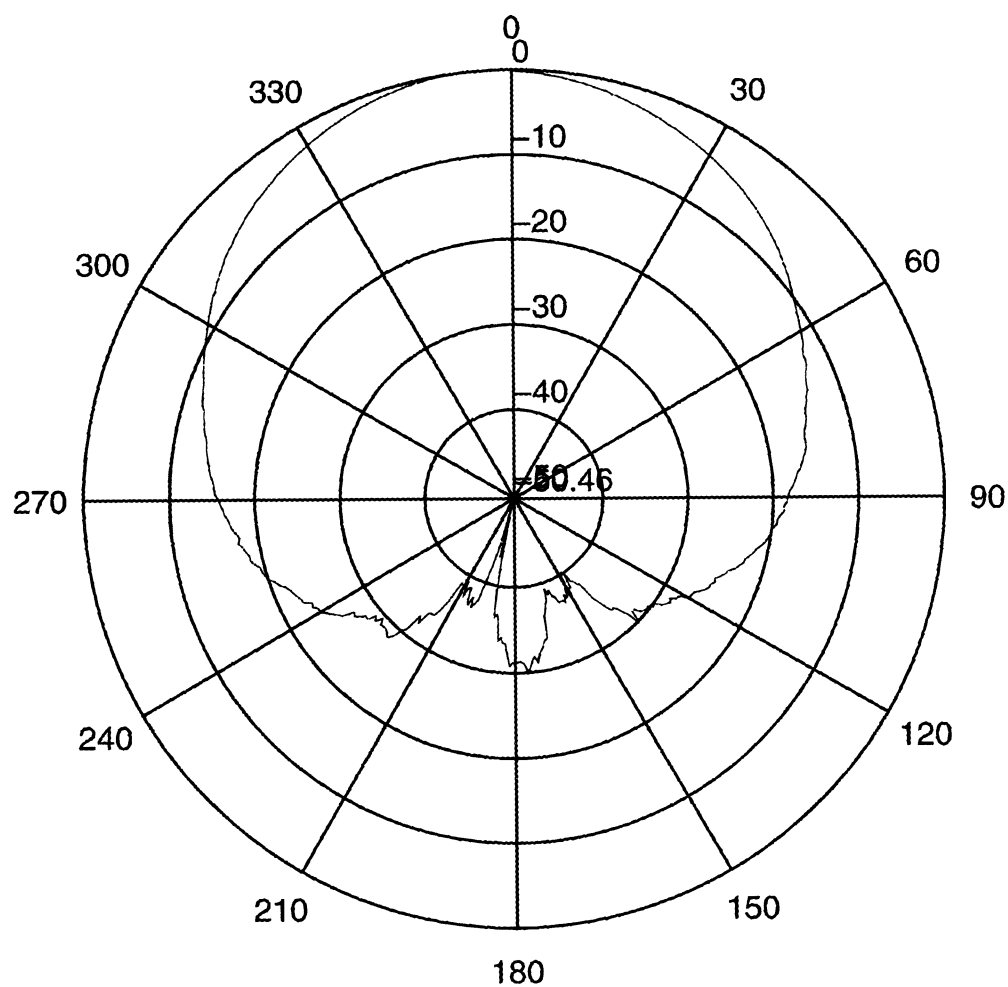


Figure 5.1.4a - Measured horizontal polarization pattern of the helibowl at azimuth angle $\phi = 90^\circ$

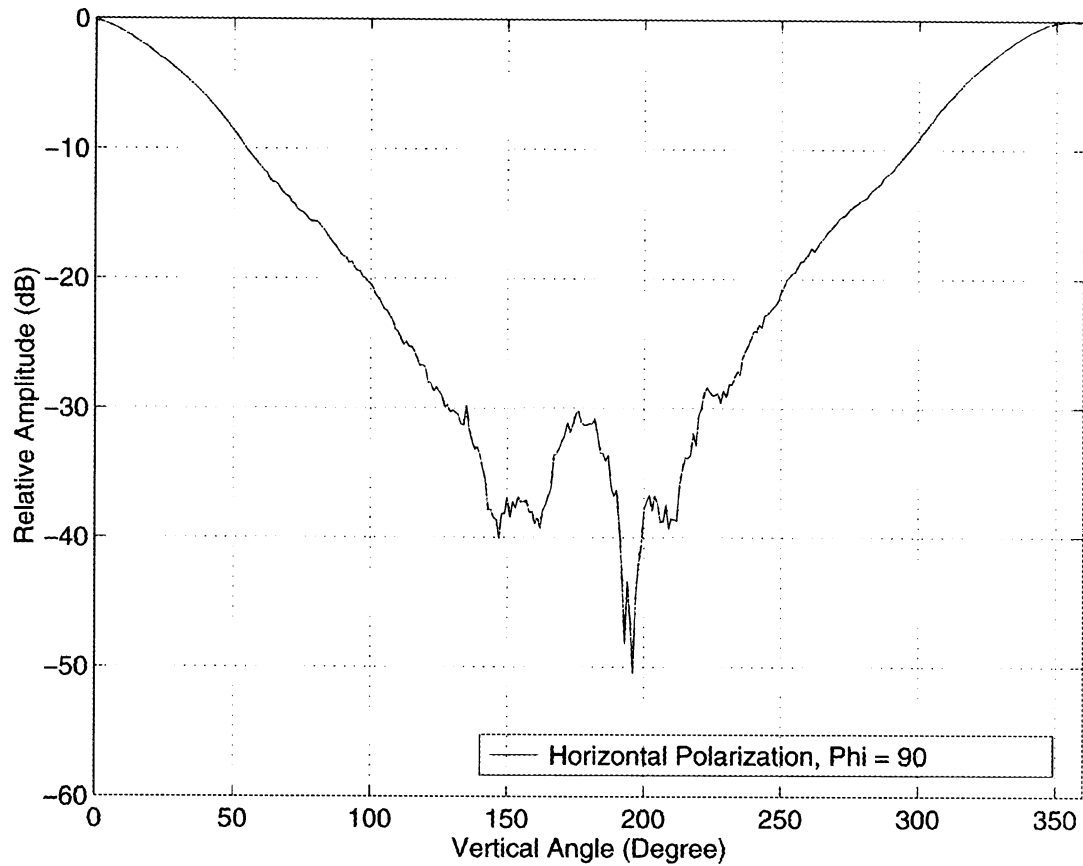


Figure 5.1.4b - Measured horizontal polarization pattern of the helibowl at azimuth angle $\phi = 90^\circ$

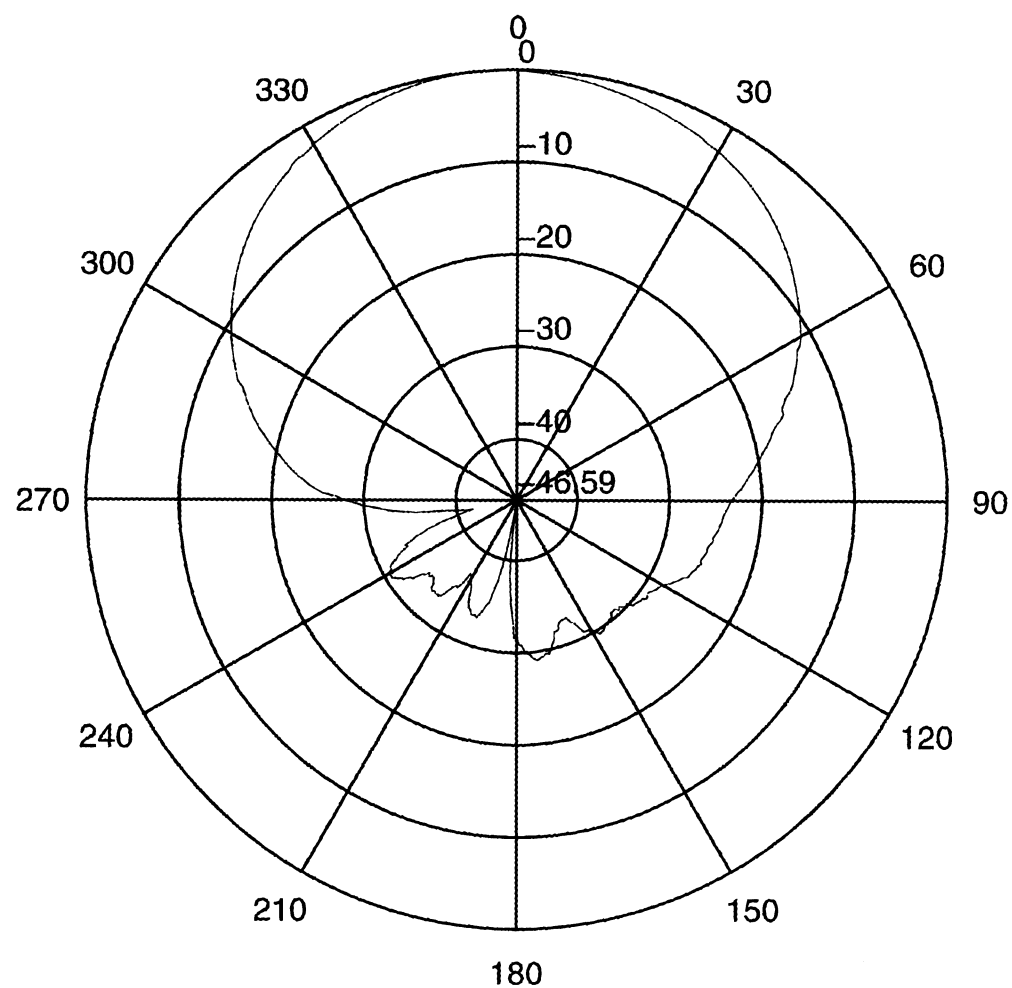


Figure 5.1.5a - Measured vertical polarization pattern of the helibowl at azimuth angle $\phi = 0^\circ$

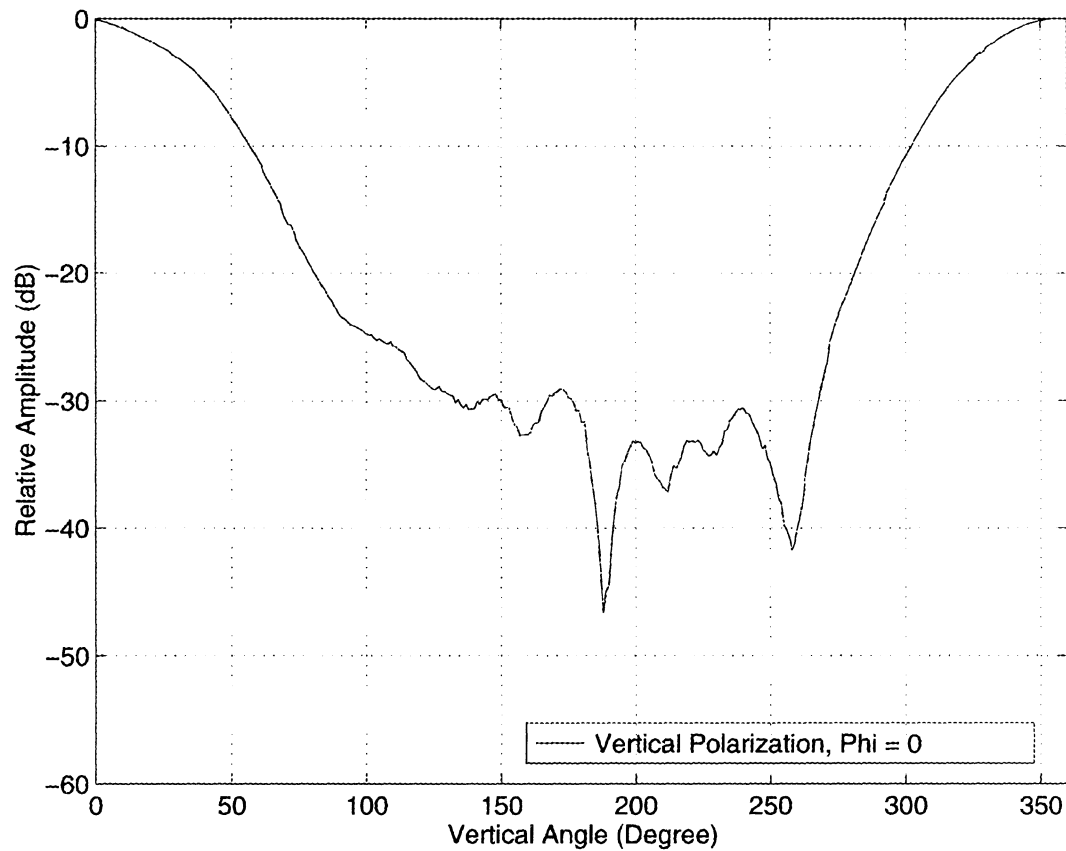


Figure 5.1.5b - Measured vertical polarization pattern of the helibowl at azimuth angle $\phi = 0^\circ$

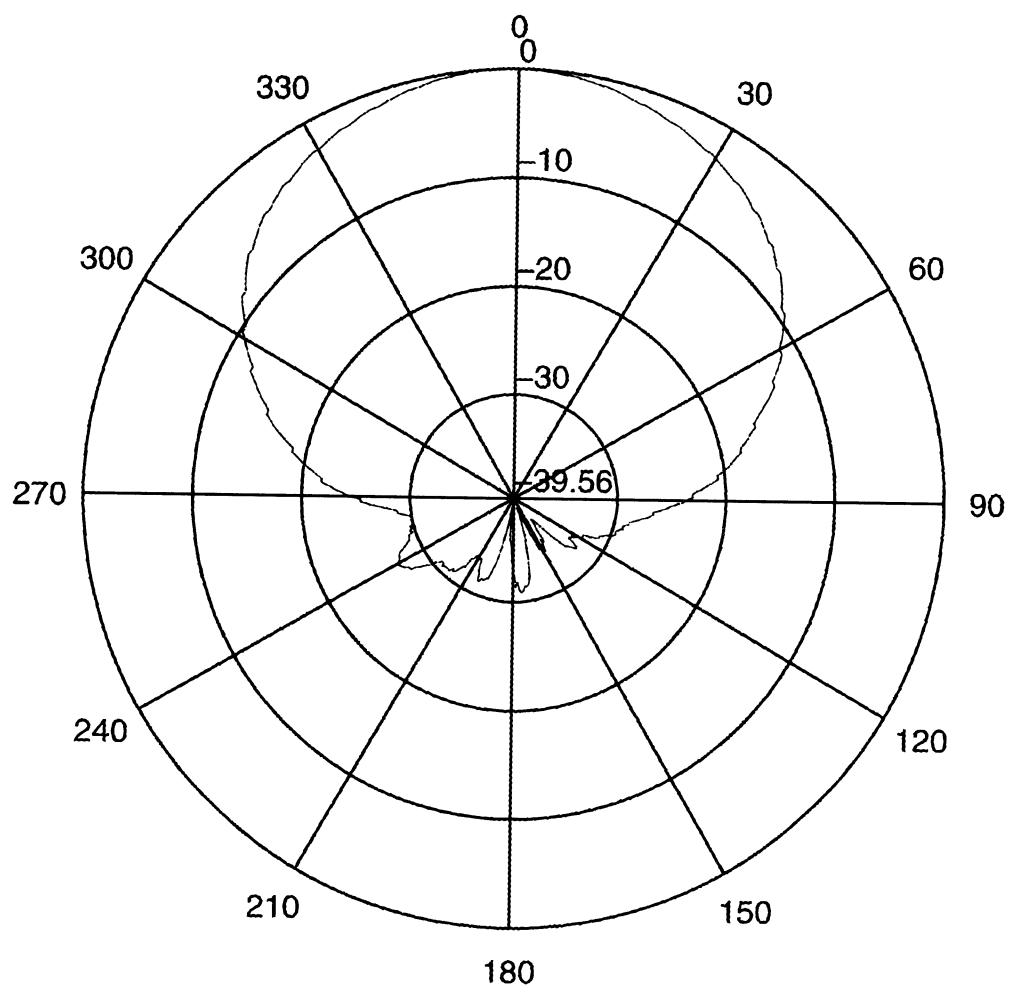


Figure 5.1.6a - Measured vertical polarization pattern of the helibowl at azimuth angle $\phi = 90^\circ$

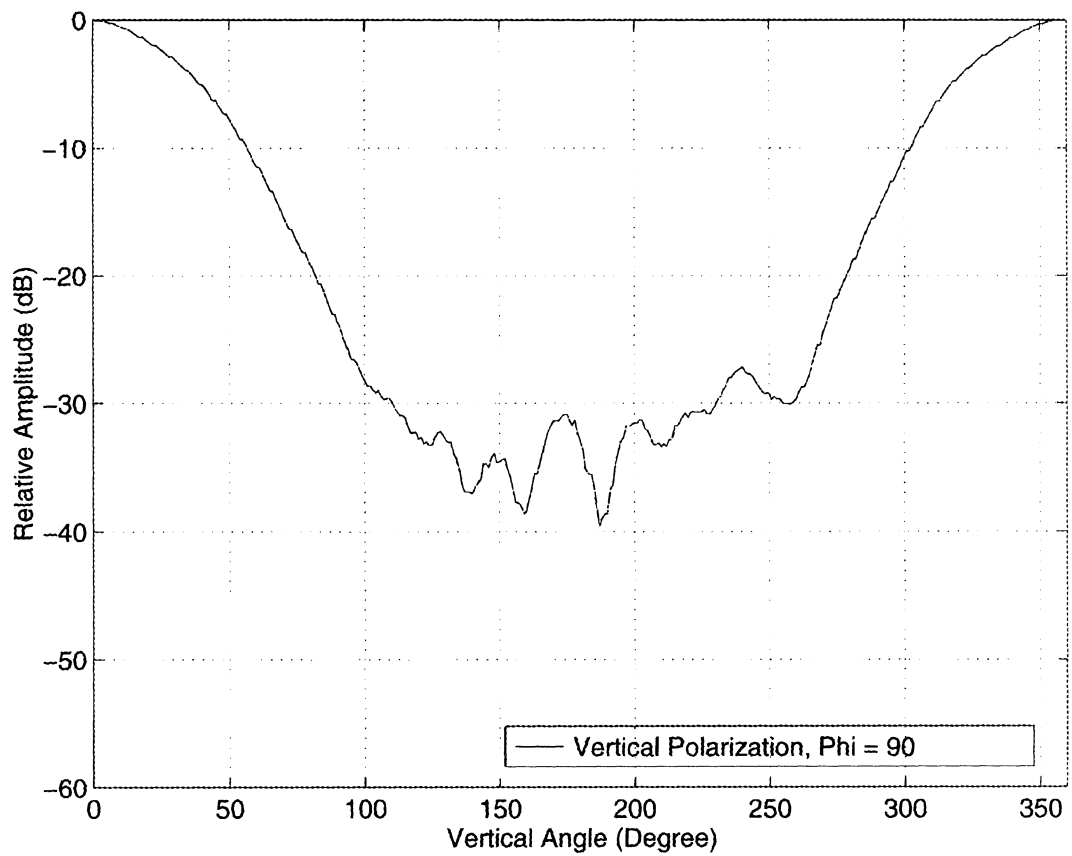


Figure 5.1.6b - Measured vertical polarization pattern of the helibowl at azimuth angle $\phi = 90^\circ$

As can be seen here, the pattern indicated that the helibowl has near perfect reception above ground. Below the horizon, the reception gain drops down to -30 dB. (See Appendix D for more information about the measured data.) One thing needs to be pointed out that the pattern will be almost the same with or without the radome. However, if the circular plate is removed away from the whole configuration, the results will vary. This will be discussed in more detail in Section 5.2.3.

5.2 Simulation Results

In other simple tests, the radome does not affect the simulation significantly. Actually, a good radome should be designed to be 'transparent' enough to the whole antenna system. Due to the NEC-2 program's limit number (1392 max.^{*}) of wire segments, the radome was not included in the simulation this time. Only a helibowl and a circular plate under the helibowl were put into the testing model.

The first model with simple wire helix didn't include the circular plate. In order to obtain better results, a ribbon-like, strip helix replaced the simple wire helix on the second model. The second model was even closer to the real helibowl, but it didn't yield any results than the first one. Its back-lobes were even larger than the first model. Therefore,

* After this research was completed, a PC version of NEC-2 which allows users to configure more wire segments into their models was found on the internet.

in the third model, a circular plate was introduced into the simulation. The last simulation of this chapter proved the circular plate plays an important role in the whole setup and cannot be neglected.

5.2.1 Model One: First One with Less Detail

This is the first model that had been created. The helical part was treated as a thin wire that, in fact, is a flat narrow ribbon. The circular plate was not included at this moment. The skeletal shape of the first model is indicated as in Figures 5.2.1a and 5.2.1b. Please pay special attention to the hole on the bottom of the bowl; the lower end of the helix goes through the hole without touching the bowl. The hole has to be small enough to prevent significant backside electromagnetic leakage from being introduced into the backlobes.

According to NEC-2 manual's guideline, the length of any wire segment has to fall between 0.1λ and 0.0001λ in order to reduce the error to acceptable range. The " λ " here denotes the wavelength. In the L1 Band (that is, 1,575 MHz), λ is equal to 0.1904 meters. Any of the segments we used to construct wire-grid model here has to be smaller than 0.01904 meters and larger than 0.0001904 meters. NEC-2 won't accept any wire segment that is larger than a wavelength.

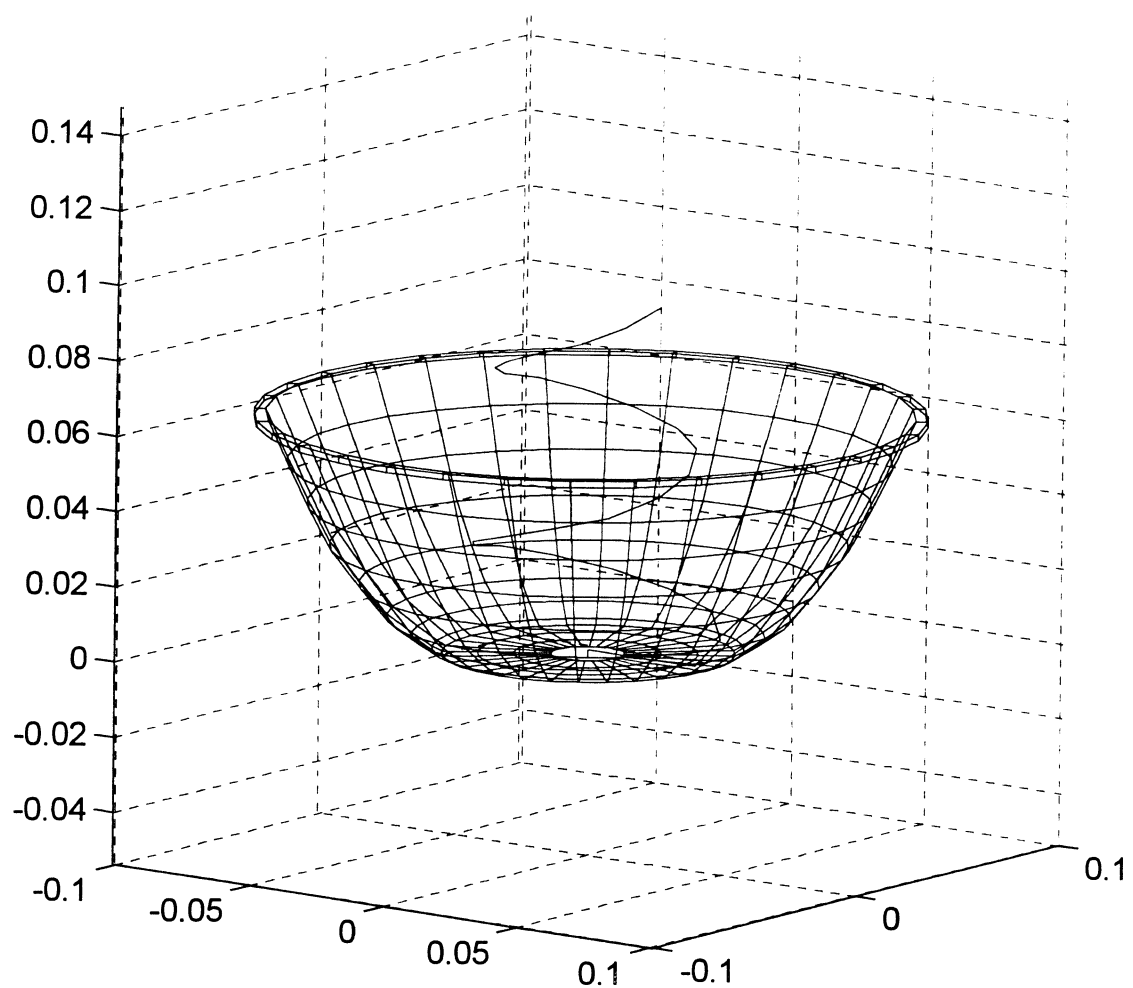


Figure 5.2.1a - Geometry of the wire-grid model for helibowl in Section 5.2.1

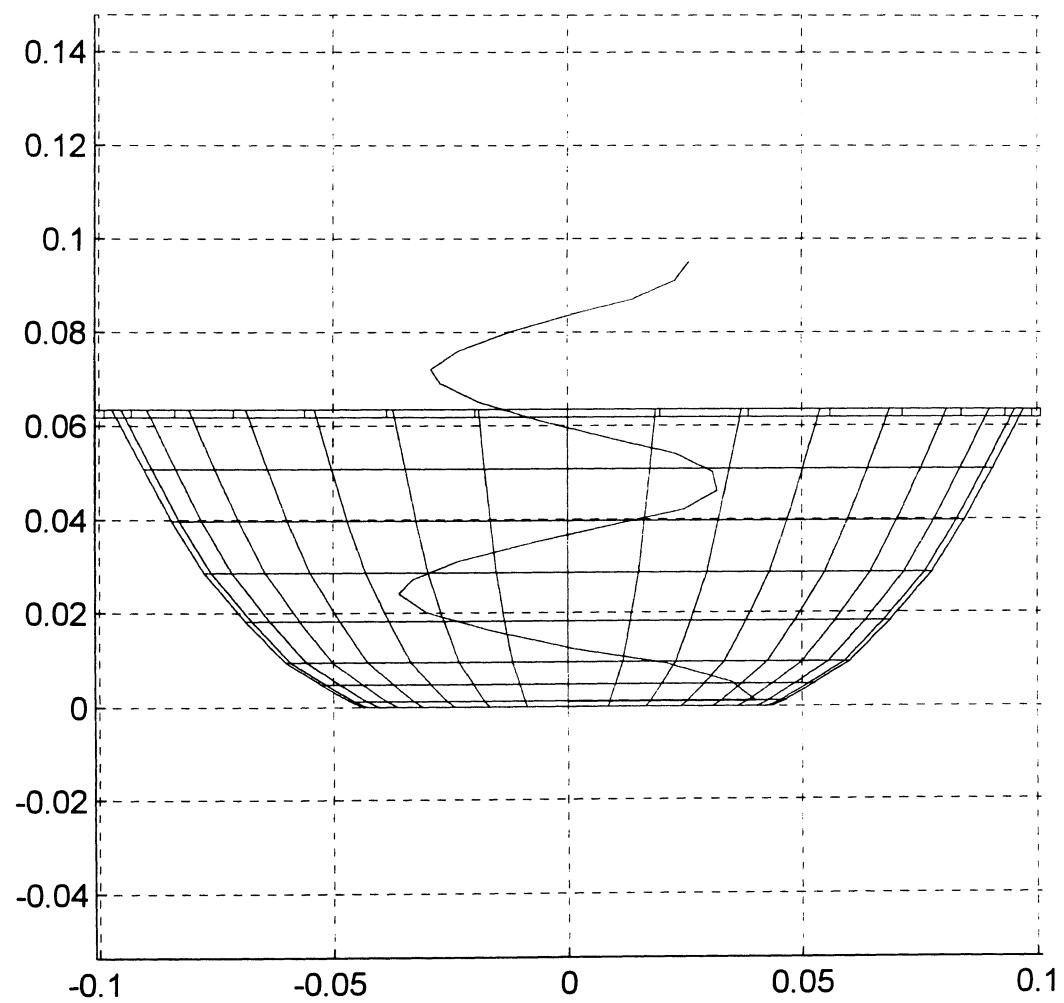


Figure 5.2.1b - 2-D geometry of the wire-grid model for helibowl in Section 5.2.1

Another thing to mention is that during the measurement, dB Systems did not record the relative position of the helibowl. Therefore, more than one pair of simulations is needed. From these patterns obtained from the simulations, the most likely pair of patterns (ϕ and $\phi+90^\circ$) was chosen to compare with the measured patterns.

The space was divided by twelve (12) elevation planes with $\phi=0^\circ, 22.5^\circ, 45^\circ, 67.5^\circ, 90^\circ, 112.5^\circ, 135^\circ$ and 157.5° . Eight simulations on eight different elevation planes were performed.

The following figures (Figure 5.2.2 - 5.2.25) are the patterns at $\phi=0^\circ, 22.5^\circ, 45^\circ, 67.5^\circ, 90^\circ, 112.5^\circ, 135^\circ$ and 157.5° , respectively. After being compared with the measured pattern, the pattern at $\phi=0^\circ$ is most similar to the measured pattern at $\phi=0^\circ$ (Figure 5.1.3) and pattern at $\phi=90^\circ$ is most similar to the measured pattern at $\phi=90^\circ$. Therefore, in the next section, only two sets of simulations ($\phi = 0^\circ$ and 90°) were performed based on these results.

However, as can be seen, these patterns are not perfect enough to call the simulation complete. The amplitude of the backside lobes is still too high and the curves didn't match favorably. In Section 5.2.2, a similar simulation will be performed. The testing model will be the wire-grid helibowl model whose helical radiator was a ribbon-like, strip helix.

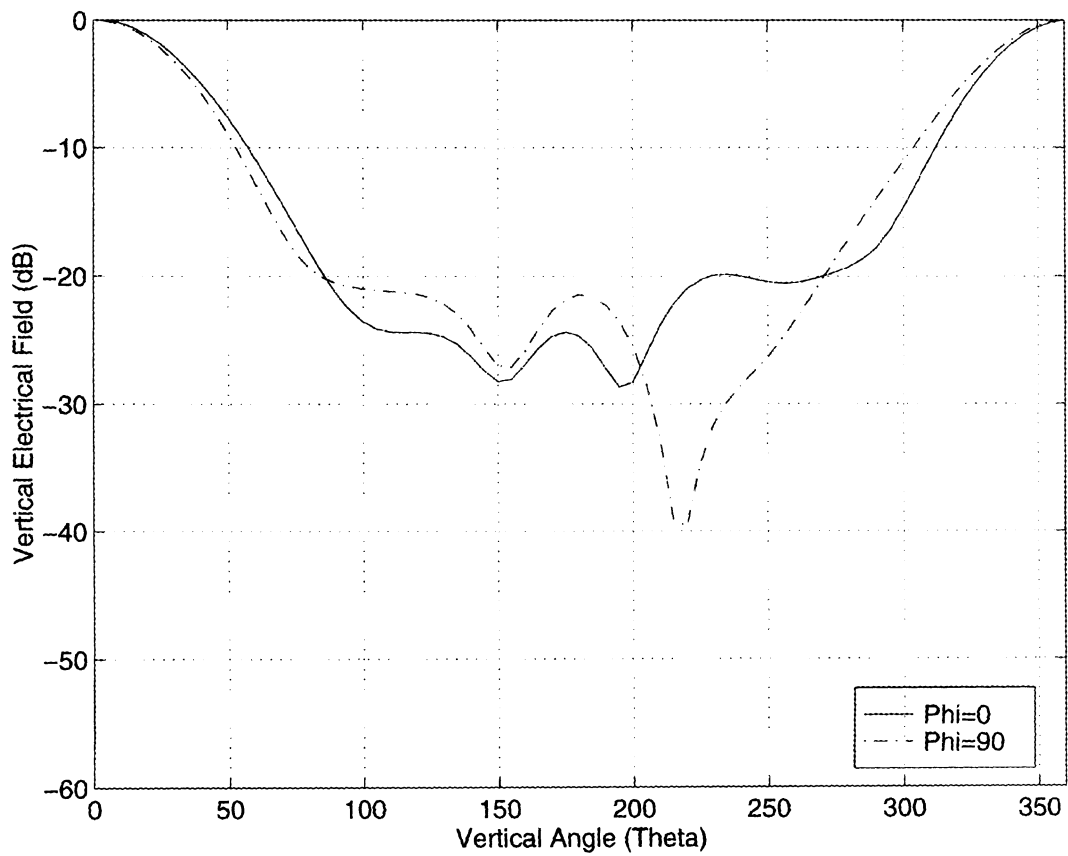


Figure 5.2.2 - Vertical radiation patterns for helibowl model in Section 5.2.1,
Simple helix, No circular plate, $\phi = 0^\circ$ and 90° , 1575 MHz

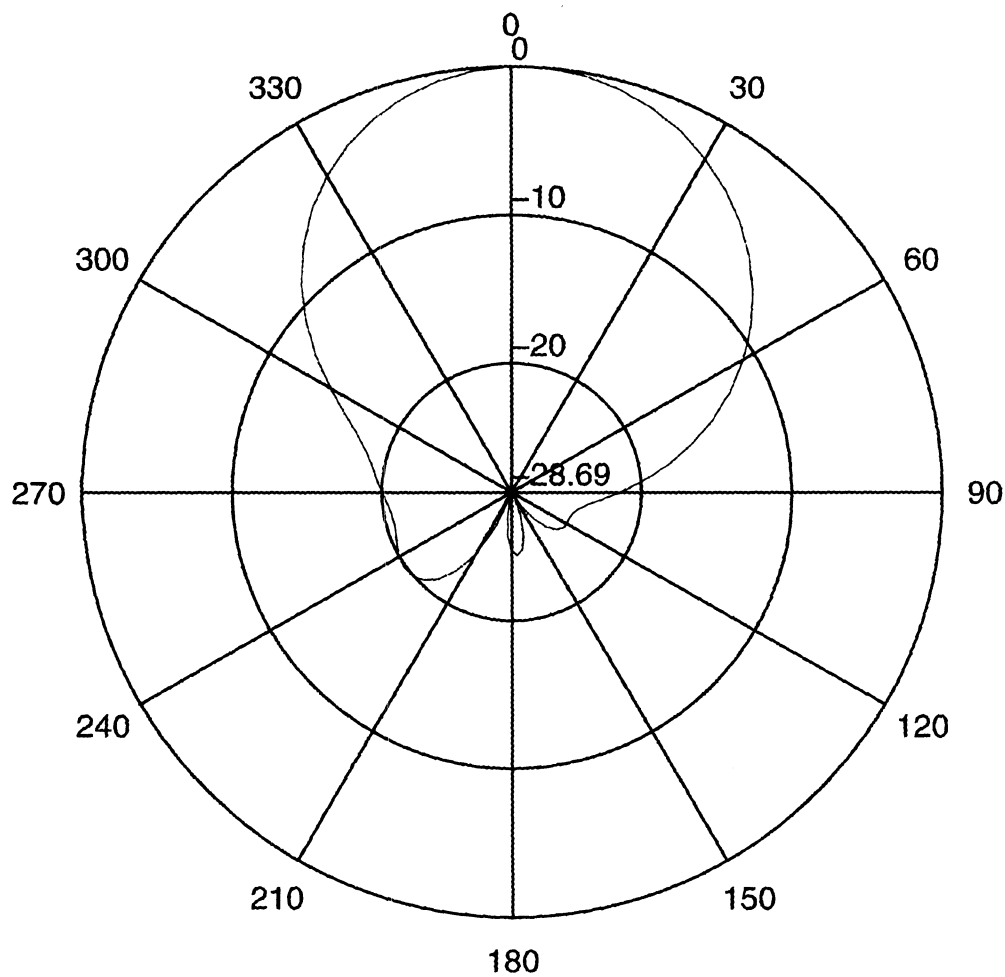


Figure 5.2.3 - Vertical radiation pattern for helibowl model in Section 5.2.1,
Simple helix, No circular plate, $\phi = 0^\circ$, 1575 MHz

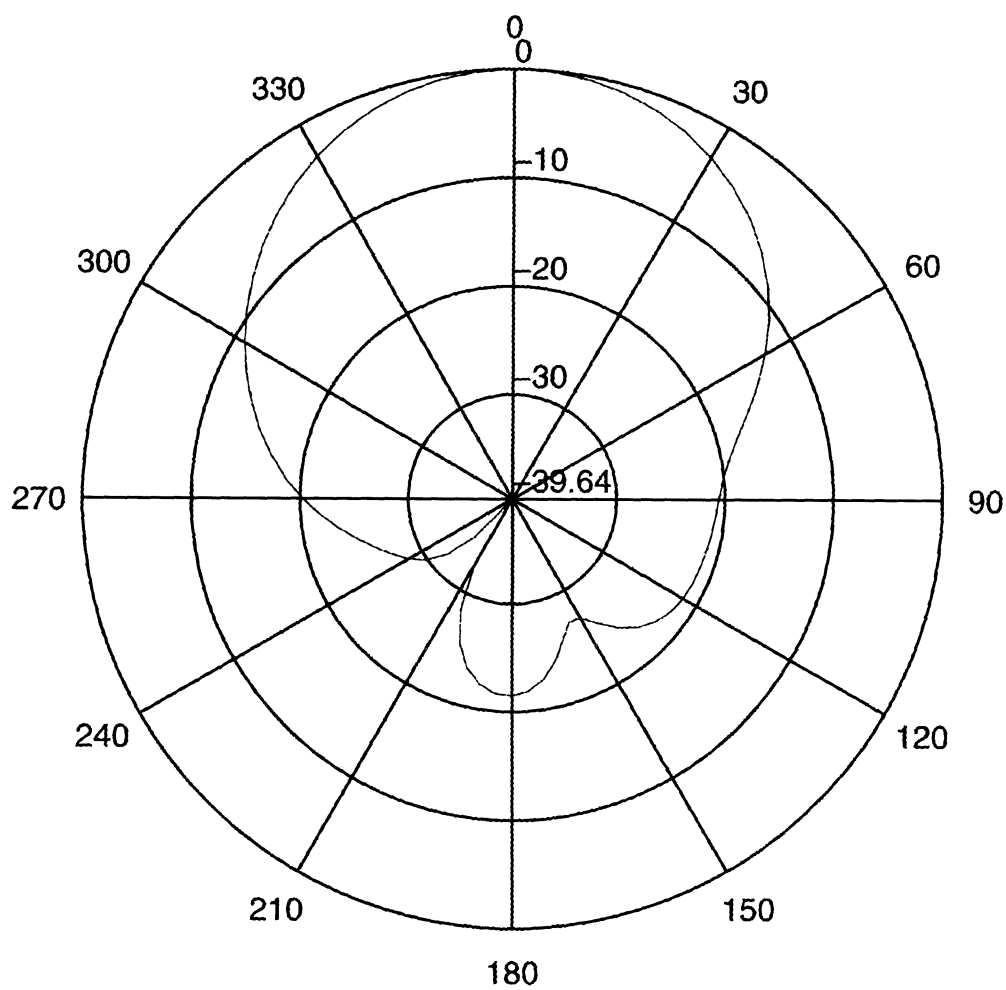


Figure 5.2.4 - Vertical radiation pattern for helibowl model in Section 5.2.1,
Simple helix, No circular plate, $\phi = 90^\circ$, 1575 MHz

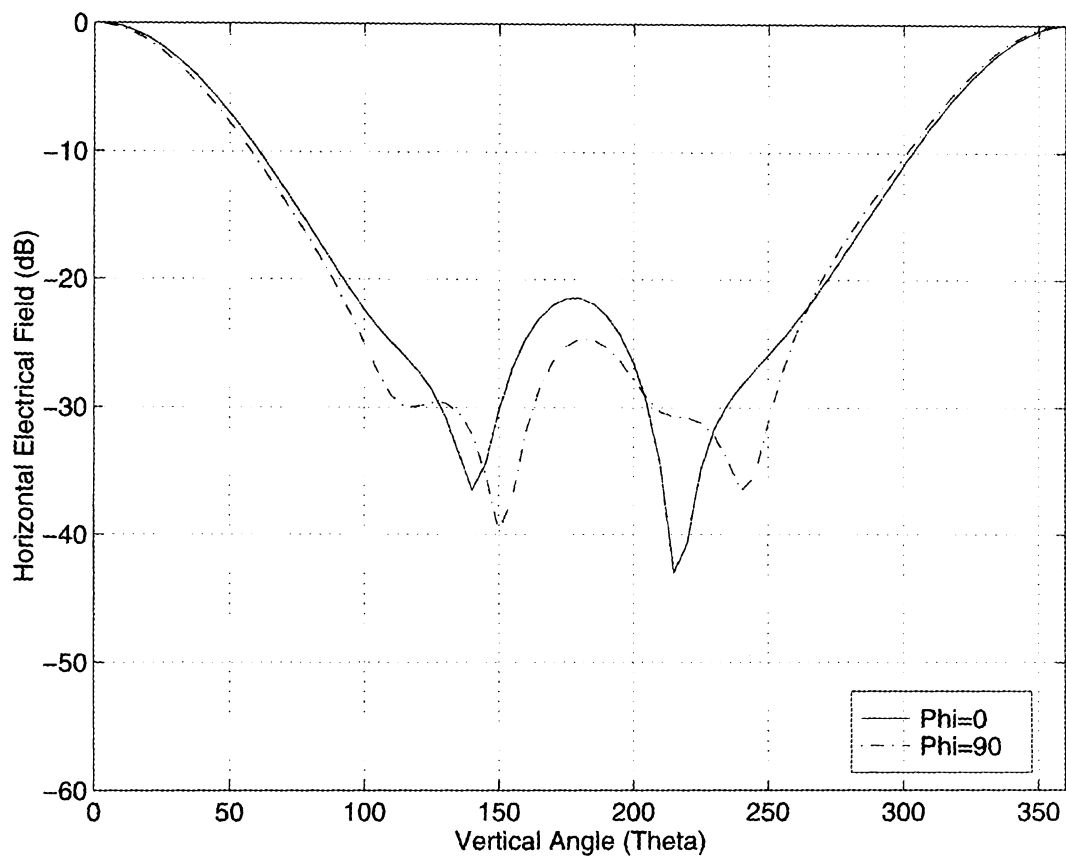


Figure 5.2.5 - Horizontal radiation patterns for helibowl model in Section 5.2.1,
Simple helix, No circular plate, $\phi = 0^\circ$ and 90° , 1575 MHz

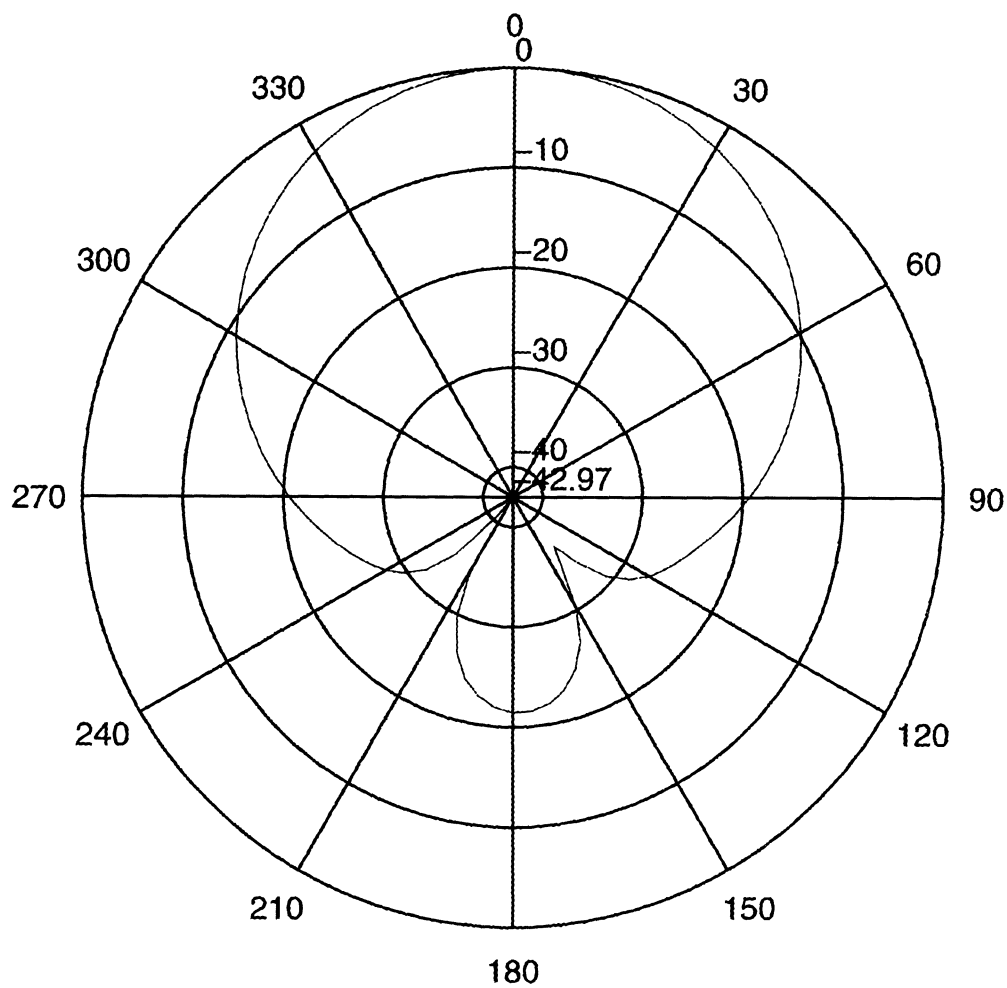


Figure 5.2.6 - Horizontal radiation pattern for helibowl model in Section 5.2.1,
Simple helix, No circular plate, $\phi = 0^\circ$, 1575 MHz

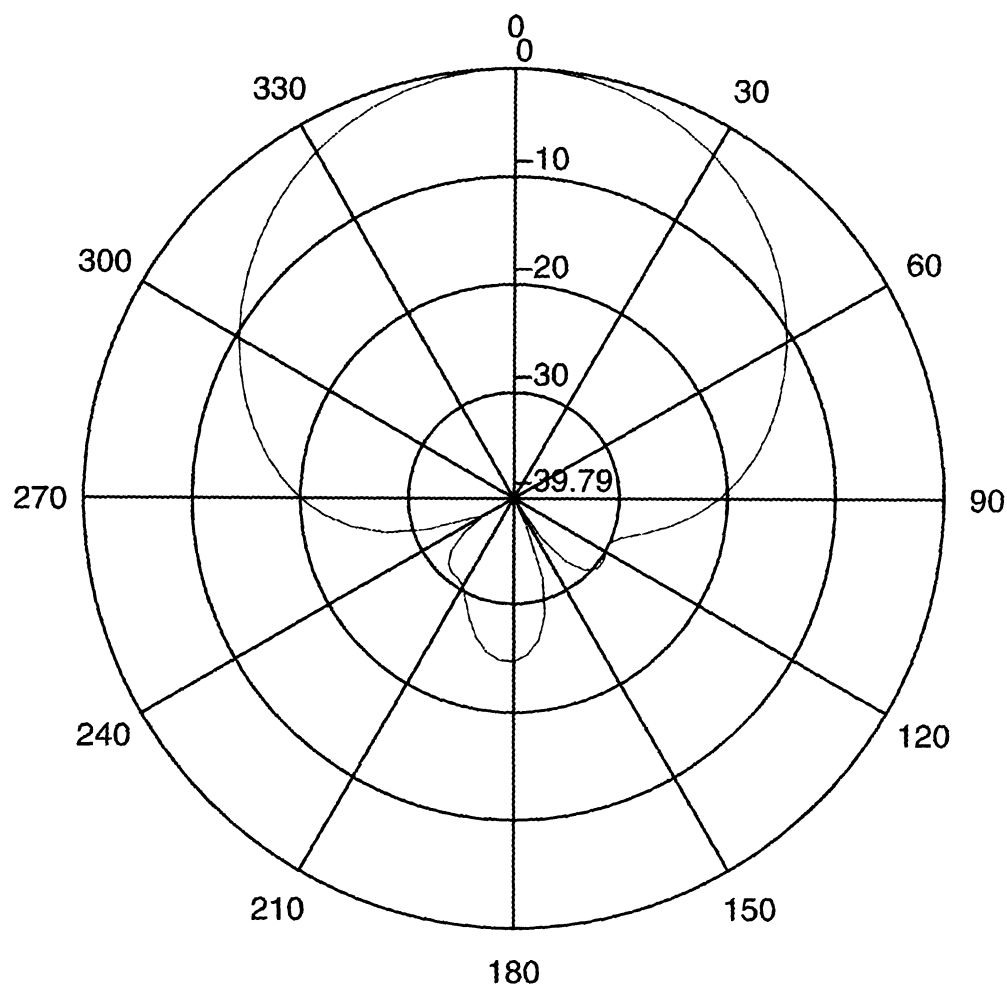


Figure 5.2.7 - Horizontal radiation pattern for helibowl model in Section 5.2.1,
Simple helix, No circular plate, $\phi = 90^\circ$, 1575 MHz

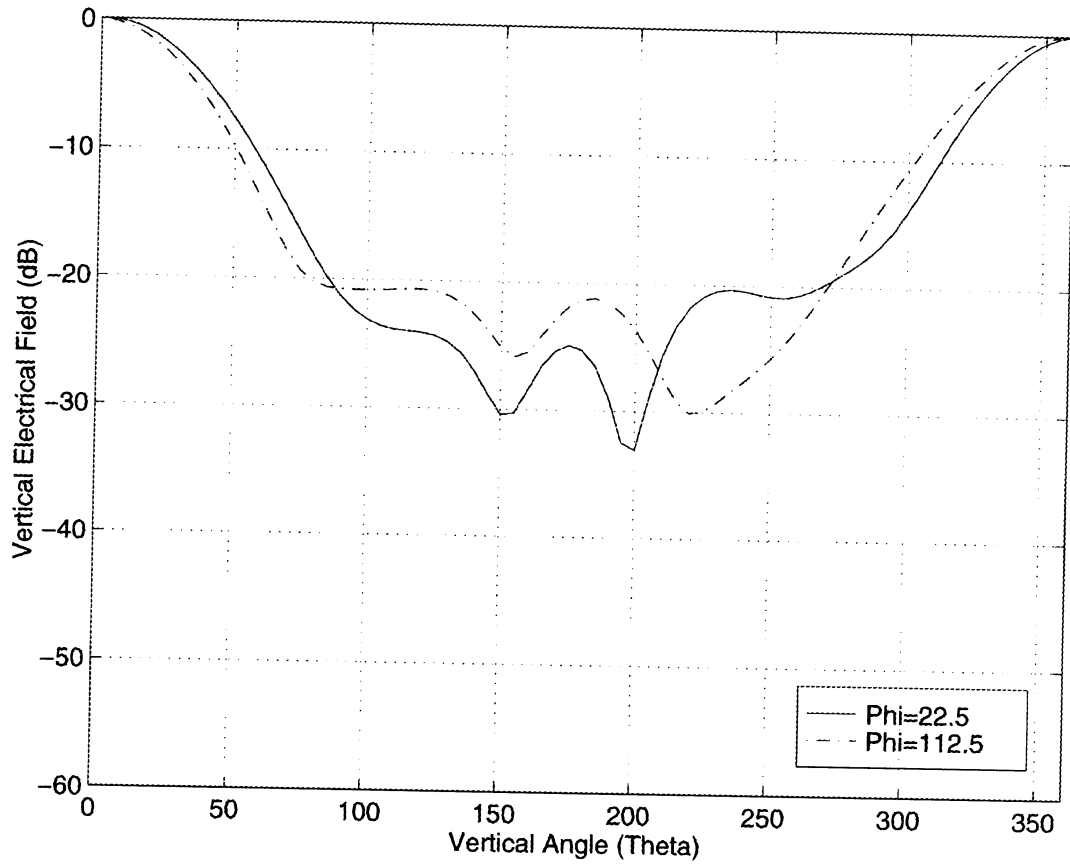


Figure 5.2.8 - Vertical radiation patterns for helibowl model in Section 5.2.1,
Simple helix, No circular plate, $\phi = 22.5^\circ$ and 112.5° , 1575 MHz

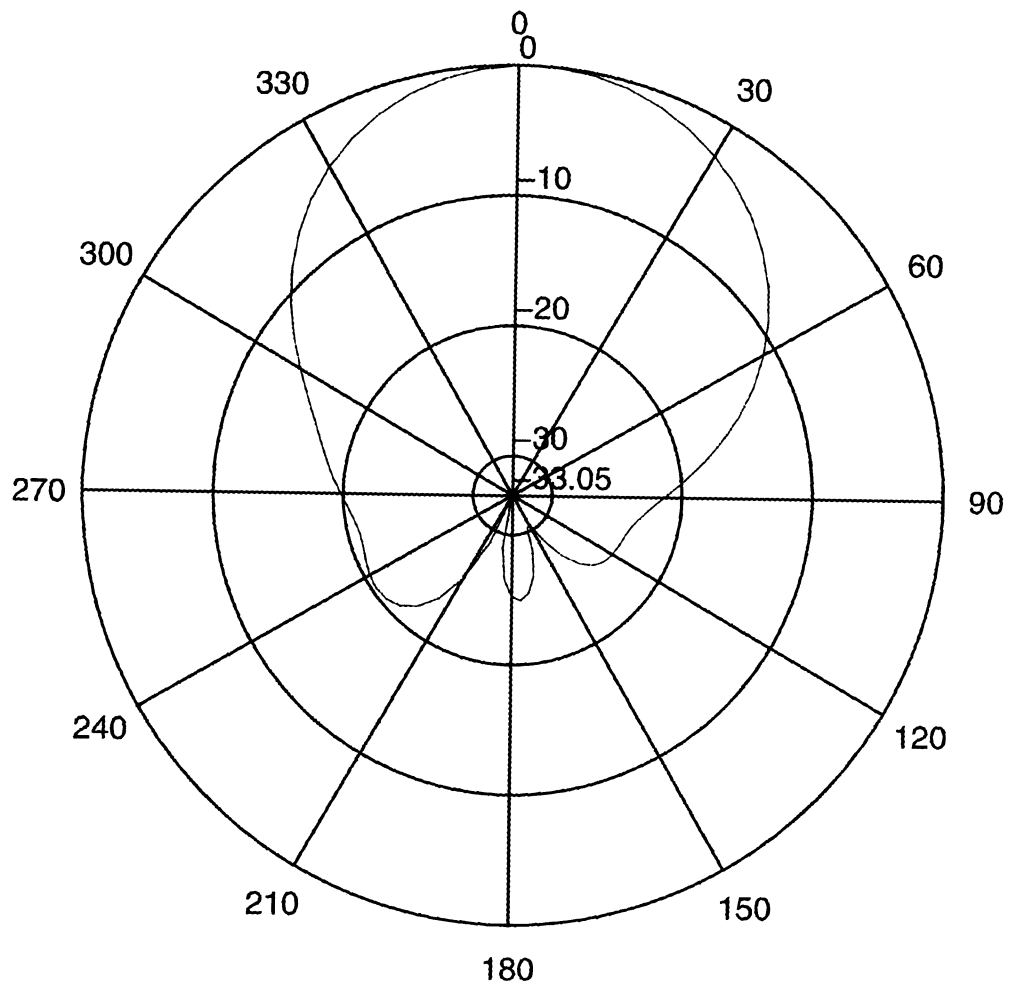


Figure 5.2.9 - Vertical radiation pattern for helibowl model in Section 5.2.1,
Simple helix, No circular plate, $\phi = 22.5^\circ$, 1575 MHz

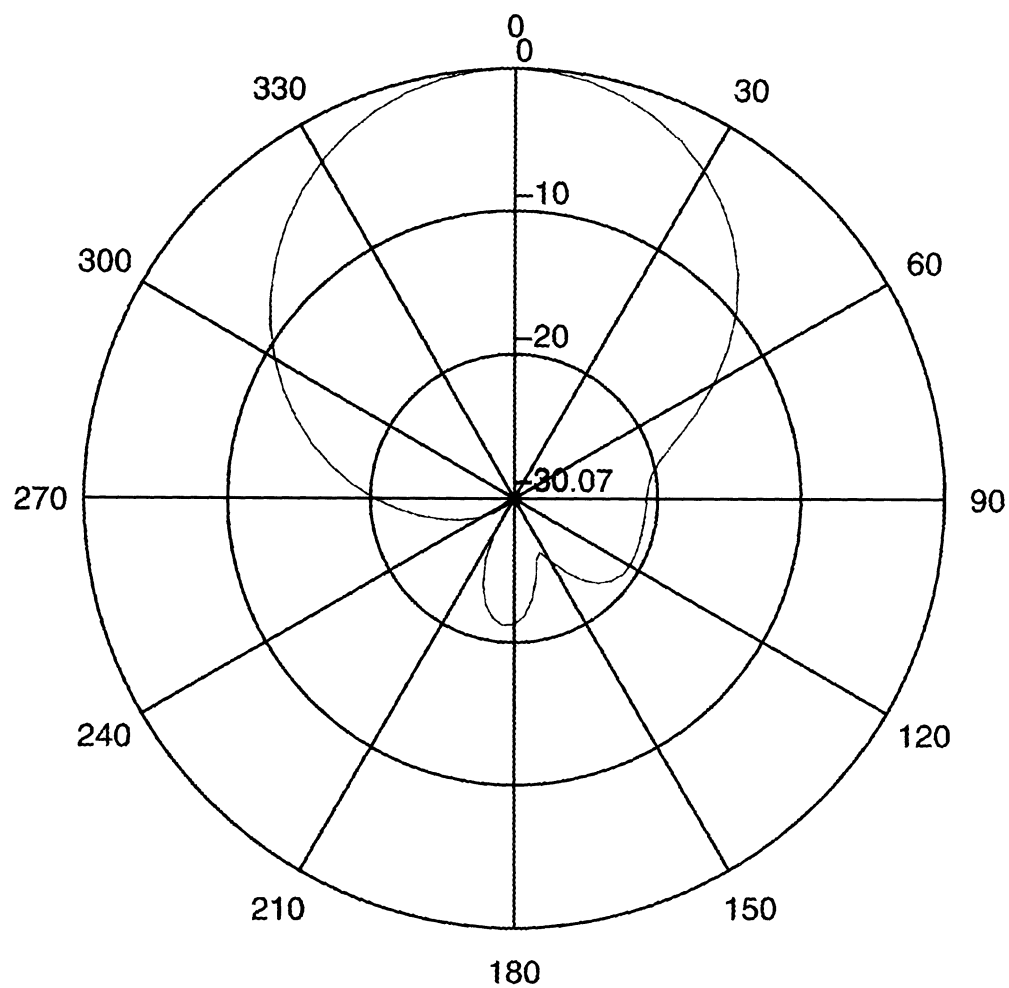


Figure 5.2.10 - Vertical radiation pattern for helibowl model in Section 5.2.1,
Simple helix, No circular plate, $\phi = 112.5^\circ$, 1575 MHz

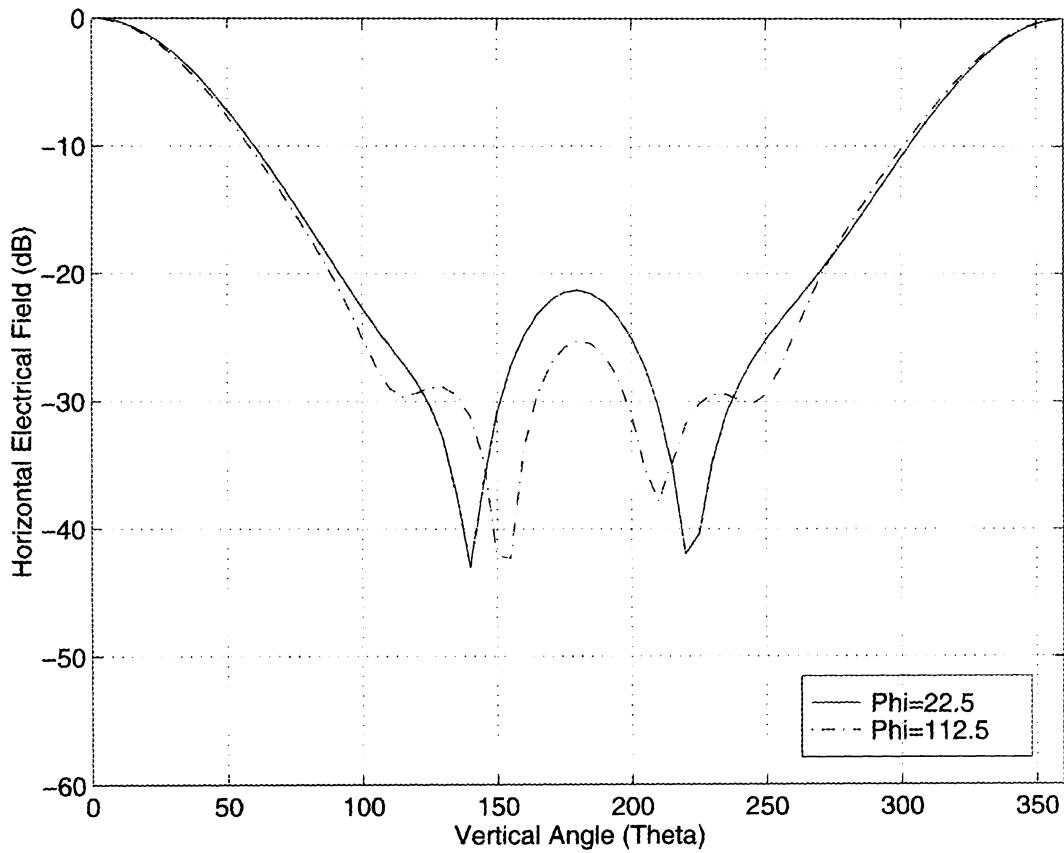


Figure 5.2.11 - Horizontal radiation patterns for helibowl model in Section 5.2.1,
Simple helix, No circular plate, $\phi = 22.5^\circ$ and 112.5° , 1575 MHz

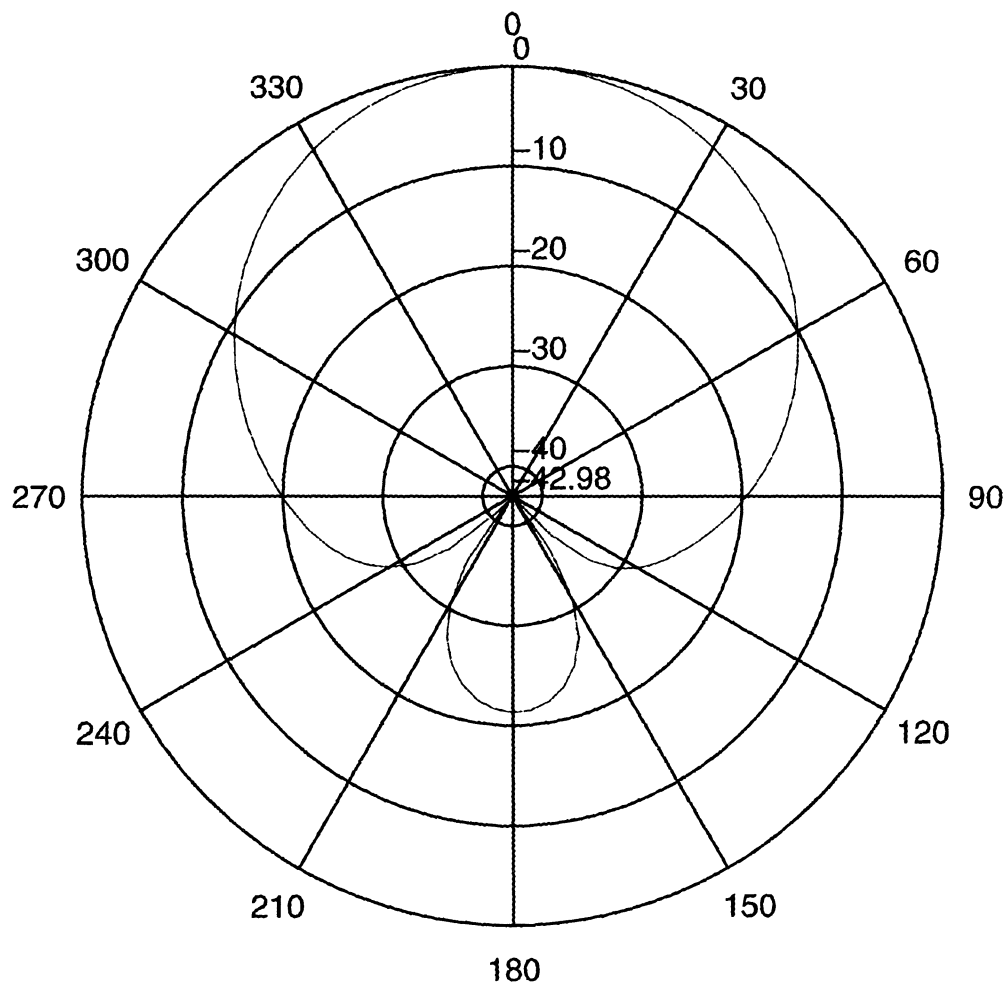


Figure 5.2.12 - Horizontal radiation pattern for helibowl model in Section 5.2.1,
Simple helix, No circular plate, $\phi = 22.5^\circ$, 1575 MHz

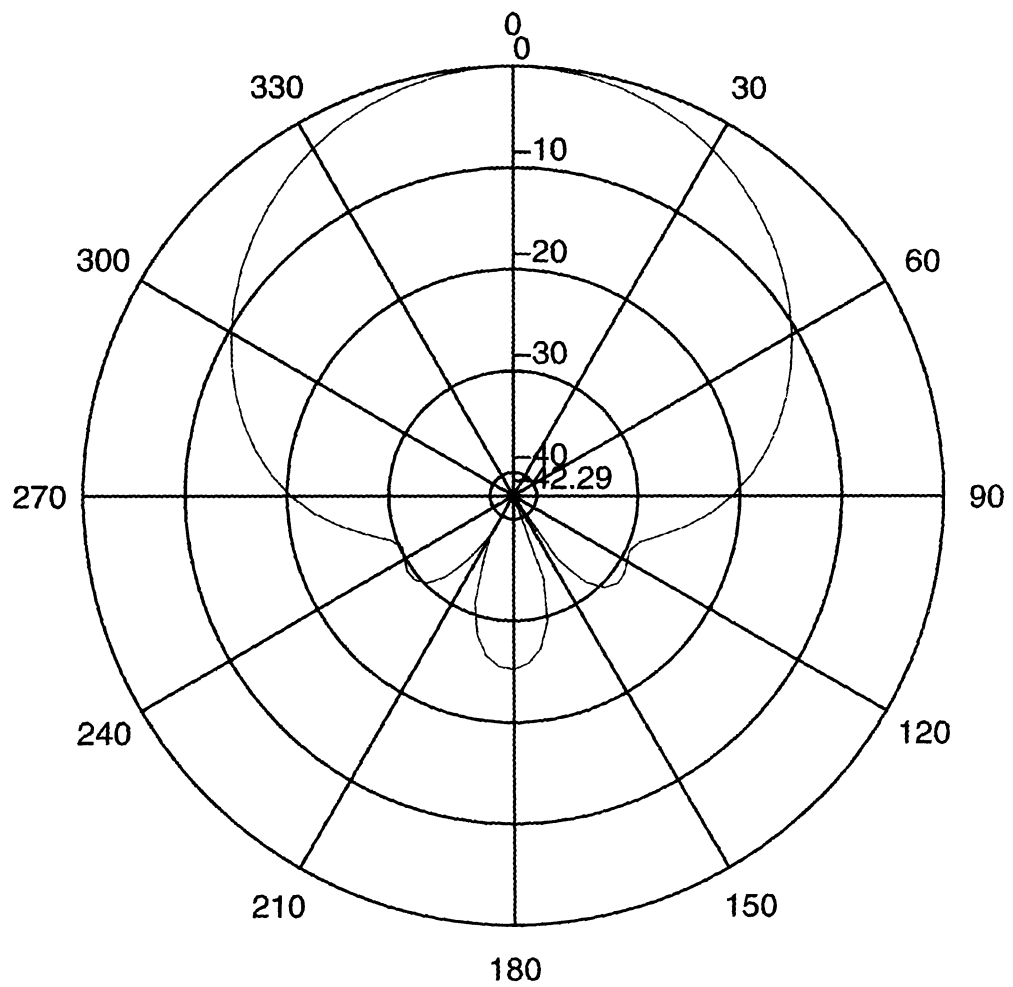


Figure 5.2.13 - Horizontal radiation pattern for helibowl model in Section 5.2.1,
Simple helix, No circular plate, $\phi = 112.5^\circ$, 1575 MHz

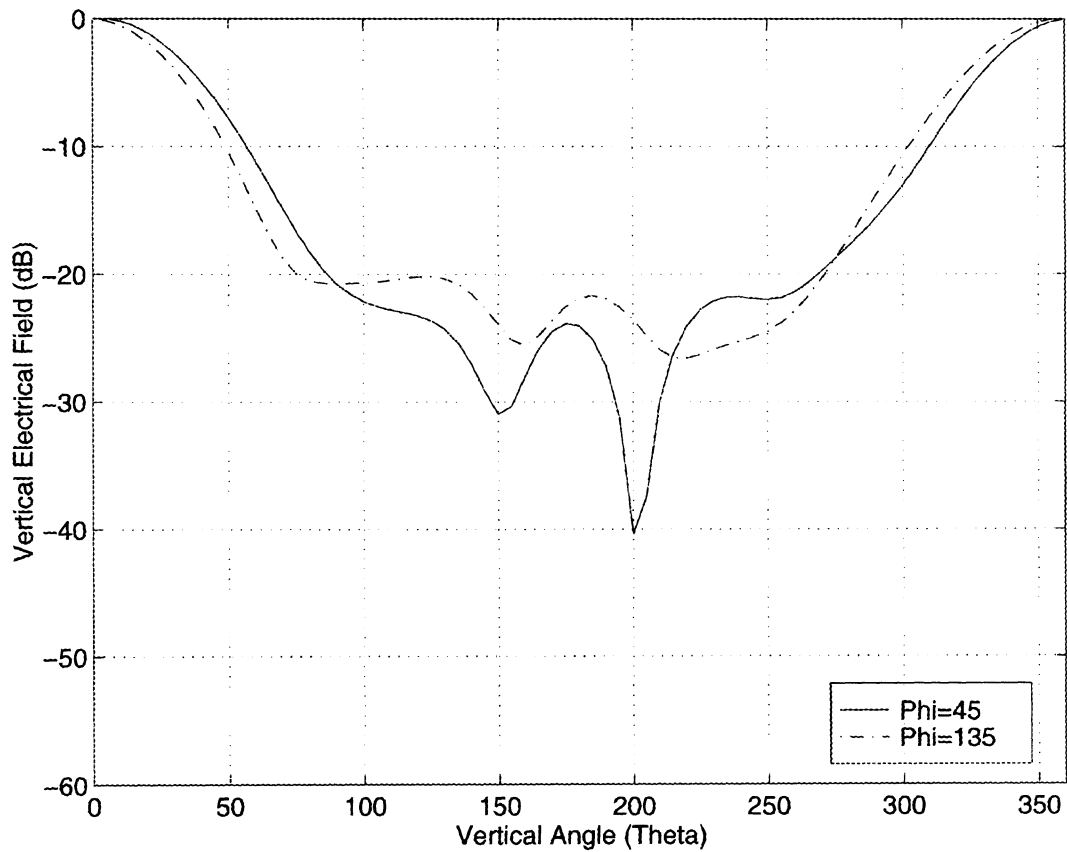


Figure 5.2.14 - Vertical radiation patterns for helibowl model in Section 5.2.1,
Simple helix, No circular plate, $\phi = 45^\circ$ and 135° , 1575 MHz

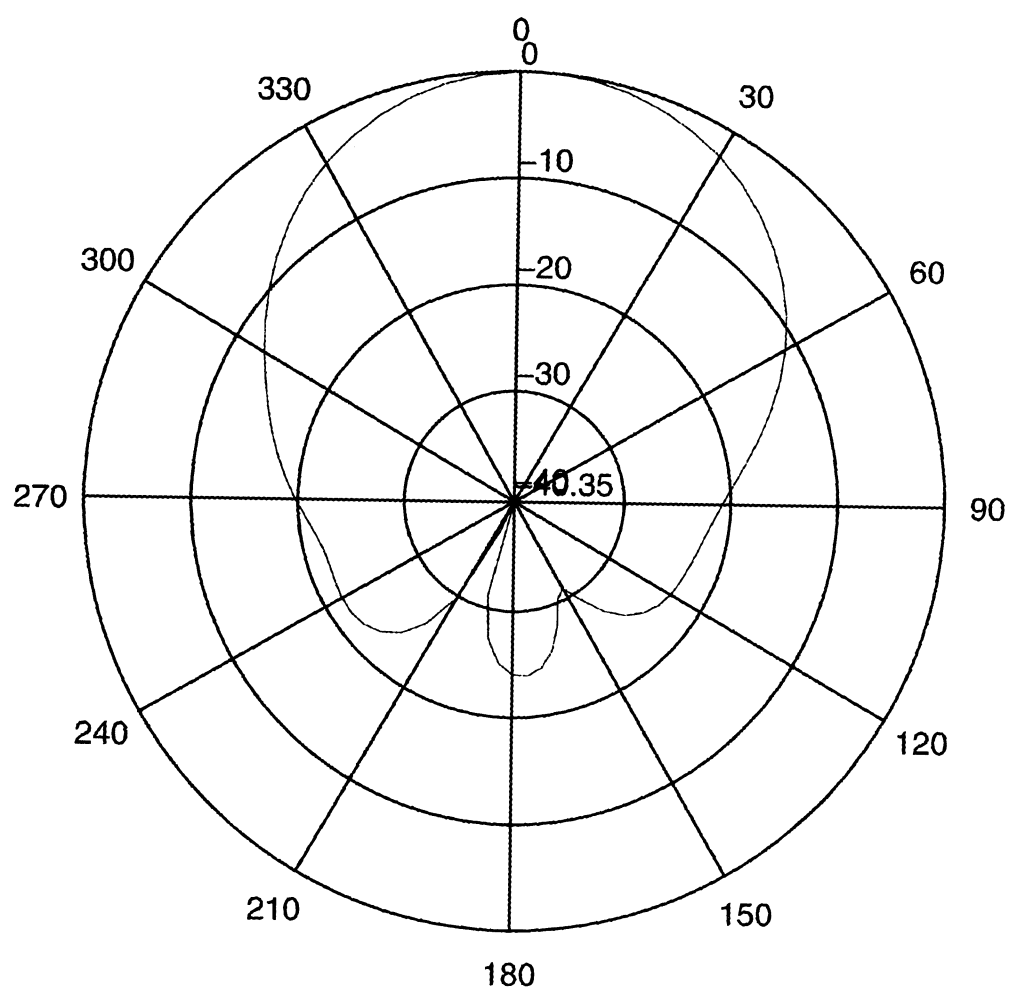


Figure 5.2.15 - Vertical radiation pattern for helibowl model in Section 5.2.1,
Simple helix, No circular plate, $\phi = 45^\circ$, 1575 MHz

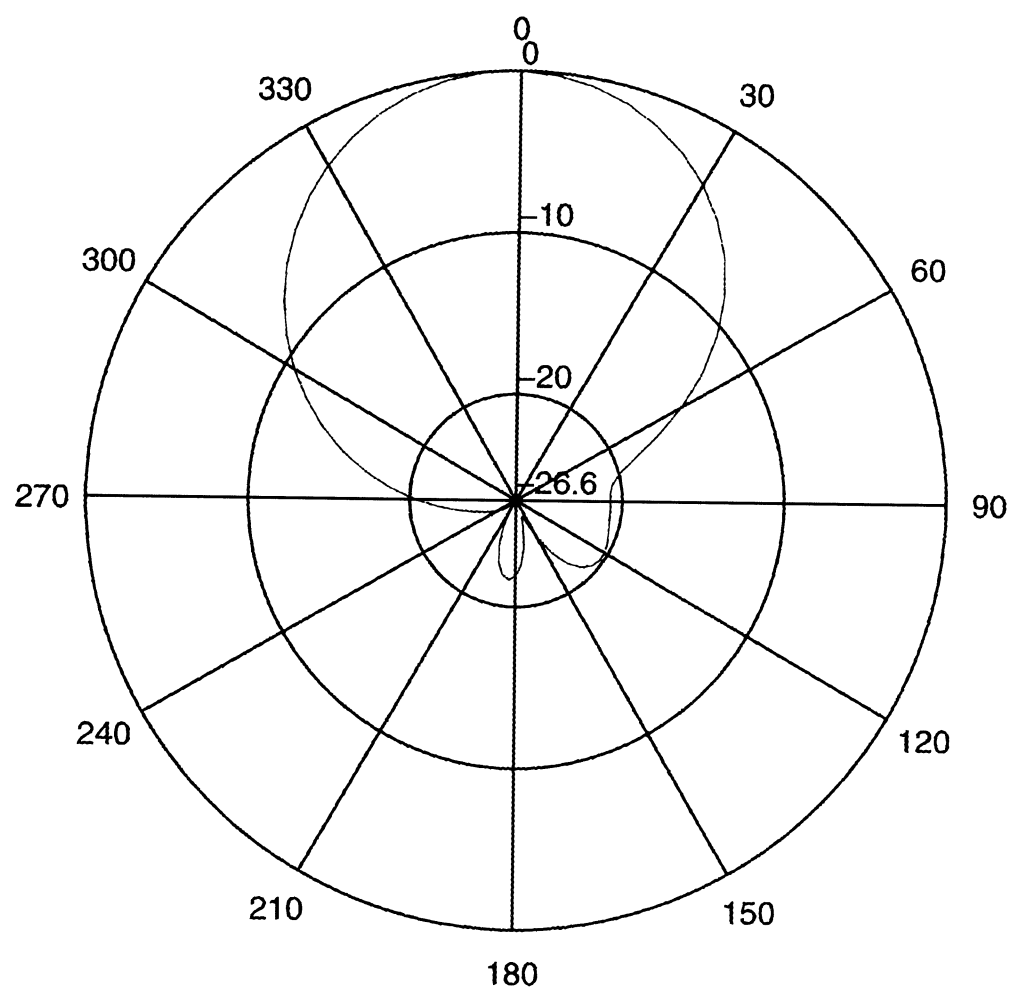


Figure 5.2.16 - Vertical radiation pattern for helibowl model in Section 5.2.1,
Simple helix, No circular plate, $\phi = 135^\circ$, 1575 MHz

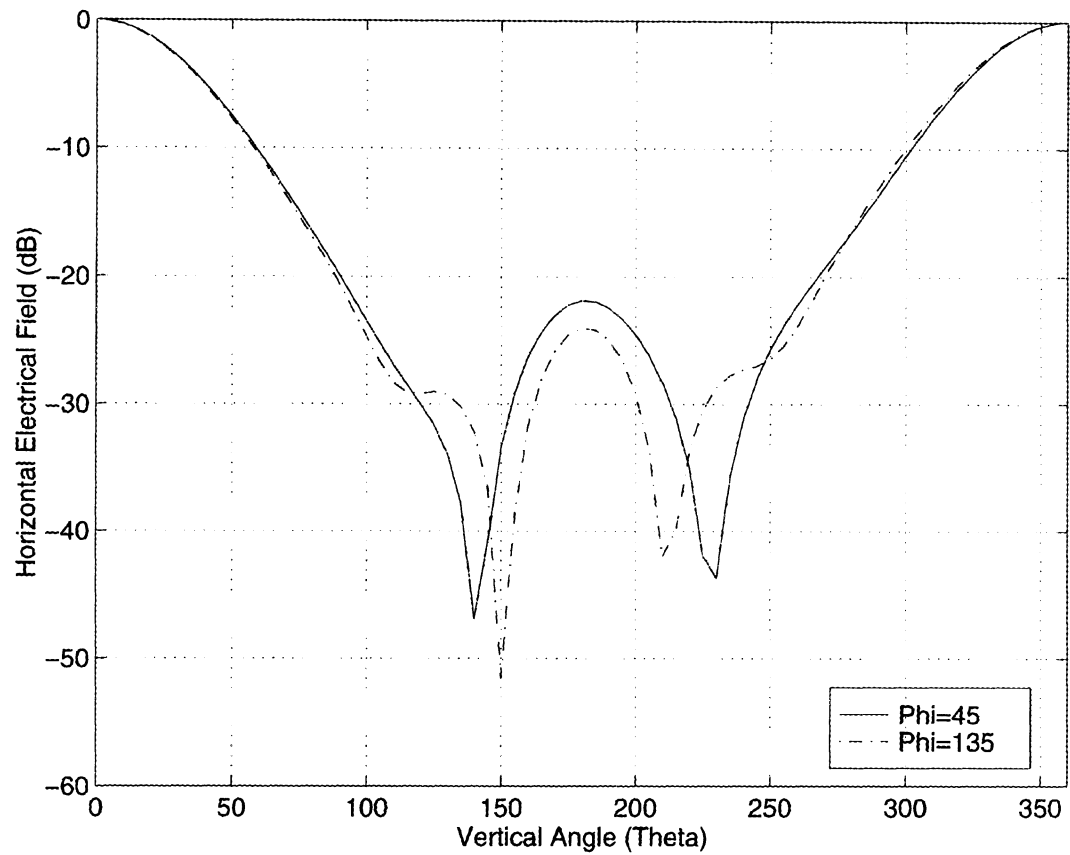


Figure 5.2.17 - Horizontal radiation patterns for helibowl model in Section 5.2.1,
Simple helix, No circular plate, $\phi = 45^\circ$ and 135° , 1575 MHz

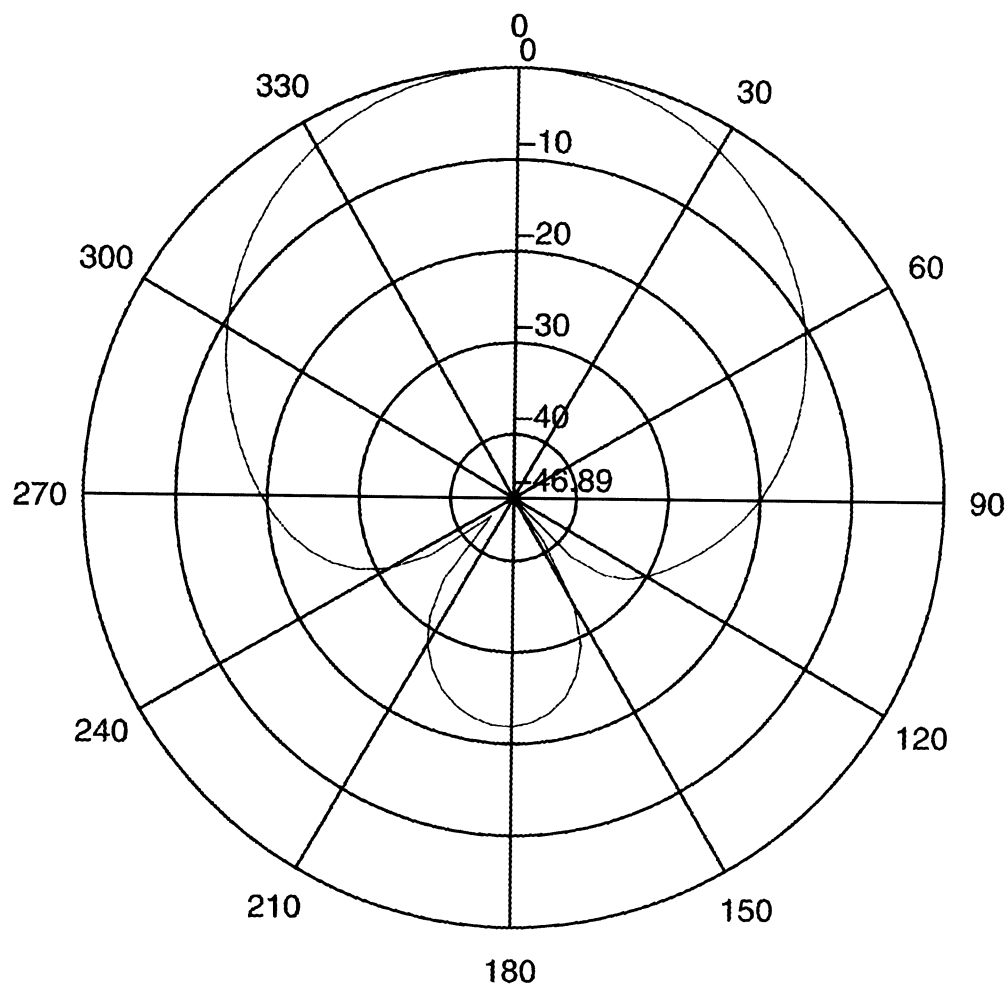


Figure 5.2.18 - Horizontal radiation pattern for helibowl model in Section 5.2.1,
Simple helix, No circular plate, $\phi = 45$, 1575 MHz

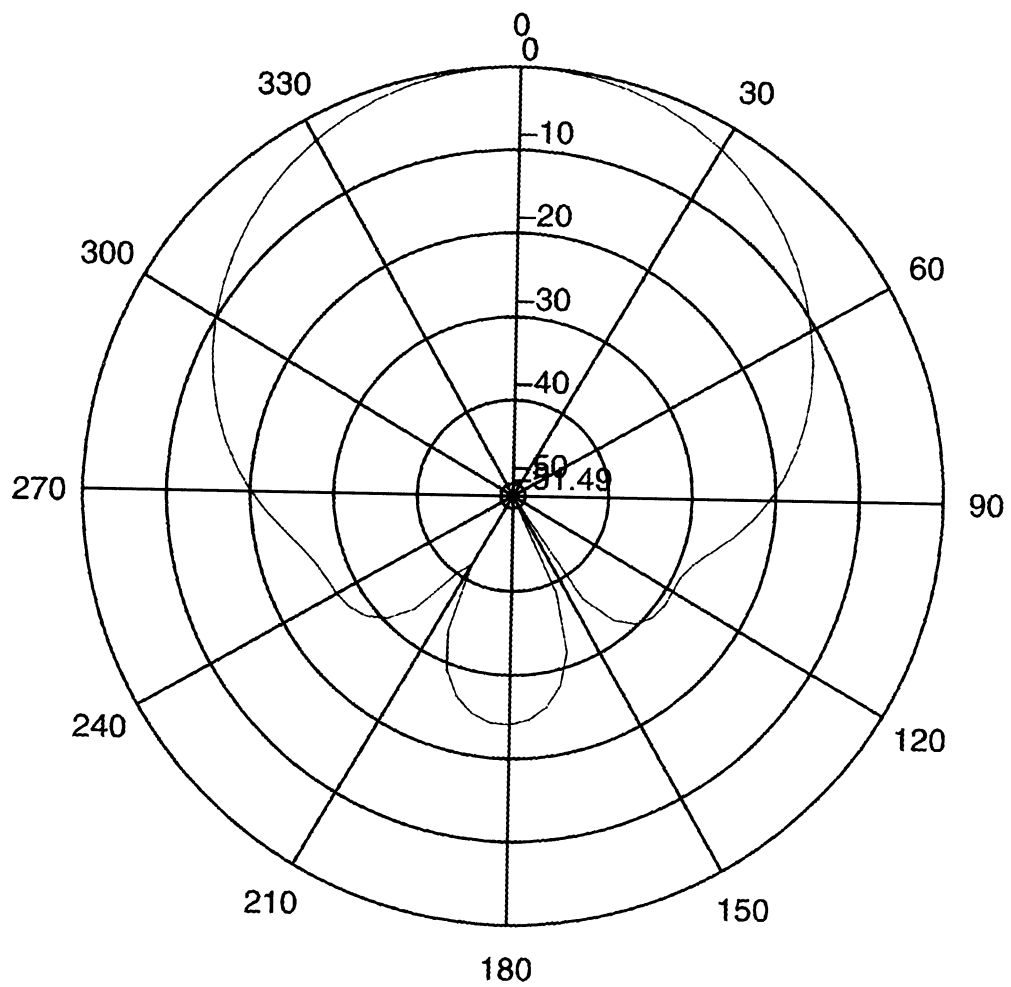


Figure 5.2.19 - Horizontal radiation pattern for helibowl model in Section 5.2.1,
Simple helix, No circular plate, $\phi = 135^\circ$, 1575 MHz

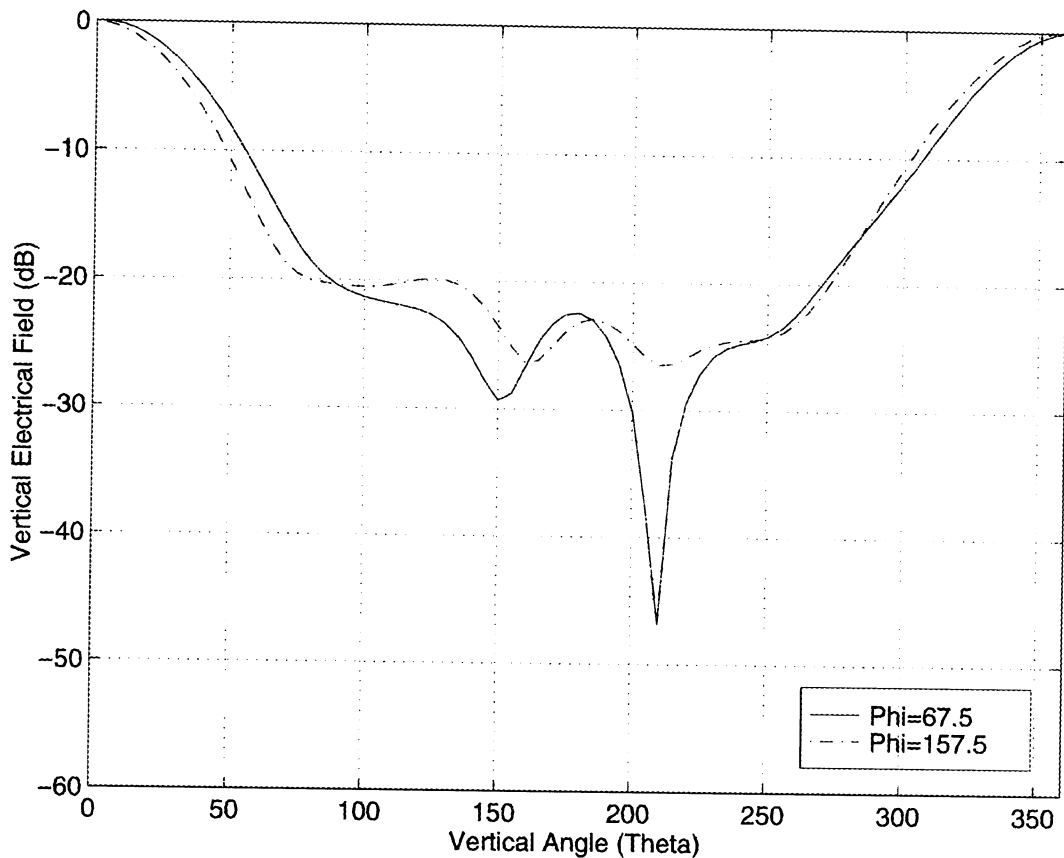


Figure 5.2.20 - Vertical radiation patterns for helibowl model in Section 5.2.1,
Simple helix, No circular plate, $\phi = 67.5^\circ$ and 157.5° , 1575 MHz

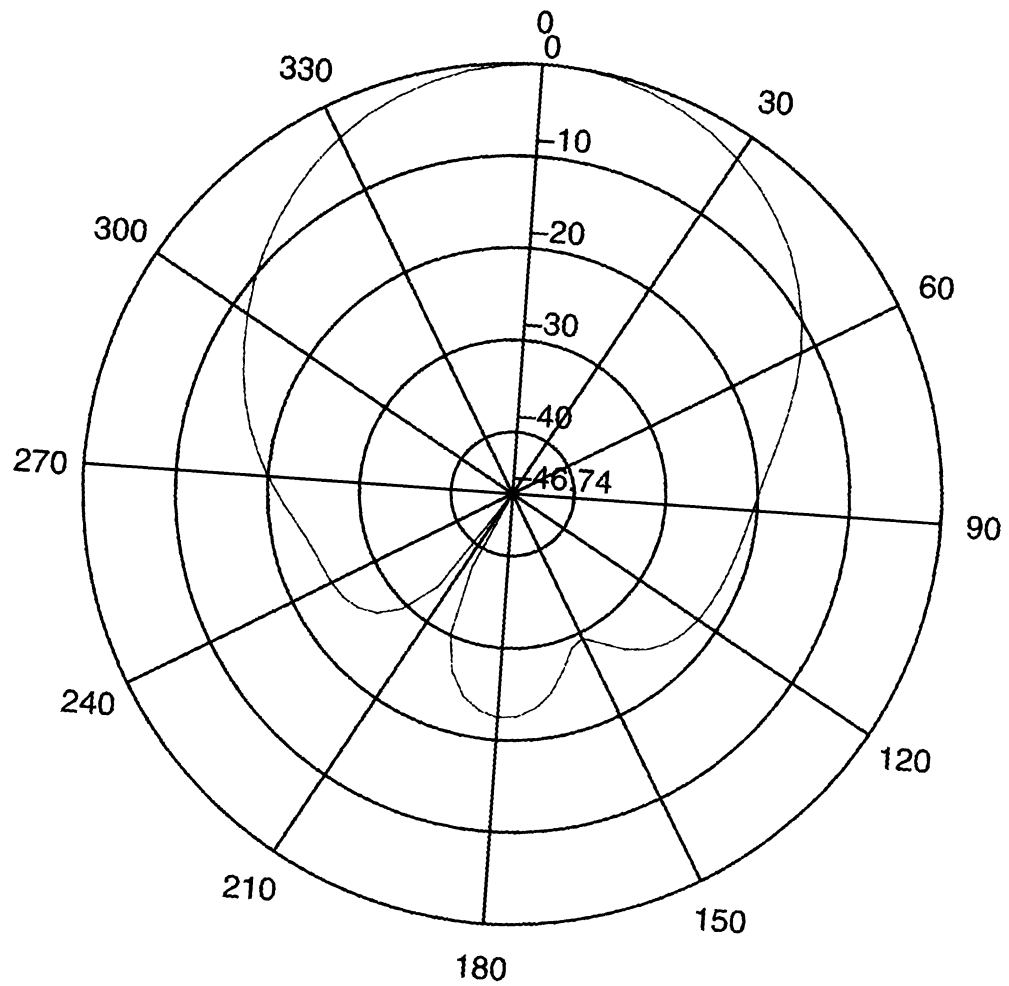


Figure 5.2.21 - Vertical radiation pattern for helibowl model in Section 5.2.1,
Simple helix, No circular plate, $\phi = 67.5^\circ$, 1575 MHz

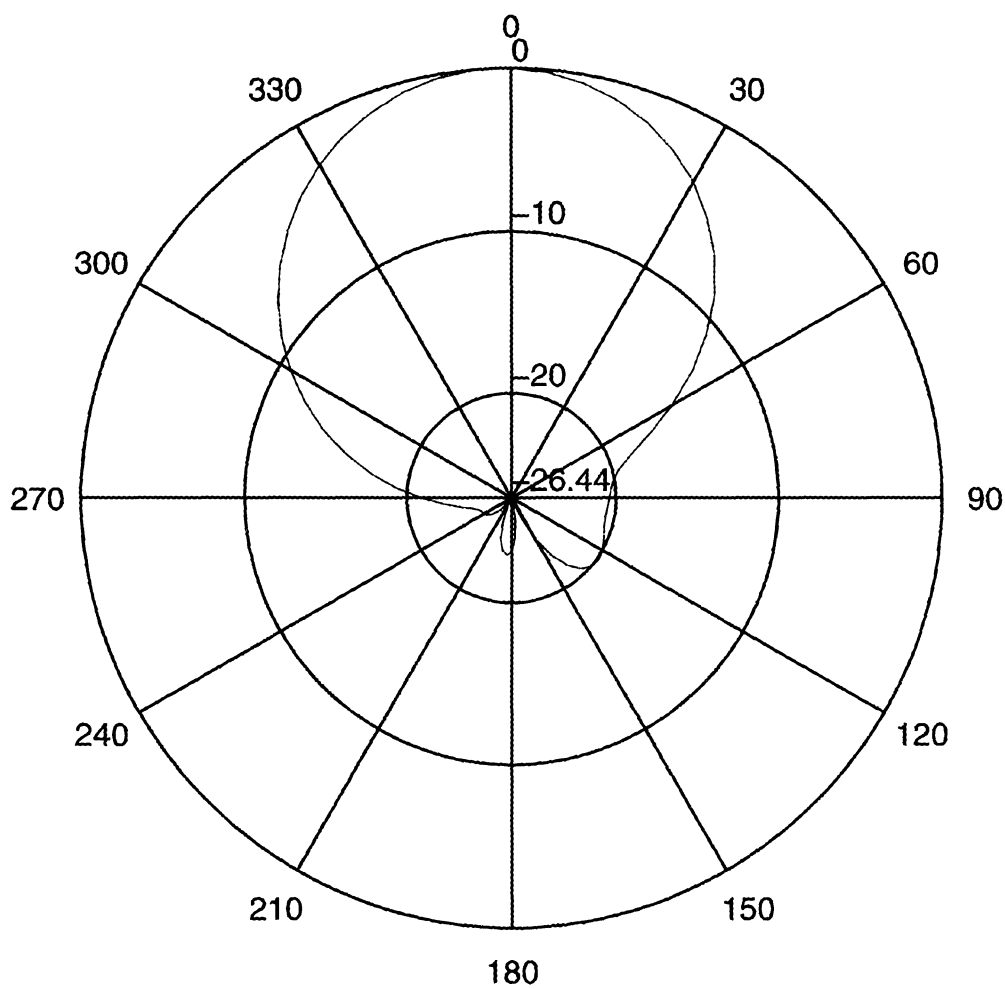


Figure 5.2.22 - Vertical radiation pattern for helibowl model in Section 5.2.1,
Simple helix, No circular plate, $\phi = 157.5^\circ$, 1575 MHz

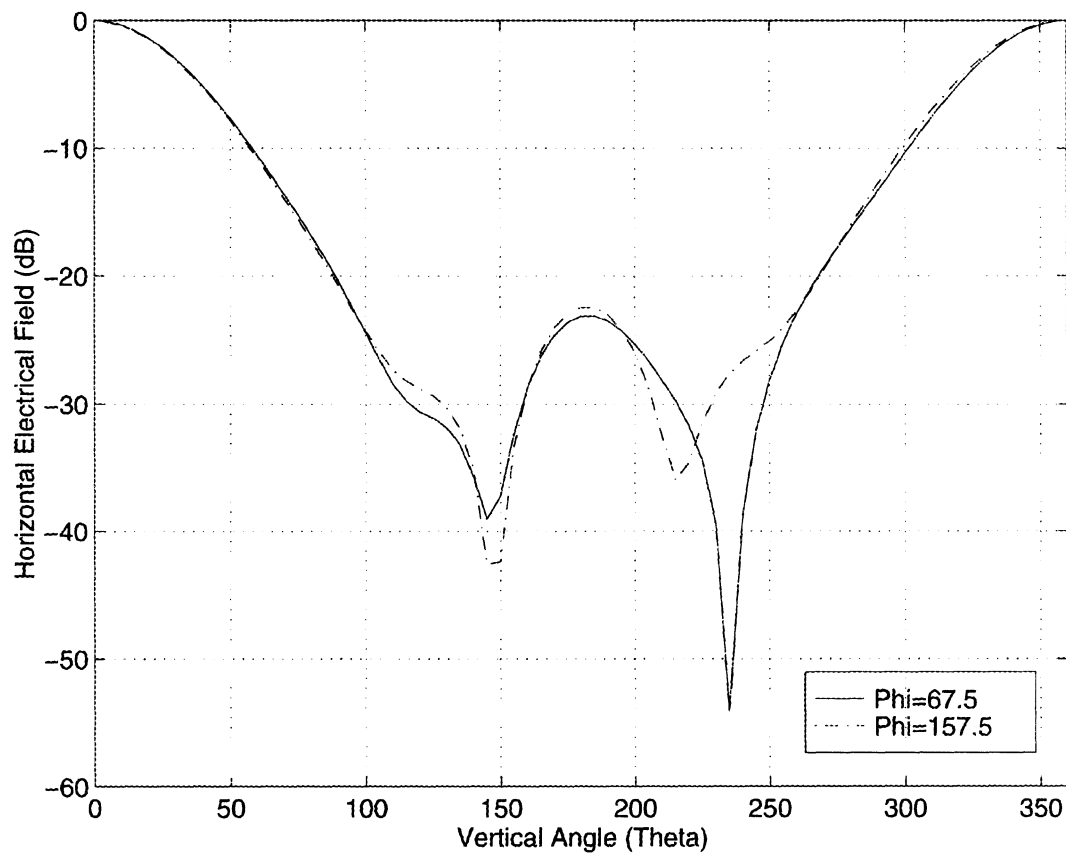


Figure 5.2.23 - Horizontal radiation patterns for helibowl model in Section 5.2.1,
Simple helix, No circular plate, $\phi = 67.5^\circ$ and 157.5° , 1575 MHz

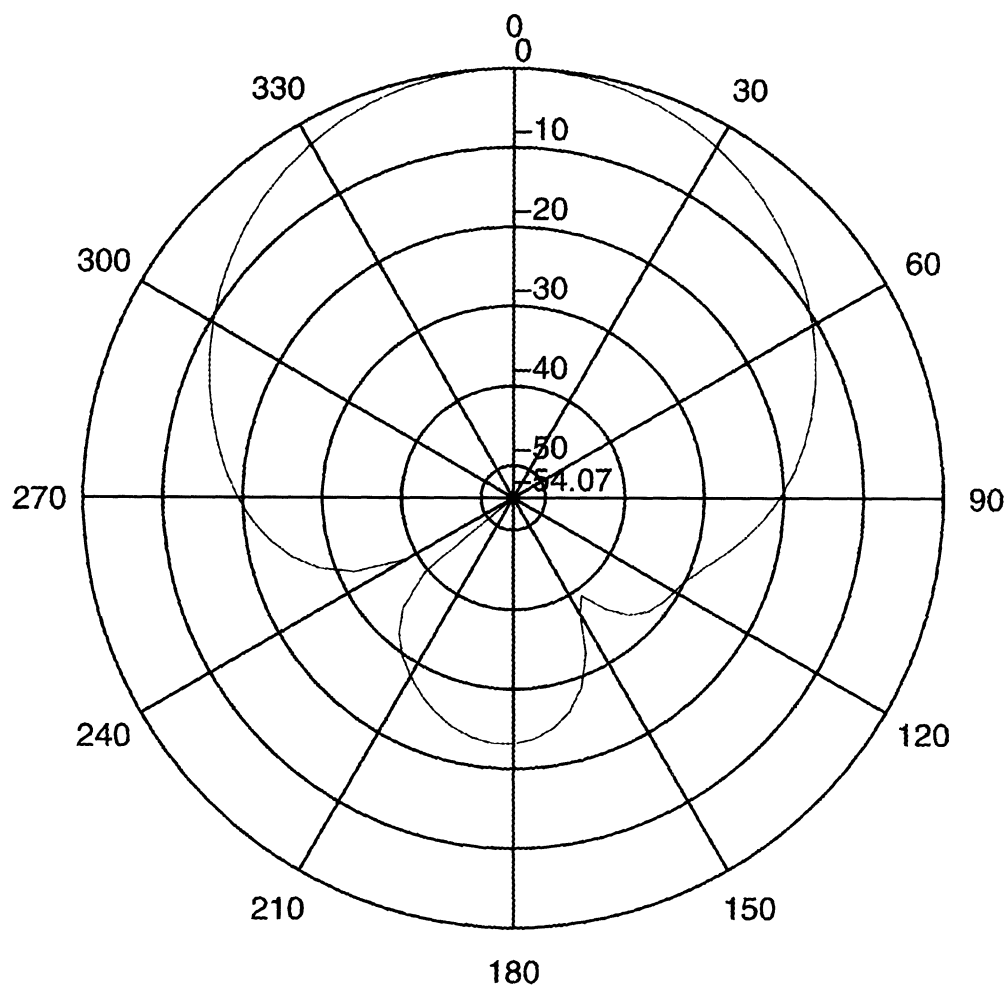


Figure 5.2.24 - Horizontal radiation pattern for helibowl model in Section 5.2.1,
Simple helix, No circular plate, $\phi = 67.5^\circ$, 1575 MHz

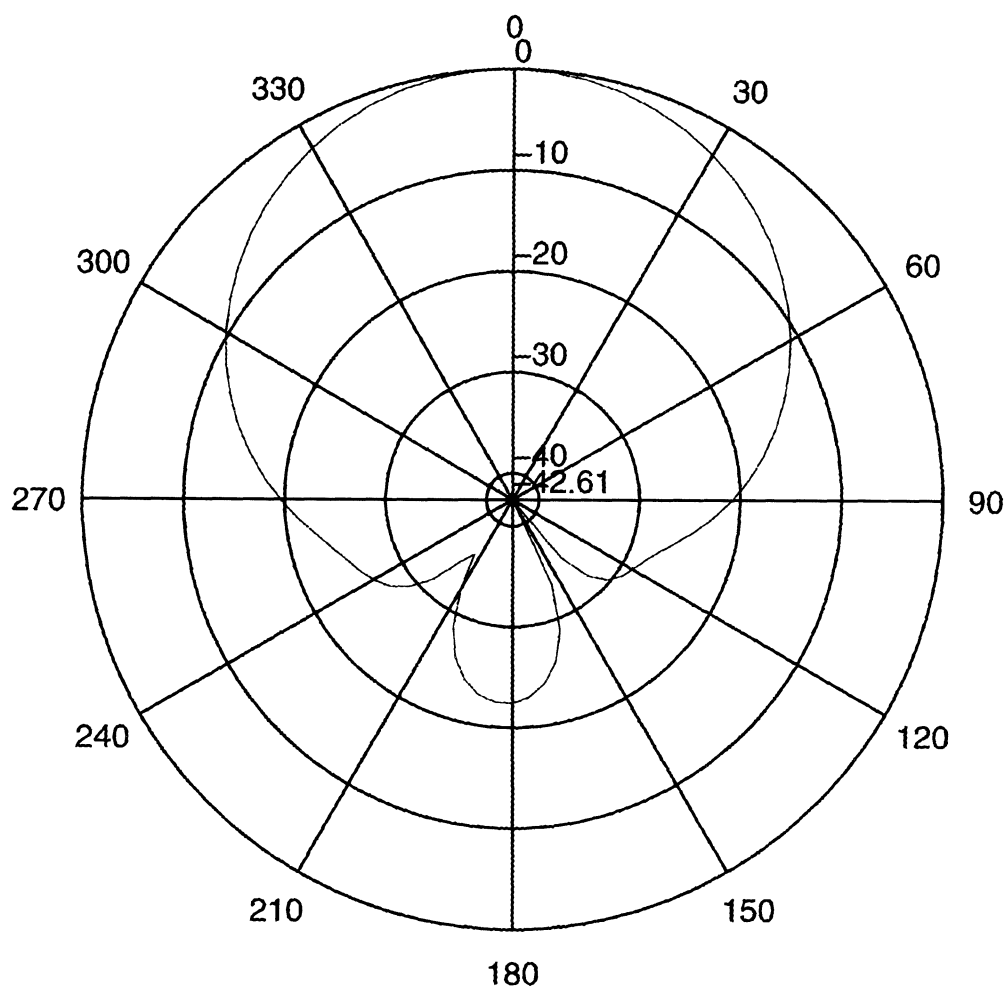


Figure 5.2.25 - Horizontal radiation pattern for helibowl model in Section 5.2.1,
Simple helix, No circular plate, $\phi = 157.5^\circ$, 1575 MHz

5.2.2 Model Two: Modified Helical Part

Beginning with the configured model described in section 5.2.1, the helical part of the wire-grid model was made to look like a spiral ribbon. The bowl was kept the same without any modification. In Figure 5.2.26, it shows the new wire-grid model with the helical part modified.

Now consider the pattern obtained from the simulation (Figure 5.2.27 - 5.2.32). The new results were changed slightly but the sidelobes on the backside were still too large. They are even larger than the result mentioned in Section 5.2.1. Therefore, the helical part should be modeled as a spiral wire instead of a spiral ribbon. In next section, the helix will be left unchanged, but a circular conducting plate will be added to the bottom of the helibowl.

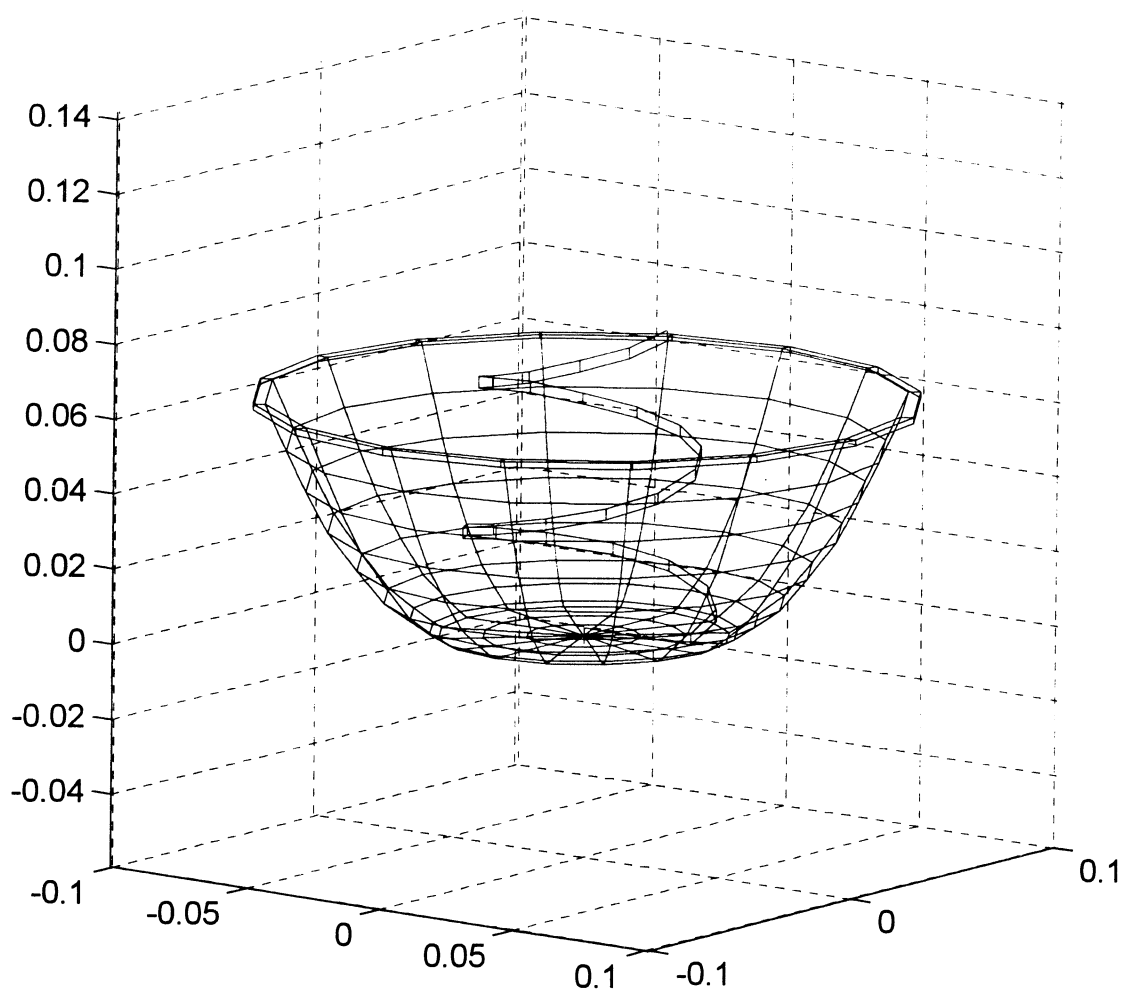


Figure 5.2.26 - Geometry of the wire-grid model for helibowl in
Section 5.2.2, Ribbon Helix

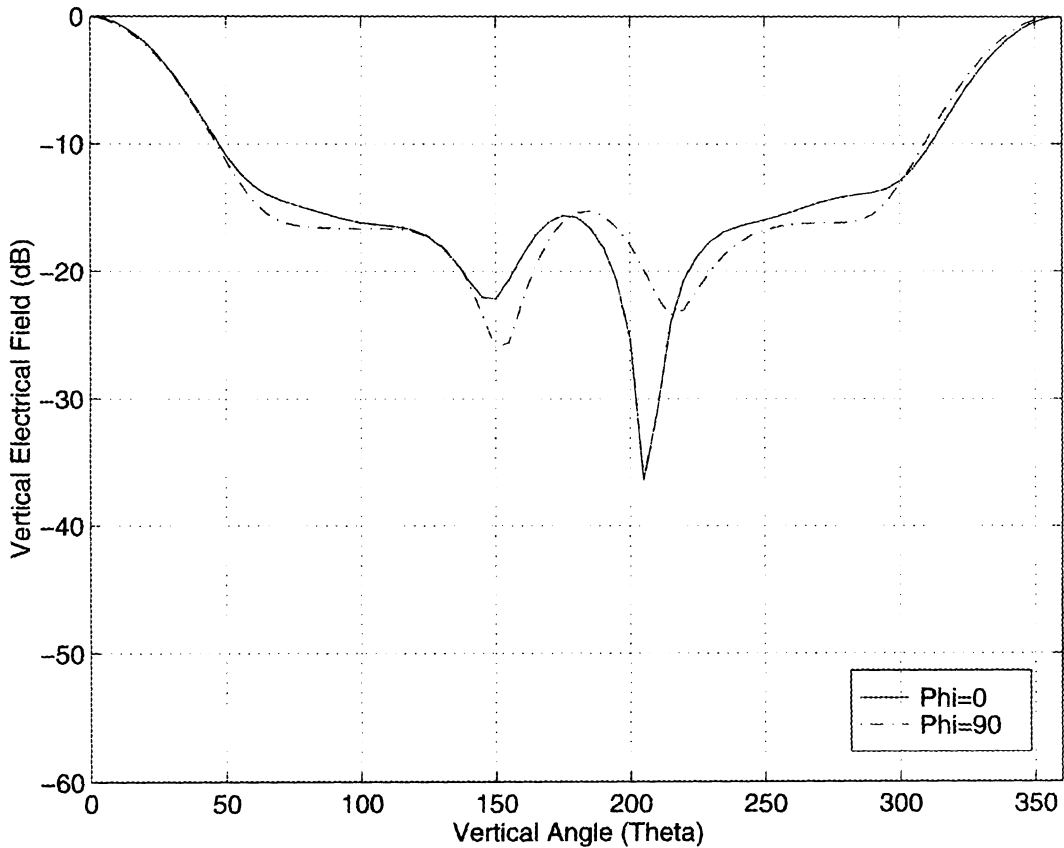


Figure 5.2.27 - Vertical radiation patterns for helibowl model in Section 5.2.2,
Ribbon helix, No circular plate, $\phi = 0^\circ$ and 90° , 1575 MHz

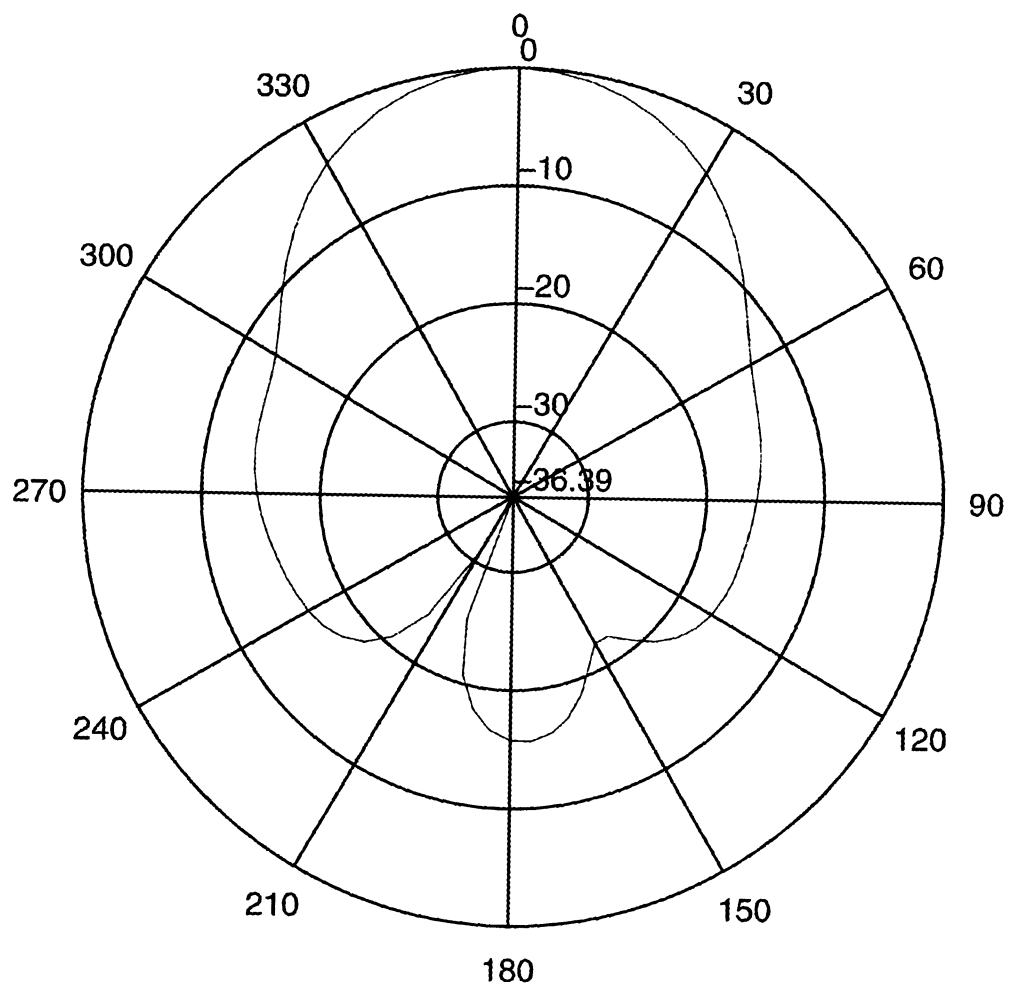


Figure 5.2.28 - Vertical radiation pattern for helibowl model in Section 5.2.2,
Ribbon helix, No circular plate, $\phi = 0^\circ$, 1575 MHz

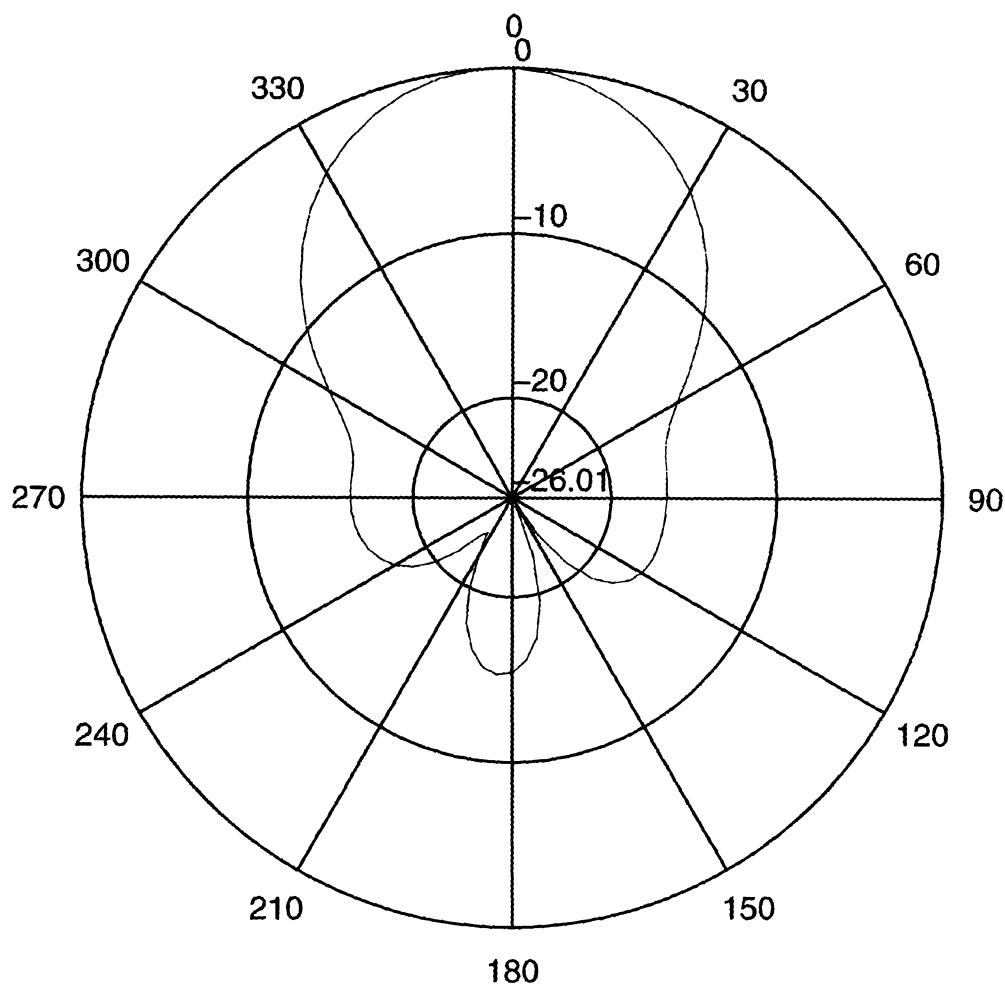


Figure 5.2.29 - Vertical radiation pattern for helibowl model in Section 5.2.2,
Ribbon helix, No circular plate, $\phi = 90^\circ$, 1575 MHz

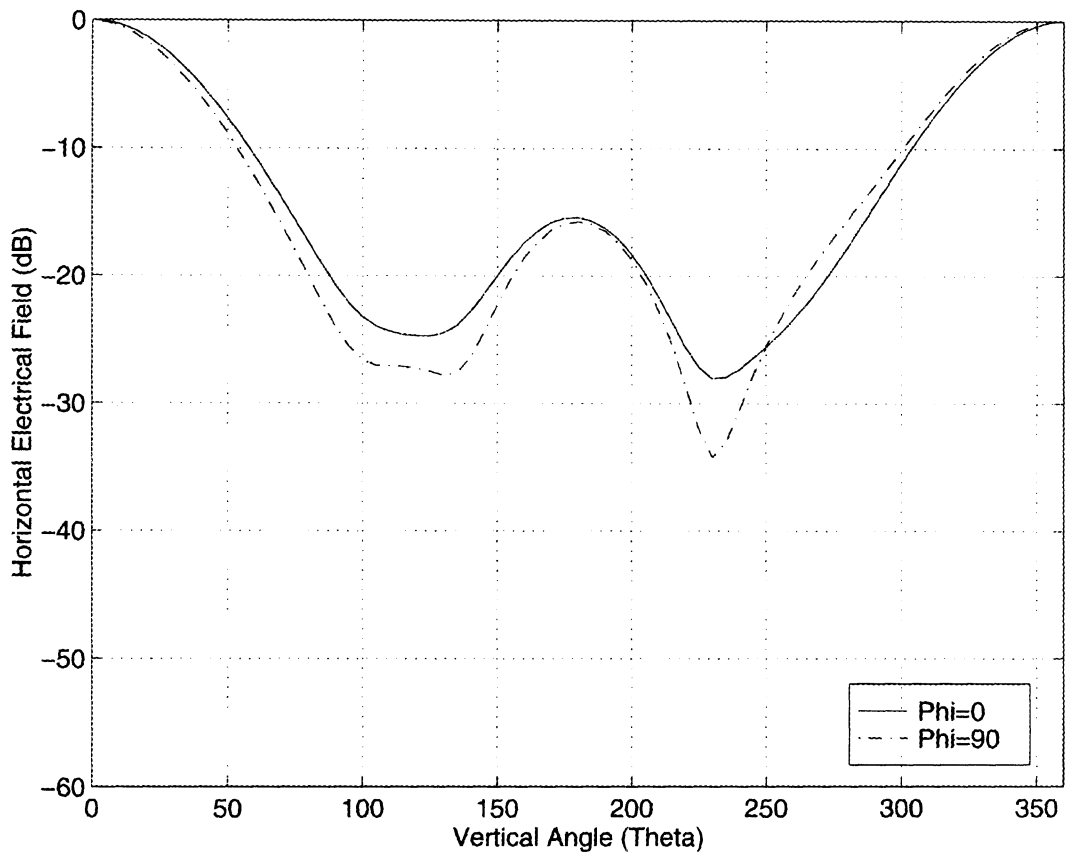


Figure 5.2.30 - Horizontal radiation patterns for helibowl model in Section 5.2.2,
Ribbon helix, No circular plate, $\phi = 0^\circ$ and 90° , 1575 MHz

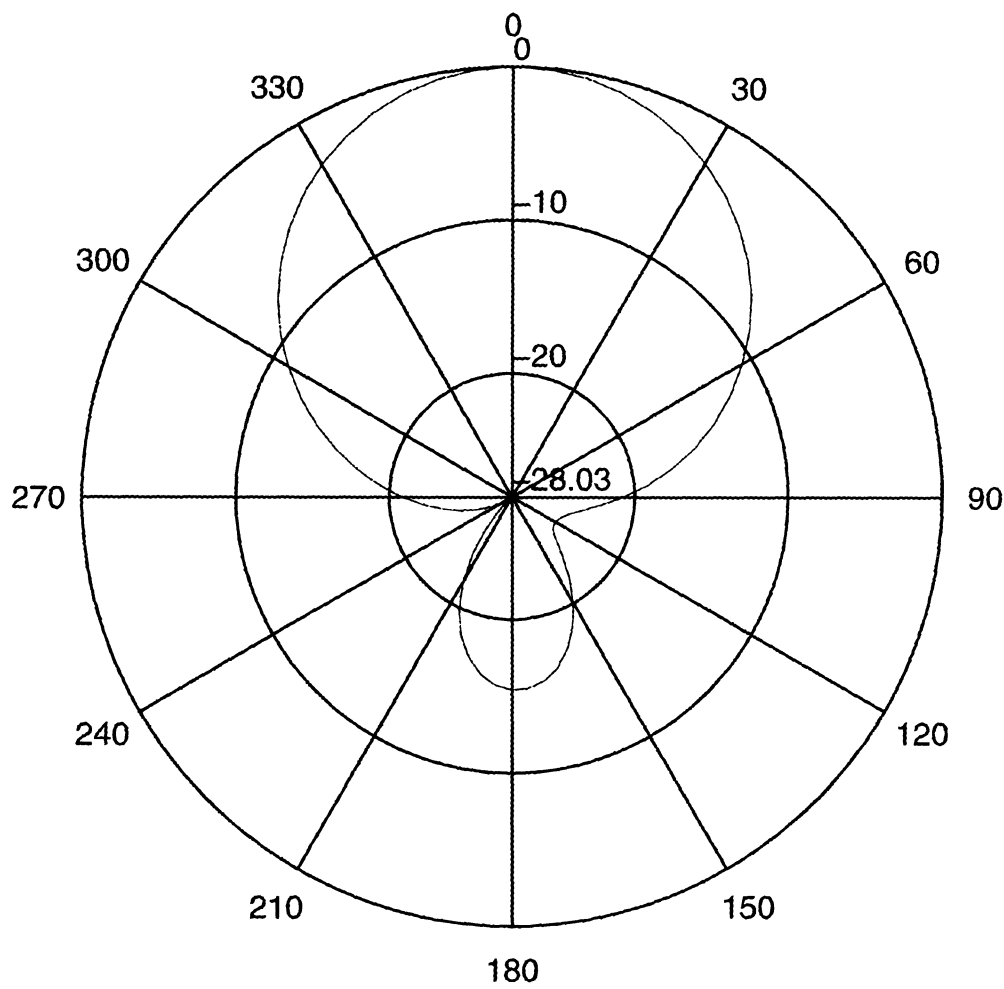


Figure 5.2.31 - Horizontal radiation pattern for helibowl model in Section 5.2.2,
Ribbon helix, No circular plate, $\phi = 0^\circ$, 1575 MHz

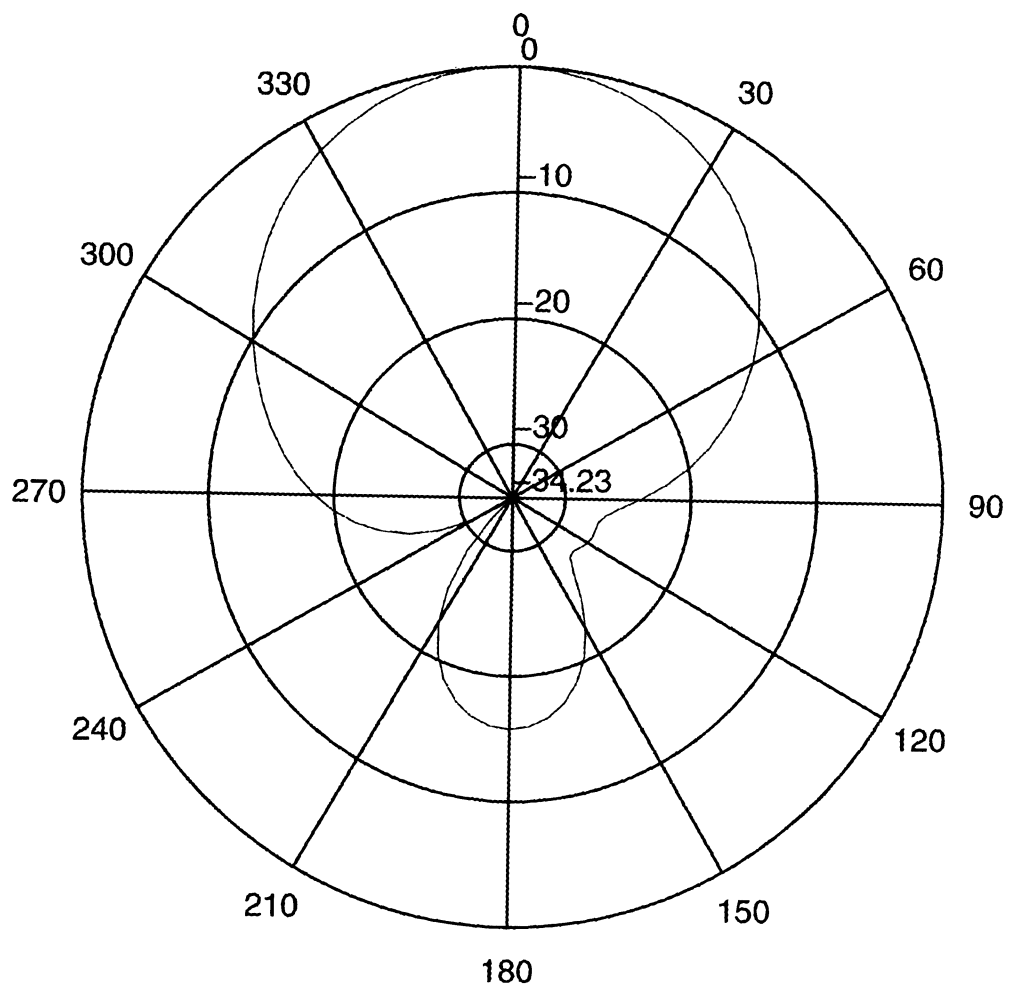


Figure 5.2.32 - Horizontal radiation pattern for helibowl model in Section 5.2.2,
Ribbon helix, No circular plate, $\phi = 90^\circ$, 1575 MHz

5.2.3 Model Three: With the Circular Plate Added

In the previous two sections, the simulation results were not close enough to the measurements. In this section, the circular plate is added to the bottom of the helibowl model. The circular plate is made of aluminum with a diameter of 16.5 inches and a thickness of 1/4 inch. It was inserted in between the helibowl and ground with the distance of 3 inches to the bottom of helibowl. The skeletal frame of model three is shown in Figure 5.2.33. The helibowl remained the same as was in Section 5.2.2.

After the computation from NEC-2, we found the radiation patterns (Figures 5.2.34 - 5.2.39) were dramatically changed. It was found that they match the measured data considerably better. Although, there was 5 dB difference on the backlobe between the simulated data and measured data, it was still within tolerable limits. It must be noted that the measurements themselves are not error-free. Sidelobe measurements 30 dB or more below the main lobe cannot be measured to better than 5 dB of accuracy. Therefore, the simulation results on model three are considered to be acceptable.

Although the wire-grid model is almost as good as the surface patch model when simulating a conducting surface like the bowl reflector, it still shows minor differences. More than one simulation on same models with different sized holes must be performed

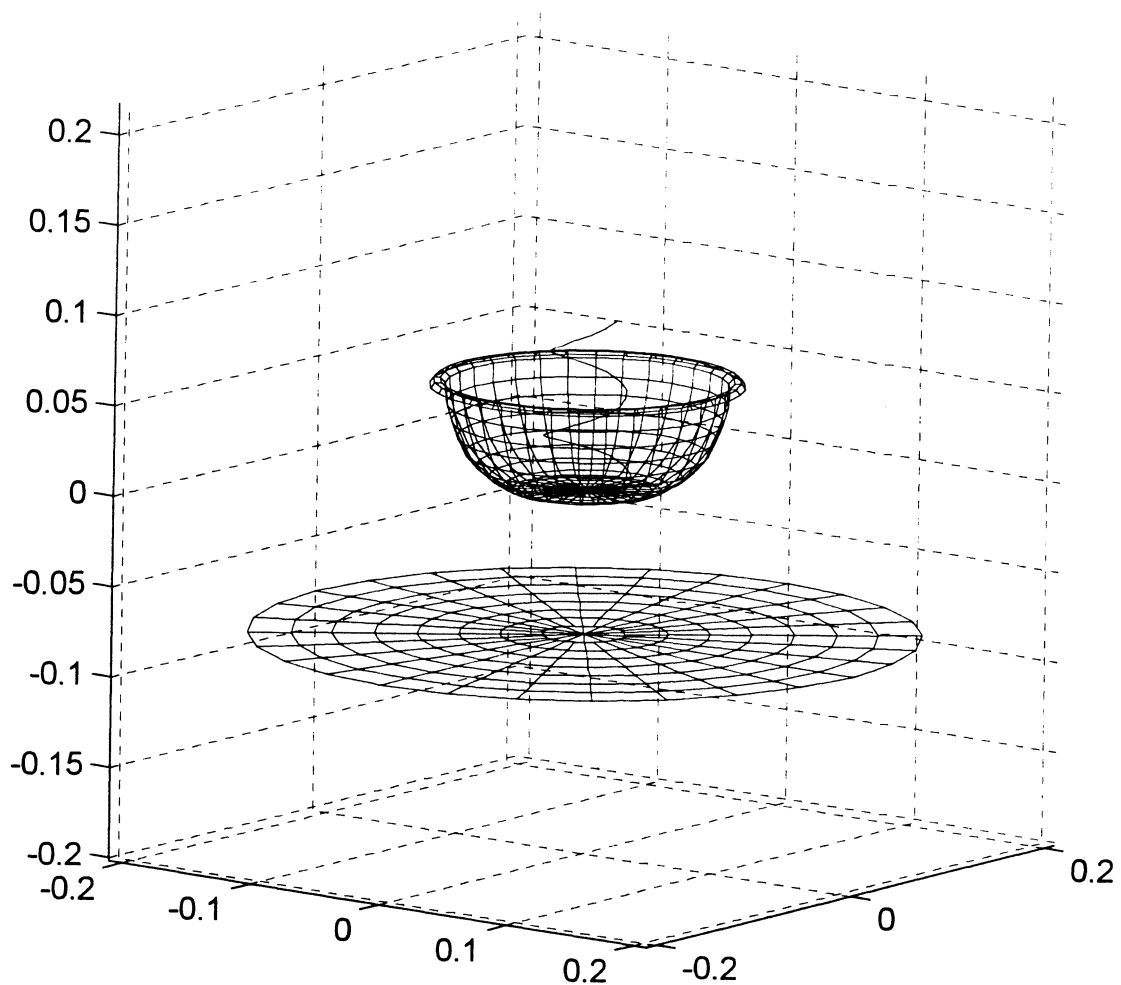


Figure 5.2.33 - Geometry of the wire-grid model for helibowl in
Section 5.2.3, Simple helix, with circular plate

in order to figure out how small the hole has to be. The result indicates that, if the hole on the bottom is opened up wider, the backlobe will become larger. The same fact is applicable to the wire-grid model. The wire-grid model actually has lots of 'holes' on it. The energy which leaks through those holes will boost the backlobe to an even higher level of magnitude. This is at least one significant reason for the 5 dB difference.

To sum up, the numerical electromagnetic codes are meant to be used to anticipate problems at the early stages of antenna design, cost-effectively and efficiently. They will not provide you 100% accuracy and neither will the measurements in the lab. Only through the practical use of many applications, can the antenna's data and pattern be collected and interpreted properly. Even so, the modeling software is still the best tool for information about a specific antenna in its designing stage. Therefore, the goal of this research is now achieved.

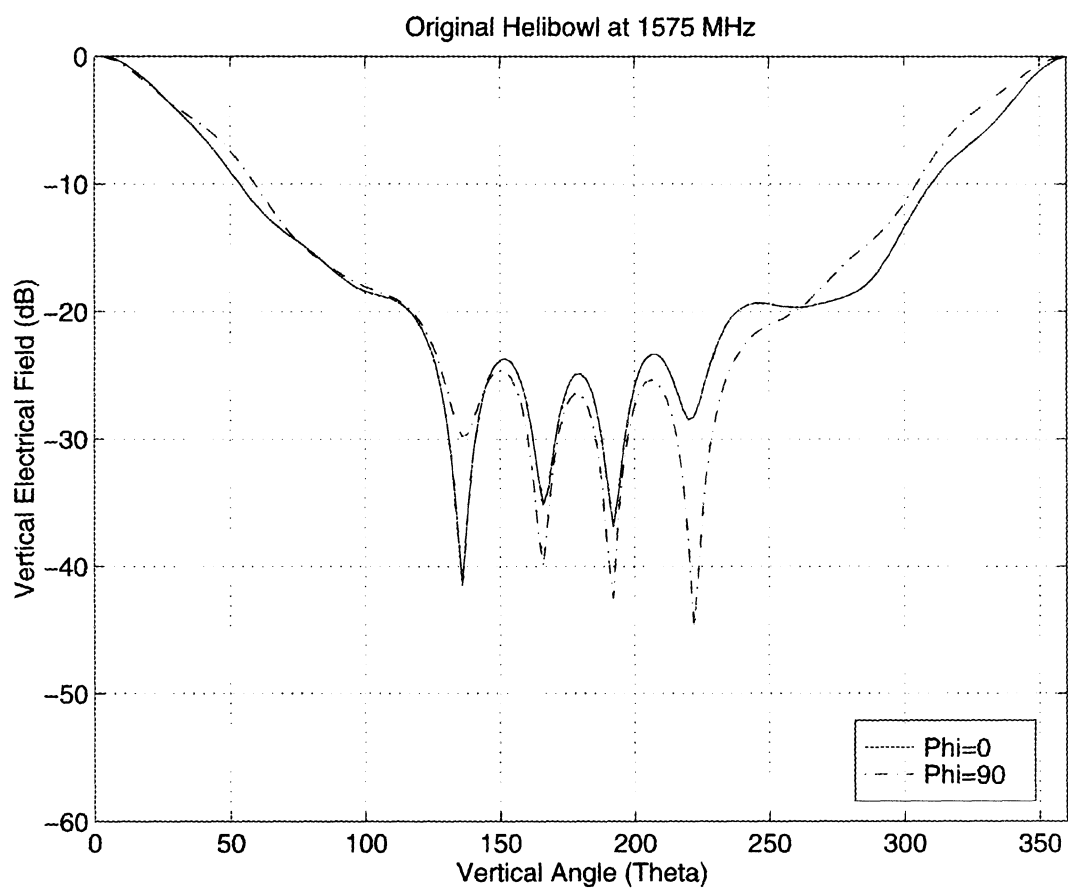


Figure 5.2.34 - Vertical radiation patterns for helibowl model in section 5.2.3,
Simple helix, With circular plate, $\phi = 0^\circ$ and 90° , 1575 MHz

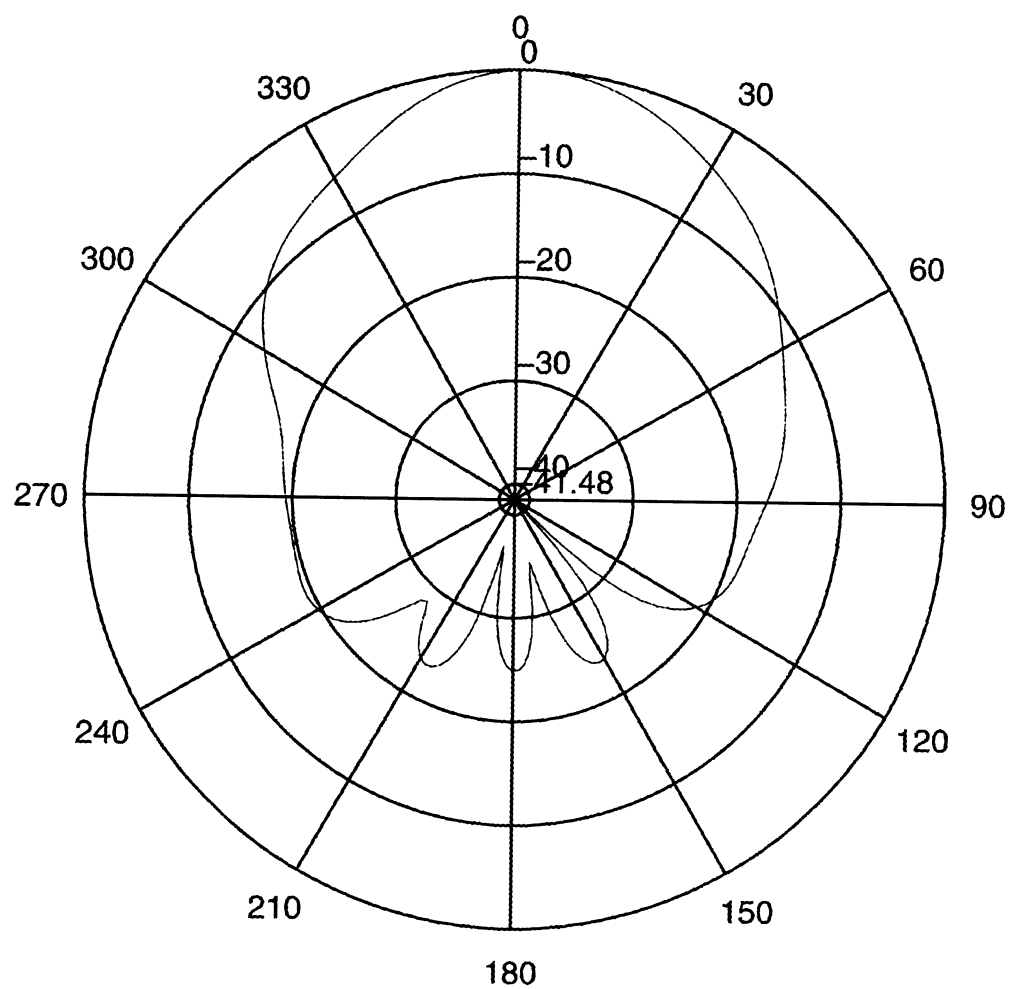


Figure 5.2.35 - Vertical radiation pattern for helibowl model in section 5.2.3,
Simple helix, With circular plate, $\phi = 0^\circ$, 1575 MHz

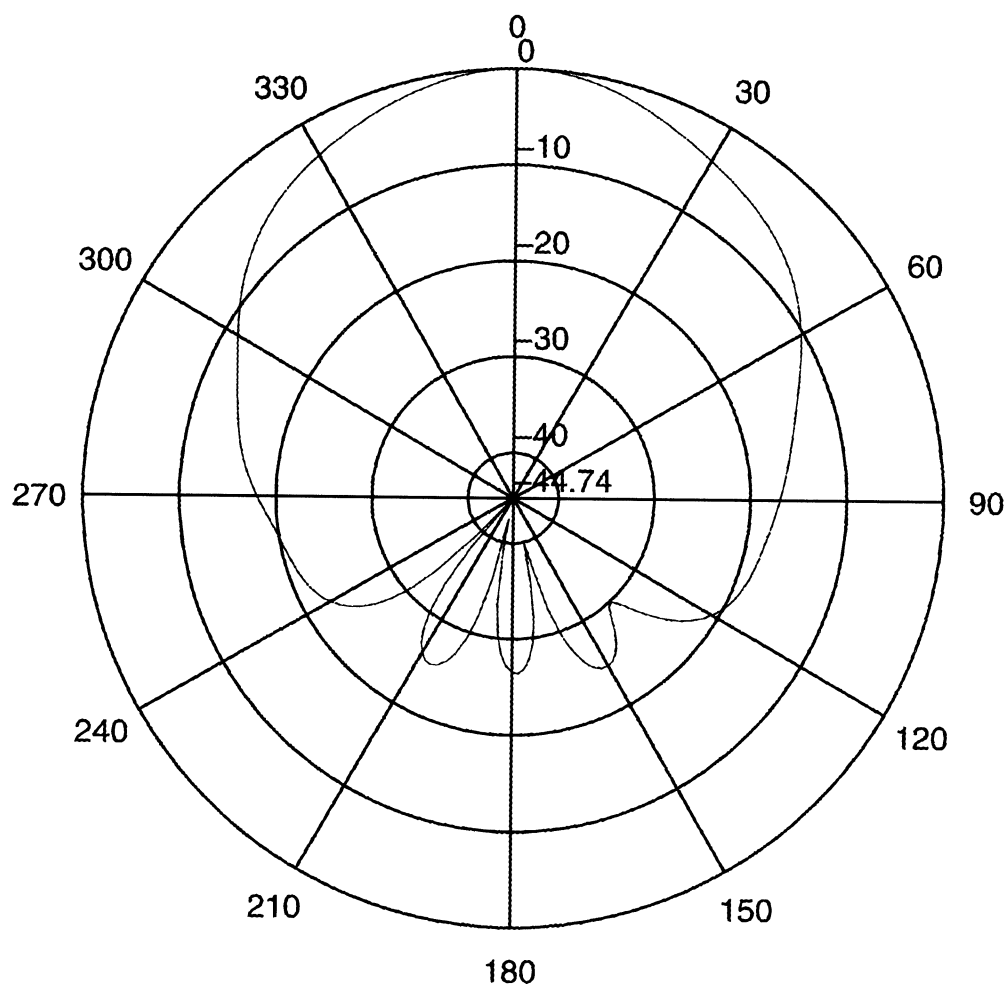


Figure 5.2.36 - Vertical radiation pattern for helibowl model in section 5.2.3,
Simple helix, With circular plate, $\phi = 90^\circ$, 1575 MHz

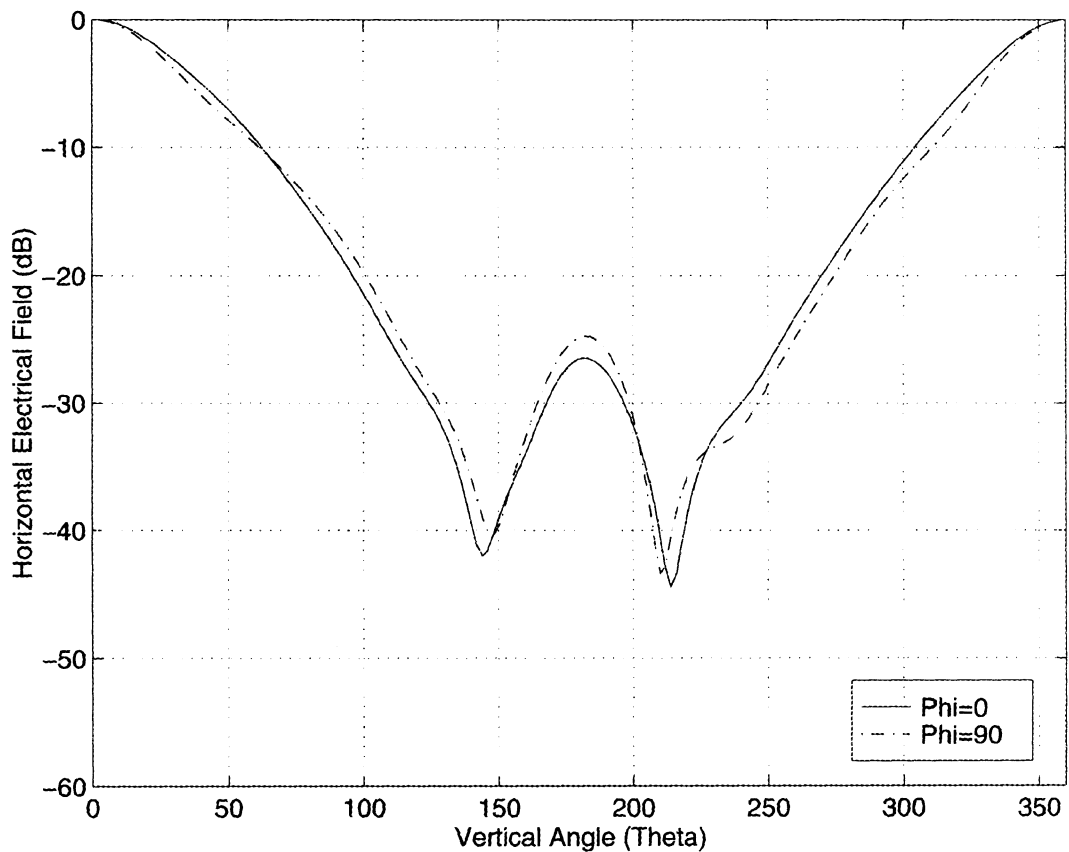


Figure 5.2.37 - Horizontal radiation patterns for helibowl model in section 5.2.3,
Simple helix, With circular plate, $\phi = 0^\circ$ and 90° , 1575 MHz

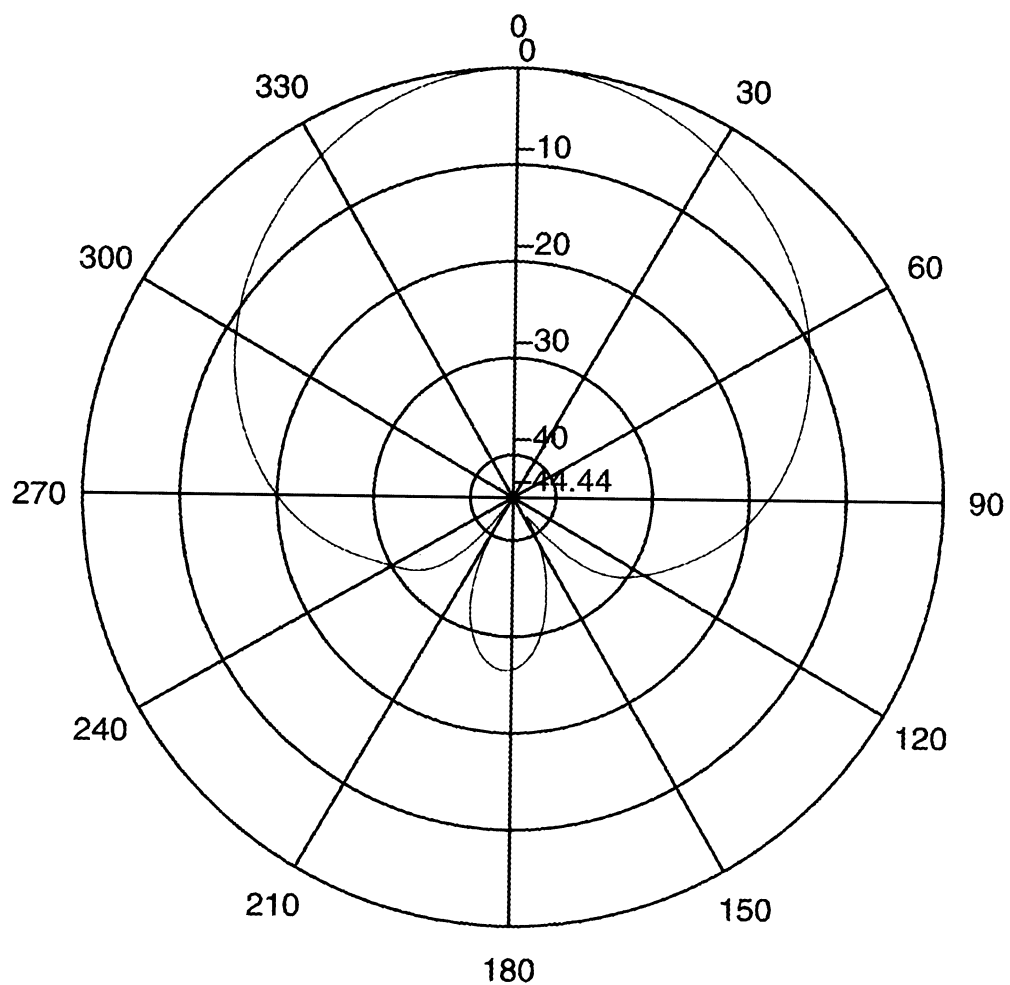


Figure 5.2.38 - Horizontal radiation pattern for helibowl model in section 5.2.3,
Simple helix, With circular plate, $\phi = 0^\circ$, 1575 MHz

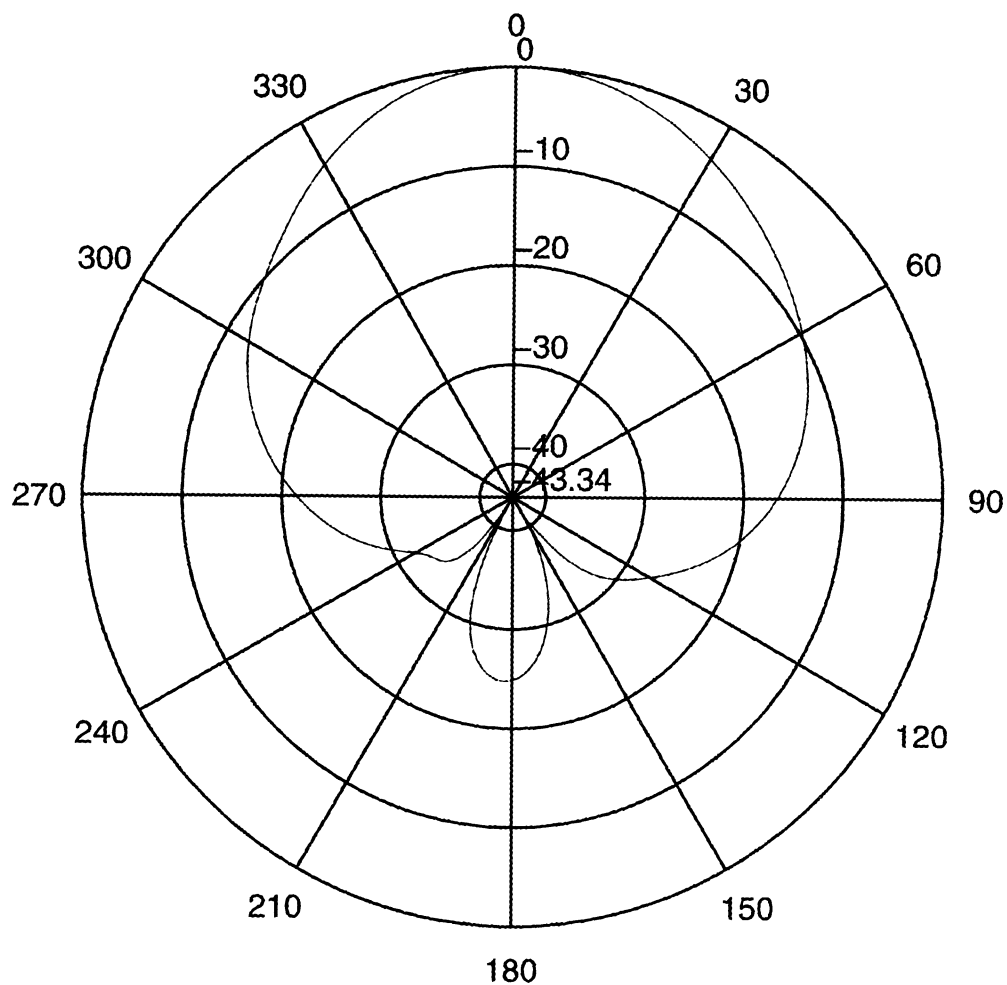


Figure 5.2.39 - Horizontal radiation pattern for helibowl model in section 5.2.3,
Simple helix, With circular plate, $\phi = 90^\circ$, 1575 MHz

5.3 Extensive Simulations on Two Models with Their Shapes Changed

After the helibowl antenna had been successfully modeled, helibowls of different dimensions were modeled by following the same procedure described in the previous sections. However, the goal of this research is to develop a series of procedures to model the helibowl correctly. Simulations on different types of helibowls should not be included in here. But, in order to find out how applicable the modeling method can be, a couple of simulations are necessary.

In this section, two helibowl models will be simulated. The first model is almost the same as the original helibowl except its bowl's size had been doubled (see Figure 5.3.1). By using program 3 listed in Appendix B, a bowl's wire-grid model can be easily created. The second model is the same except the length of the helix had been doubled by adding two turns to it (see Figure 5.3.8). Those radiation patterns for each model are placed right behind Figure 5.3.1 and Figure 5.3.8, respectively.

First of all, it's pretty certain that the modeling method is workable. All models that had been created ran successfully. No error message occurred when the NEC-2 program was calculating the models' radiation patterns. Now, consider the patterns. In the first model, where the bowl was doubled, the beamwidths of both polarization patterns reduced but the reception gain on the backside increased. In the second model, where the helix was doubled in length, the beamwidth of vertical polarization pattern increased but the

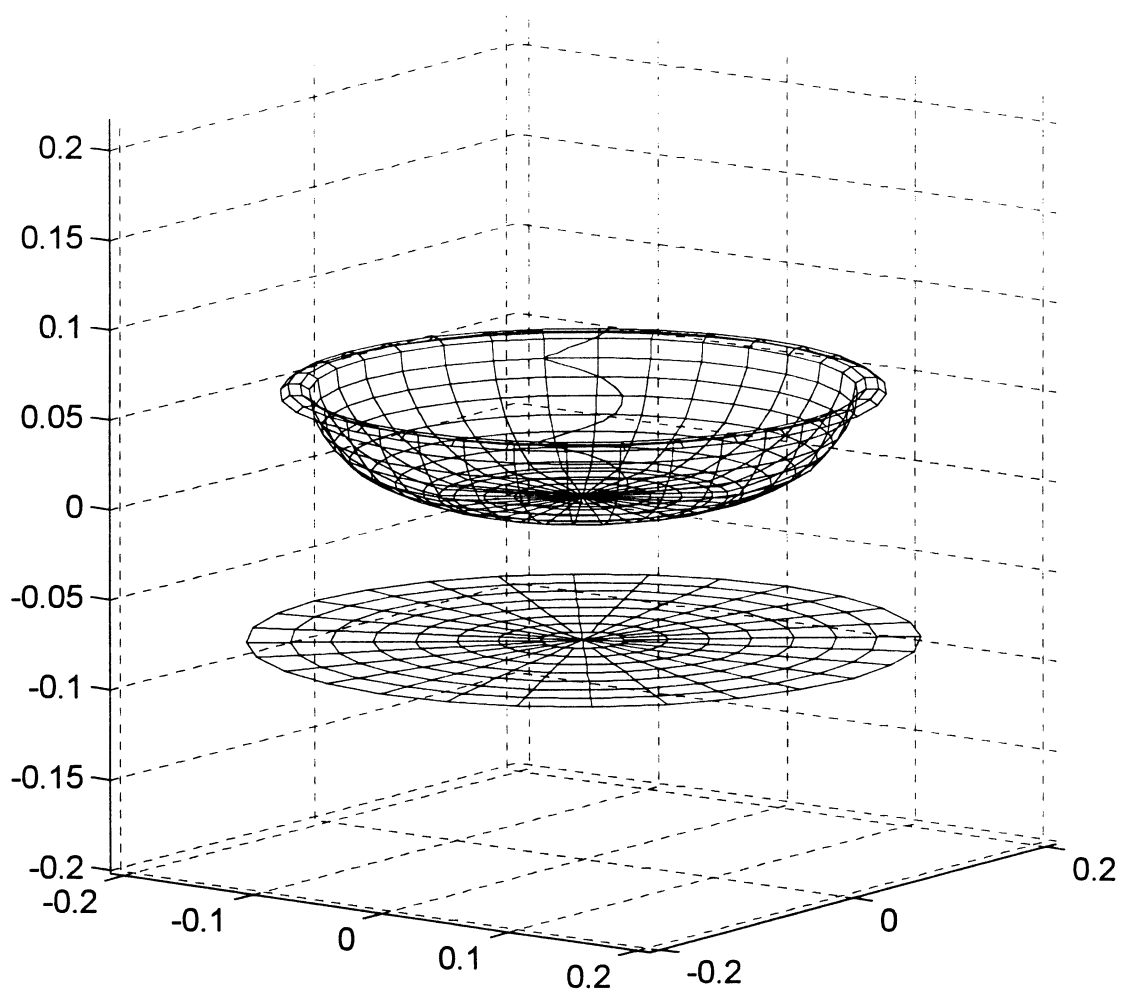


Figure 5.3.1 - Geometry of the wire-grid model for helibowl in
Section 5.3, bowl's size doubled

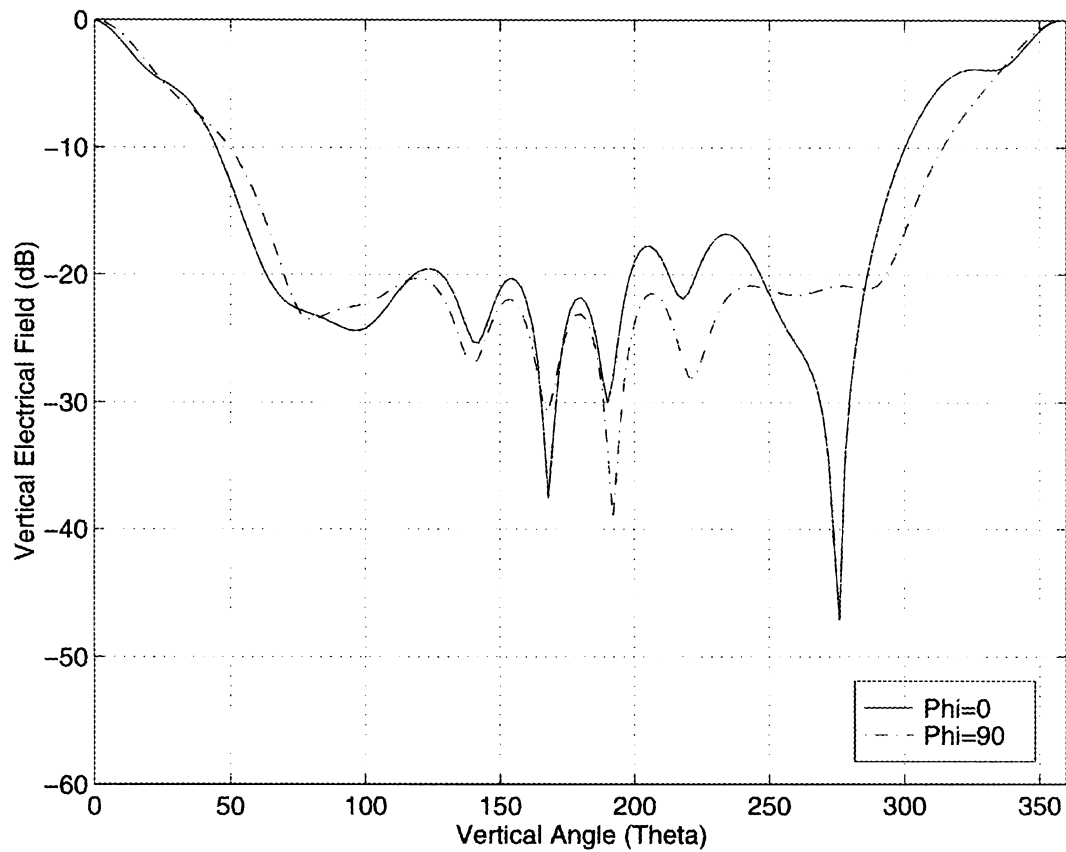


Figure 5.3.2 - Vertical radiation patterns for helibowl model in Section 5.3,
Bowl's diameter doubled, $\phi = 0^\circ$ and 90° , 1575 MHz

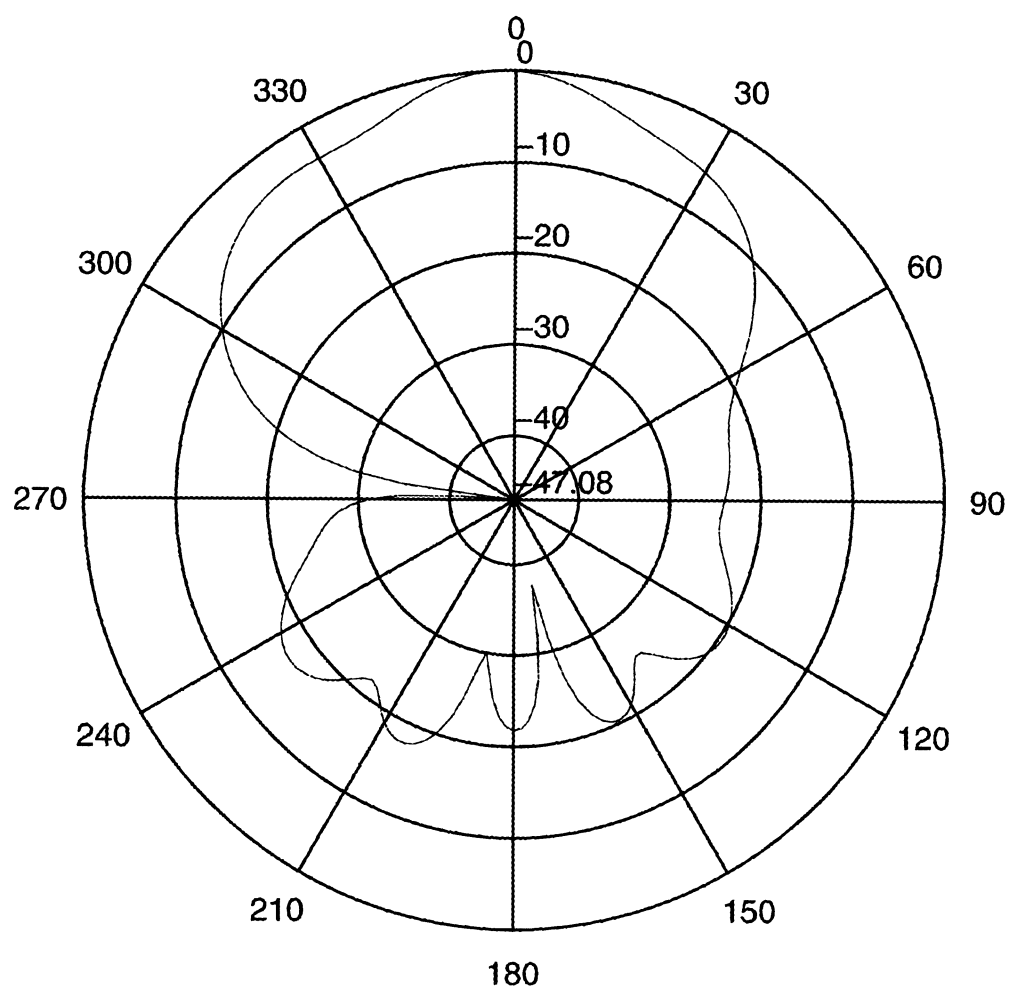


Figure 5.3.3 - Vertical radiation pattern for helibowl model in Section 5.3,
Bowl's diameter doubled, $\phi = 0^\circ$, 1575 MHz

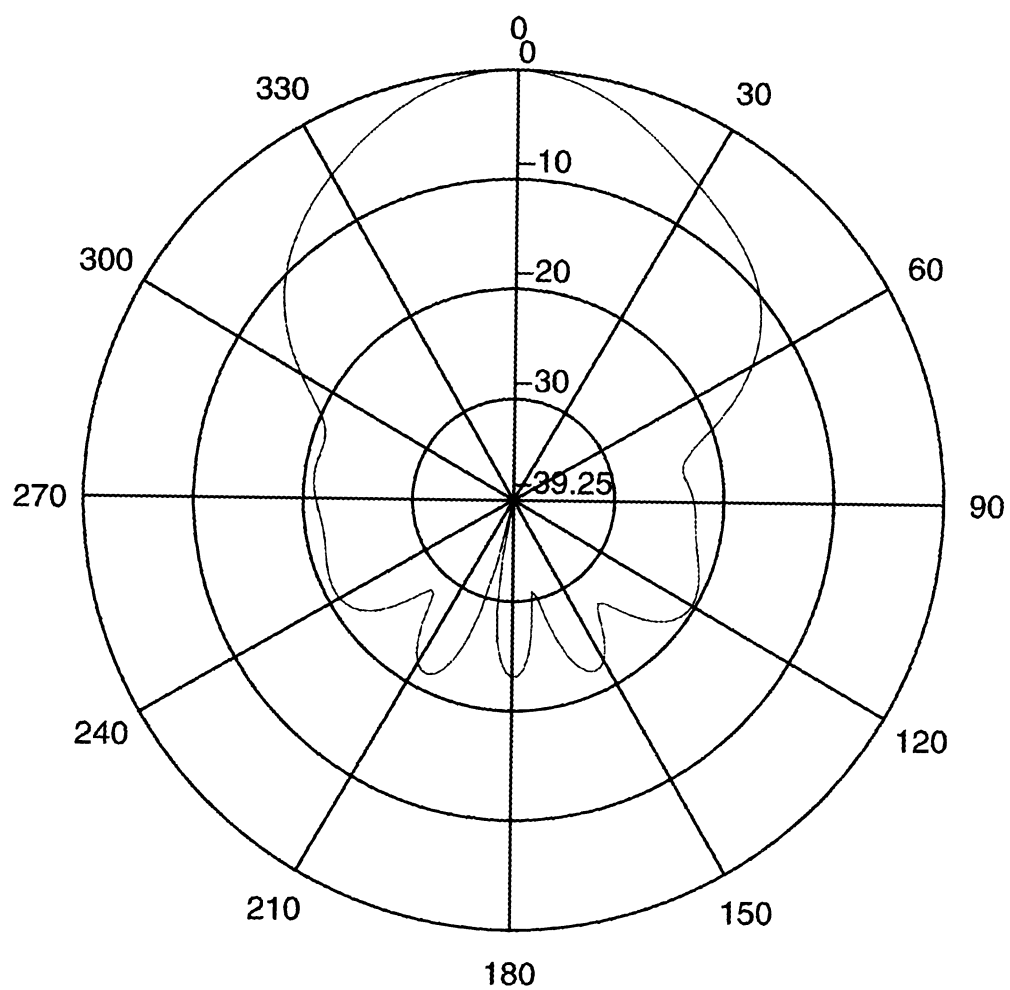


Figure 5.3.4 - Vertical radiation pattern for helibowl model in Section 5.3,
Bowl's diameter doubled, $\phi = 90^\circ$, 1575 MHz

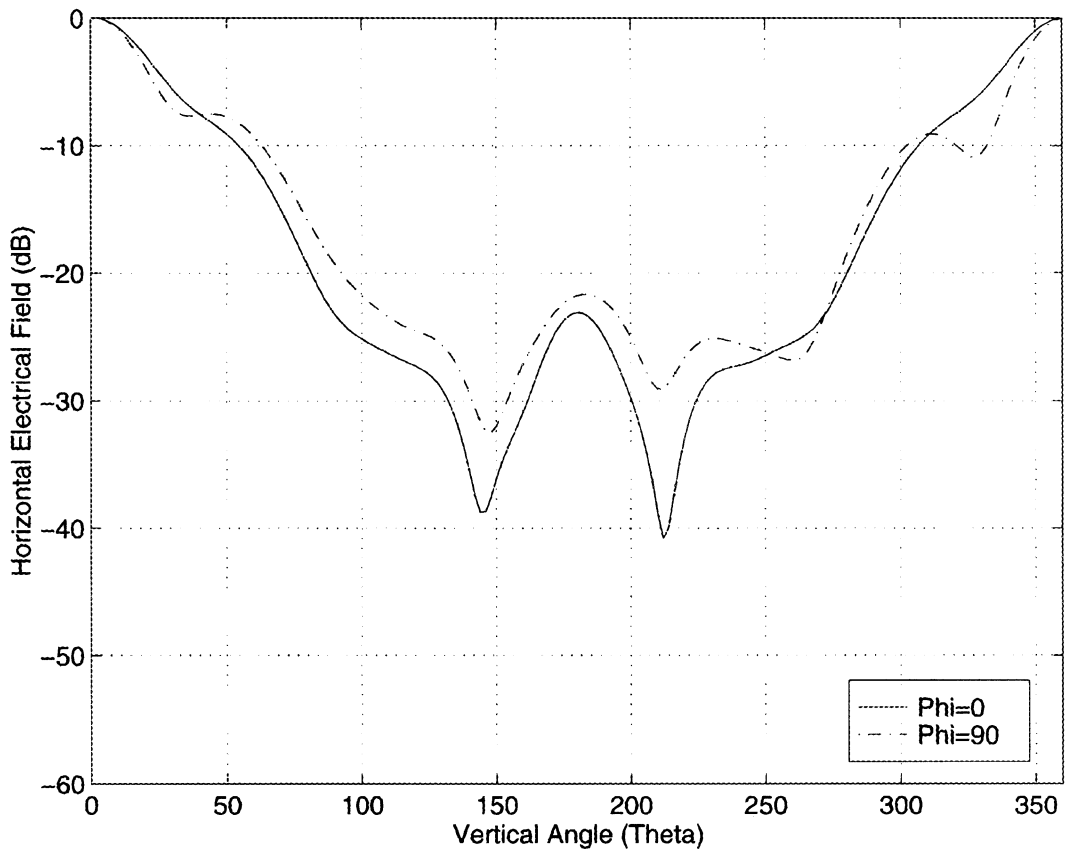


Figure 5.3.5 - Horizontal radiation patterns for helibowl model in Section 5.3,
Bowl's diameter doubled, $\phi = 0^\circ$ and 90° , 1575 MHz

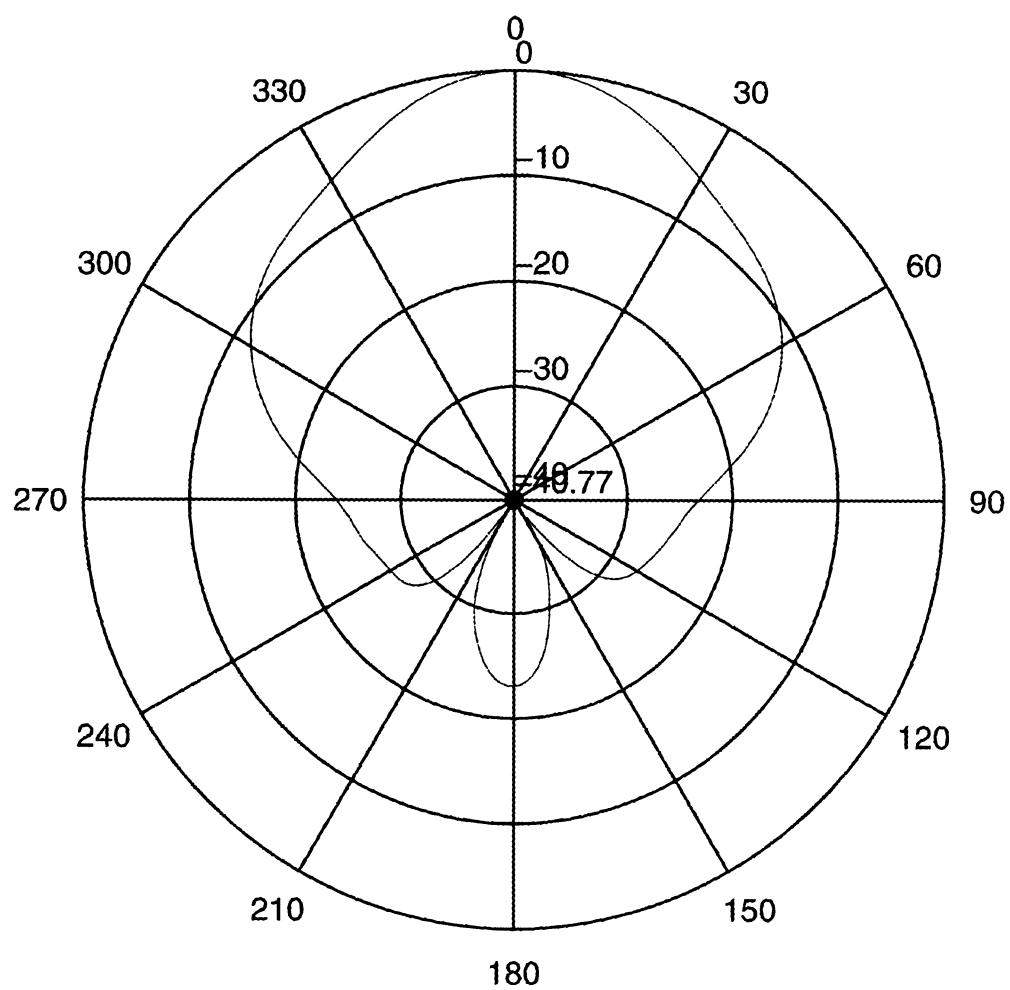


Figure 5.3.6 - Horizontal radiation pattern for helibowl model in Section 5.3,
Bowl's diameter doubled, $\phi = 0^\circ$, 1575 MHz

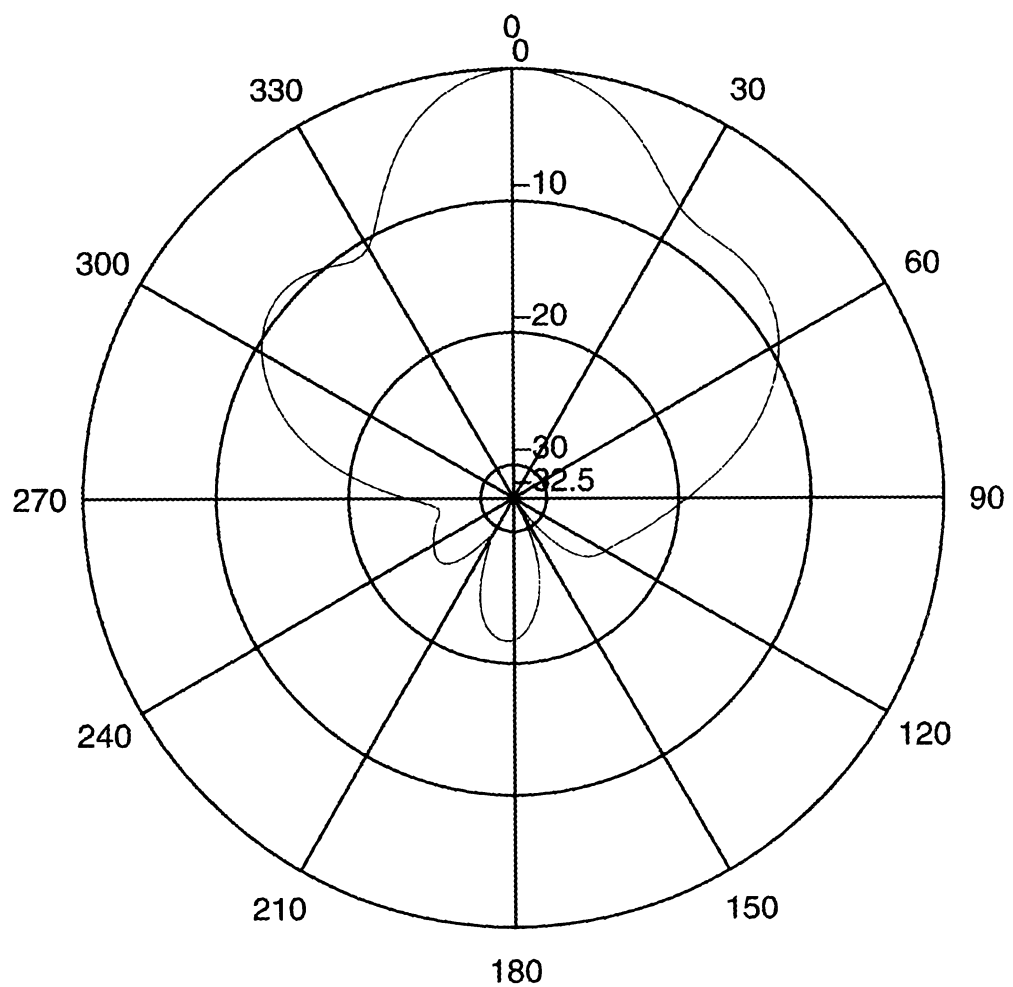


Figure 5.3.7 - Horizontal radiation pattern for helibowl model in Section 5.3,
Bowl's diameter doubled, $\phi = 90^\circ$, 1575 MHz

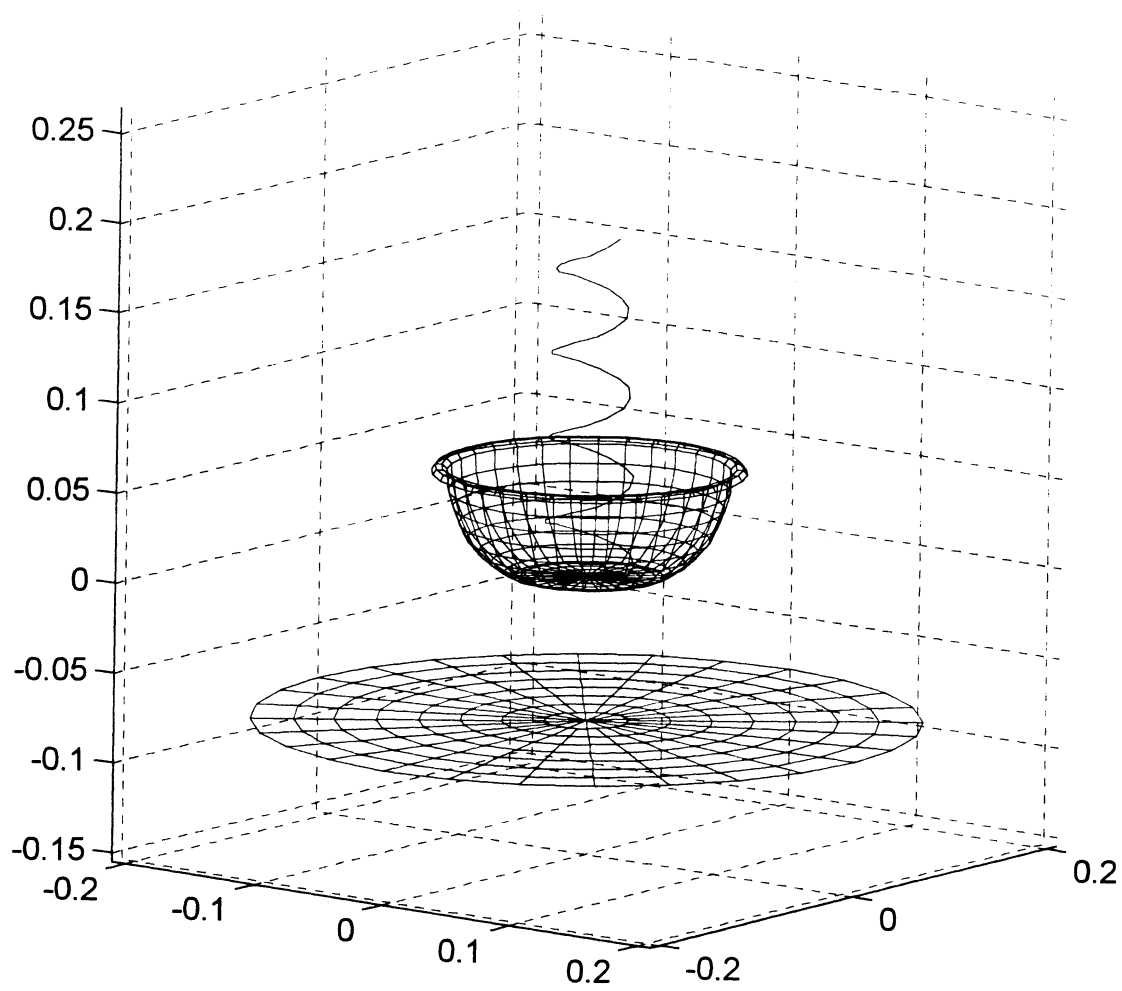


Figure 5.3.8 - Geometry of the wire-grid model for helibowl in
Section 5.3, Length of the helix doubled

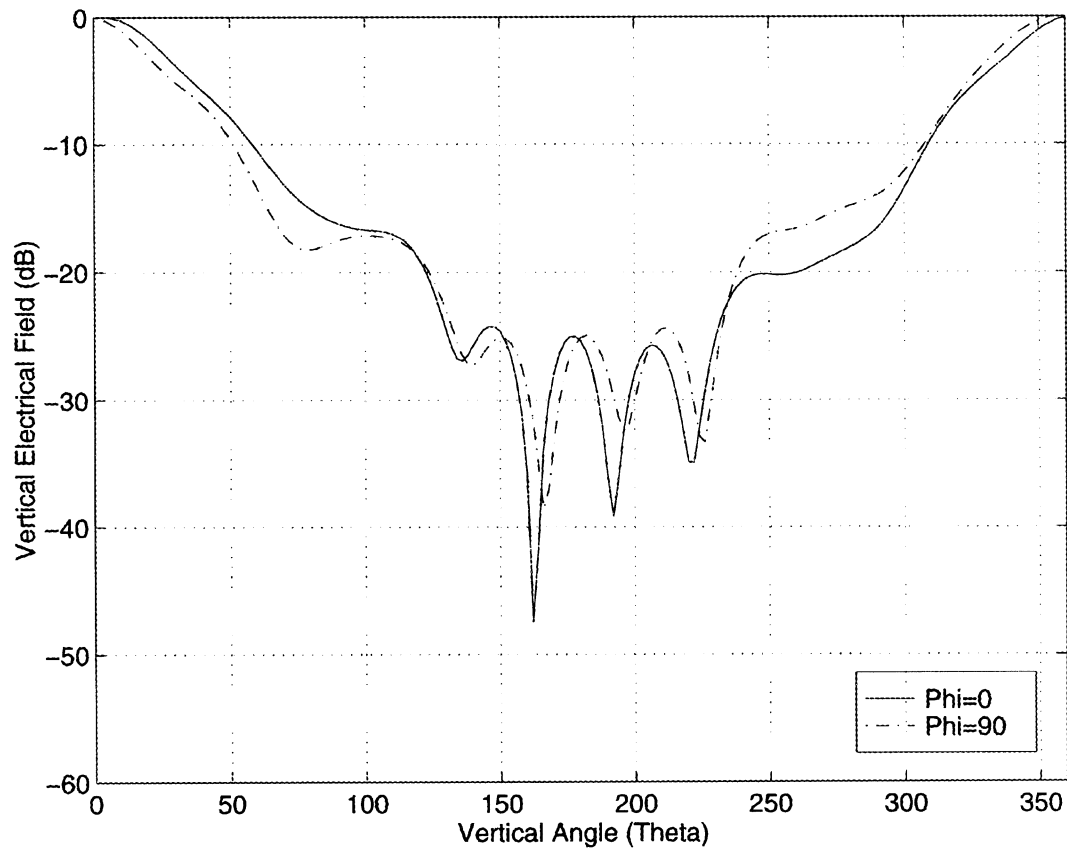


Figure 5.3.9 - Vertical radiation patterns for helibowl model in Section 5.3,
Length of the helix doubled, $\phi = 0^\circ$ and 90° , 1575 MHz

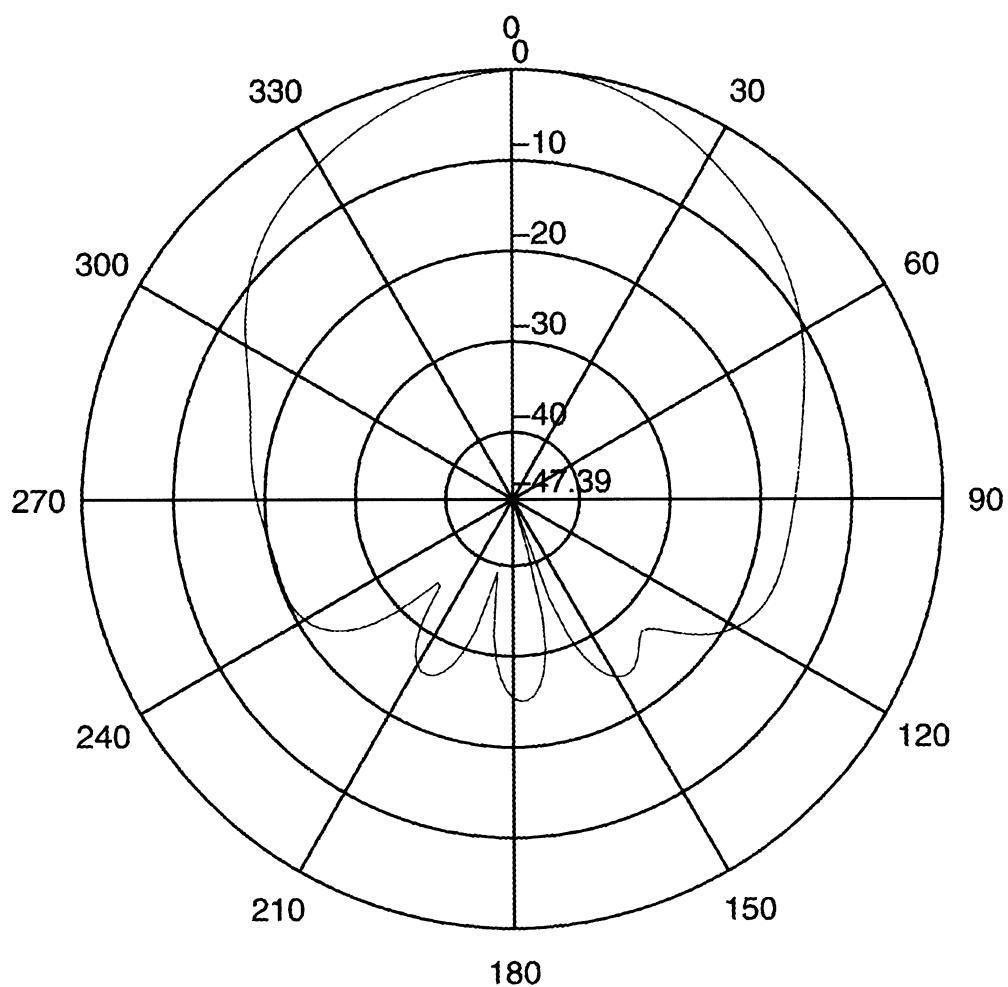


Figure 5.3.10 - Vertical radiation pattern for helibowl model in Section 5.3,
Length of the helix doubled, $\phi = 0^\circ$, 1575 MHz

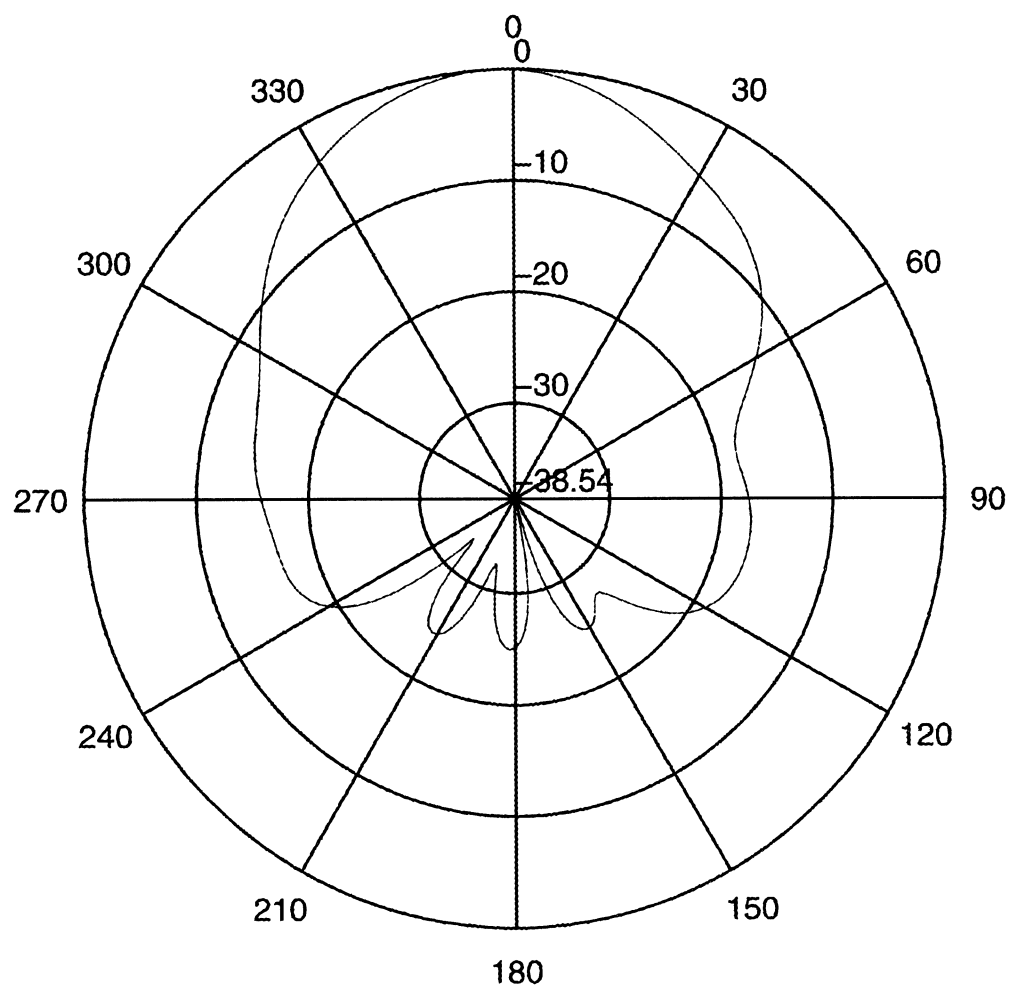


Figure 5.3.11 - Vertical radiation pattern for helibowl model in Section 5.3,
Length of the helix doubled, $\phi = 90^\circ$, 1575 MHz

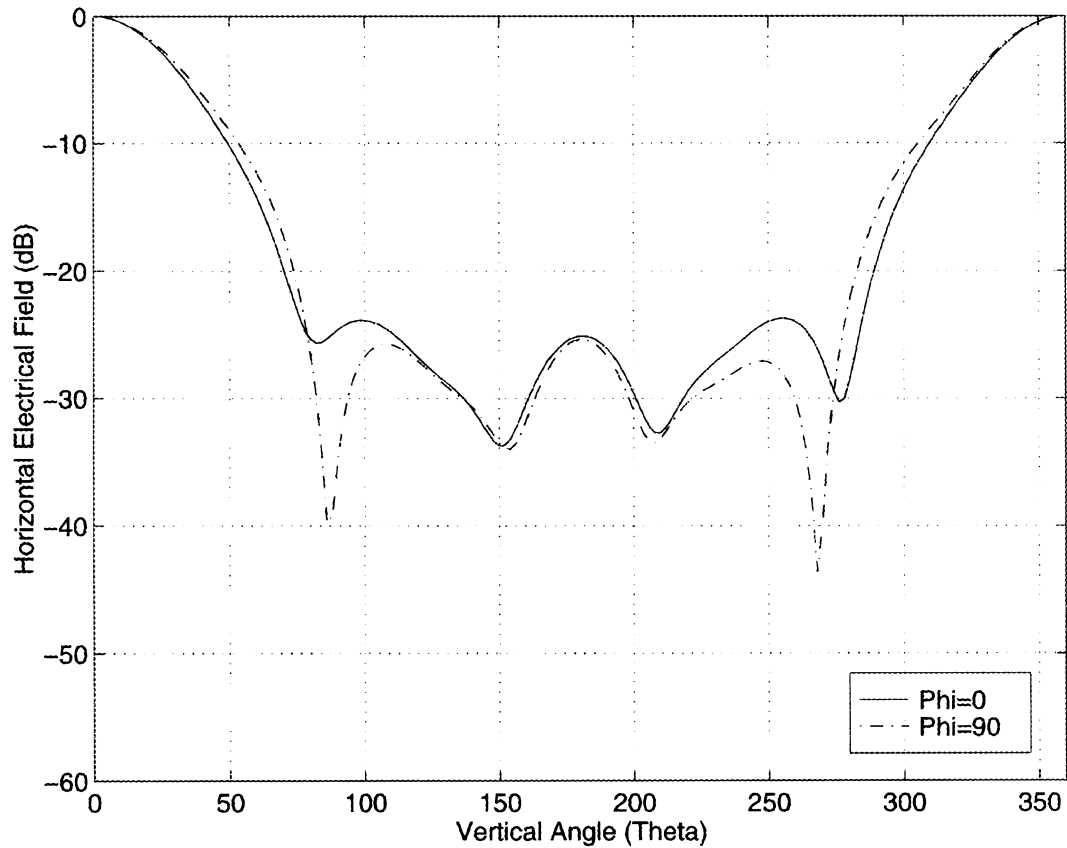


Figure 5.3.12 - Horizontal radiation patterns for helibowl model in Section 5.3,
Length of the helix doubled, $\phi = 0^\circ$ and 90° , 1575 MHz

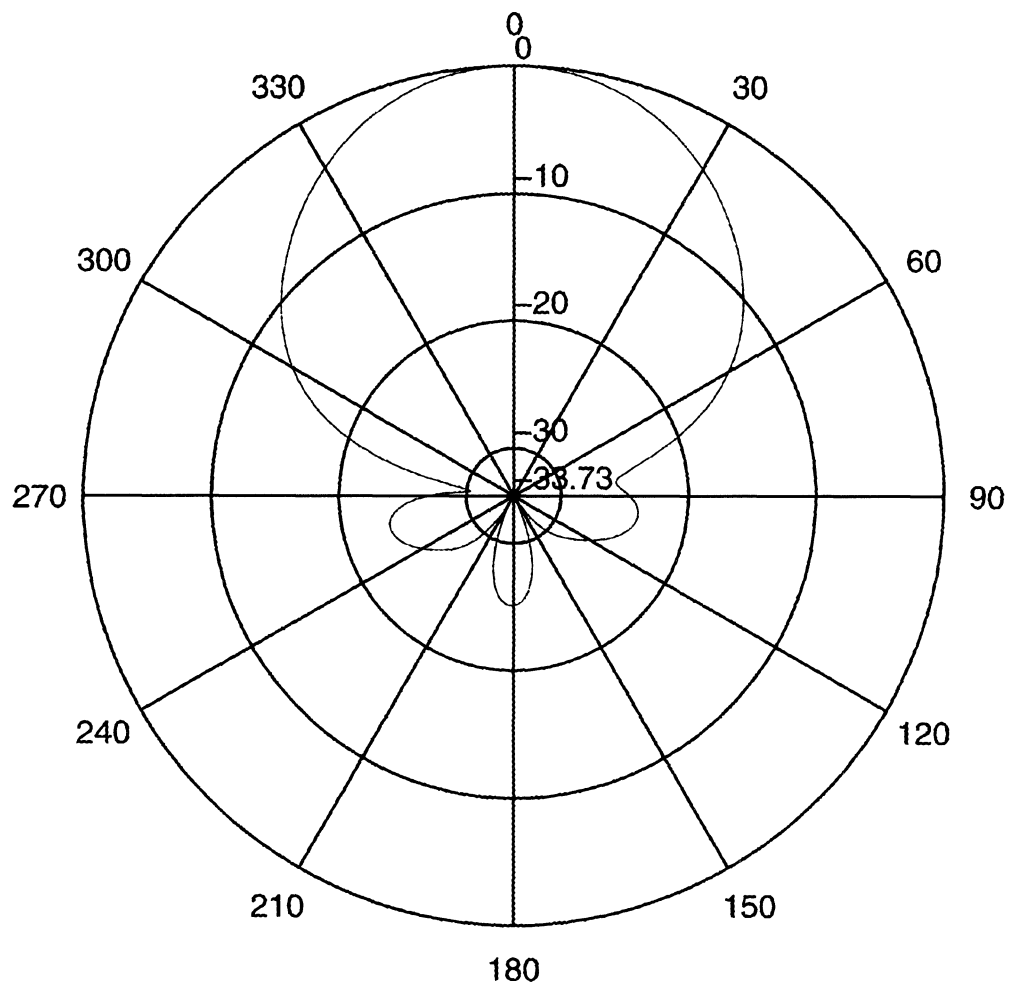


Figure 5.3.13 - Horizontal radiation pattern for helibowl model in Section 5.3,
Length of the helix doubled, $\phi = 0^\circ$, 1575 MHz

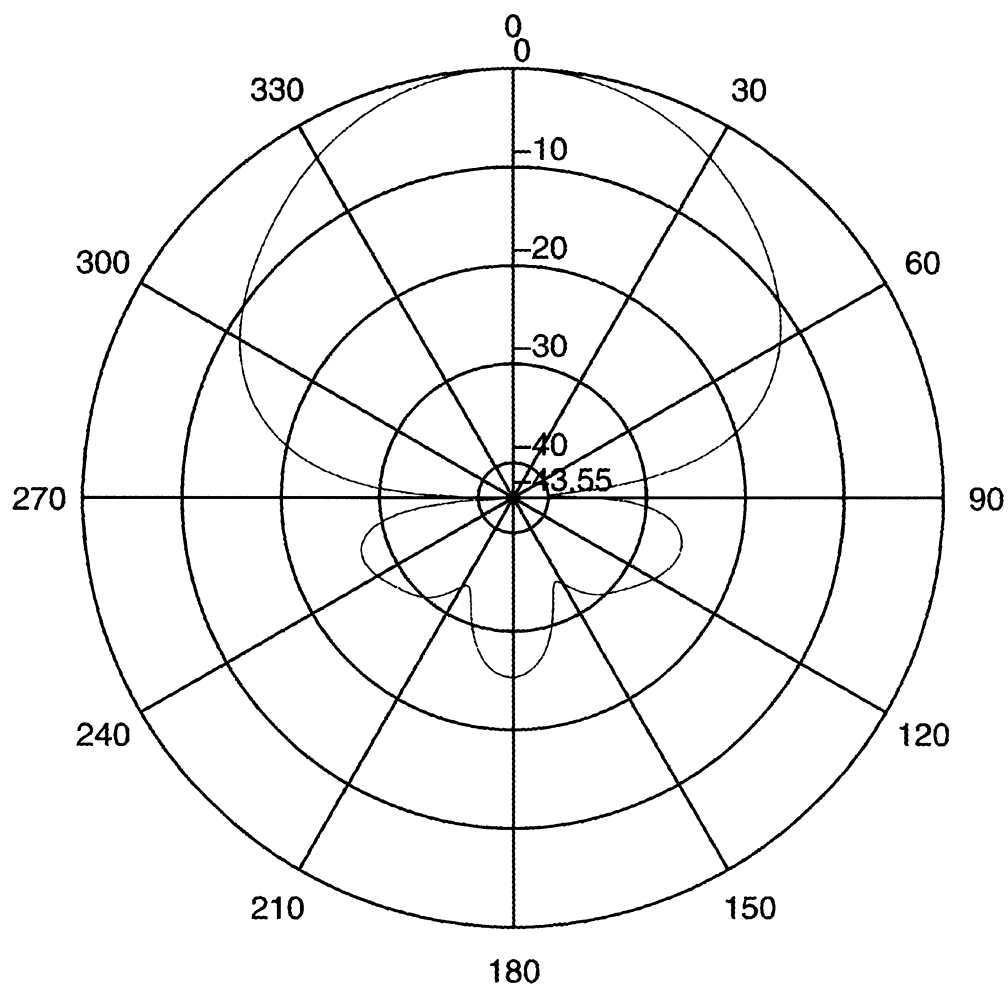


Figure 5.3.14 - Horizontal radiation pattern for helibowl model in Section 5.3,
Length of the helix doubled, $\phi = 90^\circ$, 1575 MHz

beamwidth of horizontal polarization pattern and the backlobe's reception gain decreased. This means that the change on the size of helix could probably affect the radiation patterns and the reception gain in a certain way. Changing the size of bowl may cause the helibowl to become inoperable on the GPS application. This is because GPS signal is a right-hand circular polarized signal. The axial ratio (AR) has to be roughly equal to one.

According to [25], in order to work under the circular polarization condition, the design of helical radiator has to comply with the Equation (5.3.1):

$$\pi D = \sqrt{2S\lambda} \quad (5.3.1)$$

where,

D : The diameter of the helix

S : The space between turns

λ : The wavelength of target signal

When Spitzmesser [20] first designed the helibowl, he wanted to develop a helibowl that could be used on both GPS L1 (1575.42 MHz) and L2 (1227.6 MHz) bands. That's why he created a helibowl with a tapered helical radiator. In the same manner, those factors can be swapped around to see how they would improve the performance of an antenna.

Chapter 6

Conclusion and Recommendations

6.1 Conclusion

In this research paper, the multipath effect and the adopted strategies to fight the multipath were discussed. However, the first line of defense in mitigating multipath, the antenna, has never been fully studied. In order to improve the reception and cut off the multipath effectively, research on analyzing the GPS antenna is necessary. Among many GPS antennas, the helibowl antenna is very suitable for rejecting multipath. Just as predicted, it has near perfect receiving gain above the horizon and good rejection below the horizon. Based on the same idea, an optimum helibowls can be designed to meet DGPS ground reference station requirements.

The quest to find a perfect multipath-rejecting antenna is based on how well the antenna can be simulated. The research goal was to find an acceptable procedure to model the helibowl antenna and analyze it. In Chapter 5, it was certified that the result obtained through the simulation was correct. In addition, it was proved that the modeling approach could correctly analyze the helibowl. The same method can be applied to other helibowl cases.

Besides the simulation of the known helibowl, other helibowls of different shapes were also modeled. Below is the conclusions:

First, if the bowl's opening is enlarged to twice the size, the beamwidth for both vertical and horizontal polarization is decreased but the reception gain of the backlobe is increased. However, if the length of the helix is doubled by adding two turns to it, the beamwidth of vertical polarization grows but the beamwidth of horizontal polarization and the reception gain of the backlobe are decreased. That means it is not possible to design the optimum helibowl antenna by only changing the bowl's size or the length of helix. Both must be changed simultaneously to find out what kind of helibowl to design.

Please refer to Figures 5.3.1 - 5.3.14 to see the geometry of these two helibowls and how the shape of helibowl is related to the radiation pattern. Those patterns of total fields for models in this section and Section 5.2.3 are shown in Appendix E.

One thing is to be pointed out here. Why can the helical radiator not be simply pulled up to add some lengths to it? Why must two turns be added to the helix, in order to increase its total length? The reason is obvious. DGPS signal is the right-hand polarized signal at GPS L1 band (1575.42 MHz). In order to maintain a better reception, the gap between each turn on the helix must remain approximately the same. Otherwise, the antenna will not be used favorably.

6.2 Recommendations for Future Work

During the period of this research, electromagnetic modeling improvements were discovered. First of all, as was mentioned in Section 5.2, the NEC-2 program for IBM PC has limited total number of wire segments. It is not convenient for large objects at a very high frequency. That's because, at a very high frequency, the largest length of wire segment that meets the criterion for better accuracy will become even smaller. That means more wire segments are needed to build the model. If the target object is bigger, more wire segments are needed to implement the model, too. Hence, the PC version of NEC-2 in public domain will not be sufficient. Fortunately, the NEC-2's source code is open for everybody's use. The barrier can be broken by downloading it over the internet and compiling it onto any platform. The problem of insufficient segment numbers thus can be solved.

Second, the NEC-2 program can only handle the first scattering problem. However, for the helibowl, there are two reflectors, one bowl one circular plate. The induced current on the bowl produced by the radiator (i.e., the helix) will generate a field that illuminates again on the circular plate. The second scattering field can be ignored assuming that it is very weak.

The last thing to mention is about the availability of electromagnetic software. The NEC program has many different versions. The current released version is NEC-4. It solves some computational issues and gives more accuracy. It will improve simulation results significantly. In addition, the surface patch modeling program can be used to deal with surface objects (e.g., the bowl and circular plate). Surface patch software like the Electromagnetics Surface Patch code (ESP) [23] and Triangular Surface Patch code [11] [24] yield better calculation results than wire-grid software. Although it is more difficult to apply than the wire-grid method, it will improve simulation results.

References

1. Braasch, M., "Isolation of GPS multipath and receiver Tracking Errors", NAVIGATION: Journal of the Institute of Navigation, Vol. 41, No. 4, Winter 1994-1995.
2. Van Graas, F., et al., "Ohio University/FAA Flight Test Demonstration Results of the Local Area Augmentation System (LAAS)," Proceedings of ION GPS-97, Kansas City, MO, Sept. 1997, pp. 1623-1629.
3. Braasch, M., "Optimum Antenna Design for DGPS Ground Reference Stations," Proceedings of ION GPS-94, Salt Lake City, UT, Sept. 1994, pp. 1291-1297.
4. Braasch, M., "Multipath Effects," Chapter 14, Global Positioning Systems: Theory and Applications, Vol. I, American Institute of Aeronautics and Astronautics, Washington D.C., 1996, pp. 547-568.
5. Kanekal, S., "Spread Spectrum Multipath Mitigation Studies," M.S.E.E. thesis, Ohio University, Athens Ohio, August 1998.
6. Kaplan, E. D., Understanding GPS: Principles and Applications, Artech House Publishers, Boston, 1996, pp. 256-260.
7. ibid., pp. 218-219.

8. Burke, G. J. and A. J. Poggio, Numerical Electromagnetics Code (NEC) - Method of Moments, part III: User's Guide, Lawrence Livermore National Laboratory, January 1981, p. 5.
9. ibid.
10. Richmond, J. H., "A wire-grid model for scattering by conducting bodies," IEEE Trans. Antennas Propagation, vol. AP-14, no. 6, November 1966, pp. 782-786.
11. Rao, S. M., D. R. Wilton and A. W. Glisson, "Electromagnetic Scattering by Surfaces of Arbitrary Shape", IEEE Trans. on Antennas and Propagation, vol. AP-30, no. 3, May 1982, p. 409.
12. Balanis, C. A., Advanced Engineering Electromagnetics, John Wiley & Sons, Inc., New York, 1989, pp. 670-742.
13. Harrington, R. F., Field Computation by Moment Methods, The Macmillan Company, New York, 1968.
14. Mittra, R. (Editor), Computer Techniques for Electromagnetics, Hemisphere Publishing Corporation, New York, 1987, pp. 15-16.
15. Balanis, C. A., Antenna Theory: Analysis and Design, John Wiley & Sons, Inc., New York, 1982, pp. 515 and 519.
16. "Heli-Bowl Vertical Pattern", dB Systems Inc., Salt Lake City, UT, June 8, 1997.
17. Sennott, J. and D. Pietraszewski, "Experimental Measurement and Characterization of Ionospheric and Multipath Errors in Differential GPS," NAVIGATION: Journal of The Institute of Navigation, Vol. 34, No. 2, 1987, pp. 160-173.
18. Sennott, J. and J. Spalding, "Multipath Sensitivity and Carrier Slip Tolerance of an Integrated Doppler DGPS Navigation Algorithm," Record of the Position Location and Navigation Symposium, Las Vegas, March 1990, pp. 638-644.
19. Braasch, M. and F. Van Graas, "Guidance Accuracy Considerations for Realtime GPS Interferometry," Proceedings of ION GPS-91, Albuquerque, NM, September 1991, pp. 373-386.
20. Private communication with Michael Braasch, Ohio University, Athens Ohio, 1998.
21. Carver, K., "The Helicone - A Circularly Polarized Antenna with Low Sidelobe Level," Proceedings of the IEEE, Vol. AP-55, No. 4, April 1967, p. 559.

22. Private communication with Michael DiBenedetto, Ohio University, Athens Ohio, 1998.
23. Newman, E. H. and D. L. Dilsavor, A user's manual for the electromagnetic surface patch code: ESP version III, Technical Report No. 716148-19, ElectroScience Laboratory, The Ohio State University, May 1987.
24. Umashankar, K., A. Taflove and S. M. Rao, "Electromagnetic Scattering by Arbitrary Shaped Three-Dimensional Homogeneous Lossy Dielectric Objects", IEEE Trans. on Antennas and Propagation, Vol. AP-34, No. 6, June 1986, pp. 758-766.
25. Balanis, C. A., Antenna Theory: Analysis and Design, John Wiley & Sons, Inc., New York, 1982, p.389.

Appendix A

About NEC-2

Preface

The Numerical Electromagnetics Code (NEC) has been developed at the Lawrence Livermore Laboratory, Livermore, California, under the sponsorship of the Naval Ocean Systems Center and the Air Force Weapons Laboratory. It is an advanced version of the Antenna Modeling Program (AMP) developed in the early 1970's by MBAssociates for the Naval Research Laboratory, Naval Ship Engineering Center, U.S. Army ECOM/Communications Systems, U.S. Army Strategic Communications Command, and Rome Air Development Center under Office of Naval Research Contract N00014-71-C-0187. The present version of NEC is the result of efforts by G. J. Burke and A. J. Poggio of Lawrence Livermore Laboratory. [9]

Abstract

The Numerical Electromagnetics code (NEC-2) is a computer code for analyzing the electromagnetic response of an arbitrary structure consisting of wires and surfaces in free space or over a ground plane. The analysis is accomplished by the numerical solution of integral equations for induced currents. The excitation may be an incident plane wave or a voltage source on a wire, while the output may include current and charge density, electric or magnetic field in the vicinity of the structure, and radiated fields. NEC-2 includes several features not contained in NEC-1, including an accurate method for modeling grounds, based on the Sommerfeld integrals, and an option to modify a structure without repeating the complete solution. [9]

Example of NEC-2 Input File: (chart extracted from [9])

```

CM 12 ELEMENT LOG PERIODIC ANTENNA IN FREE SPACE
CM 78 SEGMENTS. SIGMA=0/L RECEIVING AND TRANS. PATTERNS.
CM DIPOLE LENGTH TO DIAMETER RATIO=150.
CE TAU=0.93. SIGMA=0.70. BOOM IMPEDANCE=50. OHMS.
GW 1   5    0.0000   -1.0000    0.0000    0.0000    1.0000    0.0000    .00667
GW 2   5   -7527   -1.0753     0   -7527   1.0753     0   .00717
GW 3   5   -1.562   -1.1562     0   -1.562   1.1562     0   .00771
GW 4   5  -2.4323   -1.2432     0  -2.4323   1.2432     0   .00829
GW 5   5   -3.368   -1.3368     0   -3.368   1.3368     0   .00891
GW 6   7  -4.3742   -1.4374     0  -4.3742   1.4374     0   .00958
GW 7   7  -5.4562   -1.5456     0  -5.4562   1.5456     0   .0103
GW 8   7  -6.6195   -1.6619     0  -6.6195   1.6619     0   .01108
GW 9   7  -7.8705   -1.7870     0  -7.8705   1.787     0   .01191
GW 10  7  -9.2156   -1.9215     0  -9.2156   1.9215     0   .01281
GW 11  9  -10.6619  -2.0662     0  -10.6619   2.0662     0   .01377
GW 12  9  -12.2171  -2.2217     0  -12.2171   2.2217     0   .01481
GE
FR  0   0      0      0    46.29      0
EX  0   1      3      10      1
RP  0   37      1     1110      90      0      -5      0
EN

```

Appendix B

Programs of Some Visualization and Converting Tools

Program 1:

Matlab program is used to draw the total electrical field radiation pattern from NEC-2 output file. Lower clamp is applied. A special version of polar graph script, 'polarhg.m', is needed. It can be downloaded from <<http://www.mathworks.com>> website.

```
% Draw the total E-field radiation pattern from NEC-2 output file
% Clamp applied.
%
% 07/19/98
%
clear all
%
% Default: Phi=0 degrees
%
phi1='0';
%
% Default = Circular Plate
%
st='c'; % c: Circular Plate / r: Rectangular Plate
if st=='c'
    st='Circular';
else
    st='Rectangular';
end
%
% Set clamp for the min.
% Default = -60 dB
%
cp=-60;
%
%-ANGLES- - DIRECTIVE GAINS - - - POLARIZATION - - - E(THETA) - - - E(PHI) -
% THETA     VERT.    HOR.    TOTAL      AXIAL    TILT    MAGNITUDE    PHASE    MAGNITUDE    PHASE
% DEGREES    DB       DB       DB        RATIO   DEG.    VOLTS/M    DEGREES    VOLTS/M    DEGREES
%
mdata=[];
% Insert NEC-2 output data below. Items as indicated above
%
%
];
%
% Start calculation
%
z=size(mdata,1);
for ix=1:z
    a=mdata(ix,7)*cos(mdata(ix,8)*pi/180)+mdata(ix,9)*cos(mdata(ix,10)*pi/180);
    b=mdata(ix,7)*sin(mdata(ix,8)*pi/180)+mdata(ix,9)*sin(mdata(ix,10)*pi/180);
    etmp(ix)=sqrt((a^2)+(b^2));
end
maxdb=20*log10(max(etmp));
mindb=20*log10(min(etmp));
for ix=1:z
    et(ix)=20*log10(etmp(ix))-maxdb;
    if et(ix) <= cp
        et(ix)=cp;
    end
end
%
% Calculate the 'rlim' and 'rtick' matrices
%
ck=min(et(:));
rlm=[ck 0];
if ck==round(ck)
    rtk=[];
else
    rtk=ck;
end
if abs(ck)<100
    for ii=1:abs(round(ck/10))
        rtk=[rtk round(ck/10)*10];
        ck=ck+10;
    end
elseif abs(ck)<1000
    for ii=1:abs(round(ck/100))
        rtk=[rtk round(ck/100)*100];
        ck=ck+100;
    end
else
    disp('Amplitude is smaller than -1000. Clamp was set at -1000dB!')
    rtk=[rtk -1000 -500];
end
rtk=[rtk 0];
```

```

%
% Polar Plot
%
figure
h = polarhg(mdata(:,1)*pi/180,et(:,1),'tdir','clockwise','rlim',[min(et(:)) 0], ...
    'rtick',rtk,'tstep',30,'torig','up', ...
    'color','r','linestyle','--');
title(['Fig. Total E-Field for 1/4-Wavelength Monopole above a ', st, ...
    ' Plate (1 GHz, Phi=',phi1,')'])
legend(['The lower clamp sets to ', num2str(cp)])
%
% Retangular Plot
%
figure
plot(mdata(:,1), et(:,1))
axis([0 360 -60 0])
title(['1/4-Wavelength Monopole above a ', st, 'Plate (1 GHz, Phi=',phi1,')'])
xlabel('Vertical Angle (Theta)')
ylabel('Total Electrical Field (dB)')
legend(['The lower clamp sets to ', num2str(cp)])
grid
%
% Show Minimum of the total field
%
Minimum=mindb-maxdb
%
% Program ends

```

Program 2:

Matlab program is used to show two sets of radiation patterns at two perpendicular elevation planes (i.e. ϕ and $\phi+90^\circ$). Each set included the vertical and horizontal patterns. Lower clamp is applied. A special version of polar graph script, 'polarhg.m', is needed. It can be downloaded from <<http://www.mathworks.com>> website.

```

% Show two sets of radiation patterns at two perpendicular elevation planes
% (i.e. Phi and (phi+90)). Each set includes the vertical and horizontal
% patterns. Clamp applied.
%
% 7/19/98
%
phi1='0'; %degree
phi2='90'; %degree
%
% Set clamps for the minimum.
% Default = -60 dB
%
cp1=-60; % Clamp for Vertical Pattern 1
cp2=-60; % Clamp for Horizontal Pattern 1
cp3=-60; % Clamp for Vertical Pattern 2
cp4=-60; % Clamp for Horizontal Pattern 2
%
%ANGLES - - DIRECTIVE GAINS - - POLARIZATION - - - E(THETA) - - - - - E(PHI) - - -
% THETA   VERT. HOR. TOTAL   AXIAL   TILT    MAGNITUDE   PHASE    MAGNITUDE   PHASE
%DEGREES   DB      DB      DB      RATIO   DEG.    VOLTS/M   DEGREES   VOLTS/M   DEGREES
%
hb=[
% Insert the data for the first one below!!!
%
%
%
% Insert the data for the second one below!!!
%
%
];
%
% Start calcuation
%
z=size(hb,1)/2;
max1=max(hb(1:z,7));
max2=max(hb(1:z,9));
max3=max(hb(z+1:2*z,7));
max4=max(hb(z+1:2*z,9));
min1=min(hb(1:z,7));

```

```

min2=min(hb(1:z,9));
min3=min(hb(z+1:2*z,7));
min4=min(hb(z+1:2*z,9));
%
% Show Minimum of each pattern
%
Min_Ver_1=20*log10(min1/max1) % for Vertical Pattern 1
Min_Ver_2=20*log10(min3/max3) % for Vertical Pattern 2
Min_Hor_1=20*log10(min2/max2) % for Horizontal Pattern 1
Min_Hor_2=20*log10(min4/max4) % for Horizontal Pattern 2
%
% Calculation for pattern 1
%
a=0;
%
% Set the max of dB to zero. Clamp at work.
%
for i=1:z;
    a=a+1;
    hbtmp(a,1)=hb(i,1)*2*pi/360;
    hbtmp(a,2)=20*(log10(hb(i,7)/max1));
    if hbtmp(a,2) <= cp1
        hbtmp(a,2)=cp1;
    end
    hbtmp(a,3)=20*(log10(hb(i,9)/max2));
    if hbtmp(a,3) <= cp2
        hbtmp(a,3)=cp2;
    end
end
%
% Calculation for pattern 2
%
% Set the max of dB to zero. Clamp at work.
%
for i=z+1:2*z;
    a=a+1;
    hbtmp(a,1)=hb(i,1)*2*pi/360;
    hbtmp(a,2)=20*(log10(hb(i,7)/max3));
    if hbtmp(a,2) <= cp3
        hbtmp(a,2)=cp3;
    end
    hbtmp(a,3)=20*(log10(hb(i,9)/max4));
    if hbtmp(a,3) <= cp4
        hbtmp(a,3)=cp4;
    end
end
%
% Start Ploting...
%
% Polar plot for Vertical pattern 1:
%
figure
%
% Calculate the 'rlim' and 'rtick' matrices first.
%
ck=min(hbtmp(1:z,2));
rlm=[ck 0];
if ck==round(ck)
    rtk=[];
else
    rtk=ck;
end
if abs(ck)<100
    for ii=1:abs(round(ck/10))
        rtk=[rtk round(ck/10)*10];
        ck=ck+10;
    end
elseif abs(ck)<1000
    for ii=1:abs(round(ck/100))
        rtk=[rtk round(ck/100)*100];
        ck=ck+100;
    end
else
    disp('Amplitude is smaller than -1000. Clamp was set at -1000dB!')
    cp1=-1000;
    rtk=[rtk -1000 -500];
end
rtk=[rtk 0];
%
% Ploting
%
h = polarhg(hbtmp(1:z,1),hbtmp(1:z,2),'tdir','clockwise','rlim',[min(hbtmp(1:z,2)) 0], ...
    'rtick', rtk,'tstep',30,'torig','up', ...
    'color','r','linestyle','-' );
title(['Vertical Pattern, Phi = ',phi1])
legend(['Clamp at ',num2str(cp1),' dB'])
%
% Polar plot for Vertical pattern 2:
%
figure

```

```

%
% Calculate the 'rlim' and 'rtick' matrices
%
ck=min(hbtmp(z+1:2*z,2));
rlm=[ck 0];
if ck==round(ck)
    rtk=[];
else
    trk=ck;
end
if abs(ck)<100
    for ii=1:abs(round(ck/10))
        rtk=[rtk round(ck/10)*10];
        ck=ck+10;
    end
elseif abs(ck)<1000
    for ii=1:abs(round(ck/100))
        rtk=[rtk round(ck/100)*100];
        ck=ck+100;
    end
else
    disp('Amplitude is smaller than -1000. Clamp was set at -1000dB!')
    cp3=-1000;
    rtk=[rtk -1000 -500];
end
rtk=[rtk 0];
%
% Plotting
%
h = polarhg(hbtmp(z+1:2*z,1),hbtmp(z+1:2*z,2),'tdir','clockwise','rlim',[min(hbtmp(z+1:2*z,2)) 0], ...
    'rtick', rtk,'tstep',30,'torig','up', ...
    'color','r','linestyle','-');
title(['Vertical Pattern, Phi = ',phi2])
legend(['Clamp at ',num2str(cp3),' dB'])
%
% Rectangular plot for Vertical pattern 1 & 2:
%
figure
plot(hbtmp(1:z,1)*180/pi,hbtmp(1:z,2),'-',hbtmp(z+1:2*z,1)*180/pi,hbtmp(z+1:2*z,2),':')
axis([0 360 -60 0])
title('Original Helibowl at 1575 MHz')
xlabel('Vertical Angle (Theta)')
ylabel('Vertical Electrical Field (dB)')
grid
legend(['Phi=',phi1,', Clamp at ',num2str(cp1),' dB'], ['Phi=',phi2,', Clamp at ',num2str(cp3),' dB'])
%
% Polar plot for Horizontal pattern 1:
%
figure
%
% Calculate the 'rlim' and 'rtick' matrices
%
ck=min(hbtmp(1:z,3));
rlm=[ck 0];
if ck==round(ck)
    rtk=[];
else
    trk=ck;
end
if abs(ck)<100
    for ii=1:abs(round(ck/10))
        rtk=[rtk round(ck/10)*10];
        ck=ck+10;
    end
elseif abs(ck)<1000
    for ii=1:abs(round(ck/100))
        rtk=[rtk round(ck/100)*100];
        ck=ck+100;
    end
else
    disp('Amplitude is smaller than -1000. Clamp was set at -1000dB!')
    cp2=-1000;
    rtk=[rtk -1000 -500];
end
rtk=[rtk 0];
%
% Plotting
%
h = polarhg(hbtmp(1:z,1),hbtmp(1:z,3),'tdir','clockwise','rlim',[min(hbtmp(1:z,3)) 0], ...
    'rtick', rtk,'tstep',30,'torig','up', ...
    'color','r','linestyle','-');
title(['Horizontal Pattern, Phi = ',phi1])
legend(['Clamp at ',num2str(cp2),' dB'])
%
% Polar plot for Horizontal pattern 2:
%
figure
%
% Calculate the 'rlim' and 'rtick' matrices
%
```

```

ck=min(hbtmp(z+1:2*z,3));
rlm=[ck 0];
if ck==round(ck)
  rtk=[];
else
  rtk=ck;
end
if abs(ck)<100
  for ii=1:abs(round(ck/10))
    rtk=[rtk round(ck/10)*10];
    ck=ck+10;
  end
elseif abs(ck)<1000
  for ii=1:abs(round(ck/100))
    rtk=[rtk round(ck/100)*100];
    ck=ck+100;
  end
else
  disp('Amplitude is smaller than -1000. Clamp was set at -1000dB!')
  cp4=-1000;
  rtk=[rtk -1000 -500];
end
rtk=[rtk 0];
%
% Plotting
%
h = polarhg(hbtmp(z+1:2*z,1),hbtmp(z+1:2*z,3),'tdir','clockwise','rlim',[min(hbtmp(z+1:2*z,3)) 0], ...
  'rtick', rtk,'tstep',30,'torig','up', ...
  'color','r','linestyle','-');
title(['Horizontal Pattern, Phi = ',phi2])
legend(['Clamp at ',num2str(cp4),' dB'])
%
% Rectangular plot for Horizontal pattern 1 & 2:
%
figure
plot(hbtmp(1:z,1)*180/pi,hbtmp(1:z,3),'-',hbtmp(z+1:2*z,1)*180/pi,hbtmp(z+1:2*z,3),':')
axis([0 360 -60 0])
title('Original Helibowl at 1575 MHz')
xlabel('Vertical Angle (Theta)')
ylabel('Horizontal Electrical Field (dB)')
grid
legend(['Phi=',phi1,', Clamp at ',num2str(cp2),' dB'], ['Phi=',phi2,', Clamp at ',num2str(cp4),' dB'])
%
%Program ends

```

Program 3:

Matlab program is used to build the NEC-2 input file of the bowl part with only one set of coordinate data from the radial.

```

% Configure the bowl part of the helibowl antenna.
%
% Input: Diameter and its relative height.
% Output: File 'hldt.txt' in the format of NEC-2 input file.
%
% [Note]: No hole in the bottom
%
% 07/16/98
%
clear all
%
% hldata = [Height, Diameter]: Measured in Centimeters
%
hldata=[
% Insert the bowl's coordinate data of one radial below!!!
%
%
]
;
s1=size(hldata,1);
s2=input('How many wire-segment on each ring: ');
tg=input('What is the tag number: ');
sg=input('How many sub-segment on each wire: ');
rd=input('What is the radius of the wire: ');
a=2*pi/s2;
%
% Results is saved in "hldf" (Unit: Meters)

```

```

%
k=0;
for ik=1:s1
    for jk=1:s2
        k=k+1;
        hldf(k,1)=hldata(ik,2)*cos((jk-1)*a)/200;
        hldf(k,2)=hldata(ik,2)*sin((jk-1)*a)/200;
        hldf(k,3)=hldata(ik,1)/100;
    end
end
%
% Final Output:
%
hldt='';
hldtmp=sprintf('\n-- Kill this line and above --\n');
hldt=[hldt, hldtmp];
%
% Configure the Helibowl - Start with the rings.
%
for kk=1:s1
    for jj=1:s2
        if jj<s2
            dd=jj+1;
        else
            dd=1;
        end
        hldtmp=sprintf('GW%3i%5i%10.5f%10.5f%10.5f%10.5f%10.5f\n',...
            tg,sg,hldf(s2*(kk-1)+jj,1),hldf(s2*(kk-1)+jj,2),hldf(s2*(kk-1)+jj,3),...
            hldf(s2*(kk-1)+dd,1),hldf(s2*(kk-1)+dd,2),hldf(s2*(kk-1)+dd,3),rd);
        hldt=[hldt,hldtmp];
    end
end
%
% Put note 1 here
%
hldtmp=sprintf('-- Up: Rings - Down: Radials --\n');
hldt=[hldt, hldtmp];
%
% Configure the radials:
%
for jj=1:s2
    for kk=1:(s1-1)
        hldtmp=sprintf('GW%3i%5i%10.5f%10.5f%10.5f%10.5f%10.5f%10.5f\n',...
            tg,sg,hldf(s2*(kk-1)+jj,1),hldf(s2*(kk-1)+jj,2),hldf(s2*(kk-1)+jj,3),...
            hldf(s2*kk+jj,1),hldf(s2*kk+jj,2),hldf(s2*kk+jj,3),rd);
        hldt=[hldt,hldtmp];
    end
end
%
% Fill the hole in the bottom of bowl.
%
% Put note 2 here
%
hldtmp=sprintf('-- Last Set of Radials - To keep the hole --\n');
hldt=[hldt, hldtmp];
hldtmp=sprintf('-- Kill lines from here till the end --\n');
hldt=[hldt, hldtmp];
kk=s1;
for jj=1:s2
    hldtmp=sprintf('GW%3i%5i%10.5f%10.5f%10.5f%10.5f%10.5f%10.5f\n',...
        tg,sg,hldf(s2*(kk-1)+jj,1),hldf(s2*(kk-1)+jj,2),hldf(s2*(kk-1)+jj,3),...
        0,0,0,rd);
    hldt=[hldt,hldtmp];
end
%
% Final output is in: "hldt"
% It is also saved to file "hldt.txt".
% Try location - c:/matlab/hldt.txt
%
save hldt.txt hldt
mg=sprintf('\n***** Done! : Output is saved in c:/matlab/hldt.txt *****\n');
disp(mg);
%
% Program ends

```

Appendix C

NEC-2 Input Files for $\lambda/4$ Monopoles in Chapter 4

The NEC-2 input file for a $\lambda/4$ monopole above a finite square ground plane (1.22 m on each side of the square ground plane). The frequency is set at 1 GHz.

```

CM ****
CM *
CM * A 1/4-wavelength monopole above finite square ground *
CM * plane (1.22 m on each side).
CM * Freq. at 1.0 GHz
CM *
CM * NEC-2 input file created by MatNEC on 10-Apr-97
CM *
CM ****
CE
GW 2 3 0.000 0.000 0.075 0.000 0.000 0.000 0.000 0.003
GW 1 1 -0.610 -0.610 0.000 -0.549 -0.610 0.000 0.000 0.003
GW 1 1 -0.549 -0.610 0.000 -0.488 -0.610 0.000 0.000 0.003
GW 1 1 -0.488 -0.610 0.000 -0.427 -0.610 0.000 0.000 0.003
GW 1 1 -0.427 -0.610 0.000 -0.366 -0.610 0.000 0.000 0.003
GW 1 1 -0.366 -0.610 0.000 -0.305 -0.610 0.000 0.000 0.003
GW 1 1 -0.305 -0.610 0.000 -0.244 -0.610 0.000 0.000 0.003
GW 1 1 -0.244 -0.610 0.000 -0.183 -0.610 0.000 0.000 0.003
GW 1 1 -0.183 -0.610 0.000 -0.122 -0.610 0.000 0.000 0.003
GW 1 1 -0.122 -0.610 0.000 -0.061 -0.610 0.000 0.000 0.003
GW 1 1 -0.061 -0.610 0.000 0.000 -0.610 0.000 0.000 0.003
GW 1 1 0.000 -0.610 0.000 0.061 -0.610 0.000 0.000 0.003
GW 1 1 0.061 -0.610 0.000 0.122 -0.610 0.000 0.000 0.003
GW 1 1 0.122 -0.610 0.000 0.183 -0.610 0.000 0.000 0.003
GW 1 1 0.183 -0.610 0.000 0.244 -0.610 0.000 0.000 0.003
GW 1 1 0.244 -0.610 0.000 0.305 -0.610 0.000 0.000 0.003
GW 1 1 0.305 -0.610 0.000 0.366 -0.610 0.000 0.000 0.003
GW 1 1 0.366 -0.610 0.000 0.427 -0.610 0.000 0.000 0.003
GW 1 1 0.427 -0.610 0.000 0.488 -0.610 0.000 0.000 0.003
GW 1 1 0.488 -0.610 0.000 0.549 -0.610 0.000 0.000 0.003
GW 1 1 0.549 -0.610 0.000 0.610 -0.610 0.000 0.000 0.003
GW 1 1 -0.610 -0.549 0.000 -0.549 -0.549 0.000 0.000 0.003
GW 1 1 -0.549 -0.549 0.000 -0.488 -0.549 0.000 0.000 0.003
GW 1 1 -0.488 -0.549 0.000 -0.427 -0.549 0.000 0.000 0.003
GW 1 1 -0.427 -0.549 0.000 -0.366 -0.549 0.000 0.000 0.003
GW 1 1 -0.366 -0.549 0.000 -0.305 -0.549 0.000 0.000 0.003
GW 1 1 -0.305 -0.549 0.000 -0.244 -0.549 0.000 0.000 0.003
GW 1 1 -0.244 -0.549 0.000 -0.183 -0.549 0.000 0.000 0.003
GW 1 1 -0.183 -0.549 0.000 -0.122 -0.549 0.000 0.000 0.003
GW 1 1 -0.122 -0.549 0.000 -0.061 -0.549 0.000 0.000 0.003
GW 1 1 -0.061 -0.549 0.000 0.000 -0.549 0.000 0.000 0.003
GW 1 1 0.000 -0.549 0.000 0.061 -0.549 0.000 0.000 0.003
GW 1 1 0.061 -0.549 0.000 0.122 -0.549 0.000 0.000 0.003
GW 1 1 0.122 -0.549 0.000 0.183 -0.549 0.000 0.000 0.003
GW 1 1 0.183 -0.549 0.000 0.244 -0.549 0.000 0.000 0.003
GW 1 1 0.244 -0.549 0.000 0.305 -0.549 0.000 0.000 0.003
GW 1 1 0.305 -0.549 0.000 0.366 -0.549 0.000 0.000 0.003
GW 1 1 0.366 -0.549 0.000 0.427 -0.549 0.000 0.000 0.003
GW 1 1 0.427 -0.549 0.000 0.488 -0.549 0.000 0.000 0.003
GW 1 1 0.488 -0.549 0.000 0.549 -0.549 0.000 0.000 0.003
GW 1 1 0.549 -0.549 0.000 0.610 -0.549 0.000 0.000 0.003
GW 1 1 -0.610 -0.488 0.000 -0.549 -0.488 0.000 0.000 0.003
GW 1 1 -0.549 -0.488 0.000 -0.488 -0.488 0.000 0.000 0.003
GW 1 1 -0.488 -0.488 0.000 -0.366 -0.488 0.000 0.000 0.003
GW 1 1 -0.366 -0.488 0.000 -0.305 -0.488 0.000 0.000 0.003
GW 1 1 -0.305 -0.488 0.000 -0.244 -0.488 0.000 0.000 0.003
GW 1 1 -0.244 -0.488 0.000 -0.183 -0.488 0.000 0.000 0.003
GW 1 1 -0.183 -0.488 0.000 -0.122 -0.488 0.000 0.000 0.003
GW 1 1 -0.122 -0.488 0.000 -0.061 -0.488 0.000 0.000 0.003
GW 1 1 -0.061 -0.488 0.000 0.000 -0.488 0.000 0.000 0.003
GW 1 1 0.000 -0.488 0.000 0.061 -0.488 0.000 0.000 0.003
GW 1 1 0.061 -0.488 0.000 0.122 -0.488 0.000 0.000 0.003
GW 1 1 0.122 -0.488 0.000 0.183 -0.488 0.000 0.000 0.003
GW 1 1 0.183 -0.488 0.000 0.244 -0.488 0.000 0.000 0.003
GW 1 1 0.244 -0.488 0.000 0.305 -0.488 0.000 0.000 0.003
GW 1 1 0.305 -0.488 0.000 0.366 -0.488 0.000 0.000 0.003
GW 1 1 0.366 -0.488 0.000 0.427 -0.488 0.000 0.000 0.003
GW 1 1 0.427 -0.488 0.000 0.488 -0.488 0.000 0.000 0.003
GW 1 1 0.488 -0.488 0.000 0.549 -0.488 0.000 0.000 0.003
GW 1 1 0.549 -0.488 0.000 0.610 -0.488 0.000 0.000 0.003
GW 1 1 -0.610 -0.427 0.000 -0.549 -0.427 0.000 0.000 0.003
GW 1 1 -0.549 -0.427 0.000 -0.488 -0.427 0.000 0.000 0.003
GW 1 1 -0.488 -0.427 0.000 -0.427 -0.427 0.000 0.000 0.003
GW 1 1 -0.427 -0.427 0.000 -0.366 -0.427 0.000 0.000 0.003
GW 1 1 -0.366 -0.427 0.000 -0.305 -0.427 0.000 0.000 0.003
GW 1 1 -0.305 -0.427 0.000 -0.244 -0.427 0.000 0.000 0.003
GW 1 1 -0.244 -0.427 0.000 -0.183 -0.427 0.000 0.000 0.003
GW 1 1 -0.183 -0.427 0.000 -0.122 -0.427 0.000 0.000 0.003
GW 1 1 -0.122 -0.427 0.000 -0.061 -0.427 0.000 0.000 0.003
GW 1 1 -0.061 -0.427 0.000 0.000 -0.427 0.000 0.000 0.003
GW 1 1 0.000 -0.427 0.000 0.061 -0.427 0.000 0.000 0.003
GW 1 1 0.061 -0.427 0.000 0.122 -0.427 0.000 0.000 0.003

```


GW	1	1	-0.488	-0.122	0.000	-0.427	-0.122	0.000	0.003
GW	1	1	-0.427	-0.122	0.000	-0.366	-0.122	0.000	0.003
GW	1	1	-0.366	-0.122	0.000	-0.305	-0.122	0.000	0.003
GW	1	1	-0.305	-0.122	0.000	-0.244	-0.122	0.000	0.003
GW	1	1	-0.244	-0.122	0.000	-0.183	-0.122	0.000	0.003
GW	1	1	-0.183	-0.122	0.000	-0.122	-0.122	0.000	0.003
GW	1	1	-0.122	-0.122	0.000	-0.061	-0.122	0.000	0.003
GW	1	1	-0.061	-0.122	0.000	0.000	-0.122	0.000	0.003
GW	1	1	0.000	-0.122	0.000	0.061	-0.122	0.000	0.003
GW	1	1	0.061	-0.122	0.000	0.122	-0.122	0.000	0.003
GW	1	1	0.122	-0.122	0.000	0.183	-0.122	0.000	0.003
GW	1	1	0.183	-0.122	0.000	0.244	-0.122	0.000	0.003
GW	1	1	0.244	-0.122	0.000	0.305	-0.122	0.000	0.003
GW	1	1	0.305	-0.122	0.000	0.366	-0.122	0.000	0.003
GW	1	1	0.366	-0.122	0.000	0.427	-0.122	0.000	0.003
GW	1	1	0.427	-0.122	0.000	0.488	-0.122	0.000	0.003
GW	1	1	0.488	-0.122	0.000	0.549	-0.122	0.000	0.003
GW	1	1	0.549	-0.122	0.000	0.610	-0.122	0.000	0.003
GW	1	1	-0.610	-0.061	0.000	-0.549	-0.061	0.000	0.003
GW	1	1	-0.549	-0.061	0.000	-0.488	-0.061	0.000	0.003
GW	1	1	-0.488	-0.061	0.000	-0.427	-0.061	0.000	0.003
GW	1	1	-0.427	-0.061	0.000	-0.366	-0.061	0.000	0.003
GW	1	1	-0.366	-0.061	0.000	-0.305	-0.061	0.000	0.003
GW	1	1	-0.305	-0.061	0.000	-0.244	-0.061	0.000	0.003
GW	1	1	-0.244	-0.061	0.000	-0.183	-0.061	0.000	0.003
GW	1	1	-0.183	-0.061	0.000	-0.122	-0.061	0.000	0.003
GW	1	1	-0.122	-0.061	0.000	-0.061	-0.061	0.000	0.003
GW	1	1	-0.061	-0.061	0.000	0.000	-0.061	0.000	0.003
GW	1	1	0.000	-0.061	0.000	0.122	-0.061	0.000	0.003
GW	1	1	0.061	-0.061	0.000	0.183	-0.061	0.000	0.003
GW	1	1	0.122	-0.061	0.000	0.244	-0.061	0.000	0.003
GW	1	1	0.183	-0.061	0.000	0.305	-0.061	0.000	0.003
GW	1	1	0.244	-0.061	0.000	0.366	-0.061	0.000	0.003
GW	1	1	0.305	-0.061	0.000	0.427	-0.061	0.000	0.003
GW	1	1	0.366	-0.061	0.000	0.488	-0.061	0.000	0.003
GW	1	1	0.427	-0.061	0.000	0.549	-0.061	0.000	0.003
GW	1	1	0.549	-0.061	0.000	0.610	-0.061	0.000	0.003
GW	1	1	-0.610	0.000	0.000	-0.549	0.000	0.000	0.003
GW	1	1	-0.549	0.000	0.000	-0.488	0.000	0.000	0.003
GW	1	1	-0.488	0.000	0.000	-0.427	0.000	0.000	0.003
GW	1	1	-0.427	0.000	0.000	-0.366	0.000	0.000	0.003
GW	1	1	-0.366	0.000	0.000	-0.305	0.000	0.000	0.003
GW	1	1	-0.305	0.000	0.000	-0.244	0.000	0.000	0.003
GW	1	1	-0.244	0.000	0.000	-0.183	0.000	0.000	0.003
GW	1	1	-0.183	0.000	0.000	-0.122	0.000	0.000	0.003
GW	1	1	-0.122	0.000	0.000	-0.061	0.000	0.000	0.003
GW	1	1	-0.061	0.000	0.000	0.000	-0.061	0.000	0.003
GW	1	1	0.000	0.000	0.000	0.061	0.000	0.000	0.003
GW	1	1	0.061	0.000	0.000	0.122	0.000	0.000	0.003
GW	1	1	0.122	0.000	0.000	0.183	0.000	0.000	0.003
GW	1	1	0.183	0.000	0.000	0.244	0.000	0.000	0.003
GW	1	1	0.244	0.000	0.000	0.305	0.000	0.000	0.003
GW	1	1	0.305	0.000	0.000	0.366	0.000	0.000	0.003
GW	1	1	0.366	0.000	0.000	0.427	0.000	0.000	0.003
GW	1	1	0.427	0.000	0.000	0.488	0.000	0.000	0.003
GW	1	1	0.488	0.000	0.000	0.549	0.000	0.000	0.003
GW	1	1	0.549	0.000	0.000	0.610	0.000	0.000	0.003
GW	1	1	-0.610	0.061	0.000	-0.549	0.061	0.000	0.003
GW	1	1	-0.549	0.061	0.000	-0.488	0.061	0.000	0.003
GW	1	1	-0.488	0.061	0.000	-0.427	0.061	0.000	0.003
GW	1	1	-0.427	0.061	0.000	-0.366	0.061	0.000	0.003
GW	1	1	-0.366	0.061	0.000	-0.305	0.061	0.000	0.003
GW	1	1	-0.305	0.061	0.000	-0.244	0.061	0.000	0.003
GW	1	1	-0.244	0.061	0.000	-0.183	0.061	0.000	0.003
GW	1	1	-0.183	0.061	0.000	-0.122	0.061	0.000	0.003
GW	1	1	-0.122	0.061	0.000	-0.061	0.061	0.000	0.003
GW	1	1	-0.061	0.061	0.000	0.000	-0.061	0.000	0.003
GW	1	1	0.000	0.061	0.000	0.061	0.000	0.000	0.003
GW	1	1	0.061	0.061	0.000	0.122	0.000	0.000	0.003
GW	1	1	0.122	0.061	0.000	0.183	0.000	0.000	0.003
GW	1	1	0.183	0.061	0.000	0.244	0.000	0.000	0.003
GW	1	1	0.244	0.061	0.000	0.305	0.000	0.000	0.003
GW	1	1	0.305	0.061	0.000	0.366	0.000	0.000	0.003
GW	1	1	0.366	0.061	0.000	0.427	0.000	0.000	0.003
GW	1	1	0.427	0.061	0.000	0.488	0.000	0.000	0.003
GW	1	1	0.488	0.061	0.000	0.549	0.000	0.000	0.003
GW	1	1	0.549	0.061	0.000	0.610	0.000	0.000	0.003
GW	1	1	-0.610	0.122	0.000	-0.549	0.122	0.000	0.003
GW	1	1	-0.549	0.122	0.000	-0.488	0.122	0.000	0.003
GW	1	1	-0.488	0.122	0.000	-0.427	0.122	0.000	0.003
GW	1	1	-0.427	0.122	0.000	-0.366	0.122	0.000	0.003
GW	1	1	-0.366	0.122	0.000	-0.305	0.122	0.000	0.003
GW	1	1	-0.305	0.122	0.000	-0.244	0.122	0.000	0.003
GW	1	1	-0.244	0.122	0.000	-0.183	0.122	0.000	0.003
GW	1	1	-0.183	0.122	0.000	-0.122	0.122	0.000	0.003
GW	1	1	-0.122	0.122	0.000	-0.061	0.122	0.000	0.003
GW	1	1	-0.061	0.122	0.000	0.000	0.122	0.000	0.003
GW	1	1	0.000	0.122	0.000	0.061	0.122	0.000	0.003
GW	1	1	0.061	0.122	0.000	0.122	0.122	0.000	0.003

GW	1	1	-0.488	0.427	0.000	-0.427	0.427	0.000	0.003
GW	1	1	-0.427	0.427	0.000	-0.366	0.427	0.000	0.003
GW	1	1	-0.366	0.427	0.000	-0.305	0.427	0.000	0.003
GW	1	1	-0.305	0.427	0.000	-0.244	0.427	0.000	0.003
GW	1	1	-0.244	0.427	0.000	-0.183	0.427	0.000	0.003
GW	1	1	-0.183	0.427	0.000	-0.122	0.427	0.000	0.003
GW	1	1	-0.122	0.427	0.000	-0.061	0.427	0.000	0.003
GW	1	1	-0.061	0.427	0.000	0.000	0.427	0.000	0.003
GW	1	1	0.000	0.427	0.000	0.061	0.427	0.000	0.003
GW	1	1	0.061	0.427	0.000	0.122	0.427	0.000	0.003
GW	1	1	0.122	0.427	0.000	0.183	0.427	0.000	0.003
GW	1	1	0.183	0.427	0.000	0.244	0.427	0.000	0.003
GW	1	1	0.244	0.427	0.000	0.305	0.427	0.000	0.003
GW	1	1	0.305	0.427	0.000	0.366	0.427	0.000	0.003
GW	1	1	0.366	0.427	0.000	0.427	0.427	0.000	0.003
GW	1	1	0.427	0.427	0.000	0.488	0.427	0.000	0.003
GW	1	1	0.488	0.427	0.000	0.549	0.427	0.000	0.003
GW	1	1	0.549	0.427	0.000	0.610	0.427	0.000	0.003
GW	1	1	-0.610	0.488	0.000	-0.549	0.488	0.000	0.003
GW	1	1	-0.549	0.488	0.000	-0.488	0.488	0.000	0.003
GW	1	1	-0.488	0.488	0.000	-0.427	0.488	0.000	0.003
GW	1	1	-0.427	0.488	0.000	-0.366	0.488	0.000	0.003
GW	1	1	-0.366	0.488	0.000	-0.305	0.488	0.000	0.003
GW	1	1	-0.305	0.488	0.000	-0.244	0.488	0.000	0.003
GW	1	1	-0.244	0.488	0.000	-0.183	0.488	0.000	0.003
GW	1	1	-0.183	0.488	0.000	-0.122	0.488	0.000	0.003
GW	1	1	-0.122	0.488	0.000	-0.061	0.488	0.000	0.003
GW	1	1	-0.061	0.488	0.000	0.000	0.488	0.000	0.003
GW	1	1	0.000	0.488	0.000	0.061	0.488	0.000	0.003
GW	1	1	0.061	0.488	0.000	0.122	0.488	0.000	0.003
GW	1	1	0.122	0.488	0.000	0.183	0.488	0.000	0.003
GW	1	1	0.183	0.488	0.000	0.244	0.488	0.000	0.003
GW	1	1	0.244	0.488	0.000	0.305	0.488	0.000	0.003
GW	1	1	0.305	0.488	0.000	0.366	0.488	0.000	0.003
GW	1	1	0.366	0.488	0.000	0.427	0.488	0.000	0.003
GW	1	1	0.427	0.488	0.000	0.488	0.488	0.000	0.003
GW	1	1	0.488	0.488	0.000	0.549	0.488	0.000	0.003
GW	1	1	0.549	0.488	0.000	0.610	0.488	0.000	0.003
GW	1	1	-0.610	0.549	0.000	-0.549	0.549	0.000	0.003
GW	1	1	-0.549	0.549	0.000	-0.488	0.549	0.000	0.003
GW	1	1	-0.488	0.549	0.000	-0.427	0.549	0.000	0.003
GW	1	1	-0.427	0.549	0.000	-0.366	0.549	0.000	0.003
GW	1	1	-0.366	0.549	0.000	-0.305	0.549	0.000	0.003
GW	1	1	-0.305	0.549	0.000	-0.244	0.549	0.000	0.003
GW	1	1	-0.244	0.549	0.000	-0.183	0.549	0.000	0.003
GW	1	1	-0.183	0.549	0.000	-0.122	0.549	0.000	0.003
GW	1	1	-0.122	0.549	0.000	-0.061	0.549	0.000	0.003
GW	1	1	-0.061	0.549	0.000	0.000	0.549	0.000	0.003
GW	1	1	0.000	0.549	0.000	0.061	0.549	0.000	0.003
GW	1	1	0.061	0.549	0.000	0.122	0.549	0.000	0.003
GW	1	1	0.122	0.549	0.000	0.183	0.549	0.000	0.003
GW	1	1	0.183	0.549	0.000	0.244	0.549	0.000	0.003
GW	1	1	0.244	0.549	0.000	0.305	0.549	0.000	0.003
GW	1	1	0.305	0.549	0.000	0.366	0.549	0.000	0.003
GW	1	1	0.366	0.549	0.000	0.427	0.549	0.000	0.003
GW	1	1	0.427	0.549	0.000	0.488	0.549	0.000	0.003
GW	1	1	0.488	0.549	0.000	0.549	0.549	0.000	0.003
GW	1	1	0.549	0.549	0.000	0.610	0.549	0.000	0.003
GW	1	1	-0.610	0.610	0.000	-0.549	0.610	0.000	0.003
GW	1	1	-0.549	0.610	0.000	-0.488	0.610	0.000	0.003
GW	1	1	-0.488	0.610	0.000	-0.427	0.610	0.000	0.003
GW	1	1	-0.427	0.610	0.000	-0.366	0.610	0.000	0.003
GW	1	1	-0.366	0.610	0.000	-0.305	0.610	0.000	0.003
GW	1	1	-0.305	0.610	0.000	-0.244	0.610	0.000	0.003
GW	1	1	-0.244	0.610	0.000	-0.183	0.610	0.000	0.003
GW	1	1	-0.183	0.610	0.000	-0.122	0.610	0.000	0.003
GW	1	1	-0.122	0.610	0.000	-0.061	0.610	0.000	0.003
GW	1	1	-0.061	0.610	0.000	0.000	0.610	0.000	0.003
GW	1	1	0.000	0.610	0.000	0.061	0.610	0.000	0.003
GW	1	1	0.061	0.610	0.000	0.122	0.610	0.000	0.003
GW	1	1	0.122	0.610	0.000	0.183	0.610	0.000	0.003
GW	1	1	0.183	0.610	0.000	0.244	0.610	0.000	0.003
GW	1	1	0.244	0.610	0.000	0.305	0.610	0.000	0.003
GW	1	1	0.305	0.610	0.000	0.366	0.610	0.000	0.003
GW	1	1	0.366	0.610	0.000	0.427	0.610	0.000	0.003
GW	1	1	0.427	0.610	0.000	0.488	0.610	0.000	0.003
GW	1	1	0.488	0.610	0.000	0.549	0.610	0.000	0.003
GW	1	1	0.549	0.610	0.000	0.610	0.610	0.000	0.003
GW	1	1	-0.610	-0.610	0.000	-0.610	-0.549	0.000	0.003
GW	1	1	-0.549	-0.610	0.000	-0.610	-0.488	0.000	0.003
GW	1	1	-0.488	-0.610	0.000	-0.610	-0.427	0.000	0.003
GW	1	1	-0.427	-0.610	0.000	-0.610	-0.366	0.000	0.003
GW	1	1	-0.366	-0.610	0.000	-0.610	-0.305	0.000	0.003
GW	1	1	-0.305	-0.610	0.000	-0.610	-0.244	0.000	0.003
GW	1	1	-0.244	-0.610	0.000	-0.610	-0.183	0.000	0.003
GW	1	1	-0.183	-0.610	0.000	-0.610	-0.122	0.000	0.003
GW	1	1	-0.122	-0.610	0.000	-0.610	-0.061	0.000	0.003
GW	1	1	-0.061	-0.610	0.000	-0.610	0.000	0.000	0.003
GW	1	1	0.000	-0.610	0.000	-0.610	0.061	0.000	0.003
GW	1	1	0.061	-0.610	0.000	-0.610	0.122	0.000	0.003

GW	1	1	0.488	0.122	0.000	0.488	0.183	0.000	0.003
GW	1	1	0.488	0.183	0.000	0.488	0.244	0.000	0.003
GW	1	1	0.488	0.244	0.000	0.488	0.305	0.000	0.003
GW	1	1	0.488	0.305	0.000	0.488	0.366	0.000	0.003
GW	1	1	0.488	0.366	0.000	0.488	0.427	0.000	0.003
GW	1	1	0.488	0.427	0.000	0.488	0.488	0.000	0.003
GW	1	1	0.488	0.488	0.000	0.488	0.549	0.000	0.003
GW	1	1	0.488	0.549	0.000	0.488	0.610	0.000	0.003
GW	1	1	0.549	-0.610	0.000	0.549	-0.549	0.000	0.003
GW	1	1	0.549	-0.549	0.000	0.549	-0.488	0.000	0.003
GW	1	1	0.549	-0.488	0.000	0.549	-0.427	0.000	0.003
GW	1	1	0.549	-0.427	0.000	0.549	-0.366	0.000	0.003
GW	1	1	0.549	-0.366	0.000	0.549	-0.305	0.000	0.003
GW	1	1	0.549	-0.305	0.000	0.549	-0.244	0.000	0.003
GW	1	1	0.549	-0.244	0.000	0.549	-0.183	0.000	0.003
GW	1	1	0.549	-0.183	0.000	0.549	-0.122	0.000	0.003
GW	1	1	0.549	-0.122	0.000	0.549	-0.061	0.000	0.003
GW	1	1	0.549	-0.061	0.000	0.549	0.000	0.000	0.003
GW	1	1	0.549	0.000	0.000	0.549	0.061	0.000	0.003
GW	1	1	0.549	0.061	0.000	0.549	0.122	0.000	0.003
GW	1	1	0.549	0.122	0.000	0.549	0.183	0.000	0.003
GW	1	1	0.549	0.183	0.000	0.549	0.244	0.000	0.003
GW	1	1	0.549	0.244	0.000	0.549	0.305	0.000	0.003
GW	1	1	0.549	0.305	0.000	0.549	0.366	0.000	0.003
GW	1	1	0.549	0.366	0.000	0.549	0.427	0.000	0.003
GW	1	1	0.549	0.427	0.000	0.549	0.488	0.000	0.003
GW	1	1	0.549	0.488	0.000	0.549	0.549	0.000	0.003
GW	1	1	0.549	0.549	0.000	0.549	0.610	0.000	0.003
GW	1	1	0.610	-0.610	0.000	0.610	-0.549	0.000	0.003
GW	1	1	0.610	-0.549	0.000	0.610	-0.488	0.000	0.003
GW	1	1	0.610	-0.488	0.000	0.610	-0.427	0.000	0.003
GW	1	1	0.610	-0.427	0.000	0.610	-0.366	0.000	0.003
GW	1	1	0.610	-0.366	0.000	0.610	-0.305	0.000	0.003
GW	1	1	0.610	-0.305	0.000	0.610	-0.244	0.000	0.003
GW	1	1	0.610	-0.244	0.000	0.610	-0.183	0.000	0.003
GW	1	1	0.610	-0.183	0.000	0.610	-0.122	0.000	0.003
GW	1	1	0.610	-0.122	0.000	0.610	-0.061	0.000	0.003
GW	1	1	0.610	-0.061	0.000	0.610	0.000	0.000	0.003
GW	1	1	0.610	0.000	0.000	0.610	0.061	0.000	0.003
GW	1	1	0.610	0.061	0.000	0.610	0.122	0.000	0.003
GW	1	1	0.610	0.122	0.000	0.610	0.183	0.000	0.003
GW	1	1	0.610	0.183	0.000	0.610	0.244	0.000	0.003
GW	1	1	0.610	0.244	0.000	0.610	0.305	0.000	0.003
GW	1	1	0.610	0.305	0.000	0.610	0.366	0.000	0.003
GW	1	1	0.610	0.366	0.000	0.610	0.427	0.000	0.003
GW	1	1	0.610	0.427	0.000	0.610	0.488	0.000	0.003
GW	1	1	0.610	0.488	0.000	0.610	0.549	0.000	0.003
GW	1	1	0.610	0.549	0.000	0.610	0.610	0.000	0.003
EN									
FR	0	1	0	0	1000.000	1.000	0.000	0.000	0.000
EX	0	2	3	0	5.000	0.000	1.000	0.000	0.000
RP	0	721	1	1010	0	0	0.5	0.5	0.000

The NEC-2 input file for a $\lambda/4$ monopole above a finite circular ground plane (The diameter of the circular ground plane is 4'). The frequency is set at 1 GHz.

```

CM ****
CM *
CM * NEC-2 input file created by MatNEC on 10-Apr-97 *
CM *
CM * 1/4-Wavelength Monopole above a circular plate *
CM * The diameter of circular plate is 4' long *
CM * Freq. at 1 GHz *
CM *
CM ****
CE
GW 2 3 0.000 0.000 0.000 0.000 0.000 0.075 0.05
GW 1 1 0.000 0.000 0.000 0.061 0.000 0.000 0.003
GW 1 1 0.061 0.000 0.000 0.122 0.000 0.000 0.003
GW 1 1 0.122 0.000 0.000 0.183 0.000 0.000 0.003
GW 1 1 0.183 0.000 0.000 0.244 0.000 0.000 0.003
GW 1 1 0.244 0.000 0.000 0.305 0.000 0.000 0.003
GW 1 1 0.305 0.000 0.000 0.366 0.000 0.000 0.003
GW 1 1 0.366 0.000 0.000 0.427 0.000 0.000 0.003
GW 1 1 0.427 0.000 0.000 0.488 0.000 0.000 0.003
GW 1 1 0.488 0.000 0.000 0.549 0.000 0.000 0.003
GW 1 1 0.549 0.000 0.000 0.610 0.000 0.000 0.003
GW 1 1 0.000 0.000 0.000 0.060 0.013 0.000 0.003
GW 1 1 0.060 0.013 0.000 0.119 0.025 0.000 0.003
GW 1 1 0.119 0.025 0.000 0.179 0.038 0.000 0.003
GW 1 1 0.179 0.038 0.000 0.239 0.051 0.000 0.003
GW 1 1 0.239 0.051 0.000 0.298 0.063 0.000 0.003

```

GW	1	1	0.298	0.063	0.000	0.358	0.076	0.000	0.003
GW	1	1	0.358	0.076	0.000	0.417	0.089	0.000	0.003
GW	1	1	0.417	0.089	0.000	0.477	0.101	0.000	0.003
GW	1	1	0.477	0.101	0.000	0.537	0.114	0.000	0.003
GW	1	1	0.537	0.114	0.000	0.596	0.127	0.000	0.003
GW	1	1	0.000	0.000	0.000	0.056	0.025	0.000	0.003
GW	1	1	0.056	0.025	0.000	0.111	0.050	0.000	0.003
GW	1	1	0.111	0.050	0.000	0.167	0.074	0.000	0.003
GW	1	1	0.167	0.074	0.000	0.223	0.099	0.000	0.003
GW	1	1	0.223	0.099	0.000	0.278	0.124	0.000	0.003
GW	1	1	0.278	0.124	0.000	0.334	0.149	0.000	0.003
GW	1	1	0.334	0.149	0.000	0.390	0.174	0.000	0.003
GW	1	1	0.390	0.174	0.000	0.446	0.198	0.000	0.003
GW	1	1	0.446	0.198	0.000	0.501	0.223	0.000	0.003
GW	1	1	0.501	0.223	0.000	0.557	0.248	0.000	0.003
GW	1	1	0.000	0.000	0.000	0.049	0.036	0.000	0.003
GW	1	1	0.049	0.036	0.000	0.099	0.072	0.000	0.003
GW	1	1	0.099	0.072	0.000	0.148	0.107	0.000	0.003
GW	1	1	0.148	0.107	0.000	0.197	0.143	0.000	0.003
GW	1	1	0.197	0.143	0.000	0.247	0.179	0.000	0.003
GW	1	1	0.247	0.179	0.000	0.296	0.215	0.000	0.003
GW	1	1	0.296	0.215	0.000	0.345	0.251	0.000	0.003
GW	1	1	0.345	0.251	0.000	0.395	0.287	0.000	0.003
GW	1	1	0.395	0.287	0.000	0.444	0.322	0.000	0.003
GW	1	1	0.444	0.322	0.000	0.493	0.358	0.000	0.003
GW	1	1	0.000	0.000	0.000	0.041	0.045	0.000	0.003
GW	1	1	0.041	0.045	0.000	0.082	0.091	0.000	0.003
GW	1	1	0.082	0.091	0.000	0.122	0.136	0.000	0.003
GW	1	1	0.122	0.136	0.000	0.163	0.181	0.000	0.003
GW	1	1	0.163	0.181	0.000	0.204	0.227	0.000	0.003
GW	1	1	0.204	0.227	0.000	0.245	0.272	0.000	0.003
GW	1	1	0.245	0.272	0.000	0.286	0.317	0.000	0.003
GW	1	1	0.286	0.317	0.000	0.326	0.362	0.000	0.003
GW	1	1	0.326	0.362	0.000	0.367	0.408	0.000	0.003
GW	1	1	0.367	0.408	0.000	0.408	0.453	0.000	0.003
GW	1	1	0.030	0.053	0.000	0.061	0.106	0.000	0.003
GW	1	1	0.061	0.106	0.000	0.091	0.158	0.000	0.003
GW	1	1	0.091	0.158	0.000	0.122	0.211	0.000	0.003
GW	1	1	0.122	0.211	0.000	0.152	0.264	0.000	0.003
GW	1	1	0.152	0.264	0.000	0.183	0.317	0.000	0.003
GW	1	1	0.183	0.317	0.000	0.213	0.370	0.000	0.003
GW	1	1	0.213	0.370	0.000	0.244	0.422	0.000	0.003
GW	1	1	0.244	0.422	0.000	0.274	0.475	0.000	0.003
GW	1	1	0.274	0.475	0.000	0.305	0.528	0.000	0.003
GW	1	1	0.000	0.000	0.000	0.019	0.058	0.000	0.003
GW	1	1	0.019	0.058	0.000	0.038	0.116	0.000	0.003
GW	1	1	0.038	0.116	0.000	0.057	0.174	0.000	0.003
GW	1	1	0.057	0.174	0.000	0.075	0.232	0.000	0.003
GW	1	1	0.075	0.232	0.000	0.094	0.290	0.000	0.003
GW	1	1	0.094	0.290	0.000	0.113	0.348	0.000	0.003
GW	1	1	0.113	0.348	0.000	0.132	0.406	0.000	0.003
GW	1	1	0.132	0.406	0.000	0.151	0.464	0.000	0.003
GW	1	1	0.151	0.464	0.000	0.170	0.522	0.000	0.003
GW	1	1	0.170	0.522	0.000	0.188	0.580	0.000	0.003
GW	1	1	0.000	0.000	0.000	0.006	0.061	0.000	0.003
GW	1	1	0.006	0.061	0.000	0.013	0.121	0.000	0.003
GW	1	1	0.013	0.121	0.000	0.019	0.182	0.000	0.003
GW	1	1	0.019	0.182	0.000	0.025	0.243	0.000	0.003
GW	1	1	0.025	0.243	0.000	0.032	0.303	0.000	0.003
GW	1	1	0.032	0.303	0.000	0.038	0.364	0.000	0.003
GW	1	1	0.038	0.364	0.000	0.045	0.424	0.000	0.003
GW	1	1	0.045	0.424	0.000	0.051	0.485	0.000	0.003
GW	1	1	0.051	0.424	0.000	0.051	0.485	0.000	0.003
GW	1	1	0.051	0.485	0.000	0.057	0.546	0.000	0.003
GW	1	1	0.057	0.546	0.000	0.064	0.606	0.000	0.003
GW	1	1	0.000	0.000	0.000	-0.006	0.061	0.000	0.003
GW	1	1	-0.006	0.061	0.000	-0.013	0.121	0.000	0.003
GW	1	1	-0.013	0.121	0.000	-0.019	0.182	0.000	0.003
GW	1	1	-0.019	0.182	0.000	-0.025	0.243	0.000	0.003
GW	1	1	-0.025	0.243	0.000	-0.032	0.303	0.000	0.003
GW	1	1	-0.032	0.303	0.000	-0.038	0.364	0.000	0.003
GW	1	1	-0.038	0.364	0.000	-0.045	0.424	0.000	0.003
GW	1	1	-0.045	0.424	0.000	-0.051	0.485	0.000	0.003
GW	1	1	-0.051	0.485	0.000	-0.057	0.546	0.000	0.003
GW	1	1	-0.057	0.546	0.000	-0.064	0.606	0.000	0.003
GW	1	1	0.000	0.000	0.000	-0.019	0.058	0.000	0.003
GW	1	1	-0.019	0.058	0.000	-0.038	0.116	0.000	0.003
GW	1	1	-0.038	0.116	0.000	-0.057	0.174	0.000	0.003
GW	1	1	-0.057	0.174	0.000	-0.075	0.232	0.000	0.003
GW	1	1	-0.075	0.232	0.000	-0.094	0.290	0.000	0.003
GW	1	1	-0.094	0.290	0.000	-0.113	0.348	0.000	0.003
GW	1	1	-0.113	0.348	0.000	-0.132	0.406	0.000	0.003
GW	1	1	-0.132	0.406	0.000	-0.151	0.464	0.000	0.003
GW	1	1	-0.151	0.464	0.000	-0.170	0.522	0.000	0.003
GW	1	1	-0.170	0.522	0.000	-0.188	0.580	0.000	0.003
GW	1	1	0.000	0.000	0.000	-0.030	0.053	0.000	0.003
GW	1	1	-0.030	0.053	0.000	-0.061	0.106	0.000	0.003
GW	1	1	-0.061	0.106	0.000	-0.091	0.158	0.000	0.003
GW	1	1	-0.091	0.158	0.000	-0.122	0.211	0.000	0.003
GW	1	1	-0.122	0.211	0.000	-0.152	0.264	0.000	0.003
GW	1	1	-0.152	0.264	0.000	-0.183	0.317	0.000	0.003

GW	1	1	-0.183	0.317	0.000	-0.213	0.370	0.000	0.003
GW	1	1	-0.213	0.370	0.000	-0.244	0.422	0.000	0.003
GW	1	1	-0.244	0.422	0.000	-0.274	0.475	0.000	0.003
GW	1	1	-0.274	0.475	0.000	-0.305	0.528	0.000	0.003
GW	1	1	-0.041	0.045	0.000	-0.082	0.091	0.000	0.003
GW	1	1	-0.082	0.091	0.000	-0.122	0.136	0.000	0.003
GW	1	1	-0.122	0.136	0.000	-0.163	0.181	0.000	0.003
GW	1	1	-0.163	0.181	0.000	-0.204	0.227	0.000	0.003
GW	1	1	-0.204	0.227	0.000	-0.245	0.272	0.000	0.003
GW	1	1	-0.245	0.272	0.000	-0.286	0.317	0.000	0.003
GW	1	1	-0.286	0.317	0.000	-0.326	0.362	0.000	0.003
GW	1	1	-0.326	0.362	0.000	-0.367	0.408	0.000	0.003
GW	1	1	-0.367	0.408	0.000	-0.408	0.453	0.000	0.003
GW	1	1	0.000	0.000	0.000	-0.049	0.036	0.000	0.003
GW	1	1	-0.049	0.036	0.000	-0.099	0.072	0.000	0.003
GW	1	1	-0.099	0.072	0.000	-0.148	0.107	0.000	0.003
GW	1	1	-0.148	0.107	0.000	-0.197	0.143	0.000	0.003
GW	1	1	-0.197	0.143	0.000	-0.247	0.179	0.000	0.003
GW	1	1	-0.247	0.179	0.000	-0.296	0.215	0.000	0.003
GW	1	1	-0.296	0.215	0.000	-0.345	0.251	0.000	0.003
GW	1	1	-0.345	0.251	0.000	-0.395	0.287	0.000	0.003
GW	1	1	-0.395	0.287	0.000	-0.444	0.322	0.000	0.003
GW	1	1	-0.444	0.322	0.000	-0.493	0.358	0.000	0.003
GW	1	1	0.000	0.000	0.000	-0.056	0.025	0.000	0.003
GW	1	1	-0.056	0.025	0.000	-0.111	0.050	0.000	0.003
GW	1	1	-0.111	0.050	0.000	-0.167	0.074	0.000	0.003
GW	1	1	-0.167	0.074	0.000	-0.223	0.099	0.000	0.003
GW	1	1	-0.223	0.099	0.000	-0.278	0.124	0.000	0.003
GW	1	1	-0.278	0.124	0.000	-0.334	0.149	0.000	0.003
GW	1	1	-0.334	0.149	0.000	-0.390	0.174	0.000	0.003
GW	1	1	-0.390	0.174	0.000	-0.446	0.198	0.000	0.003
GW	1	1	-0.446	0.198	0.000	-0.501	0.223	0.000	0.003
GW	1	1	-0.501	0.223	0.000	-0.557	0.248	0.000	0.003
GW	1	1	0.000	0.000	0.000	-0.060	0.013	0.000	0.003
GW	1	1	-0.060	0.013	0.000	-0.119	0.025	0.000	0.003
GW	1	1	-0.119	0.025	0.000	-0.179	0.038	0.000	0.003
GW	1	1	-0.179	0.038	0.000	-0.239	0.051	0.000	0.003
GW	1	1	-0.239	0.051	0.000	-0.298	0.063	0.000	0.003
GW	1	1	-0.298	0.063	0.000	-0.358	0.076	0.000	0.003
GW	1	1	-0.358	0.076	0.000	-0.417	0.089	0.000	0.003
GW	1	1	-0.417	0.089	0.000	-0.477	0.101	0.000	0.003
GW	1	1	-0.477	0.101	0.000	-0.537	0.114	0.000	0.003
GW	1	1	-0.537	0.114	0.000	-0.596	0.127	0.000	0.003
GW	1	1	0.000	0.000	0.000	-0.061	0.000	0.000	0.003
GW	1	1	-0.061	0.000	0.000	-0.122	0.000	0.000	0.003
GW	1	1	-0.122	0.000	0.000	-0.183	0.000	0.000	0.003
GW	1	1	-0.183	0.000	0.000	-0.244	0.000	0.000	0.003
GW	1	1	-0.244	0.000	0.000	-0.305	0.000	0.000	0.003
GW	1	1	-0.305	0.000	0.000	-0.366	0.000	0.000	0.003
GW	1	1	-0.366	0.000	0.000	-0.427	0.000	0.000	0.003
GW	1	1	-0.427	0.000	0.000	-0.488	0.000	0.000	0.003
GW	1	1	-0.488	0.000	0.000	-0.549	0.000	0.000	0.003
GW	1	1	-0.549	0.000	0.000	-0.610	0.000	0.000	0.003
GW	1	1	0.000	0.000	0.000	-0.060	-0.013	0.000	0.003
GW	1	1	-0.060	-0.013	0.000	-0.119	-0.025	0.000	0.003
GW	1	1	-0.119	-0.025	0.000	-0.179	-0.038	0.000	0.003
GW	1	1	-0.179	-0.038	0.000	-0.239	-0.051	0.000	0.003
GW	1	1	-0.239	-0.051	0.000	-0.298	-0.063	0.000	0.003
GW	1	1	-0.298	-0.063	0.000	-0.358	-0.076	0.000	0.003
GW	1	1	-0.358	-0.076	0.000	-0.417	-0.089	0.000	0.003
GW	1	1	-0.417	-0.089	0.000	-0.477	-0.101	0.000	0.003
GW	1	1	-0.477	-0.101	0.000	-0.537	-0.114	0.000	0.003
GW	1	1	-0.537	-0.114	0.000	-0.596	-0.127	0.000	0.003
GW	1	1	-0.056	-0.025	0.000	-0.111	-0.050	0.000	0.003
GW	1	1	-0.111	-0.050	0.000	-0.167	-0.074	0.000	0.003
GW	1	1	-0.167	-0.074	0.000	-0.223	-0.099	0.000	0.003
GW	1	1	-0.223	-0.099	0.000	-0.278	-0.124	0.000	0.003
GW	1	1	-0.278	-0.124	0.000	-0.334	-0.149	0.000	0.003
GW	1	1	-0.334	-0.149	0.000	-0.390	-0.174	0.000	0.003
GW	1	1	-0.390	-0.174	0.000	-0.446	-0.198	0.000	0.003
GW	1	1	-0.446	-0.198	0.000	-0.501	-0.223	0.000	0.003
GW	1	1	-0.501	-0.223	0.000	-0.557	-0.248	0.000	0.003
GW	1	1	0.000	0.000	0.000	-0.049	-0.036	0.000	0.003
GW	1	1	-0.049	-0.036	0.000	-0.099	-0.072	0.000	0.003
GW	1	1	-0.099	-0.072	0.000	-0.148	-0.107	0.000	0.003
GW	1	1	-0.148	-0.107	0.000	-0.197	-0.143	0.000	0.003
GW	1	1	-0.197	-0.143	0.000	-0.247	-0.179	0.000	0.003
GW	1	1	-0.247	-0.179	0.000	-0.296	-0.215	0.000	0.003
GW	1	1	-0.296	-0.215	0.000	-0.345	-0.251	0.000	0.003
GW	1	1	-0.345	-0.251	0.000	-0.395	-0.287	0.000	0.003
GW	1	1	-0.395	-0.287	0.000	-0.444	-0.322	0.000	0.003
GW	1	1	-0.444	-0.322	0.000	-0.493	-0.358	0.000	0.003
GW	1	1	0.000	0.000	0.000	-0.041	-0.045	0.000	0.003
GW	1	1	-0.041	-0.045	0.000	-0.082	-0.091	0.000	0.003
GW	1	1	-0.082	-0.091	0.000	-0.122	-0.136	0.000	0.003
GW	1	1	-0.122	-0.136	0.000	-0.163	-0.181	0.000	0.003
GW	1	1	-0.163	-0.181	0.000	-0.204	-0.227	0.000	0.003
GW	1	1	-0.204	-0.227	0.000	-0.245	-0.272	0.000	0.003
GW	1	1	-0.245	-0.272	0.000	-0.286	-0.317	0.000	0.003
GW	1	1	-0.286	-0.317	0.000	-0.326	-0.362	0.000	0.003

GW	1	1	-0.326	-0.362	0.000	-0.367	-0.408	0.000	0.003
GW	1	1	-0.367	-0.408	0.000	-0.408	-0.453	0.000	0.003
GW	1	1	0.000	0.000	0.000	-0.030	-0.053	0.000	0.003
GW	1	1	-0.030	-0.053	0.000	-0.061	-0.106	0.000	0.003
GW	1	1	-0.061	-0.106	0.000	-0.091	-0.158	0.000	0.003
GW	1	1	-0.091	-0.158	0.000	-0.122	-0.211	0.000	0.003
GW	1	1	-0.122	-0.211	0.000	-0.152	-0.264	0.000	0.003
GW	1	1	-0.152	-0.264	0.000	-0.183	-0.317	0.000	0.003
GW	1	1	-0.183	-0.317	0.000	-0.213	-0.370	0.000	0.003
GW	1	1	-0.213	-0.370	0.000	-0.244	-0.422	0.000	0.003
GW	1	1	-0.244	-0.422	0.000	-0.274	-0.475	0.000	0.003
GW	1	1	-0.274	-0.475	0.000	-0.305	-0.528	0.000	0.003
GW	1	1	0.000	0.000	0.000	-0.019	-0.058	0.000	0.003
GW	1	1	-0.019	-0.058	0.000	-0.038	-0.116	0.000	0.003
GW	1	1	-0.038	-0.116	0.000	-0.057	-0.174	0.000	0.003
GW	1	1	-0.057	-0.174	0.000	-0.075	-0.232	0.000	0.003
GW	1	1	-0.075	-0.232	0.000	-0.094	-0.290	0.000	0.003
GW	1	1	-0.094	-0.290	0.000	-0.113	-0.348	0.000	0.003
GW	1	1	-0.113	-0.348	0.000	-0.132	-0.406	0.000	0.003
GW	1	1	-0.132	-0.406	0.000	-0.151	-0.464	0.000	0.003
GW	1	1	-0.151	-0.464	0.000	-0.170	-0.522	0.000	0.003
GW	1	1	-0.170	-0.522	0.000	-0.188	-0.580	0.000	0.003
GW	1	1	0.000	0.000	0.000	-0.006	-0.061	0.000	0.003
GW	1	1	-0.006	-0.061	0.000	-0.013	-0.121	0.000	0.003
GW	1	1	-0.013	-0.121	0.000	-0.019	-0.182	0.000	0.003
GW	1	1	-0.019	-0.182	0.000	-0.025	-0.243	0.000	0.003
GW	1	1	-0.025	-0.243	0.000	-0.032	-0.303	0.000	0.003
GW	1	1	-0.032	-0.303	0.000	-0.038	-0.364	0.000	0.003
GW	1	1	-0.038	-0.364	0.000	-0.045	-0.424	0.000	0.003
GW	1	1	-0.045	-0.424	0.000	-0.051	-0.485	0.000	0.003
GW	1	1	-0.051	-0.485	0.000	-0.057	-0.546	0.000	0.003
GW	1	1	-0.057	-0.546	0.000	-0.064	-0.606	0.000	0.003
GW	1	1	0.006	-0.061	0.000	0.013	-0.121	0.000	0.003
GW	1	1	0.013	-0.121	0.000	0.019	-0.182	0.000	0.003
GW	1	1	0.019	-0.182	0.000	0.025	-0.243	0.000	0.003
GW	1	1	0.025	-0.243	0.000	0.032	-0.303	0.000	0.003
GW	1	1	0.032	-0.303	0.000	0.038	-0.364	0.000	0.003
GW	1	1	0.038	-0.364	0.000	0.045	-0.424	0.000	0.003
GW	1	1	0.045	-0.424	0.000	0.051	-0.485	0.000	0.003
GW	1	1	0.051	-0.485	0.000	0.057	-0.546	0.000	0.003
GW	1	1	0.057	-0.546	0.000	0.064	-0.606	0.000	0.003
GW	1	1	0.000	0.000	0.000	0.019	-0.058	0.000	0.003
GW	1	1	0.019	-0.058	0.000	0.038	-0.116	0.000	0.003
GW	1	1	0.038	-0.116	0.000	0.057	-0.174	0.000	0.003
GW	1	1	0.057	-0.174	0.000	0.075	-0.232	0.000	0.003
GW	1	1	0.075	-0.232	0.000	0.094	-0.290	0.000	0.003
GW	1	1	0.094	-0.290	0.000	0.113	-0.348	0.000	0.003
GW	1	1	0.113	-0.348	0.000	0.132	-0.406	0.000	0.003
GW	1	1	0.132	-0.406	0.000	0.151	-0.464	0.000	0.003
GW	1	1	0.151	-0.464	0.000	0.170	-0.522	0.000	0.003
GW	1	1	0.170	-0.522	0.000	0.188	-0.580	0.000	0.003
GW	1	1	0.000	0.000	0.000	0.030	-0.053	0.000	0.003
GW	1	1	0.030	-0.053	0.000	0.061	-0.106	0.000	0.003
GW	1	1	0.061	-0.106	0.000	0.091	-0.158	0.000	0.003
GW	1	1	0.091	-0.158	0.000	0.122	-0.211	0.000	0.003
GW	1	1	0.122	-0.211	0.000	0.152	-0.264	0.000	0.003
GW	1	1	0.152	-0.264	0.000	0.183	-0.317	0.000	0.003
GW	1	1	0.183	-0.317	0.000	0.213	-0.370	0.000	0.003
GW	1	1	0.213	-0.370	0.000	0.244	-0.422	0.000	0.003
GW	1	1	0.244	-0.422	0.000	0.274	-0.475	0.000	0.003
GW	1	1	0.274	-0.475	0.000	0.305	-0.528	0.000	0.003
GW	1	1	0.000	0.000	0.000	0.041	-0.045	0.000	0.003
GW	1	1	0.041	-0.045	0.000	0.082	-0.091	0.000	0.003
GW	1	1	0.082	-0.091	0.000	0.122	-0.136	0.000	0.003
GW	1	1	0.122	-0.136	0.000	0.163	-0.181	0.000	0.003
GW	1	1	0.163	-0.181	0.000	0.204	-0.227	0.000	0.003
GW	1	1	0.204	-0.227	0.000	0.245	-0.272	0.000	0.003
GW	1	1	0.245	-0.272	0.000	0.286	-0.317	0.000	0.003
GW	1	1	0.286	-0.317	0.000	0.326	-0.362	0.000	0.003
GW	1	1	0.326	-0.362	0.000	0.367	-0.408	0.000	0.003
GW	1	1	0.367	-0.408	0.000	0.408	-0.453	0.000	0.003
GW	1	1	0.000	0.000	0.000	0.049	-0.036	0.000	0.003
GW	1	1	0.049	-0.036	0.000	0.099	-0.072	0.000	0.003
GW	1	1	0.099	-0.072	0.000	0.148	-0.107	0.000	0.003
GW	1	1	0.148	-0.107	0.000	0.197	-0.143	0.000	0.003
GW	1	1	0.197	-0.143	0.000	0.247	-0.179	0.000	0.003
GW	1	1	0.247	-0.179	0.000	0.296	-0.215	0.000	0.003
GW	1	1	0.296	-0.215	0.000	0.345	-0.251	0.000	0.003
GW	1	1	0.345	-0.251	0.000	0.395	-0.287	0.000	0.003
GW	1	1	0.395	-0.287	0.000	0.444	-0.322	0.000	0.003
GW	1	1	0.444	-0.322	0.000	0.493	-0.358	0.000	0.003
GW	1	1	0.000	0.000	0.000	0.056	-0.025	0.000	0.003
GW	1	1	0.056	-0.025	0.000	0.111	-0.050	0.000	0.003
GW	1	1	0.111	-0.050	0.000	0.167	-0.074	0.000	0.003
GW	1	1	0.167	-0.074	0.000	0.223	-0.099	0.000	0.003
GW	1	1	0.223	-0.099	0.000	0.278	-0.124	0.000	0.003
GW	1	1	0.278	-0.124	0.000	0.334	-0.149	0.000	0.003
GW	1	1	0.334	-0.149	0.000	0.390	-0.174	0.000	0.003
GW	1	1	0.390	-0.174	0.000	0.446	-0.198	0.000	0.003
GW	1	1	0.446	-0.198	0.000	0.501	-0.223	0.000	0.003

GW	1	1	0.501	-0.223	0.000	0.557	-0.248	0.000	0.003
GW	1	1	0.060	-0.013	0.000	0.119	-0.025	0.000	0.003
GW	1	1	0.119	-0.025	0.000	0.179	-0.038	0.000	0.003
GW	1	1	0.179	-0.038	0.000	0.239	-0.051	0.000	0.003
GW	1	1	0.239	-0.051	0.000	0.298	-0.063	0.000	0.003
GW	1	1	0.298	-0.063	0.000	0.358	-0.076	0.000	0.003
GW	1	1	0.358	-0.076	0.000	0.417	-0.089	0.000	0.003
GW	1	1	0.417	-0.089	0.000	0.477	-0.101	0.000	0.003
GW	1	1	0.477	-0.101	0.000	0.537	-0.114	0.000	0.003
GW	1	1	0.537	-0.114	0.000	0.596	-0.127	0.000	0.003
GW	1	1	0.061	0.000	0.000	0.060	0.013	0.000	0.003
GW	1	1	0.122	0.000	0.000	0.119	0.025	0.000	0.003
GW	1	1	0.183	0.000	0.000	0.179	0.038	0.000	0.003
GW	1	1	0.244	0.000	0.000	0.239	0.051	0.000	0.003
GW	1	1	0.305	0.000	0.000	0.298	0.063	0.000	0.003
GW	1	1	0.366	0.000	0.000	0.358	0.076	0.000	0.003
GW	1	1	0.427	0.000	0.000	0.417	0.089	0.000	0.003
GW	1	1	0.488	0.000	0.000	0.477	0.101	0.000	0.003
GW	1	1	0.549	0.000	0.000	0.537	0.114	0.000	0.003
GW	1	1	0.610	0.000	0.000	0.596	0.127	0.000	0.003
GW	1	1	0.060	0.013	0.000	0.056	0.025	0.000	0.003
GW	1	1	0.119	0.025	0.000	0.111	0.050	0.000	0.003
GW	1	1	0.179	0.038	0.000	0.167	0.074	0.000	0.003
GW	1	1	0.239	0.051	0.000	0.223	0.099	0.000	0.003
GW	1	1	0.298	0.063	0.000	0.278	0.124	0.000	0.003
GW	1	1	0.358	0.076	0.000	0.334	0.149	0.000	0.003
GW	1	1	0.417	0.089	0.000	0.390	0.174	0.000	0.003
GW	1	1	0.477	0.101	0.000	0.446	0.198	0.000	0.003
GW	1	1	0.537	0.114	0.000	0.501	0.223	0.000	0.003
GW	1	1	0.596	0.127	0.000	0.557	0.248	0.000	0.003
GW	1	1	0.056	0.025	0.000	0.049	0.036	0.000	0.003
GW	1	1	0.111	0.050	0.000	0.099	0.072	0.000	0.003
GW	1	1	0.167	0.074	0.000	0.148	0.107	0.000	0.003
GW	1	1	0.223	0.099	0.000	0.197	0.143	0.000	0.003
GW	1	1	0.278	0.124	0.000	0.247	0.179	0.000	0.003
GW	1	1	0.334	0.149	0.000	0.296	0.215	0.000	0.003
GW	1	1	0.390	0.174	0.000	0.345	0.251	0.000	0.003
GW	1	1	0.446	0.198	0.000	0.395	0.287	0.000	0.003
GW	1	1	0.501	0.223	0.000	0.444	0.322	0.000	0.003
GW	1	1	0.557	0.248	0.000	0.493	0.358	0.000	0.003
GW	1	1	0.049	0.036	0.000	0.041	0.045	0.000	0.003
GW	1	1	0.099	0.072	0.000	0.082	0.091	0.000	0.003
GW	1	1	0.148	0.107	0.000	0.122	0.136	0.000	0.003
GW	1	1	0.197	0.143	0.000	0.163	0.181	0.000	0.003
GW	1	1	0.247	0.179	0.000	0.204	0.227	0.000	0.003
GW	1	1	0.296	0.215	0.000	0.245	0.272	0.000	0.003
GW	1	1	0.345	0.251	0.000	0.286	0.317	0.000	0.003
GW	1	1	0.395	0.287	0.000	0.326	0.362	0.000	0.003
GW	1	1	0.444	0.322	0.000	0.367	0.408	0.000	0.003
GW	1	1	0.493	0.358	0.000	0.408	0.453	0.000	0.003
GW	1	1	0.041	0.045	0.000	0.030	0.053	0.000	0.003
GW	1	1	0.082	0.091	0.000	0.061	0.106	0.000	0.003
GW	1	1	0.122	0.136	0.000	0.091	0.158	0.000	0.003
GW	1	1	0.163	0.181	0.000	0.122	0.211	0.000	0.003
GW	1	1	0.204	0.227	0.000	0.152	0.264	0.000	0.003
GW	1	1	0.245	0.272	0.000	0.183	0.317	0.000	0.003
GW	1	1	0.286	0.317	0.000	0.213	0.370	0.000	0.003
GW	1	1	0.326	0.362	0.000	0.244	0.422	0.000	0.003
GW	1	1	0.367	0.408	0.000	0.274	0.475	0.000	0.003
GW	1	1	0.408	0.453	0.000	0.305	0.528	0.000	0.003
GW	1	1	0.030	0.053	0.000	0.019	0.058	0.000	0.003
GW	1	1	0.061	0.106	0.000	0.038	0.116	0.000	0.003
GW	1	1	0.091	0.158	0.000	0.057	0.174	0.000	0.003
GW	1	1	0.122	0.211	0.000	0.075	0.232	0.000	0.003
GW	1	1	0.152	0.264	0.000	0.094	0.290	0.000	0.003
GW	1	1	0.183	0.317	0.000	0.113	0.348	0.000	0.003
GW	1	1	0.213	0.370	0.000	0.132	0.406	0.000	0.003
GW	1	1	0.244	0.422	0.000	0.151	0.464	0.000	0.003
GW	1	1	0.274	0.475	0.000	0.170	0.522	0.000	0.003
GW	1	1	0.305	0.528	0.000	0.188	0.580	0.000	0.003
GW	1	1	0.019	0.058	0.000	0.006	0.061	0.000	0.003
GW	1	1	0.038	0.116	0.000	0.013	0.121	0.000	0.003
GW	1	1	0.057	0.174	0.000	0.019	0.182	0.000	0.003
GW	1	1	0.075	0.232	0.000	0.025	0.243	0.000	0.003
GW	1	1	0.094	0.290	0.000	0.032	0.303	0.000	0.003
GW	1	1	0.113	0.348	0.000	0.038	0.364	0.000	0.003
GW	1	1	0.132	0.406	0.000	0.045	0.424	0.000	0.003
GW	1	1	0.151	0.464	0.000	0.051	0.485	0.000	0.003
GW	1	1	0.170	0.522	0.000	0.057	0.546	0.000	0.003
GW	1	1	0.188	0.580	0.000	0.064	0.606	0.000	0.003
GW	1	1	0.006	0.061	0.000	-0.006	0.061	0.000	0.003
GW	1	1	0.013	0.121	0.000	-0.013	0.121	0.000	0.003
GW	1	1	0.019	0.182	0.000	-0.019	0.182	0.000	0.003
GW	1	1	0.025	0.243	0.000	-0.025	0.243	0.000	0.003
GW	1	1	0.032	0.303	0.000	-0.032	0.303	0.000	0.003
GW	1	1	0.038	0.364	0.000	-0.038	0.364	0.000	0.003
GW	1	1	0.045	0.424	0.000	-0.045	0.424	0.000	0.003
GW	1	1	0.051	0.485	0.000	-0.051	0.485	0.000	0.003
GW	1	1	0.057	0.546	0.000	-0.057	0.546	0.000	0.003
GW	1	1	0.064	0.606	0.000	-0.064	0.606	0.000	0.003

GW	1	1	-0.006	0.061	0.000	-0.019	0.058	0.000	0.003
GW	1	1	-0.013	0.121	0.000	-0.038	0.116	0.000	0.003
GW	1	1	-0.019	0.182	0.000	-0.057	0.174	0.000	0.003
GW	1	1	-0.025	0.243	0.000	-0.075	0.232	0.000	0.003
GW	1	1	-0.032	0.303	0.000	-0.094	0.290	0.000	0.003
GW	1	1	-0.038	0.364	0.000	-0.113	0.348	0.000	0.003
GW	1	1	-0.045	0.424	0.000	-0.132	0.406	0.000	0.003
GW	1	1	-0.051	0.485	0.000	-0.151	0.464	0.000	0.003
GW	1	1	-0.057	0.546	0.000	-0.170	0.522	0.000	0.003
GW	1	1	-0.064	0.606	0.000	-0.188	0.580	0.000	0.003
GW	1	1	-0.019	0.058	0.000	-0.030	0.053	0.000	0.003
GW	1	1	-0.038	0.116	0.000	-0.061	0.106	0.000	0.003
GW	1	1	-0.057	0.174	0.000	-0.091	0.158	0.000	0.003
GW	1	1	-0.075	0.232	0.000	-0.122	0.211	0.000	0.003
GW	1	1	-0.094	0.290	0.000	-0.152	0.264	0.000	0.003
GW	1	1	-0.113	0.348	0.000	-0.183	0.317	0.000	0.003
GW	1	1	-0.132	0.406	0.000	-0.213	0.370	0.000	0.003
GW	1	1	-0.151	0.464	0.000	-0.244	0.422	0.000	0.003
GW	1	1	-0.170	0.522	0.000	-0.274	0.475	0.000	0.003
GW	1	1	-0.188	0.580	0.000	-0.305	0.528	0.000	0.003
GW	1	1	-0.030	0.053	0.000	-0.041	0.045	0.000	0.003
GW	1	1	-0.061	0.106	0.000	-0.082	0.091	0.000	0.003
GW	1	1	-0.091	0.158	0.000	-0.122	0.136	0.000	0.003
GW	1	1	-0.122	0.211	0.000	-0.163	0.181	0.000	0.003
GW	1	1	-0.152	0.264	0.000	-0.204	0.227	0.000	0.003
GW	1	1	-0.183	0.317	0.000	-0.245	0.272	0.000	0.003
GW	1	1	-0.213	0.370	0.000	-0.286	0.317	0.000	0.003
GW	1	1	-0.244	0.422	0.000	-0.326	0.362	0.000	0.003
GW	1	1	-0.274	0.475	0.000	-0.367	0.408	0.000	0.003
GW	1	1	-0.305	0.528	0.000	-0.408	0.453	0.000	0.003
GW	1	1	-0.041	0.045	0.000	-0.049	0.036	0.000	0.003
GW	1	1	-0.082	0.091	0.000	-0.099	0.072	0.000	0.003
GW	1	1	-0.122	0.136	0.000	-0.148	0.107	0.000	0.003
GW	1	1	-0.163	0.181	0.000	-0.197	0.143	0.000	0.003
GW	1	1	-0.204	0.227	0.000	-0.247	0.179	0.000	0.003
GW	1	1	-0.245	0.272	0.000	-0.296	0.215	0.000	0.003
GW	1	1	-0.286	0.317	0.000	-0.345	0.251	0.000	0.003
GW	1	1	-0.326	0.362	0.000	-0.395	0.287	0.000	0.003
GW	1	1	-0.367	0.408	0.000	-0.444	0.322	0.000	0.003
GW	1	1	-0.408	0.453	0.000	-0.493	0.358	0.000	0.003
GW	1	1	-0.049	0.036	0.000	-0.056	0.025	0.000	0.003
GW	1	1	-0.099	0.072	0.000	-0.111	0.050	0.000	0.003
GW	1	1	-0.148	0.107	0.000	-0.167	0.074	0.000	0.003
GW	1	1	-0.197	0.143	0.000	-0.223	0.099	0.000	0.003
GW	1	1	-0.247	0.179	0.000	-0.278	0.124	0.000	0.003
GW	1	1	-0.296	0.215	0.000	-0.334	0.149	0.000	0.003
GW	1	1	-0.345	0.251	0.000	-0.390	0.174	0.000	0.003
GW	1	1	-0.395	0.287	0.000	-0.446	0.198	0.000	0.003
GW	1	1	-0.444	0.322	0.000	-0.501	0.223	0.000	0.003
GW	1	1	-0.493	0.358	0.000	-0.557	0.248	0.000	0.003
GW	1	1	-0.056	0.025	0.000	-0.060	0.013	0.000	0.003
GW	1	1	-0.111	0.050	0.000	-0.119	0.025	0.000	0.003
GW	1	1	-0.167	0.074	0.000	-0.179	0.038	0.000	0.003
GW	1	1	-0.223	0.099	0.000	-0.239	0.051	0.000	0.003
GW	1	1	-0.278	0.124	0.000	-0.298	0.063	0.000	0.003
GW	1	1	-0.334	0.149	0.000	-0.358	0.076	0.000	0.003
GW	1	1	-0.390	0.174	0.000	-0.417	0.089	0.000	0.003
GW	1	1	-0.446	0.198	0.000	-0.477	0.101	0.000	0.003
GW	1	1	-0.501	0.223	0.000	-0.537	0.114	0.000	0.003
GW	1	1	-0.557	0.248	0.000	-0.596	0.127	0.000	0.003
GW	1	1	-0.060	0.013	0.000	-0.061	0.000	0.000	0.003
GW	1	1	-0.119	0.025	0.000	-0.122	0.000	0.000	0.003
GW	1	1	-0.179	0.038	0.000	-0.183	0.000	0.000	0.003
GW	1	1	-0.239	0.051	0.000	-0.244	0.000	0.000	0.003
GW	1	1	-0.298	0.063	0.000	-0.305	0.000	0.000	0.003
GW	1	1	-0.358	0.076	0.000	-0.366	0.000	0.000	0.003
GW	1	1	-0.417	0.089	0.000	-0.427	0.000	0.000	0.003
GW	1	1	-0.477	0.101	0.000	-0.488	0.000	0.000	0.003
GW	1	1	-0.537	0.114	0.000	-0.549	0.000	0.000	0.003
GW	1	1	-0.596	0.127	0.000	-0.610	0.000	0.000	0.003
GW	1	1	-0.061	0.000	0.000	-0.060	-0.013	0.000	0.003
GW	1	1	-0.122	0.000	0.000	-0.119	-0.025	0.000	0.003
GW	1	1	-0.183	0.000	0.000	-0.179	-0.038	0.000	0.003
GW	1	1	-0.244	0.000	0.000	-0.239	-0.051	0.000	0.003
GW	1	1	-0.305	0.000	0.000	-0.298	-0.063	0.000	0.003
GW	1	1	-0.366	0.000	0.000	-0.358	-0.076	0.000	0.003
GW	1	1	-0.427	0.000	0.000	-0.417	-0.089	0.000	0.003
GW	1	1	-0.488	0.000	0.000	-0.477	-0.101	0.000	0.003
GW	1	1	-0.549	0.000	0.000	-0.537	-0.114	0.000	0.003
GW	1	1	-0.610	0.000	0.000	-0.596	-0.127	0.000	0.003
GW	1	1	-0.060	-0.013	0.000	-0.056	-0.025	0.000	0.003
GW	1	1	-0.119	-0.025	0.000	-0.111	-0.050	0.000	0.003
GW	1	1	-0.179	-0.038	0.000	-0.167	-0.074	0.000	0.003
GW	1	1	-0.239	-0.051	0.000	-0.223	-0.099	0.000	0.003
GW	1	1	-0.298	-0.063	0.000	-0.278	-0.124	0.000	0.003
GW	1	1	-0.358	-0.076	0.000	-0.334	-0.149	0.000	0.003
GW	1	1	-0.417	-0.089	0.000	-0.390	-0.174	0.000	0.003
GW	1	1	-0.477	-0.101	0.000	-0.446	-0.198	0.000	0.003
GW	1	1	-0.537	-0.114	0.000	-0.501	-0.223	0.000	0.003
GW	1	1	-0.596	-0.127	0.000	-0.557	-0.248	0.000	0.003

GW	1	1	-0.056	-0.025	0.000	-0.049	-0.036	0.000	0.003
GW	1	1	-0.111	-0.050	0.000	-0.099	-0.072	0.000	0.003
GW	1	1	-0.167	-0.074	0.000	-0.148	-0.107	0.000	0.003
GW	1	1	-0.223	-0.099	0.000	-0.197	-0.143	0.000	0.003
GW	1	1	-0.278	-0.124	0.000	-0.247	-0.179	0.000	0.003
GW	1	1	-0.334	-0.149	0.000	-0.296	-0.215	0.000	0.003
GW	1	1	-0.390	-0.174	0.000	-0.345	-0.251	0.000	0.003
GW	1	1	-0.446	-0.198	0.000	-0.395	-0.287	0.000	0.003
GW	1	1	-0.501	-0.223	0.000	-0.444	-0.322	0.000	0.003
GW	1	1	-0.557	-0.248	0.000	-0.493	-0.358	0.000	0.003
GW	1	1	-0.049	-0.036	0.000	-0.041	-0.045	0.000	0.003
GW	1	1	-0.099	-0.072	0.000	-0.082	-0.091	0.000	0.003
GW	1	1	-0.148	-0.107	0.000	-0.122	-0.136	0.000	0.003
GW	1	1	-0.197	-0.143	0.000	-0.163	-0.181	0.000	0.003
GW	1	1	-0.247	-0.179	0.000	-0.204	-0.227	0.000	0.003
GW	1	1	-0.296	-0.215	0.000	-0.245	-0.272	0.000	0.003
GW	1	1	-0.345	-0.251	0.000	-0.286	-0.317	0.000	0.003
GW	1	1	-0.395	-0.287	0.000	-0.326	-0.362	0.000	0.003
GW	1	1	-0.444	-0.322	0.000	-0.367	-0.408	0.000	0.003
GW	1	1	-0.493	-0.358	0.000	-0.408	-0.453	0.000	0.003
GW	1	1	-0.041	-0.045	0.000	-0.030	-0.053	0.000	0.003
GW	1	1	-0.082	-0.091	0.000	-0.061	-0.106	0.000	0.003
GW	1	1	-0.122	-0.136	0.000	-0.091	-0.158	0.000	0.003
GW	1	1	-0.163	-0.181	0.000	-0.122	-0.211	0.000	0.003
GW	1	1	-0.204	-0.227	0.000	-0.152	-0.264	0.000	0.003
GW	1	1	-0.245	-0.272	0.000	-0.183	-0.317	0.000	0.003
GW	1	1	-0.286	-0.317	0.000	-0.213	-0.370	0.000	0.003
GW	1	1	-0.326	-0.362	0.000	-0.244	-0.422	0.000	0.003
GW	1	1	-0.367	-0.408	0.000	-0.274	-0.475	0.000	0.003
GW	1	1	-0.408	-0.453	0.000	-0.305	-0.528	0.000	0.003
GW	1	1	-0.030	-0.053	0.000	-0.019	-0.058	0.000	0.003
GW	1	1	-0.061	-0.106	0.000	-0.038	-0.116	0.000	0.003
GW	1	1	-0.091	-0.158	0.000	-0.057	-0.174	0.000	0.003
GW	1	1	-0.122	-0.211	0.000	-0.075	-0.232	0.000	0.003
GW	1	1	-0.152	-0.264	0.000	-0.094	-0.290	0.000	0.003
GW	1	1	-0.183	-0.317	0.000	-0.113	-0.348	0.000	0.003
GW	1	1	-0.213	-0.370	0.000	-0.132	-0.406	0.000	0.003
GW	1	1	-0.244	-0.422	0.000	-0.151	-0.464	0.000	0.003
GW	1	1	-0.274	-0.475	0.000	-0.170	-0.522	0.000	0.003
GW	1	1	-0.305	-0.528	0.000	-0.188	-0.580	0.000	0.003
GW	1	1	-0.019	-0.058	0.000	-0.006	-0.061	0.000	0.003
GW	1	1	-0.038	-0.116	0.000	-0.013	-0.121	0.000	0.003
GW	1	1	-0.057	-0.174	0.000	-0.019	-0.182	0.000	0.003
GW	1	1	-0.075	-0.232	0.000	-0.025	-0.243	0.000	0.003
GW	1	1	-0.094	-0.290	0.000	-0.032	-0.303	0.000	0.003
GW	1	1	-0.113	-0.348	0.000	-0.038	-0.364	0.000	0.003
GW	1	1	-0.132	-0.406	0.000	-0.045	-0.424	0.000	0.003
GW	1	1	-0.151	-0.464	0.000	-0.051	-0.485	0.000	0.003
GW	1	1	-0.170	-0.522	0.000	-0.057	-0.546	0.000	0.003
GW	1	1	-0.188	-0.580	0.000	-0.064	-0.606	0.000	0.003
GW	1	1	-0.006	-0.061	0.000	0.006	-0.061	0.000	0.003
GW	1	1	-0.013	-0.121	0.000	0.013	-0.121	0.000	0.003
GW	1	1	-0.019	-0.182	0.000	0.019	-0.182	0.000	0.003
GW	1	1	-0.025	-0.243	0.000	0.025	-0.243	0.000	0.003
GW	1	1	-0.032	-0.303	0.000	0.032	-0.303	0.000	0.003
GW	1	1	-0.038	-0.364	0.000	0.038	-0.364	0.000	0.003
GW	1	1	-0.045	-0.424	0.000	0.132	-0.406	0.000	0.003
GW	1	1	-0.051	-0.485	0.000	0.151	-0.464	0.000	0.003
GW	1	1	-0.057	-0.546	0.000	0.051	-0.485	0.000	0.003
GW	1	1	-0.064	-0.606	0.000	0.064	-0.606	0.000	0.003
GW	1	1	0.006	-0.061	0.000	0.019	-0.058	0.000	0.003
GW	1	1	0.013	-0.121	0.000	0.038	-0.116	0.000	0.003
GW	1	1	0.019	-0.182	0.000	0.057	-0.174	0.000	0.003
GW	1	1	0.025	-0.243	0.000	0.075	-0.232	0.000	0.003
GW	1	1	0.032	-0.303	0.000	0.094	-0.290	0.000	0.003
GW	1	1	0.038	-0.364	0.000	0.113	-0.348	0.000	0.003
GW	1	1	0.045	-0.424	0.000	0.132	-0.406	0.000	0.003
GW	1	1	0.051	-0.485	0.000	0.151	-0.464	0.000	0.003
GW	1	1	0.057	-0.546	0.000	0.170	-0.522	0.000	0.003
GW	1	1	0.064	-0.606	0.000	0.188	-0.580	0.000	0.003
GW	1	1	0.019	-0.058	0.000	0.030	-0.053	0.000	0.003
GW	1	1	0.038	-0.116	0.000	0.061	-0.106	0.000	0.003
GW	1	1	0.057	-0.174	0.000	0.091	-0.158	0.000	0.003
GW	1	1	0.075	-0.232	0.000	0.122	-0.211	0.000	0.003
GW	1	1	0.094	-0.290	0.000	0.152	-0.264	0.000	0.003
GW	1	1	0.113	-0.348	0.000	0.183	-0.317	0.000	0.003
GW	1	1	0.132	-0.406	0.000	0.213	-0.370	0.000	0.003
GW	1	1	0.151	-0.464	0.000	0.244	-0.422	0.000	0.003
GW	1	1	0.170	-0.522	0.000	0.274	-0.475	0.000	0.003
GW	1	1	0.188	-0.580	0.000	0.305	-0.528	0.000	0.003
GW	1	1	0.030	-0.053	0.000	0.041	-0.045	0.000	0.003
GW	1	1	0.061	-0.106	0.000	0.082	-0.091	0.000	0.003
GW	1	1	0.091	-0.158	0.000	0.122	-0.136	0.000	0.003
GW	1	1	0.122	-0.211	0.000	0.163	-0.181	0.000	0.003
GW	1	1	0.152	-0.264	0.000	0.204	-0.227	0.000	0.003
GW	1	1	0.183	-0.317	0.000	0.245	-0.272	0.000	0.003
GW	1	1	0.213	-0.370	0.000	0.286	-0.317	0.000	0.003
GW	1	1	0.244	-0.422	0.000	0.326	-0.362	0.000	0.003
GW	1	1	0.274	-0.475	0.000	0.367	-0.408	0.000	0.003
GW	1	1	0.305	-0.528	0.000	0.408	-0.453	0.000	0.003

Appendix D

Measured Data for the Helibowl (Measured by dB Systems Inc.)

dB Systems, Inc. Measured Heli-Bowl Radiation Patterns, 1575 MHz

(Table provided courtesy of db Systems, Inc.)

--6/8/97--

Pattern 1:

dBs Heli-Bowl Vertical Patterns with Radome, No Absorber & Mounting Plate, Az Angle=90, 1575 MHz, Vertical Polarization

Pattern 2:

dBs Heli-Bowl Vertical Patterns with Radome, No Absorber & Mounting Plate, Az Angle=0, 1575 MHz, Horizontal Polarization

Pattern 3:

dBs Heli-Bowl Vertical Patterns with Radome, No Absorber & Mounting Plate, Az Angle=0, 1575 MHz, Vertical Polarization

Pattern4:

dBs Heli-Bowl Vertical Patterns with Radome, No Absorber & Mounting Plate, Az Angle=90, 1575 MHz, Horizontal Polarization

Angle (Degrees)	1 (dB)	2 (dB)	3 (dB)	4 (dB)
359.0000	-0.0100	-0.0200	-0.0600	-0.0600
358.0000	0	-0.0100	-0.0300	-0.0600
357.0000	-0.0200	0	-0.0100	-0.0200
356.0000	-0.0200	0	0	0
355.0000	-0.0500	0	0	-0.0100
354.0000	-0.1000	-0.0300	-0.0300	-0.0200
353.0000	-0.1500	-0.0500	-0.0400	-0.0100
352.0000	-0.2100	-0.1100	-0.0700	-0.0700
351.0000	-0.3000	-0.1800	-0.1000	-0.0900
350.0000	-0.3000	-0.1800	-0.1500	-0.1400
349.0000	-0.3700	-0.2300	-0.2000	-0.1700
348.0000	-0.4800	-0.3300	-0.2500	-0.2600
347.0000	-0.6000	-0.4100	-0.3200	-0.2900
346.0000	-0.7200	-0.5300	-0.3900	-0.3600
345.0000	-0.7200	-0.5300	-0.4500	-0.4800
344.0000	-0.8400	-0.6500	-0.5400	-0.5800
343.0000	-0.9800	-0.7800	-0.6300	-0.6700
342.0000	-1.1100	-0.9400	-0.7200	-0.7700
341.0000	-1.2700	-1.1100	-0.8100	-0.8600
340.0000	-1.4000	-1.1100	-0.9200	-1.0000
339.0000	-1.4000	-1.2600	-1.0300	-1.1100
338.0000	-1.5700	-1.4100	-1.1500	-1.2400
337.0000	-1.7200	-1.5700	-1.2600	-1.3700
336.0000	-1.9000	-1.7800	-1.3900	-1.5300
335.0000	-2.0500	-1.7800	-1.5200	-1.6400
334.0000	-2.0500	-1.9800	-1.6400	-1.8000
333.0000	-2.2300	-2.1500	-1.8000	-1.9300
332.0000	-2.4000	-2.3600	-1.9400	-2.1100
331.0000	-2.5900	-2.3600	-2.0800	-2.2300
330.0000	-2.7600	-2.5700	-2.2200	-2.4300
329.0000	-2.7600	-2.8000	-2.5400	-2.5900
328.0000	-2.9600	-3.0100	-2.7000	-2.7700
327.0000	-3.1400	-3.2200	-2.7000	-2.9200
326.0000	-3.3600	-3.2200	-2.8800	-3.1000
325.0000	-3.5500	-3.4600	-3.2400	-3.2800
324.0000	-3.7900	-3.6700	-3.4300	-3.4200
323.0000	-3.7900	-3.8600	-3.6400	-3.6500
322.0000	-4.0200	-4.1000	-3.8500	-3.7800
321.0000	-4.2500	-4.1000	-4.0700	-4.0000
320.0000	-4.4900	-4.3800	-4.2900	-4.1800

319.0000	-4.7600	-4.6300	-4.5200	-4.3400
318.0000	-4.7600	-4.8900	-4.7800	-4.5700
317.0000	-5.0400	-5.1400	-5.0300	-4.7500
316.0000	-5.3300	-5.4600	-5.2900	-5.0000
315.0000	-5.6600	-5.4600	-5.5900	-5.2400
314.0000	-5.9700	-5.7200	-5.8800	-5.4300
313.0000	-6.3300	-6.0300	-6.1700	-5.7100
312.0000	-6.3300	-6.3200	-6.4800	-5.9600
311.0000	-6.6800	-6.6200	-6.8100	-6.1300
310.0000	-7.0900	-6.6200	-7.1200	-6.3400
309.0000	-7.4900	-6.9200	-7.4700	-6.6700
308.0000	-7.9100	-7.2300	-7.8000	-6.8900
307.0000	-8.3600	-7.6200	-8.1700	-7.1900
306.0000	-8.3600	-7.6200	-8.5200	-7.4200
305.0000	-8.8000	-7.9300	-8.8800	-7.7800
304.0000	-9.2700	-8.3100	-9.2500	-7.9500
303.0000	-9.7400	-8.5900	-9.6100	-8.2600
302.0000	-10.2100	-8.9700	-10.0100	-8.5600
301.0000	-10.2100	-9.3000	-10.4000	-8.8000
300.0000	-10.6900	-9.3000	-10.7800	-9.1500
299.0000	-11.1800	-9.7100	-11.1700	-9.3900
298.0000	-11.6300	-10.0700	-11.6000	-9.6400
297.0000	-12.1100	-10.3800	-12.0000	-9.8900
296.0000	-12.6500	-10.7400	-12.4100	-10.1500
295.0000	-12.6500	-10.7400	-12.8500	-10.4100
294.0000	-13.1400	-10.9400	-13.2800	-10.6700
293.0000	-13.6600	-11.3100	-13.6800	-10.9400
292.0000	-14.1000	-11.6500	-14.5500	-11.1900
291.0000	-14.5600	-11.9100	-14.9800	-11.4900
290.0000	-15.0600	-12.1600	-15.3700	-11.7100
289.0000	-15.5500	-12.1600	-15.9000	-11.8800
288.0000	-15.5500	-12.4600	-16.3600	-12.0500
287.0000	-15.9800	-12.7100	-16.7900	-12.2600
286.0000	-16.5000	-12.9800	-17.3400	-12.6600
285.0000	-17.0100	-13.2400	-17.8500	-12.7900
284.0000	-17.6000	-13.5200	-18.4300	-13.0300
283.0000	-18.1100	-13.5200	-18.9800	-13.1700
282.0000	-18.7100	-13.7600	-19.4900	-13.4100
281.0000	-18.7100	-13.8200	-20.0400	-13.7200
280.0000	-19.2900	-14.1800	-20.6500	-13.8400
279.0000	-19.7400	-14.3500	-21.1600	-13.9500
278.0000	-20.2600	-14.5600	-21.6800	-14.1300
277.0000	-20.8500	-14.5600	-22.2100	-14.3000
276.0000	-21.3200	-14.7900	-22.7800	-14.4700
275.0000	-21.8000	-14.9700	-23.4200	-14.6200
274.0000	-21.8000	-15.0900	-23.9300	-14.8600
273.0000	-22.5300	-15.3700	-24.7000	-15.1500
272.0000	-23.1200	-15.6100	-25.3900	-15.1600
271.0000	-23.8100	-15.6100	-26.9700	-15.3500
270.0000	-24.3900	-15.9800	-27.7500	-15.6600
269.0000	-25.4400	-16.1400	-28.7700	-15.9100
268.0000	-25.4400	-16.4300	-29.7700	-16.1900
267.0000	-26.1400	-16.9500	-30.8600	-16.3400
266.0000	-26.8900	-17.3300	-32.0000	-16.7100
265.0000	-27.6700	-17.3300	-32.8600	-16.9300
264.0000	-28.3000	-17.4400	-34.3500	-17.1500
263.0000	-28.7600	-17.8500	-35.5900	-17.4900
262.0000	-28.7600	-18.0500	-37.8600	-17.8300
261.0000	-29.2100	-18.2700	-39.1500	-17.6100
260.0000	-29.7300	-18.2700	-39.9500	-18.0700
259.0000	-29.9400	-18.7800	-41.1800	-18.2700
258.0000	-30.0800	-18.9700	-41.7000	-18.6000
257.0000	-30.0700	-19.1200	-40.6900	-18.6100
256.0000	-30.0700	-19.4300	-40.1600	-19.0200
255.0000	-30.0300	-20.1000	-39.7600	-19.4800
254.0000	-29.6600	-20.1000	-38.1300	-19.5600
253.0000	-29.7300	-19.9600	-37.6400	-19.8500

252.0000	-29.5200	-20.6600	-36.4300	-20.0600
251.0000	-29.7500	-21.0600	-35.7900	-20.6600
250.0000	-29.2600	-21.4200	-34.9200	-21.0200
249.0000	-29.2600	-21.5500	-34.6000	-21.6200
248.0000	-29.2400	-21.5500	-33.5600	-22.0200
247.0000	-29.0100	-22.0200	-33.7600	-22.2500
246.0000	-28.6900	-22.3100	-33.0100	-22.4900
245.0000	-28.3800	-22.5000	-32.4000	-22.7300
244.0000	-27.9500	-22.6200	-32.0400	-22.8400
243.0000	-27.7400	-23.1600	-31.4800	-23.7400
242.0000	-27.7400	-23.1600	-31.0600	-23.5500
241.0000	-27.5800	-23.2900	-31.0300	-24.0500
240.0000	-27.2100	-23.9700	-30.5900	-24.0500
239.0000	-27.3500	-24.1000	-30.6700	-24.5700
238.0000	-27.4900	-25.0100	-30.6900	-25.1000
237.0000	-27.6800	-25.8300	-30.9900	-25.6000
236.0000	-28.0100	-25.8300	-31.3900	-26.0100
235.0000	-28.0100	-26.0400	-31.6600	-27.4100
234.0000	-28.6400	-27.0400	-32.3200	-27.1400
233.0000	-28.9100	-28.1900	-32.4300	-27.6300
232.0000	-29.4700	-28.6300	-33.4600	-28.1700
231.0000	-29.6500	-29.3900	-33.7400	-28.1300
230.0000	-30.2000	-29.3900	-34.2800	-29.1600
229.0000	-30.4900	-29.8600	-33.9700	-28.6600
228.0000	-30.8000	-30.3300	-34.3100	-29.5800
227.0000	-30.8000	-30.9000	-34.3100	-28.8700
226.0000	-30.4900	-30.1800	-34.0100	-28.9700
225.0000	-30.6400	-30.7700	-33.8500	-29.0100
224.0000	-30.7000	-30.7700	-33.2900	-28.7600
223.0000	-30.6900	-31.0000	-33.1300	-28.4000
222.0000	-30.6800	-30.6300	-33.2700	-28.8100
221.0000	-30.6800	-31.9300	-33.1700	-30.0700
220.0000	-31.0800	-31.7300	-33.2400	-30.5200
219.0000	-30.7800	-31.7500	-33.1100	-32.8500
218.0000	-31.0300	-31.7500	-33.6200	-31.9800
217.0000	-31.4300	-33.4900	-34.4000	-33.6200
216.0000	-31.7600	-32.8900	-34.9100	-33.8200
215.0000	-31.7600	-33.0500	-35.2900	-33.8200
214.0000	-32.8300	-35.7100	-35.0900	-34.7700
213.0000	-32.8800	-35.7100	-35.9200	-36.0700
212.0000	-33.3400	-36.6700	-37.1500	-38.7100
211.0000	-33.2000	-35.0100	-36.9600	-38.6200
210.0000	-33.3700	-36.1200	-36.7800	-38.5300
209.0000	-33.1100	-34.1500	-36.3200	-39.3000
208.0000	-33.2600	-34.7600	-36.1500	-37.4700
207.0000	-33.2600	-34.2100	-35.7600	-38.7600
206.0000	-32.6200	-33.3100	-34.8700	-38.8000
205.0000	-32.1300	-33.3100	-34.2900	-37.3700
204.0000	-31.9800	-35.6000	-33.8200	-36.7700
203.0000	-31.3000	-32.8000	-33.7300	-37.9200
202.0000	-31.2800	-34.5400	-33.3000	-36.7100
201.0000	-31.5700	-34.4900	-33.2200	-37.2200
200.0000	-31.5300	-34.9700	-33.3400	-37.7500
199.0000	-31.6500	-35.5600	-33.1600	-40.5000
198.0000	-31.7800	-35.5300	-33.5800	-42.1000
197.0000	-31.7800	-35.5300	-34.1300	-44.7300
196.0000	-32.6600	-39.2000	-34.7300	-50.4600
195.0000	-32.9900	-36.6100	-35.0300	-46.4500
194.0000	-33.7800	-39.1200	-36.6700	-43.4000
193.0000	-34.7900	-40.4000	-37.4500	-48.1400
192.0000	-36.3700	-47.7200	-39.0500	-43.4000
191.0000	-36.7600	-56.7100	-41.1600	-39.3200
190.0000	-38.6100	-55.1000	-44.4100	-36.3100
189.0000	-38.6100	-55.1000	-44.9200	-36.7700
188.0000	-39.0200	-46.5500	-46.5900	-36.0700
187.0000	-39.5600	-45.5000	-43.3800	-33.6600
186.0000	-38.0400	-39.9300	-40.2700	-34.0900

185.0000	-36.4000	-37.4700	-38.1500	-33.4600
184.0000	-35.5500	-37.4700	-36.7800	-33.4600
183.0000	-35.5500	-38.1300	-35.0900	-32.1100
182.0000	-35.2200	-37.6300	-33.8100	-30.8300
181.0000	-33.6600	-36.2900	-31.6800	-31.2100
180.0000	-32.9200	-34.8200	-31.6800	-31.2100
179.0000	-32.3600	-33.8900	-30.8100	-31.3000
178.0000	-31.3200	-33.8900	-30.8100	-31.3000
177.0000	-31.7600	-34.0100	-30.1600	-31.0400
176.0000	-31.2700	-33.4500	-29.8400	-30.2400
175.0000	-30.8600	-33.7700	-29.7500	-30.4500
174.0000	-30.8500	-32.9300	-29.3200	-31.2900
173.0000	-31.0400	-34.2700	-29.1400	-31.8200
172.0000	-31.3400	-34.2700	-29.0700	-31.1000
171.0000	-31.3400	-34.8800	-29.3000	-32.0800
170.0000	-31.4000	-34.9500	-29.3700	-32.4900
169.0000	-31.8000	-35.5100	-29.6400	-33.0700
168.0000	-32.1200	-37.3200	-29.5600	-33.5500
167.0000	-32.9500	-38.9200	-30.0300	-33.6000
166.0000	-33.7600	-39.3000	-30.5000	-36.1900
165.0000	-34.7100	-41.4800	-30.8000	-36.7700
164.0000	-35.5100	-41.4800	-31.7800	-37.5000
163.0000	-35.5100	-46.8500	-31.7600	-37.8500
162.0000	-36.6100	-46.3100	-31.8500	-39.2300
161.0000	-37.4600	-51.9100	-32.4900	-38.5200
160.0000	-38.4000	-51.1300	-32.6800	-38.9200
159.0000	-38.6200	-45.7900	-32.6900	-38.0100
158.0000	-37.9500	-44.7600	-32.6900	-38.0300
157.0000	-37.7500	-44.7600	-32.7600	-37.1100
156.0000	-37.7500	-41.2200	-32.1000	-37.2400
155.0000	-36.6800	-40.7200	-31.9200	-37.2300
154.0000	-35.7500	-41.4900	-31.2700	-36.8700
153.0000	-35.1500	-38.5400	-30.5800	-37.7000
152.0000	-34.3300	-38.5100	-30.5200	-37.2400
151.0000	-34.3800	-38.5100	-30.5200	-38.4100
150.0000	-34.5900	-39.6800	-29.9500	-36.8800
149.0000	-34.5900	-37.0600	-29.9500	-38.1800
148.0000	-33.9100	-40.9500	-29.5000	-38.1100
147.0000	-34.2600	-37.2800	-29.5700	-40.0500
146.0000	-35.0100	-37.4100	-29.6300	-38.6800
145.0000	-34.7300	-37.4100	-29.8900	-38.5100
144.0000	-34.7300	-37.6900	-29.8900	-37.8700
143.0000	-35.9000	-36.1300	-29.8900	-37.8700
142.0000	-36.2500	-35.9500	-30.2800	-35.5900
141.0000	-36.5700	-35.7800	-30.0800	-34.6300
140.0000	-37.0200	-32.9100	-30.6700	-33.6500
139.0000	-36.9400	-34.2800	-30.6400	-32.9900
138.0000	-36.9100	-34.2800	-30.7400	-33.1800
137.0000	-36.9100	-32.6200	-30.3000	-32.4800
136.0000	-36.2100	-32.2700	-30.5400	-31.6400
135.0000	-35.1000	-32.4500	-30.3300	-29.8400
134.0000	-34.3900	-32.4900	-29.8900	-31.2700
133.0000	-33.9400	-31.9000	-30.1700	-31.2700
132.0000	-33.0500	-31.9000	-29.5900	-30.5300
131.0000	-33.0500	-31.8300	-29.5600	-30.3800
130.0000	-32.8200	-31.2700	-29.4400	-30.2000
129.0000	-32.4600	-31.2200	-29.2500	-30.3100
128.0000	-32.2000	-30.6500	-29.2700	-29.7800
127.0000	-32.2900	-29.5100	-28.8900	-29.8800
126.0000	-32.7100	-29.5100	-29.0300	-29.0300
125.0000	-33.2800	-29.7000	-29.1300	-28.7500
124.0000	-33.2800	-28.9200	-28.9500	-28.4100
123.0000	-33.0200	-28.2200	-28.7500	-28.7200
122.0000	-33.1600	-27.5800	-28.5300	-28.0800
121.0000	-32.6900	-27.5700	-28.4200	-28.0200
120.0000	-32.8200	-27.5700	-28.2600	-26.8900
119.0000	-32.2800	-26.8400	-27.9000	-26.7100

118.0000	-32.2800	-26.7100	-27.5100	-26.6900
117.0000	-32.3100	-26.0400	-27.2300	-26.1500
116.0000	-31.7300	-25.8200	-26.9500	-25.6700
115.0000	-31.1000	-25.8200	-26.7100	-25.2800
114.0000	-30.9200	-25.9900	-26.1800	-25.2800
113.0000	-30.9200	-24.8600	-26.1100	-24.8900
112.0000	-30.6300	-25.0500	-25.9900	-25.1000
111.0000	-30.3900	-24.2800	-25.7700	-24.5600
110.0000	-29.8900	-23.9700	-25.7000	-24.1000
109.0000	-29.5700	-23.9700	-25.4100	-23.9100
108.0000	-29.6900	-23.7000	-25.5700	-23.2300
107.0000	-29.6900	-23.3600	-25.4600	-22.9200
106.0000	-29.4000	-23.1500	-25.3400	-22.4900
105.0000	-29.0600	-22.9200	-25.1900	-22.4000
104.0000	-29.2000	-21.9200	-25.2500	-21.9900
103.0000	-28.9800	-21.9200	-25.1200	-21.5600
102.0000	-28.6800	-21.7300	-24.8400	-21.3600
101.0000	-28.6800	-21.2800	-24.8600	-20.8500
100.0000	-28.1800	-20.7000	-24.7700	-20.4600
99.0000	-27.8400	-20.3400	-24.5700	-20.2900
98.0000	-27.3400	-20.3400	-24.4300	-20.0100
97.0000	-26.8500	-19.8900	-24.3500	-19.8700
96.0000	-26.6000	-19.5700	-24.2300	-19.4700
95.0000	-26.6000	-19.0600	-24.1300	-19.4000
94.0000	-25.9400	-18.6800	-24.0800	-19.1300
93.0000	-25.3700	-18.4500	-23.8600	-18.7000
92.0000	-24.8700	-18.2300	-23.6400	-18.7800
91.0000	-24.1200	-18.2300	-23.5100	-18.4000
90.0000	-23.6700	-17.8500	-23.3300	-18.2900
89.0000	-23.0500	-17.5900	-22.8500	-18.1000
88.0000	-23.0500	-17.2500	-22.6100	-17.7800
87.0000	-22.5000	-16.9600	-22.1400	-17.4400
86.0000	-21.8700	-16.9600	-21.8800	-17.2000
85.0000	-21.2800	-16.6600	-21.5500	-16.9400
84.0000	-20.6400	-16.6300	-21.1900	-16.5900
83.0000	-20.6400	-16.0000	-20.7800	-16.2900
82.0000	-20.0800	-15.7900	-20.4600	-16.0800
81.0000	-19.5800	-15.7400	-20.1000	-15.7900
80.0000	-19.1700	-15.7400	-19.7300	-15.6100
79.0000	-18.7300	-15.6400	-19.3600	-15.6100
78.0000	-18.1700	-15.3900	-18.9700	-15.5900
77.0000	-18.1700	-15.2300	-18.5300	-15.4100
76.0000	-17.7600	-14.8700	-18.1900	-15.1000
75.0000	-17.2900	-14.8700	-17.8200	-14.9100
74.0000	-16.9000	-14.8800	-17.4100	-14.8300
73.0000	-16.3700	-14.5300	-16.6100	-14.6500
72.0000	-16.3700	-14.0900	-16.1800	-14.2900
71.0000	-15.8900	-13.6400	-16.1800	-14.1400
70.0000	-15.3900	-13.4400	-15.7500	-13.7100
69.0000	-14.9100	-13.4400	-15.3200	-13.6300
68.0000	-14.3700	-13.1800	-14.5400	-13.4400
67.0000	-13.8900	-12.8300	-14.0900	-13.1700
66.0000	-13.3900	-12.5600	-13.7000	-12.8000
65.0000	-13.3900	-12.1800	-13.3200	-12.6000
64.0000	-12.8800	-12.0100	-12.8800	-12.6000
63.0000	-12.3900	-12.0100	-12.5300	-12.3300
62.0000	-11.9000	-11.6200	-12.1700	-11.8700
61.0000	-11.4900	-11.3700	-11.4300	-11.6900
60.0000	-11.4900	-11.1100	-11.0800	-11.4500
59.0000	-11.0200	-10.7000	-10.7300	-11.2100
58.0000	-10.5600	-10.7000	-10.4000	-10.9300
57.0000	-10.1500	-10.5000	-10.0600	-10.6900
56.0000	-9.7300	-10.2000	-9.7100	-10.4000
55.0000	-9.3100	-9.8400	-9.3800	-10.1200
54.0000	-9.3100	-9.5300	-9.0400	-9.8100
53.0000	-8.8800	-9.1900	-8.7100	-9.5400
52.0000	-8.4700	-9.1900	-8.3900	-9.2100

51.0000	-8.0900	-8.8300	-8.0500	-8.9000
50.0000	-7.7200	-8.5200	-7.7200	-8.6300
49.0000	-7.3400	-8.2300	-7.3800	-8.3700
48.0000	-7.3400	-7.8800	-7.0800	-8.0800
47.0000	-6.9700	-7.8800	-6.7700	-7.7800
46.0000	-6.6000	-7.6100	-6.4800	-7.5300
45.0000	-6.2500	-7.2700	-6.1900	-7.2600
44.0000	-6.2500	-6.9300	-5.9100	-7.0200
43.0000	-5.9100	-6.6700	-5.6500	-6.7500
42.0000	-5.5900	-6.6700	-5.3800	-6.5400
41.0000	-5.2800	-6.3500	-5.1200	-6.2900
40.0000	-5.0000	-6.0800	-4.8800	-6.0500
39.0000	-5.0000	-5.8000	-4.6600	-5.8200
38.0000	-4.7100	-5.8000	-4.4300	-5.6100
37.0000	-4.4500	-5.5300	-4.2200	-5.3700
36.0000	-4.2000	-5.2800	-4.0100	-5.2000
35.0000	-3.9500	-5.0400	-3.8400	-4.9900
34.0000	-3.9500	-4.7600	-3.6500	-4.8100
33.0000	-3.7200	-4.4600	-3.4900	-4.5900
32.0000	-3.5100	-4.4600	-3.3500	-4.4200
31.0000	-3.3000	-4.2300	-3.1800	-4.2000
30.0000	-3.0800	-4.0100	-3.0300	-4.0200
29.0000	-2.8900	-3.7800	-2.9100	-3.8500
28.0000	-2.8900	-3.5300	-2.7900	-3.7200
27.0000	-2.6900	-3.5300	-2.5500	-3.5300
26.0000	-2.5100	-3.3500	-2.4400	-3.3600
25.0000	-2.3500	-3.0900	-2.3300	-3.1900
24.0000	-2.1600	-2.9000	-2.2100	-3.0500
23.0000	-1.9900	-2.6700	-2.1000	-2.9100
22.0000	-1.9900	-2.4400	-1.9900	-2.7100
21.0000	-1.8200	-2.4400	-1.8800	-2.5400
20.0000	-1.6700	-2.2800	-1.7600	-2.4000
19.0000	-1.5100	-2.0800	-1.6600	-2.2200
18.0000	-1.3500	-1.8600	-1.5600	-2.0700
17.0000	-1.3500	-1.6900	-1.4600	-1.9600
16.0000	-1.2000	-1.6900	-1.3500	-1.8100
15.0000	-1.0600	-1.5100	-1.2400	-1.6400
14.0000	-0.9100	-1.3300	-1.1400	-1.5300
13.0000	-0.7800	-1.1800	-1.0500	-1.3200
12.0000	-0.6600	-1.0200	-0.9500	-1.2300
11.0000	-0.6600	-1.0200	-0.8500	-1.1100
10.0000	-0.5400	-0.8600	-0.7600	-0.9700
9.0000	-0.4400	-0.7500	-0.6700	-0.8800
8.0000	-0.3300	-0.6000	-0.5800	-0.7600
7.0000	-0.2500	-0.4700	-0.5100	-0.6400
6.0000	-0.2500	-0.4700	-0.4400	-0.5400
5.0000	-0.1900	-0.3700	-0.3700	-0.4700
4.0000	-0.1300	-0.3200	-0.3000	-0.3700
3.0000	-0.0700	-0.2000	-0.2300	-0.2900
2.0000	-0.0700	-0.1300	-0.1800	-0.2200
1.0000	-0.0400	-0.1300	-0.1300	-0.1900
0	-0.0100	-0.0700	-0.0900	-0.1100

Appendix E

**The Simulation Results of those
Helibowl Models as Mentioned in
Sections 5.2.3 & 5.3.**

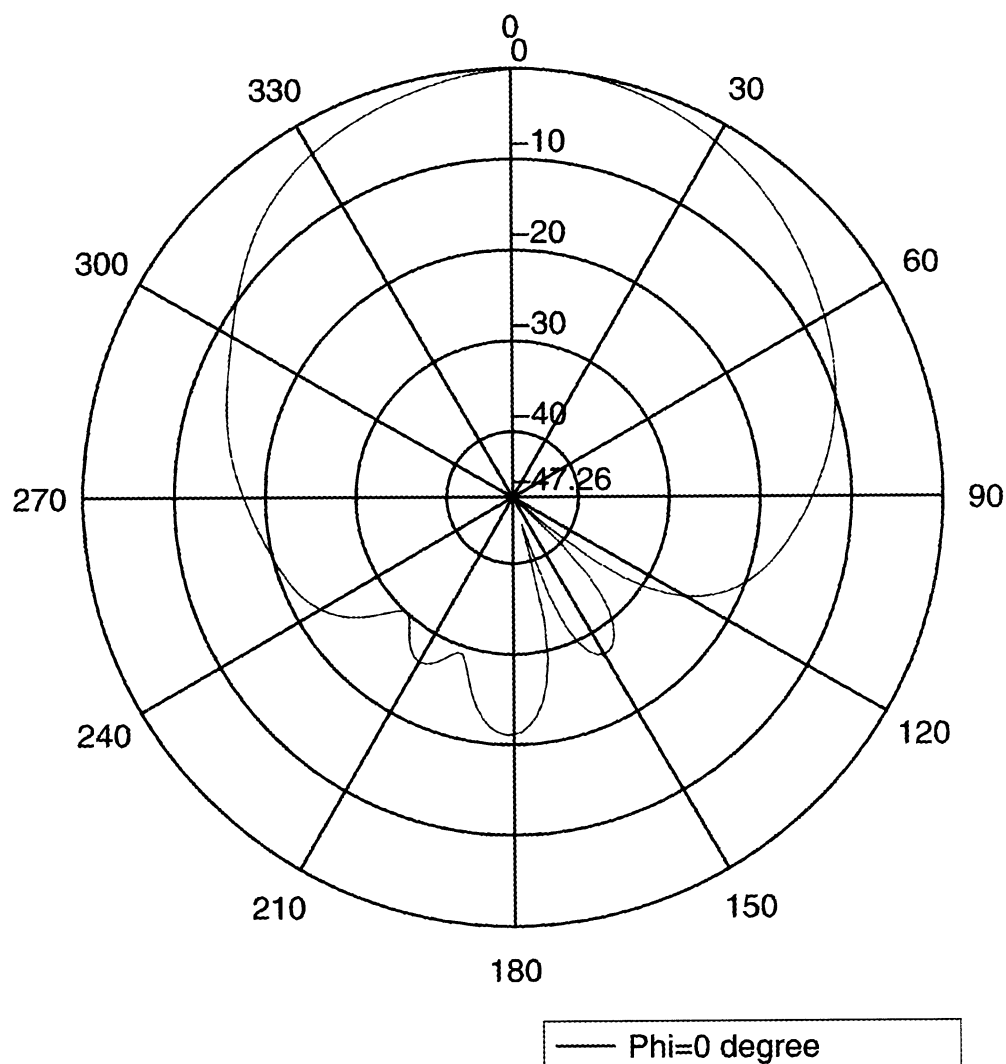


Figure E-1 Total radiation pattern for original helibowl

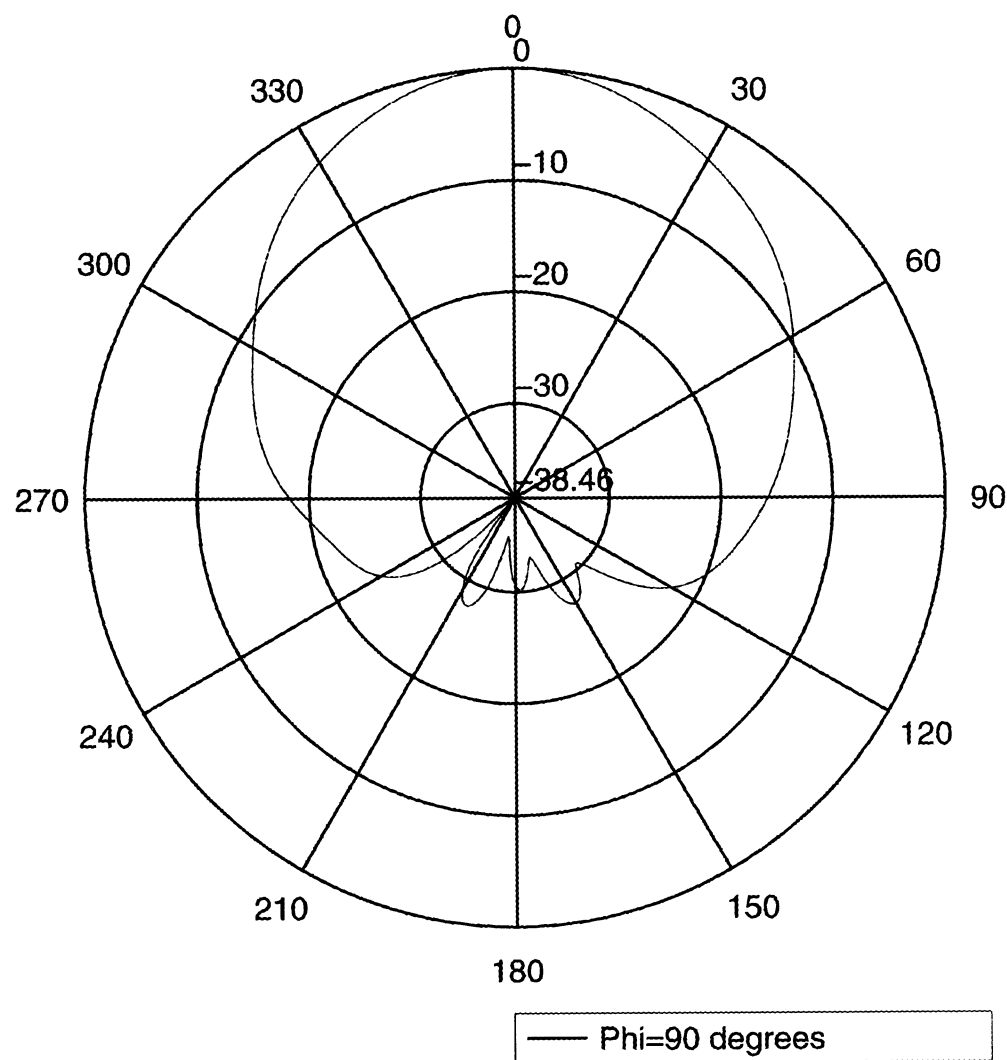


Figure E-2 Total radiation pattern for original helibowl

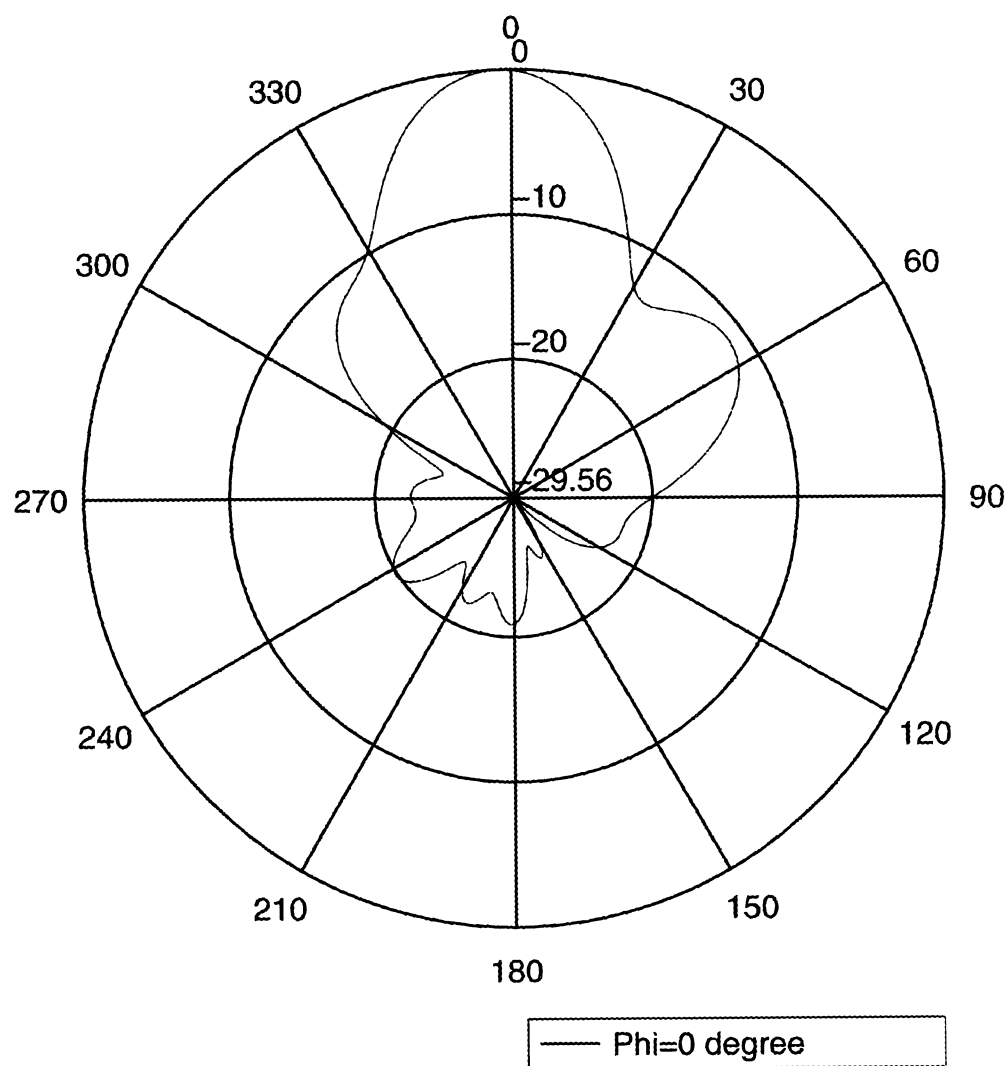


Figure E-3 Total Radiation Pattern for helibowl with double sized bowl

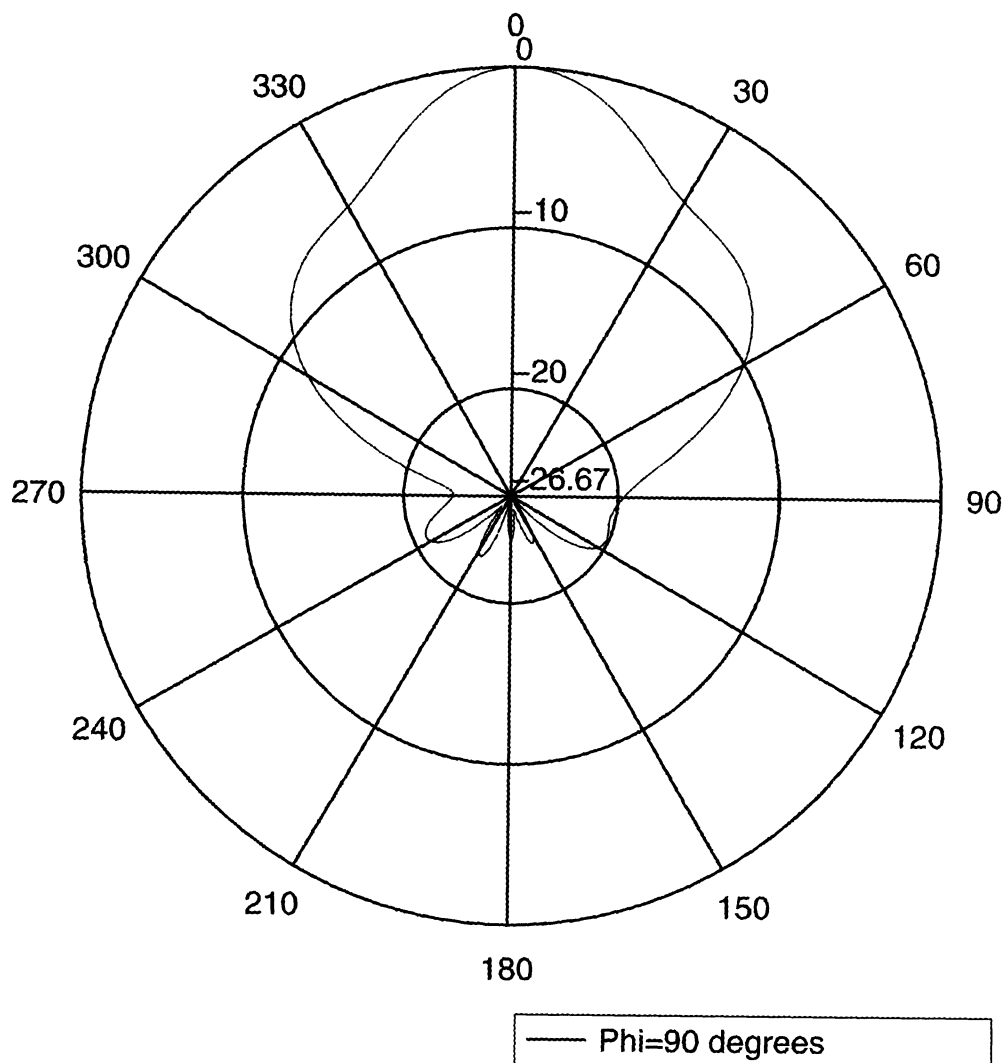


Figure E-4 Total Radiation Pattern for helibowl with doubled sized bowl

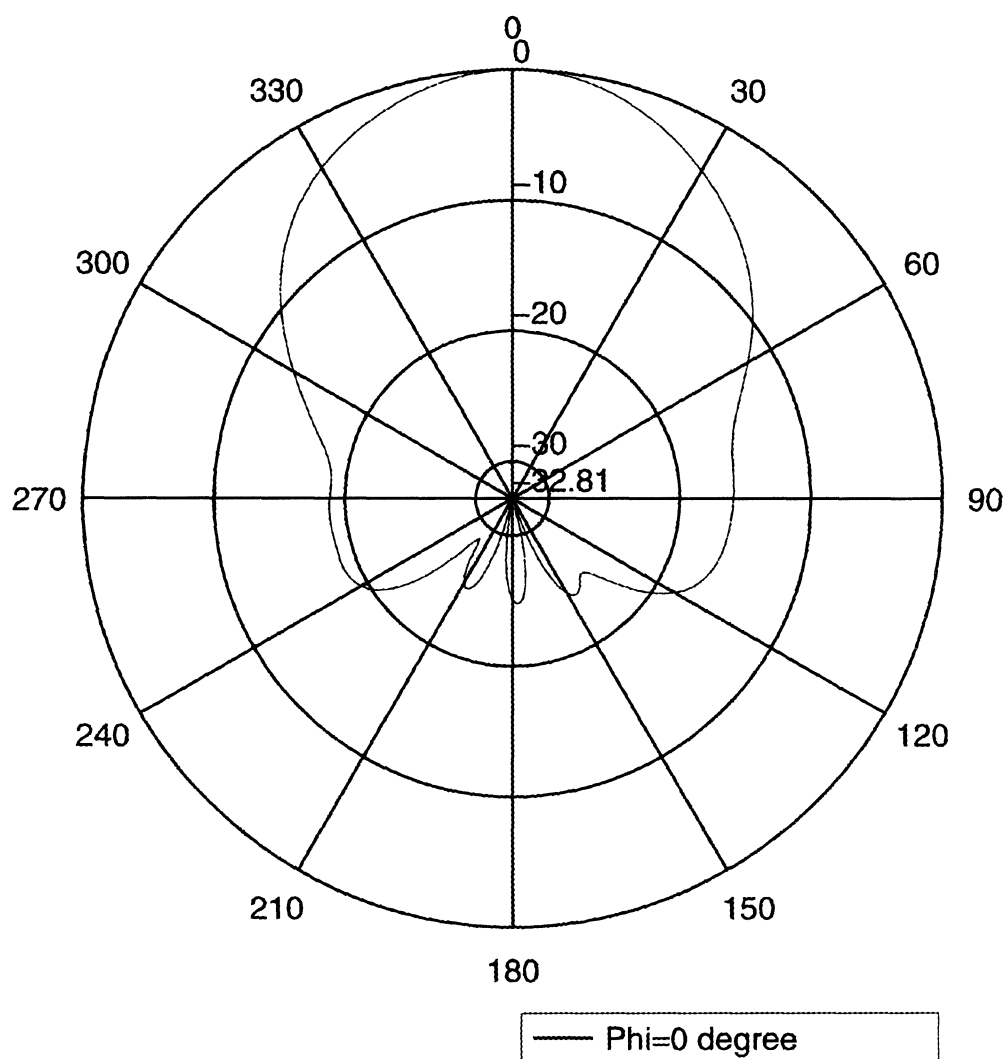


Figure E-5 Total Radiation Pattern for helibowl with length of helix doubled

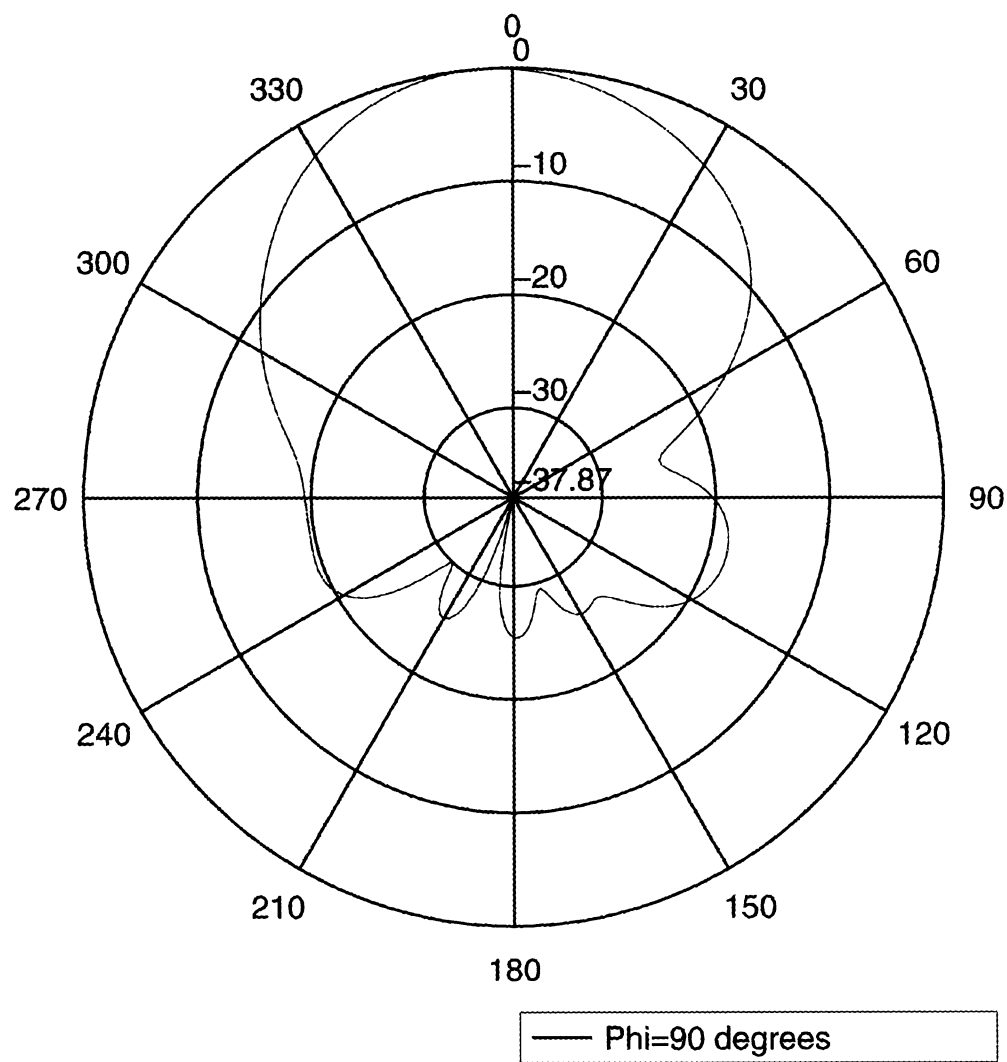


Figure E-6 Total Radiation Pattern for helibowl with length of helix doubled